RIGA TECHNICAL UNIVERSITY

Guntis Pikurs

RESEARCH ON THE NOVEL MANUFACTURING TECHNOLOGY FOR COMPACT RADIO FREQUENCY QUADRUPOLE DESIGN AND PRODUCTION

Doctoral Thesis

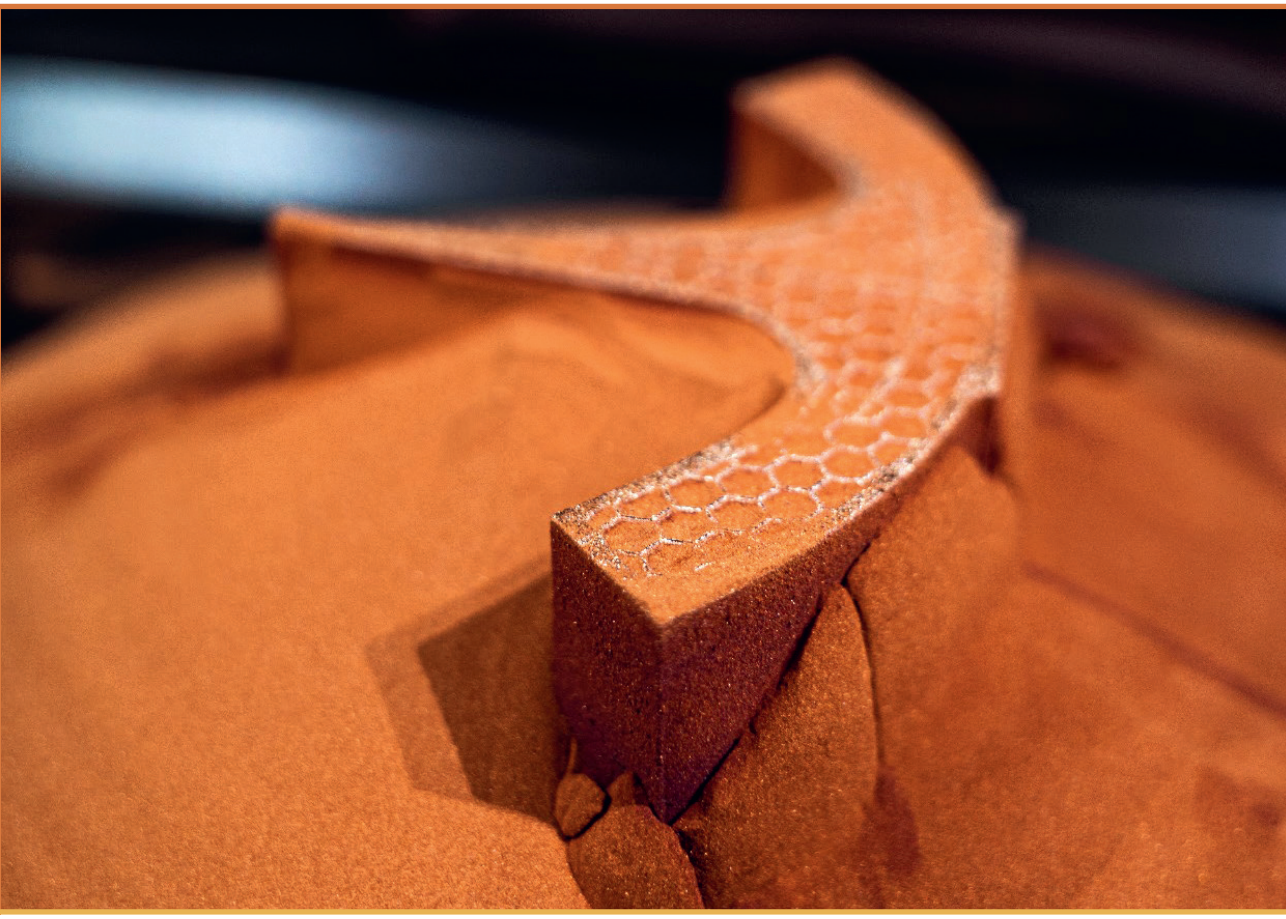

RTU Press
Riga 2024

RIGA TECHNICAL UNIVERSITY
Faculty of Civil and Mechanical Engineering
Institute of Mechanical and Biomedical Engineering

Guntis Pikurs
Doctoral Student of the Study Programme "Mechanical Engineering and Mechanics"

RESEARCH ON THE NOVEL ADDITIVE MANUFACTURING TECHNOLOGY FOR COMPACT RADIO FREQUENCY QUADRUPOLE DESIGN AND PRODUCTION

Doctoral Thesis

Scientific supervisors

Professor Dr. sc. ing.
TOMS TORIMS

Dr. phys.
MAURIZIO VRETENAR

Riga 2024

The research was carried out within the framework and with financial support of the following projects:

- State Research Programme (SRP) "High-energy physics and accelerator technologies" VPP-IZM-CERN-2020/1-0002; VPP-IZM-CERN-2022/1-0001;

- Horizon 2020 project "Innovation Fostering in Accelerator Science and Technology" (I.FAST) WP10.2. This project has received funding from the European Union's Horizon 2020 Research and Innovation programme under grant agreement No. 101004730.

Cover photo by Christoph Wilsnack/Fraunhofer IWS

ABSTRACT

This Thesis research is focused on examining the potential applicability of metal additive manufacturing (AM) in the context of accelerator technology, with a particular emphasis on the feasibility of utilising this technology for the fabrication of compact, pure copper radio frequency quadrupole (RFQ) components.

The Thesis research commences with an introduction, wherein the fundamental principles, applications and significance of accelerators are elucidated. The first chapter provides an overview of the specific challenges and conditions that have been addressed in the context of accelerator components. Subsequently, a literature review and state-of-the-art analysis on AM are presented. This includes an overview of the evolution of metal AM technology and recent advances. Furthermore, there is a growing emphasis on the rapidly increasing popularity of AM technology and its incorporation into the strategic plans of most developed countries.

The following chapter delineates the objective and scope of the study, along with any existing gaps in knowledge and potential case studies. The primary objectives, methodologies, applications, and distinctive features of the scientific findings are meticulously delineated. Further, Thesis turns to research methodology, where the quantitative and qualitative analytical techniques and tools used in this study, as well as the planning of the experiments and the steps taken to validate the results are discussed.

A survey is conducted to ascertain the requirements for the development of accelerators and components, thereby identifying the needs and challenges in this field.

Subsequently, this Thesis examines methods for enhancing RFQ designs through the utilisation of AM benefits. The study also considers the geometry design and thermal management of AM RFQs and presents a mathematical model for predicting the Q factor of AM RFQs. Additionally, the potential challenges and difficulties faced by both AM and traditional manufacturing processes are discussed.

This concept prototype RFQ, created using AM, encompasses the experimental setup, the AM process employing pure copper, and post-processing methods such as conventional mass finishing, chemically assisted finishing, and MMP TECHNOLOGY®. The methodology employed to assess the geometrical accuracy and surface roughness quality of the additively built RFQ prototype is elucidated. This comprised measurements conducted using coordinate measuring devices, optical scanning, and surface roughness evaluations for both the as-built and post-processed components.

Subsequent studies of technical and physical validation are conducted to substantiate the findings of the research. In order to evaluate the manufacturing time of AM for the production of RFQ, a comparison is made between the machining times for AM and traditional machining methods. The Thesis concludes with a synthesis of the findings, recommendations for future research, and a discussion of the challenges that remain to be addressed.

The bibliography provides list of 117 supplementary resources for those wishing to pursue a more in-depth investigation of the subject matter, offering a comprehensive list of the sources cited throughout the Thesis.

ANOTĀCIJA

Promocijas darba fokuss ir vērsts uz metāla aditīvās ražošanas (AM) tehnoloģijas pielietojumu daļiņu paātrinātāju izgatavošanā. Darba mērķis ir iegūt priekšstatu par tehnoloģiskajiem ierobežojumiem un izaicinājumiem kompakta izmēra, tīra vara radiofrekvences kvadrupola (RFQ) izgatavošanā.

Promocijas darba ievadā, tiek aprakstīti paātrinātāju vispārīgie principi, pielietojumi un to industriālā nozīme. Šajā daļā ir ietverts pārskats par īpašajiem izaicinājumiem un nosacījumiem, kas tiek attiecināti uz paātrinātāju komponentēm. Ievadam seko literatūras un jaunāko sasniegumu apskats metālu AM tehnoloģijā, ietverot evolūcijas vēsturi un izceļot aktuālos jaunos sasniegumus. Uzsvars apskatā tiek likts uz strauji augošo AM tehnoloģiju popularitāti un tās izvirzīšanu vispārējos rūpniecības stratēģiskajos plānos ne tikai Eiropā un ASV, bet arī strauji progresējošajās Āzijas valstīs.

Sekojošajā nodaļā ir aprakstīts pētījuma mērķis, un izvirzītie uzdevumi tā sasniegšanai, kā arī pieminētas iztrūstošās zināšanas un nepieciešamie pētījumi. Nodaļā ir izskaidroti pētījuma zinātnisko atziņu pamatmērķi, uzdevumi, pielietojamība un pētījuma unikalitāte.

Izmantotās kvantitatīvās un kvalitatīvās analītiskās metodes un to rīki ir aprakstīti sadaļā par pētījumu metodoloģiju, kā arī detalizētāka eksperimentu plānošana un soļi, kas veikti, lai salīdzinātu un pārbaudītu iegūtos rezultātus. Papildus, lai noskaidrotu paātrinātāju kopienas vajadzības tika veikta aptauja, par kopienas interesi AM tehnoloģiju izmantošanai kā nākotnes potenciālu.

Sekojoši darba fokuss tika virzīts uz RFQ dizaina uzlabošanu un pielāgošanu AM tehnoloģijai. Pētījums ietver ģeometrijas un siltuma pārvaldības modelēšanu, piedāvājot vienkāršotu matemātisko modeli AM RFQ Q faktora aprēķinam dizaina fāzē, kā arī pievērsta uzmanība izaicinājumiem, ar kuriem saskaras AM un tradicionālie ražošanas procesi.

Turpmāk seko eksperimenālā daļa, kurā tiek aprakstīta izmantotā TRUMPF "zaļā" lāzera PBF-LB/M/Cu-OFE 3D printēšanai, un Rösler Italiana Srl. pēcapstrādes metodes: abrazīvā un pēcapstrāde ar papildu ķīmisko katalizatoru pielietošanu, kā arī unikālā MMP TECHNOLOGY®. Ir paskaidrots, kā tika novērtēta AM RFQ prototipa ģeometriskā precizitāte un virsmas raupjuma kvalitātes novērtēšana, kas ietvēra mērījumus, kas veikti, izmantojot koordinātu mērīšanas ierīces, optisko skenēšanu un virsmas raupjuma novērtējumus gan gatavām, gan pēcapstrādātam 1/4 sektora RFQ prototipam.

Rezultātu ticamības novērtēšanai, tika veikta validācija, Savukārt lai novērtētu AM cikla laiku RFQ prototipa ražošanai, tika salīdzināti apstrādes laiki gan AM, gan tradicionālajai RFQ izgatavošanas metodei. Promocijas darbs noslēdzas ar konkrētiemm, praktiskas ievirzes secinājumiem, priekšlikumiem un rekomendācijām turpmākajai AM tehnoloģijas sagatavošanai RFQ izgatavošanai.

Promocijas darbs ietver 117 literatūras avotu sarakstu uz kuriem ir norādes darbā.

ABBREVIATIONS

Abbreviation	Meaning
AM	Additive Manufacturing
AMAZE	Additive Manufacturing Aiming Towards Zero Waste & Efficient
AMCM	Additive Manufacturing Customized Machines & Production of High–Tech Metal Products
ARIES	Accelerator Research and Innovation for European Science and Society
ARIES-CS	Advanced Research Innovation and Evaluation Study-Compact Stellarator
ASTM	American Society for Testing and Materials
BPM	Beam Position Monitoring
CAD	Computer-Aided Design
CAMF	Chemically Assisted Mass Finishing
CATIA	Computer Aided Three–Dimensional Interactive Application
CERN	European Organization for Nuclear Research
CLIC	Compact Linear Collider
CMMI	Civil, Mechanical and Manufacturing Innovation
CORDIS	Community Research and Development Information Service
CMM	Coordinate Measurement Machine
CNC	Computer Numerical Control
DARPA	Defense Advanced Research Projects Agency
DED	Direct Energy Deposition
DESY	Deutsches Elektronen–Synchrotron
DMD	Direct Metal Deposition
DMLS	Direct Metal Laser Sintering
DREAM	Driving up Reliability and Efficiency of Additive Manufacturing
DOE	Department of Energy
EBM	Electron Beam Melting
EDM	Electro Discharge Machining
EDMS	Engineering Data Management Service
ELISA	Experimental LINAC for Surface Analysis
EPSRC	Engineering and Physical Sciences Research Council
ESA	European Space Agency
EuCARD2	European Coordinated Accelerator Research and Development
H2020	Horizon 2020
HEP	High Energy Physics
HF-RFQ	High Frequency Radio Frequency Quadrupole
IACS	International Annealed Copper Standard
I.FAST	Innovation Fostering in Accelerator Science and Technology
IJCLab	Irene Joliot-Curie named Laboratorie in Orsay

ISO	International Standard Organisation
IWS	Institut für Werkstoff und Strahltechnik
JACoW	Joint Accelerator Conferences Website
KEK	Japanese High Energy Accelerator Research Organization
MANUELA	Additive Manufacturing using Metal Pilot Line
MDPI	Multidisciplinary Digital Publishing Institute
MMP	Micro Machining Process
NCSU	North Carolina State University
NSF	National Science Foundation
NIST	National Institute of Standards and Technology
ONR	Office of Naval Research
PA	Particle Accelerator
PAC	Particle Accelerator Conference
PAM^2	Precision Additive Metal Manufacturing
PBF	Powder Bed Fusion
PIXE	Proton–Induced X–ray Emission[1]
PLM	Product Lifecycle Management
RF	Radio Frequency
RFQ	Radio Frequency Quadrupole
RP	Rapid Prototyping
SBIR/STTR	Small Business Innovation Research/Small Business Technology Transfer
SEM	Scanning Electron Microscope
SLAC	Stanford Linear Accelerator Center
SLS	Selective Laser Sintering
STL/ .stl	Stereo Lithography/ .stl file format used for Stereo Lithography
STP/.stp/.step	Standard for the Exchange of Product Data (STEP) format, conforms to the STEP Application Protocols ISO 10303-2xx
TIARA	Test Infrastructure and Accelerator Research Area
TRL	Technology Readiness Level
TQ	Technology Qualification
TUV SUD	Technischer Überwachungsverein SUD
UL	Underwriters Laboratories (US)
UK	The United Kingdom
USA	The United States of America
USPAS	U.S. Particle Accelerator School
3DP	Three Dimensional Printing

GLOSSARY

Symbol	Meaning
A	– total quadrant area of cavity, mm^2
B	– magnetic field in the quadrant, T
c	– the specific heat, $J \cdot K^{-1} \cdot kg^{-1}$
C_ℓ	– shunt capacitance for unit length, F/m
C'	– cavity quadrant shunt capacitance per unit length, F/m
CI	– statistics confidence interval
I	– peak current, A
k	– the coefficient of thermal conductivity
Ku	– statistics kurtuosis value
κ	– coefficient, which covers OFE-Cu 750 Mhz cavities specifics
L	– perimeter of cavity quadrant, mm
ℓ_{V}	– vane(cavity) length, mm
L'	– quadrant shunt inductance, $H \cdot m$
μ_0	–permeability of free space (physical constant), Tm/A
P	– power dissipation, W
P_ℓ	– power per unit of length, W/m
π	– mathematical constant that is the ratio of a circle's circumference to its diameter, approximately equal to 3.1415
r	– circle radius, mm
Ra	– arithmetic mean deviation of roughness profile, μm
Rz	– arithmetic mean deviation of roughness profile, μm
ρ	– the density of the studied solid material, kg/m^3
Q_0	– unloaded cavity quality factor
$Q_{0,2\mathrm{D}}$	– unloaded two dimensional cavity quality factor
$\dot{q}$	– the internal heat generation rate, per unit volume, per unit time, $W/m^3/h$
s	– statistics standard deviation
S	– cavity quadrant area, mm^2
SE	– statistics standard error value
Sk	– statistics skewness value
σ	– electric conductivity, S/m
t	– time, s
T	– the variable temperature for the coordinates x, y, z and time t
x, y, z	– coordinates, mm
$\overline{x}$	– aritmethic mean for x_{i} values
ω_0	– resonant frequency of cavity, Hz
W_0	– stored energy for unit lenght, J/m

CONTENTS

INTRODUCTION

Particle accelerators and their applications

Particle accelerators are sophisticated devices that provide energy to subatomic particles, enabling them to interact with atomic nuclei, generate new particles, produce intense streams of X-rays or neutrons, and deliver their energy with precision to materials or biological cells [2].

In the relatively short period of less than 90 years since their inception, accelerators have become a pivotal tool in the advancement of modern science, accounting for over one-third of all Nobel Prizes in the field of physics. Their impact has extended well beyond basic research into applied science and market applications. Although the most visible accelerators are the large machines employed in particle physics, it is notable that of the more than 30,000 accelerators that currently exist in the world, only less than 1 % operate for the benefit of fundamental research. The vast majority are small accelerators used for healthcare or in industry [2].

A particle accelerator is a device that accelerates electrically charged subatomic particles, such as protons, electrons and ions. The acceleration of charged particles requires the input of energy, which is achieved by applying an electric field. Magnetic fields are deployed to deflect the paths of charged particles, thus offering a means to focus and steer the particle beam, which is essential for the practical application of an accelerator device [3].

Particle accelerators are widely employed in a multitude of sectors, such as medicine and healthcare, security and defence, material science, cultural heritage preservation, manufacturing and industry, nuclear energy and enviromental applications. In the present time, accelerators have been instrumental in the treatment of thousands of cancer patients worldwide. They have also been employed in the production of isotopes for medical imaging and nuclear medicine, the sterilisation of medical paraphernalia and food products, the non-destructive testing of hidden pipes and structures for defects and cracks, and the security of our borders. The aforementioned applications include the cutting and welding of steel beams, the processing of semiconductor chips for computers, the modification of the characteristics of polymers, the location of oil and minerals in the earth, and the determination of the age of ancient artefacts by archaeologists. These applications are described in greater detail by T. Taccetti et.al. [4]. The current annual global sales of these commercial accelerators are estimated to be in the billions of dollars [5].

On 1st May of 2013 **EuCARD²** (Enhanced European Coordination for Accelerator Research & Development) project started with the goal to build upon, consolidate and extend the broad collaboration started by the two Integrating Activities: **CARE** in FP6 and **EuCARD** in FP7, which was co–funded by the European Commission under the FP7 Capacities Programme. The project contributed to positioning European accelerator

infrastructures at the forefront of global research. EuCARD^2 [2] has summarised its key recommendations and some of them were taken as a lighthouse for this research:

Improved designs and cost − effectiveness − the necessity for simpler and lower-cost designs and concepts, with higher efficiency, reliability, robustness, and reduced costs of operation, is evident in many accelerator applications, particularly in the fields of health, industry, and security. Additionally, the ready mobility of accelerator equipment is becoming increasingly important for certain applications.

Improved academia − industry interactions − the advancement of accelerators for "big science" is the primary driver of progress in accelerator R&D on a global scale.

Improved R&D collaboration within EU − a stronger coordination of R&D eforts and collaborations at the EU level would be highly beneficial.

Compact accelerators − the development of more compact accelerator technology is a crucial factor in all applications.

Radio Frequency Quadrupole (RFQ)

In general, accelerators are composed of a multitude of intricate assemblies, sub-assemblies, and discrete components. It is often challenging to ascertain the specific importance of each individual part. Nevertheless, one of the most crucial components of the accelerator assembly is the part responsible for the initial acceleration, focusing and bunching of particles. In many accelerator laboratories, this task is performed by a RFQ. RFQ is a low-velocity, high-current linear accelerator with high capture efficiency, capable of accelerating ion species from protons through to uranium. Ion sources only require relatively low extraction and pre-acceleration voltages to inject the RFQ [2]. The RFQ output energy is well aligned with the input energy demand of linear accelerators, including drift-tube linacs. A considerable number of laboratories have integrated the RFQ as a primary accelerator for injectors in hadron synchrotrons [6]. As previously stated RFQ has a critical role in medical accelerators as they are able to accelerate medically applicable protons and ions. Also the unique efficiency level of RFQ allows for the construction of more compact medical accelerators. Unfortunately, RFQ design is highly complex and has numerous manufacturing challenges due to used **material (oxygen free pure copper), machining accuracy, roughness and assembling accuracy** requirements. However, today are available new technologies which potentially can solve most of the previously mentioned issues, but initially they must be tested and tuned for application in accelerators. In case of success this will significantly reduce the manufacturing time and costs of RFQs and significantly increase accessibility of society to advanced medical treatments.

RFQ manufacturing: engineering challenges versus available technologies

Accelerators constitute a significant component of the field of high–energy physics. It is therefore necessary to consider the specific requirements of this field, which are not common to other industries. These include high and ultra–high vacuum compatibility, as well as good outgassing behaviour. Typically, additive manufacturing (AM) technology represents the next level of manufacturing method, enabling the production of final products with greater efficiency and cost-effectiveness than those manufactured through traditional methods. Currently, AM technology has reached a level of maturity where it can be considered a viable replacement for traditional manufacturing processes. Figure 0.1. illustrates the common requirements for AM applications, as identified by the AM expert at CERN R. Gerard. Currently, most of requirements are technically reachable by combination of fine tuned AM cycle and post-processing adaptation for each specific case. The AM technology is relatively new and promising game changer for many of industries,

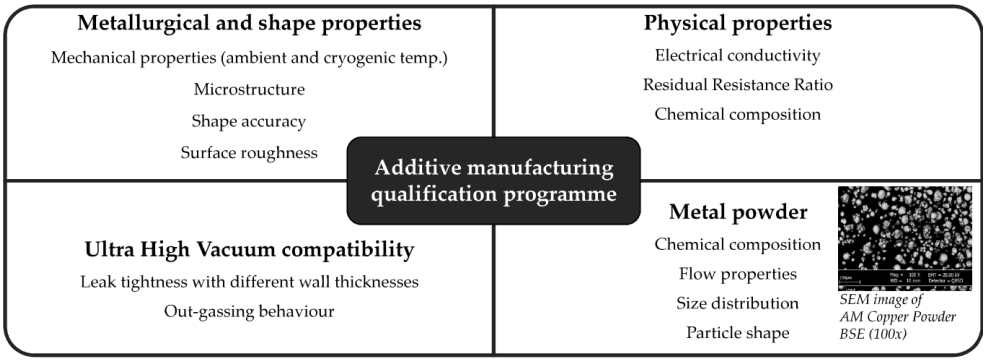

Fig. 0.1. Qualification programme for Additive Manufacturing at CERN [7].

but despite that there are still many opinions on first historical event. Many publishers are giving different cases on the first AM launch. In the opinions of AM Power analytics the metal AM history started in 1983 with the invention of stereolitography by Charles Hull (Fig. 1.2.). However, in other articles authors place the start of AM history even later, for exsample Jemghili et.al. [8], started the history timeline from year 1987.

Most beneficial AM results could be reached by new non-traditional designs for ultimate level of efficiency and performance. AM could also allow manufacturing of spare parts locally, which could give transportation and time savings to business owners and would contribute to a more efficient machine and plant operation. Similarly AM is a technology that can be used for the manufacturing of prototypes and end–use parts. This technology can be used at any stage of the development process of a product [9].

Meanwhile, the automotive, aviation and medical implant industries already use this relatively new technology with good results [10]. However, the standardization process and

implementation of even more precise monitoring techniques to ensure consistent results are continuously evolving. Presently, the consistency and outcome quality repeatability are still challenging for some areas of the industry, where it is problematic to afford the failure of manufactured part, either due to production costs or safety reasons. The strategies that are mainly process parameter control oriented to laser power, scanning speed, and layer thickness; or material science–oriented. In European AM community there are several initiatives and AM developing groups which are focused on new projects to advance in accelerator technology. Among leaders in the field are Fraunhofer IWS(Dresden), PoliMi(Milano), INFN DIAM(Padova) and TRUMPF SE+Co.KG.

1. METAL ADDITIVE MANUFACTURING REWIEV AND STATE OF ART ANALYSIS

It is imperative to acknowledge that metals serve as indispensable resources for advancing economic and industrial development. It is a well-established fact that approximately three-quarters of all known chemical elements are metals. The most prevalent varieties within the Earth's crust are aluminium, iron, calcium, sodium, potassium and magnesium. The majority of metals are found in ores, which are mineral-bearing substances. However, a few metals, including copper, gold, platinum, and silver, frequently occur in the free state due to their low reactivity with other elements [11]. The processing of non-ferrous metals, including aluminium, copper, zinc and ferrous materials, such as steel, is a critical aspect of the European Union's (EU) economy, competitiveness, and industrial development. The European Commission's objective is to ensure that EU legislation allows these sectors to achieve a high level of competitiveness and encourages their participation in meeting the EU's energy efficiency and environmental goals [12].

In order to explore the current state of the art in the field of metal AM and specifically on applications in field of high energy physics, number of public and institutional databases were explored; such as: Google Scholar; JACoW Publishing; ScienceDirect/Elsevier; Springer; MDPI; IEEEXplore; arXiv.org; ResearchGate; indico.cern.ch; CORDIS; etc. For more specific and focused search keywords *metal AM*, *metal 3D printing*, *powder bed fusion*, *solid freeform fabrication*, *accelerator, linear accelerator*, *LINAC*, *radio frequency quadrupole*, *pure copper* were applied. In addition, international patent and intellectual properties search were executed using European Patent Office and World Intelectual Property Organization search engines.

In general, the highest number of scientific articles (25 articles on 2/10/2022) about applications of AM for accelerators are published by JACoW Publishing [13]. It is well known that JACoW (Joint Accelerator Conferences Website) holds status of authority in accelerator community and AM is the technology, which has a good potential for next generation accelerators. Exponential growth of AM application cases are visible during the last decade. Geographical distribution of previous research in the field of accelerators still is more concentrated in the western part of Europe and in the USA. Asian region is most known by Japanese KEK and Chinas BEPC, and activities around these research centers. However, in the Asia region AM activities are appearing to be on the low level and even invisible on the public domain. It has been challenging to identify any joint activities with AM, which probably is due to the novelty of the technology and the limited access to it. Further application of Chinese search engines like Baidu, Sogou, Shenma, Haosou and Youdao did not give any visible results.

The majority of the research results are on technology developments from EU and USA region. Practically the same situation is in Russia, where the most powerful cyrillic search engine, Yandex, also did not produce any tangible results.

1.1. Evolution of the technology

AM already is part of the modern manufacturing curricula, however, it is still a relatively young and continuously developing technology, which progresses in close step with the latest inventions in industry. AM has numerous advantages over conventional manufacturing technologies. The one of the best known advantages of AM technology is its high potential for manufacturing of top-performance and high complexity parts. AM is capable of building parts from various materials such as plastics, metals, alloys, as well as biomaterials and ceramics. Over the last three decades, AM technology has served many sectors of industry such as automotive, aerospace, manufacturing, and medical. Starting from parts manufactured in plastics to metals and bioprinting of organs, the technology is making a progress, which is a breakthrough innovation [14].

Patents and historical outlook. By looking at history, the roots of AM can be recognized in photo sculpturing in 1860s and topography in 1890s [15], which later led to the "Photo-glyph recording" technique (patented in 1951) [16]. Practically at same time as the first photo-glyph recordings, the idea of laminated horseshoes was patented by Peacock in 1899 [17]. Relatively soon after R.Baker was granted the US Patent 1533300 on "Method of Making Decorative Articles" (Fig. 1.1.). Soon after the World War II

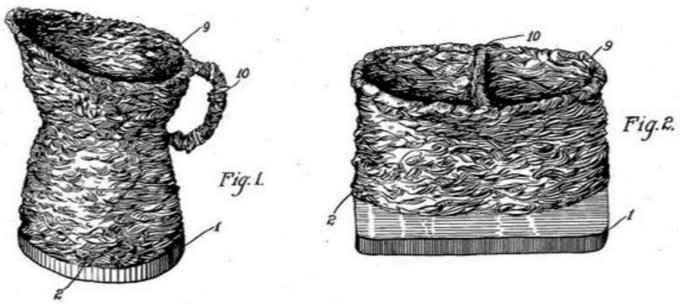

Fig. 1.1. Metal parts produced layer by layer, R.Baker's patent [18].

Kojima demonstrated the benefits of layer manufacturing processes. Several additional patents and demonstrations took place in the period of the 60–80's that further solidified the idea of producing a three-dimensional object using a layer-wide approach and set the stage for the introduction and development of processes based on this principle to produce physical prototypes [19].

History of patents using the terminology *"AM"* as it is today started with Sandia Corp(US) company and its inventors Greene Donald L (US); Griffith Michelle L (US); Harwell Lane D (US); Pressly Gary A (US) with the US patent number US6143378A, titled "Energetic AM process with feed wire" with earliest priority 1998–05–12 and official publication date in 2000–11–07. During the last 20 years, a patent number where are words *"AM"* are used in the patent title has risen to 5'328. Patents with the phrase

"AM" somewhere in textfield has risen to an enormous 39'252. This tendency shows that AM technology is expanding at an incredible speed, especially in last two decades. Nowadays the main players in the AM business are large-size innovative companies and research institutes. Mostly they look for future business perspectives and key technologies, which will be dominating soon. As it is seen from the patent applications, the US company "General Electric" is one of the leaders in number of granted patents on AM technology. Keywords *"Additive manufacturing + copper"* were in titles of 22 patents, but unfortunately none of them were on pure copper processing, what is one of most interesting materials for the accelerator community.

Wohlers Associates. Since the middle of the 1990s, Wohlers Associates prepare annual reports on AM industry trends and the overall impact on whole tendencies of economics. However, the Wohlers reports and the access to them are not for free, most AM community rely on them for business planning and being granted an access to the updated trends in industry. Wohlers Associates is a more than a 35-year-old consulting company, which is based in Washington, DC and Fort Collins, Colorado. The company focuses on the technical and strategic consulting on the new developments and trends in rapid prototyping and AM technologies. The company helps to recognize the opportunities in mergers and acquisitions, provides advice on product positioning and competitive issues, as well as offers expert testimony in litigation.

Metal AM technology is a relatively new and promising game changer for most industries. There are still many opinions on the first historical event. Many publishers are mentioning different cases as the first metal AM launch event. In the opinion of AMPower analytics, the history of metal AM started in 1983 with the invention of stereolithography by Charles Hull (Fig. 1.2.). As usual it is difficult to define exact event as the first one, because of an unclear definition, for exsample Jemghili et al. started metal AM history timeline in 1987 [8].

The compilation of the history of AM technology should be credited to Wohlers Associates, who have been involved with 280 client organisations in 27 countries. The company has advised nearly 200 additional companies in the investment community, including institutional investors and private equity valued at billions of dollars. For 27 consecutive years, the company has published the Wohlers Report, which provides a worldwide review and analysis of AM and 3D printing. This report has been the undisputed industry-leading document on the subject for over two decades. Many participants of the community have graciously referred to it as the "bible" of 3D printing [21], [22]. However, Wohler's Report does not provide the technical details of the AM process itself [23].

1.2. AM technology and recent advances

As this Thesis is generally focused on AM of accelerator components, it is necessary to mention that the most beneficial AM results could be reached by new non-traditional designs for the ultimate level of efficiency and performance. AM allows the manufacture

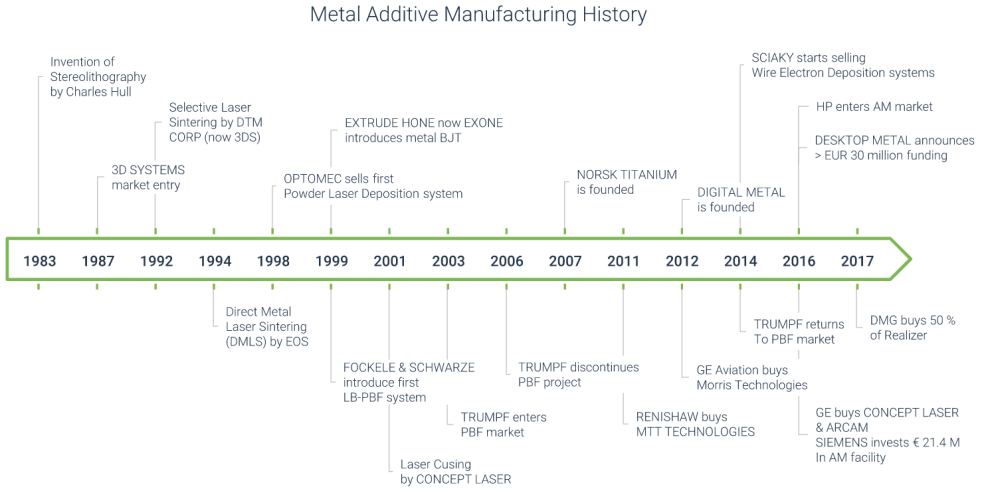

Fig. 1.2. Metal AM history timeline [20].

of spare parts locally, saving transportation and time expenses and contributing to more efficient machine and plant operations. Similarly, AM is a technology that can be used for the manufacturing of prototypes as well as the end-use parts. The advantage of AM technology is flexibility, which can be used at any development stage of a product [9]. The manufacturing capability and classification of the technology is devided in seven groups. Figure 1.3. demonstrates the standardized classification of the International Standard Organization (ISO) [25] and the American Society for Testing and Materials (ASTM) [24]. Both organizations agreed to classify AM technologies according to their functional principle, and in general terms, the technology can be used at any stage of the development process of a product. Other classification methods are assigned according to the working material and shape building technique; the equipment employed here, the physical state of the raw material, and the characteristics of the embodiment. Lastly, AM methods have also been classified according to the physics of material transformation [24]. These methods are often seen in several publications, and the selection criteria are often related to the preferences or the approach of each author.

Technologies. Research outlined further in this Thesis will be exclusively focused on AM techniques used in the manufacture of metal parts, particularly as applied to pure copper. Therefore, only few AM methods and techniques could be considered:

1. Powder bed fusion (PBF), which divides into two subgroups PBF-LB and PBF-EB, for Laser Beam and Electron Beam as power source, respectively;
2. Direct energy deposition (DED), such as direct metal deposition (DMD);
3. Material jetting, such as drop on demand (DOD);
4. Binder jetting (BJ).

The latest industry news for pure copper AM is described in AM community review on

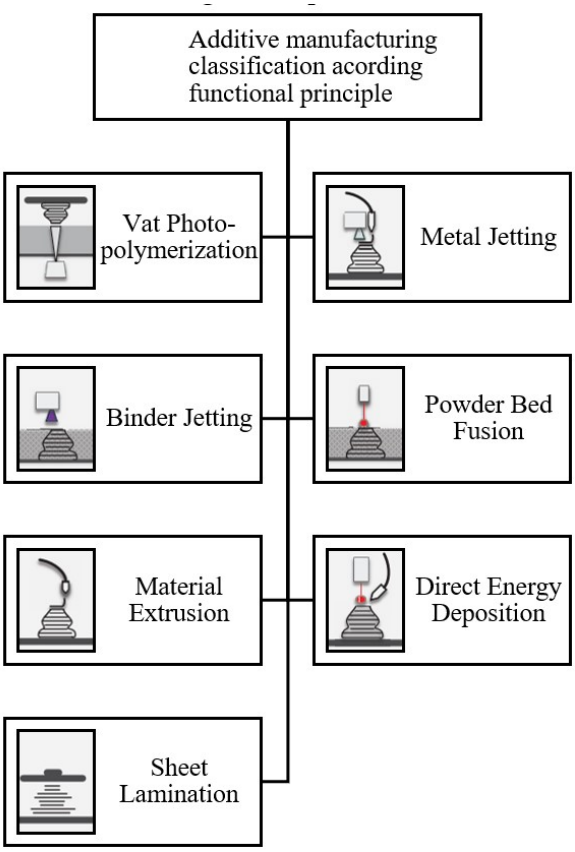

Fig. 1.3. Functional AM classification according to ISO 17296–2:2015 [24].

copper related 3D printing technology guide [27]. In this Thesis only one of the mentioned technologies (powder bed fusion) is an acceptable candidate for further technology development and exploration for accelerator parts as only PBF can provide high resolution printing for complex parts (Fig. 1.4.). The choice of PBF-LB technology is based on such parameters as applicability to pure copper material, build accuracy, material density and build size. Furthermore, PBF is one of the most widely used and well developed among other 3D printing technologies. Several reports, including Wohlers Associates, states that PBF-LB covers up to 80 % from overall metal AM turnover [28].

Furthermore, PBF technology at current status gives a more optimistic view for future developments to reach the specific demands of the field of high energy physics. Meanwhile, industry already uses this relatively new technology in areas where high performance parts are required. However, the standardization process and implementation for more precise and strict monitoring techniques is ongoing to ensure a higher technology reliability. Presently, the outcome quality repeatability is still challenging and does not have full acceptance, especially in industry areas where failure occurring may impact

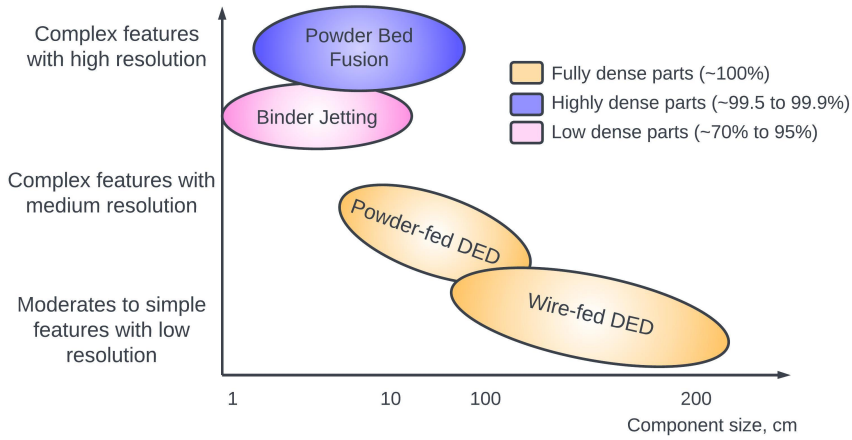

Fig. 1.4. Metal AM features [26].

safety. PBF process is quite complex and the final results are impacted by a large number of parameters, which must be kept in stable narrow band during the whole build process. Researchers of AMAZE project tried to structurize the causes of PBF process defect generation, which are shown in Fig. 1.5..

Additionally, the use of artificial inteligence (AI) methods in the development of highly complex designs must be emphasised as one of the latest advancements in the use of AM technologies. Now pre-trained AI tools are able to develop extremely efficient CAD models, adapted for AM, and providing exceptionally high performance level. In 2022, Aerospike rocket launcher, developed by Hyperganic, received the title of the most complex AM part ever built. Since this case AI tools have become more extensively used in various design developments for improved weight, structural stiffness, heat exchange and thermal distortion topology developments. Similarly, AM machine manufacturers have been racing for hardware developments by scaling AM machine sizes and power, as well as targeting ISO 2768 fine class tolerances for 3D printed parts. In 2024, the PBF-LB/M machine market has several manufacturers, including Farsoon, Eplus3D, Velo and BLT, which offer machines with build volume above 1 m^3. One of the world largest PBF-LB/M machines from Eplus3D EP-M2050, has 36 up to 64 $\times$ 500 W lasers within the build volume of 2050 $\times$ 2050 $\times$ 1000 (2000) mm and theoretical printspeed 1080 cm^3/h [32]. Unfortunately, these machines target for space applications and are not tuned for pure copper part printing.

Conclusions. Research outlined further in this Thesis the challenges of the demanding material, accuracy and surface quality mentioned, the scientific and industrial community is working on solutions to eliminate them. Among the leaders are the H2020 I.FAST WP10 project partners, Fraunhofer IWS (Dresden), PoliMi (Milano), INFN

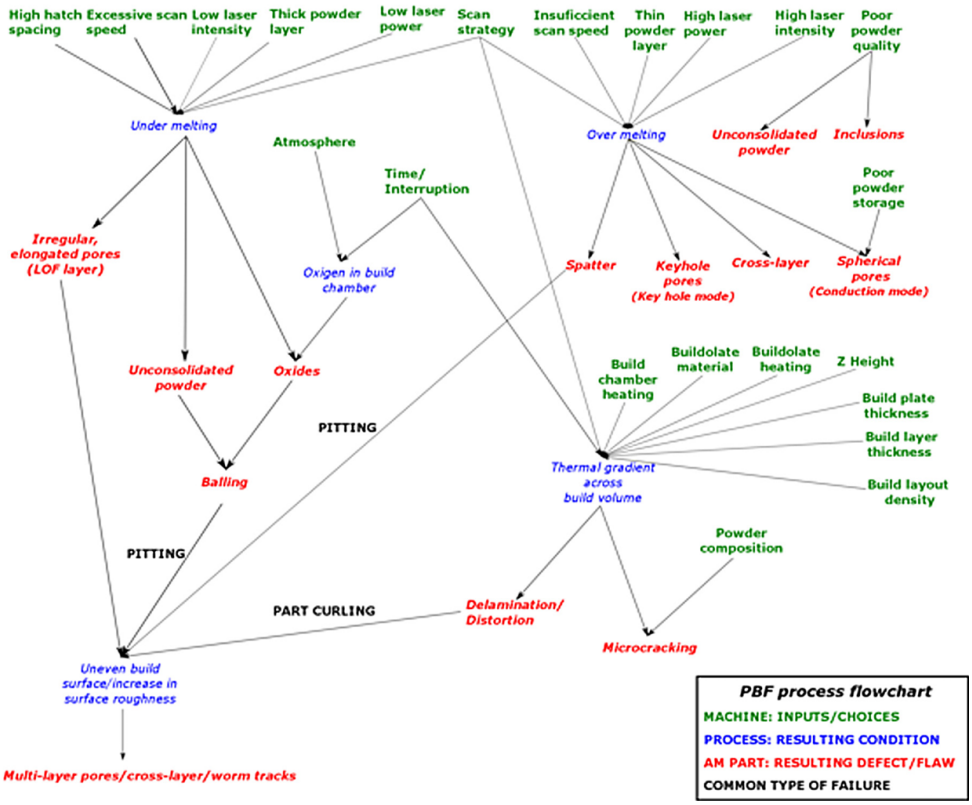

Fig. 1.5. Flowchart showing the complexity of defect generation within the PBF-LB/M process. In the legend, PBF machine inputs (green), processing conditions (red), AM resulting defect/flaws (blue) and common type of failure (black). (Courtesy of H2020 AMAZE EU Project) [29].

DIAM (Padova), TRUMPF SE+Co.KG (holding) and Rösler Italiana Srl., also RTU (Latvia). It is necessary to add that **TRUMPF SE+Co.KG** is a laser source and AM machine manufacturer. The company is famous in the metal industry as the leader in laser processing technology and system development. Although, TRUMPF is not a market leader in AM machine sales, it is one of most experienced manufacturers of laser processing systems. At the FORMNEXT'2018 exibition in Frankfurt, TRUMPF presented the world premiere of green laser application for AM [33]. The "green laser" light has several advantages over traditional infra-red laser light, especially for highly reflective material processing [34]. However, initially the "green laser" technology was developed for pure copper welding applications [35] and later TRUMPF SE+Co.KG. made the effort to develop the technology for PBF machines. One of the main advantages of a 515 nm wavelength laser in Cu processing is the six to ten-fold higher absorptivity for AM powder and flat surface material. Therefore, "green" laser has a significantly higher beam power absorption and process stability [36].

Fig. 1.6. Aerospike rocket launcher engine designed with help of AI based algorithms at Hyperganic and built by AMCM[30], [31].

1.3. Overview of international research projects

Being a so-called Key Enabling Technology (KET), AM advances many application fields and is at the centre of the fast and comprehensive transformation, currently observable in the global economy. In the future it will be crucial that manufacturing and production are not only agile and digitized, but also come with a reduced environmental footprint in processing value chains [37]. In the last decades large number of countries started progressively focus on developments in AM. Moreover, several of countries included AM in their strategic plans for the current and next decades. Among the USA and Asian players, the European Union has strong strategic plans for AM promotion and technology development. Currently in Europe are several funding programs to support new initiatives and developments for economical and environmental growth. Most known are Horizon Europe programs, first review of EU funded AM related projects was published in 2017 by "AM-motion" project deliverable [38]. the project report includes also overview of the EU national initiatives [39].

The emphasis of current research is on metal AM and the subchapter is mainly focussed to the metal AM overwiev and developments : Since CERN is an active participant

in Horizon Europe project calls. Organization is more focusing on projects, which are dedicated to HEP field innovations like accelerator and detector physics, and in most of projects there are workpackages dedicated to innovative manufacturing developments like AM technologies. As good samples are: **H2020 I.FAST** (Innovation Fostering in Accelerator Science and Technology) WP10 (Toms Torims ATS-DO), where whole workpackage is dedicated for promoting of advanced AM solutions for high energy physics community and especially for accelerator components; **H2020 AIDA** (Advanced European Infrastructures for Detectors at Accelerators) WP HM(Horizontal Mechanics) Microchannel cooling for detectors (Paulo Petagna EP-DT).

H2020-EU FP7-2012-NMP-ICT-FoF AMAZE (AM Aiming Towards Zero Waste and Efficient Production of High-Tech Metal Products) Coordinated by The Manufacturing Technology Centre Limited, (UK), overall budget € 18 088 574,46 [40]. The team of project comprises 31 partners: 21 from industry, eight from academia and two from intergovernmental agencies. AMAZE project represented the largest and most ambitious team ever builded on AM topic. Names of consortium participants here are well known in industry as European Space Agency (FR), Concept Laser GmbH (DE), Airbus Defence and Space GmbH (DE), Volvo Technology AB (SE), Renishaw PLC (UK), TRUMPF Laser und Systemtechnik GmbH (DE), Thales Alenia Space France SAS (FR), etc.

H2020-EU.1.3. PAM2 (Precision Additive Metal Manufacturing) Coordinated by Katholieke Universiteit Leuven, EU contribution € 3 896 180,44 [41] Participants from six universities and seven countries. In list of participants and partners here were Danmarks Tekniske Universitet (DK), Universita Degli Studi di Padova (IT), Karlsruher Institut fuer Technologie (DE), Technische Universiteit Delft (NL), The University of Nottingham (UK), LayerWise (B), Alicona Imaging GmbH (A), LEGO System AS (DK), Nuovo Pignone Tecnologie Srl (IT) and partners ASML Netherlands B.V. (NL), Magma Giessereitechnologie GmbH (DE). All of involved participants and partners are high class experts in AM related fields. For introduction MAGMA is one of the world's leading developers and providers of software for casting process simulation and virtual optimization, Alicona is global supplier of optical, industrial metrology for quality assurance of complex components of different shapes, sizes and materials, and their non-contact measuring systems are used in all areas of precision manufacturing. ASML is global manufacturer of complex lithography systems for production of microcrochips, LayerWise currently already is part of 3D Systems, initially grown from KU Leuven and at begining only experts of AM in Benelux countries. Under the project was developed submicron optical measurement system prototype for surface and geometry measurements, written 30 journal papers, 41 conference papers and four chapters for book "Precision Metal Additive Manufacturing" [29].

H2020 DREAM (Driving up Reliability and Efficiency of AM) is research and innovation project, which was aimed to significant improvements of the performance of laser Powder Bed Fusion (PBF) of titanium, aluminum and steel components in terms of speed,

costs, material use and reliability, also using an LCA/LCC approach, whilst producing workpieces with controlled and significantly increased fatigue life, as well with higher strength-to-weight ratios. DREAM targeted the development of a competitive supply chain to increase the productivity of laser-based AM and to bring it a significant step further toward larger-scale industrial manufacturing. To upscale the results and reach an industrial relevant level of productivity, the project was focused on the following four main challenges:

1. Part modeling and topology optimization;
2. Raw material optimization to avoid powder contamination;
3. Process optimization, including innovations of the control software of the AM machine, to enable high throughput production;
4. Setup of laser-PBF of nanostructured Titanium alloys with unchanged granulometric dimension for an additional push to higher productivity, since nanostructured metal powders can be sintered with lower energy input and faster speed.

Additionally, thanks to the three end-users involved, the project is focused on components for prosthetic, automotive and molding applications to optimize the procedure for three different materials, respectively titanium, aluminum and steel [42], [43].

H2020 MANUELA(AM using Metal Pilot Line) is innovation action project. The goal of MANUELA is the development and realization of a metal AM pilot line service covering the full AM cycle including simulation, manufacturing and on-line process control, characterization, real-time feedback, post-treatment, AM qualification protocols and associated business model. Metal AM enables the production of high value-added components not reachable by conventional manufacturing techniques. However, as the AM-based manufacturing sequence implies several critical steps, key competencies implementation at the industrial level is limited. The EU-funded MANUELA project deploys an open-access pilot line facility covering the entire production sequence to demonstrate the full potential of metal AM for industrial production. The project relies on two major AM technologies, laser powder bed fusion (LPBF) and electron beam melting (EBM). MANUELA's task is to perform careful instrumentation and adaptation of PBF and EBM machines to enable increased process reliability and speed and deploy the pilot line – including the adapted processes[42], [44].

H2020-EU.2.1.5.1.-Technologies for Factories of the Future OpenHybrid (Developing a novel hybrid AM approach, which will offer unrivalled flexibility, part quality and productivity), Coordinated by The Manufacturing Technology Centre Limited, (UK), EU contribution € 5 133 381,25 (01/10/2016 – 30/09/2019) The OpenHybrid project aimed for breakthrough thru the technical and commercial barriers of past hybrid manufacturing systems to deliver a single manufacturing system capable of undertaking a wider range of processes in a seamless automated operation. Project comprises

well known and ambitious players, similar like two above mentioned projects. Some of them was Siemens Aktiengesellschaft (DE), GF Machining Solutions AG (CH), Gudel AG (CH), ESI Group (FR), Centro Ricerche FIAT SCPA (IT), European Federation for Welding Joining and Cutting (B). The project in general was focused mainly on direct energy deposition techniques, and as result here was four counference articles and practical development of manufacturing equipment.

Besides EU funded programs, several countries have their own strategies and initiatives to develop AM technologies for further leadership in new fields. Already in 90-ties of past century in UK was established National Centre for AM. NCAM was created for accelerating of uptake of AM by developing the technology and systems required to address the key challenges within the AM value chain. The National Centre for AM is based at the Manufacturing Technology Centre (MTC), which is part of the High Value Manufacturing Catapult.There is also home of The European Space Agency (ESA) AM Benchmarking Centre and a founding partner of the ASTM AM Center of Excellence. IUK project No. 133086 and the EPSRC grants EP/R024111/1 and EP/M013294/1 and by the European Commission grant ErBeStA (No. 800942).

Meanwhile the US is global player in technologies and innovations and have serious plans to keep leadership as long as possible. Already historically US is keeping AM as strategical technology for future developments. In US innovation in AM has been dominated by the private sector, especially when it comes to the total number of patents and the continual advancement of the technology beyond initial invention. Still the government, particularly NSF, has played a role in the early development of the AM field. There are recognized three main supporting sources:

Department of Defense - some of the earliest investors in AM were the Office of Naval Research (ONR) and the Defense Advanced Research Projects Agency (DARPA), which provided steady streams of funding for both academic and industry-based researchers;

National Science Foundation (NSF) has awarded almost 600 grants for AM research and other activities, amounting to more than $200 million (year 2005. value) in funding. Within NSF, the Engineering Directorate (ENG), and within ENG, the Civil, Mechanical and Manufacturing Innovation (CMMI) program and its precursors, have provided more than two-thirds of these AM grants and more than half of NSF's total funding in support of AM. All told, NSF support of AM-related research has been instrumental in several ways.

Other support: The Department of Energy (DOE), NASA, and the National Institute of Standards and Technology (NIST) have also been involved in aspects of developing the AM field. DOE in particular played a role in developing directed energy deposition technologies [15].

As one of the first projects where HEP and AM were joined took place in 2007, then Americas Seed Fund SBIR/STTR startup granted Radiabeam Technologies, LLC

for Novel Fabrication Techniques for the Production of RF Photoinjectors. This was one year grant for development of novel manufacturing technology for accelerator technologies [45].

1.4. Applications within accelerator community

Metal AM currently is almost only of AM subdivisions, which is able to fulfill specific requirements, which are set by high energy physics community. As AM technology is relatively new, it is still developing rapidly, and as it is often for new technologies there time to time appearing innovations, which are giving some acceleration to technology development process. But despite to that accelerator community is still far behind other industries and cases of successful applications within AM are still countable. Current Thesis chapter is limited only to metal AM application cases within the accelerator community to collect most visible applications. The aim of the review is to give new ideas for applications and motivate community for further developments. It is built on publicly available information resources. The first known proposal on application of metal AM in physics field appeared in 2003, then L.Waganer from Boeing Company presented metal deposition proposal for ARIES Compact Stellator coil structure (Fig. 1.7.), [46]. The initial aim was to build cost effective shell for magnet coil winding, which can make structure much cheaper and improve most of parameters in such way decreasing large capital investments. The proposal how to reach this aim was based on DED AM process, which in general is predecessor of welding - cladding technique. During next two years ARIES-CS team developed concept and published results in article [47]. Final calculations showed that cost is less than 1/3 the cost of conventional approach and is only 50 % above the raw material cost.

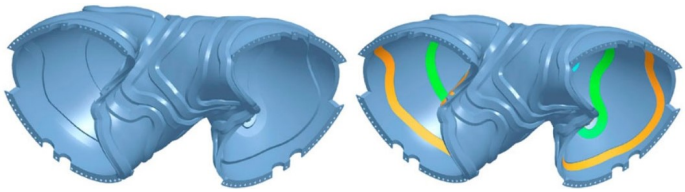

Fig. 1.7. ARIES-CS Stellator coil structure without and with coils in the internal grooves [47].

Soon after ARIES-CS Stellator appearance US SBIR funds started financial grants for metal AM developments in field of accelerators, thereby already in 2006 appeared targeted collaborations among leading accelerator and AM technology developers like SLAC, NCSU, RadiaBeam, UTEP and LLNL. On 6th November of 2006. Ronald B. Agustsson and team from RadiaBeam Technologies LLC filled registration for first patent in AM and accelerator field US2008129203A1, where they claimed method and apparatus how to build RF cavity. In general they claimed accelerator building by layers and further

approach to more complex and advanced shapes of cooling channels. Practically in same year then patent was accepted, P.Frigola presented this idea on EPAC'08 poster session further article in conference proceedings. This became first officially known AM proposal for accelerator devices, which was developed in RadiaBeam/UCLA/INFN collaboration [48]. Initial proposal of 100 Hz photo injector model with integrated cooling channels and improved geometry can be seen in Fig. 1.8. Next year collaboration presented updated version of previous model at PAC'09, they tuned their 100 Hz model to 500 Hz, improved version [49].

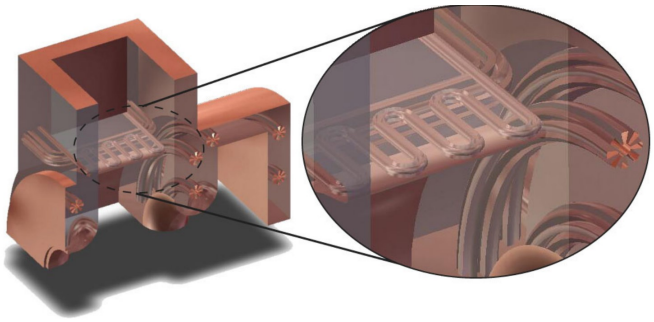

Fig. 1.8. Quarter section of the RF Gun with star-shaped, conformal cooling channels. Detailed image shows the snake-like channels at the coupling window [50].

Couple years later in 2012 at IBIC2012 CERN's scientists reported about ongoing studies on new design concept their of fast beam scanner. The new proposal included application of AM for beam scanning fork, aim was to create more advanced and faster beam scanner. Design concept was based on topology development for wire fork. Weight reduction and stiffness improvement was key factors for design proposal [51]. However model of scanner fork wasn't presented at Tsubukas conference in 2012, first official pictures of model appeared only at IBIC2015, where design analysis and tests was reported. Beam scanner fork design, stiffness and stability calculations were done by Master's student S. Samuelsson under supervision of his Thesis supervisor R. Veness [52].

In 2012 appeared first AM projects at CERN. These activities at CERN are able to track by public documents in CERN's Indico, EDMS and CDS servers. CERN's engineers started to promote first application ideas, and it looks that beam instrumentation group's idea about fast beam scanner is the first official AM project in field of accelerators from CERN. This was also time then several developments started in European accelerator research centers INFN, CRNS, IJCLab. In general looks that year 2012 is the first official start of AM projects at CERN. At that time appeared first contributions, and public documents in CERN's Indico, EDMS and CDS servers. CERN's engineers started to promote first application ideas, and it looks that beam instrumentation group's idea about fast beam scanner is the first official AM project in field of accelerators from CERN. However in 2012 AM was mentioned as potential technology. Year 2012. is time then

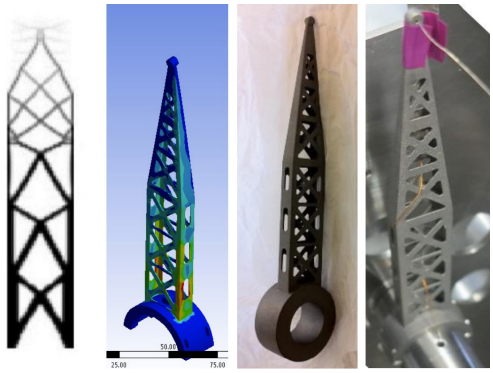

Fig. 1.9. Designed and manufactured fast beam scanning forks [53].

invited lecturers from AM industry started giving lectures on AM topics in dedicated seminars. By analyzing CERN's Indico server seems that first lecturer who started to promote AM for CERN's audience is P.Kilburn from 3T RPD Ltd [54]. However in P.Kilburn's presentation already was presented parts, which are produced for accelerators, these cases was like inspiration for those who didn't know anything about AM. The part, which already was made by AM in that time was spacers for MQXC coils, see Fig. 1.10. In that time AM technology was proposed as an integral part of the next LHC high luminosity upgrade. AM then was used in the development of several magnet types: starting from the LHC standard Nb-Ti till the high field Nb3Sn, and high temperature superconductors HTS. AM parts was targeted to resist Nb3Sn processing reaction at temperature of 650 °C. Metallic end spacers were designed to replace the old fiber glass parts [55].

Fig. 1.10. AM Ti end spacers for MQXC [54].

Practically this was time then number of AM projects in European accelerator community started arising. There is difficult to recognize, which of European accelerator centers

was first, but looks that INFN already on that time participated in AM developments with Radiabeam, as they were in coauthor list [48]–[50], [56].

The 2013 was year then UK AM company Croft Additive joined to STFC CERN BIC based in Sci-Tech Daresbury [57]. The aim of project was to accelerate AM development and engineering knowledge transfer to industry. Croft was interested in CERN's expertise of metal alloys and materials science to improve their competitiveness in rapidly growing metal AM market.

Practically after couple months, in the beginning of next year arrived new proposal from CERN's CLIC experiment, during CLIC14 workshop Alexej Grudiev presented results of additively manufactured Ti6Al4V WR90 wave guide prototype demonstrator, see Fig. 1.11.. There should be mentioned that CLIC RF team is one of first who did most needed tests of AM samples: DC conductivity, RF loss, leak tightness, outgassing, shape accuracy, surface roughness, mechanical strength and material micro structure analysis. For next developments RF group proposed to manufacture samples with integrated cooling for high power tests [58].

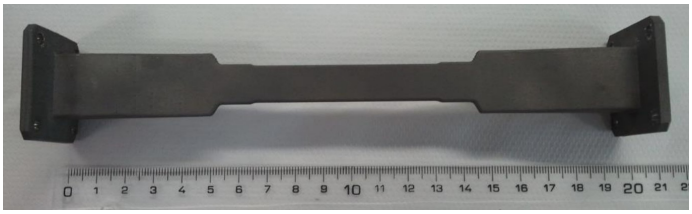

Fig. 1.11. Additively manufactured Ti6Al4V WR90 waveguide prototype [58].

At that time CERN hadn't metal AM machines, and five samples were ordered from three different AM companies. It was like acceptance test to see and compare quality and recognize gray areas of newly arrived technology. In addition two of companies did manufacturing by PBF-LB technology, but one by PBF-EB. CERN's experts did metrology, vacuum and conductivity tests. Final conclusions from first tests were that PBF-LB technology was more successful than PBF-EB. Final conclusions was, that electron beam process need more focused improvements, as second major issue was recognized surface roughness and geometrical accuracy, which became more challenging part for validating of AM technology [58]. Further development for next stage were applied, and already after couple months appeared updated report from M. Colling [59]. In new design was increased wall thickness, added vacuum flanges and water cooling jacket (Fig. 1.12.).

As next development after simplest versions, in IPAC'2018 appeared version of High power conditioning of X-band load with implemented complex shape geometry and tuned cooling configuration [60].

In middle of 2014 joint author team from Radiabeam, NCSU and UTEP published article in Advanced materials & processes journal about their experience on pure copper AM. Article was mainly focused to give reader information about current status of PBF-

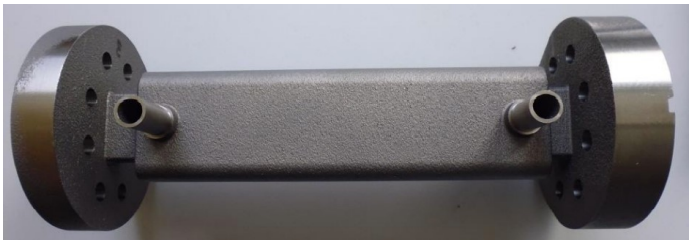

Fig. 1.12. Upgraded version of AM Ti6Al4V X-band load [59].

EB technology, and in same time to show already reached goals. As sample piece there was given case of pure copper cathode for UCLA Pegasus 1.6 cell Photoinjector (Fig. 1.13.).

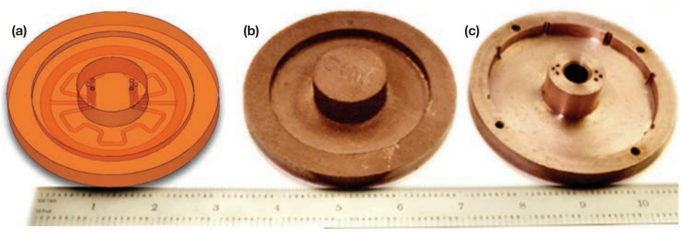

Fig. 1.13. Additively manufactured cathode with internal cooling channels for UCLA Pegasus 1.6 cell Photoinjector: a) 3D model; b) as build part; c) postmachined part [61].

At the 2014 Annual Solid Free Form Manufacturing Symposium in Austin, Texas, C.A. Terrazas, a team from UTEP, and P. Frigola from Radiabeam presented their research on PBF EB for high-purity niobium superconducting applications. The SRF cavity was selected as a case study example. The potential of AM technology as a promising alternative to conventional forming was presented, with particular focus on the achievement of uniform wall thicknesses, enhanced structural rigidity and material purity. However, the study primarily focused on optimising the PBF-EB process parameters [62]. At that time author team didn't mentioned that several months ago patent application has been filled, and in 5th of May in 2015 US9023765B1 patent "Additive manufacturing method for SRF components of various geometries" was published [63]. Soon after receiving of patent RadiaBeam, JLab and UTEP prepared presentation for SRF2015, where they reported their results on PBF-EB application for single cavity, design was based on Fermilab's 3.9 GHz 3rd Harmonic Cavity. Furthermore it was manufactured as completely functioning single SRF cavity, however it still was made from two parts and included additional steps of internal surface machining, polishing and final EB welding (Fig. 1.14.). In 2015, a workshop on advanced manufacturing methods was held at Lockheed Martin, during, which P. Frigola presented the most recent developments achieved by Radiabeam and its partners. [64].

Starting from 2012 AM number of cases and overall interest about technology started

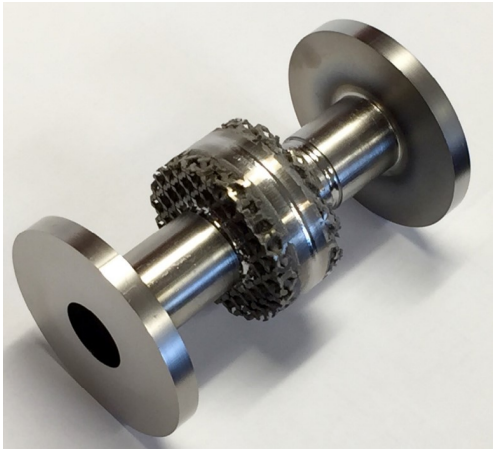

Fig. 1.14. Photograph of the PBF-EB/M/Ni single-cell cavity[65].

to rise more rapidly. Already at that time RF group had their first development of AM RF load, which already has been presented in CLIC14 Workshop by A.Grudiev [58]. Soon under hostage of several more interested and progressive minded groups in November of 2014 at CERN was organized AM Workshop [66]. This was first event at CERN, which was dedicated exclusively to AM topics, there was 115 registered participants, mostly they were from different CERN's groups, others were already in CERN projects involved AM industry and institutional representatives. Workshop was split in two parts, metal and plastic AM.

End of 2015 came with new report from CERN's CLIC's RF group. Bachelor student Gian Luigi D'Alessandro under supervision of experts A.Grudiev and W. Wuensch prepared development of X-band High-Power RF load application study for AM [67]. In general Thesis was focused on spiral load 3D model development, including mathematics and physics phenomena analysis. Technically D'Alessandro's Thesis was preparation of physics model for further real part 3D model and application of AM, spiral load model (Fig. 1.15.).

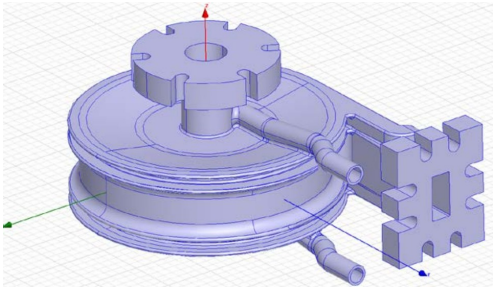

Fig. 1.15. Developed 3D spiral load model for AM 3D model [67].

After preparatory work CERN's RF group did next step toward, and already at CLIC

2017 workshop, team presented additively manufactured X-band spiral load and various tests, which proved concept [68]. However RF groups team already had plans about design improvements group still continuing work on developments and already at IPAC'2018 N. Catalan-Lashera was giving overwiev about high power conditioning for RF loads [60]. when main geometry studies was tuned RF group team arrived with proposal for concept of mass production of RF spiral loads, complete concept was presented in IPAC'2021 by Bursali [69]. Latest model was approved for mass production (Fig. 1.16.).

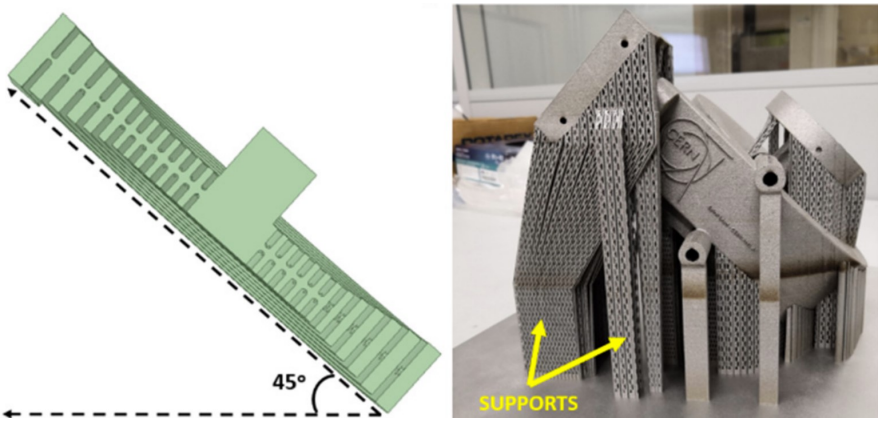

Fig. 1.16. Spiral load model optimal placing on buildplate (left) and spiral load with supports "as-built" (right) [69].

One of most typical applications where AM can prove their advantages over standard manufacturing systems are heat exchangers. AM allows to build highly specific heat exchange structures by heat transfer ratio and shape of structure itself. Already at the beginning of 2015 CERN's LIEBE WP3 team started looking on advantages of AM [70] Finally after several steps of development studies they build lead-bismuth/water heat exchanger (Fig. 1.17.).

Fig. 1.17. AM lead-bismuth eutectic/water heat exchanger for LIEBE experiment [71].

At the beginning of 2017 scientists from french institutions LAL and CNRS/IN2P3 from Orsay joint to race for AM applications at high energy physics field. The first

approach was to prove vacuum tightness of AM technology. They ordered 130 mm long DN40KF tubes to study vacuum tightness of 316L AM products. Manufacturing was done by PBF/LB technology at two different companies: BV Proto and AGS Fusion [72]. In general results of vacuum tests was promising for further investigation and development of AM projects. Then as next step came design proposal for slightly more complex structure – beam pipe monitor (BPM). In classic design BPM consists from several parts with high alignment tolerances. Already at the beginning it was clear that AM could good alternative for tolerances, cost effectiveness and manufacturing speed. The first test results of AM BPM was presented in IPAC2018 [73].

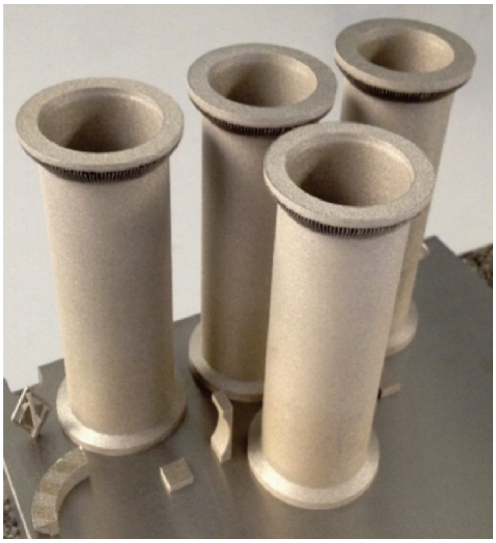

Fig. 1.18. AM DN40KF tubes for vacuum tests [72].

Since CERN started dealing with AM parts, the engineering department (EN-MME) became involved in testing of AM samples more often. Mostly mechanical, geometric accuracy and surface roughness tests were carried out soon after AM. The first registered EDMS report on AM parts is dated by January of 2014, it was made by Santillana [74]. But one of most crucial parameter for AM applicability in high energy field is vacuum tightness and outgassing. For proving AM applicability of different materials and AM proceses from point of vacuum tightness care was on TE-VSC team and L. Mourier. First review of applicability was reported at the end of 2016 [75]. The easiest way to test vacuum tightness and not to fail on expenses of inappropriate quality are manufacturing of ISO KF or CF type membranes for vacuum tests, before manufacturing of more complex and expensive shapes. Typical ISO-KF type membranes (Fig. 1.19.).

One year later in FFC conference J. Gargiulo gave presentation on investigating of the vacuum tightness for AM parts [76]. In summary of presentation has been concluded that stainless steel 316L is helium leak tight with thicknesses from 0.25 mm, but Ti and

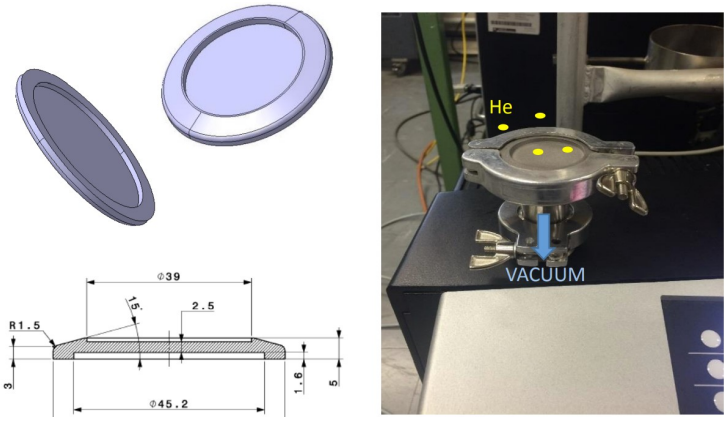

Fig. 1.19. AM ISO-KF type vacuum test membrane 3D model, drawing and test assembly [75].

Al by HIP is helium tight starting from 0.5 mm. However the presenter mentioned that these limits are strongly influenced from manufacturers experience.
As one of relatively simple and often developed pieces for AM technology are various types of beam dumps. Parts have been developed by different institutions and from various materials. In 2018 INFN DIAM developed pure copper beam dump prototype (Fig. 1.20.) with internal cooling channels it has been designed for SPES LNL INFN. Specific design feature is that AM part has been built directly on pure copper substrate plate, which is half of whole structure [77].

Fig. 1.20. AM pure copper beam dump prototype [78].

In 2018 CERN's RADIATE collaboration team introduced new design of AD target, which was named PROTAD Target (PROTotype AD Target). The new design version has several advantages over old one, it has larger core diameter, multi material configuration (Ta, Ir) and expanded graphite as matrix material. In addition new design target has double wall Ti-6Al-4V assembly with an internal spiral channel for pressurized (5 bar –

6 bar) compressed air cooling [79]. Part of new targets was made by PBF-LB technology at the CERN's AM workshop, AM parts in Fig. 1.21.

Fig. 1.21. AM Ti-6Al-4V PROTAD target housings [80].

Since 2014 when the first AM workshop dedicated to HEP was held in CERN, three of the European particle physics centers started to develop applications of AM parts for their core projects. CERN and INFN even managed to open their own AM laboratories. In spring of 2015 T. Sanher from EN-MME team gave presentation in TE-MSC MDT technical seminar, where he mentioned about the plans to have a metal AM machine by the end of year [81]. Technically this was starting point of metal AM workshop at CERN. Administratively it was developed under CERN's EN-MME department and still continue successful work. Practically several months later INFN's DIAM workgroup was created in Padova. It still is multi-disciplinary team including engineers, researchers, technicians, etc. with a background in mechanical design and material sciences [82].

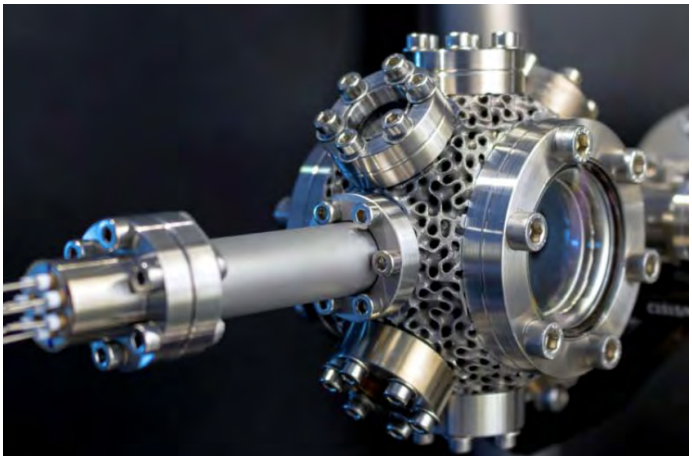

Fig. 1.22. 3D printed UHV chamber [83].

Relatively recent development of an ultra high vacuum chamber build by PBF-LB process was developed in 2018 by young scientists and experts from UK. The production of AM systems for ultra-high vacuum applications has so far proved as highly challenging

and even been considered as impossible. At that time UK team demonstrated the first additively manufactured vacuum chamber operating at a pressure below 10^{-10} mbar. In addition to that they included exclusive design features, which are not available by standard manufacturing. For part rigidity, weight and cooling improvement they implemented gyroid lattice structures (Fig. 1.22.).

1.5. Survey of demands for accelerator and parts development

The purpose of this survey was to assess the size and interest of the accelerator community in the further development of AM technology for High Energy Physics (HEP) and to understand their specific demands. A comprehensive survey was conducted to answer these questions. Despite the low number of active participants, the results of the survey clearly showed that AM technology is an attractive solution for the challenges faced by the accelerator community.

The survey was conducted several weeks before of the 1st Annual I.FAST project meeting with the topic "Accelerator community response to the use of AM in the production and repairs of accelerator components" [84]. The survey consisted of participants from the accelerator community and aimed to gather information on their views and experiences with AM technology. The results of the survey showed that approximately 50 % of the participants had prior experience with AM. The data indicated that all of the participants saw AM as a potential technology for future accelerators, but only 80 % were considering using it for their current applications. The survey also included questions about the use of AM for repairs, with a more pessimistic response. Only 40 % of the participants were considering using AM for repairs, 30 % stated that they may consider using it in the future, and 20 % had a negative response towards using AM for repairs. These results provide valuable insights into the accelerator community's perception of AM technology and its potential applications.

Summary of survey. In general survey clearly confirmed tendencies in accelerator community: it is informed about AM possibilities, but there is still some doubts about performance level and technological possibilities of technology. The community have trust on AM potential for future developments, but the technology is not proved yet for highest technical readiness level. Despite to low number of participants, the results showed that AM is seen as a potential solution for challenges faced by the accelerator community. The results indicated a positive outlook towards the potential use of AM for future accelerators, although a slightly less optimistic response towards its use for repairs. These results provide valuable insights into the accelerator community's perception of AM technology.

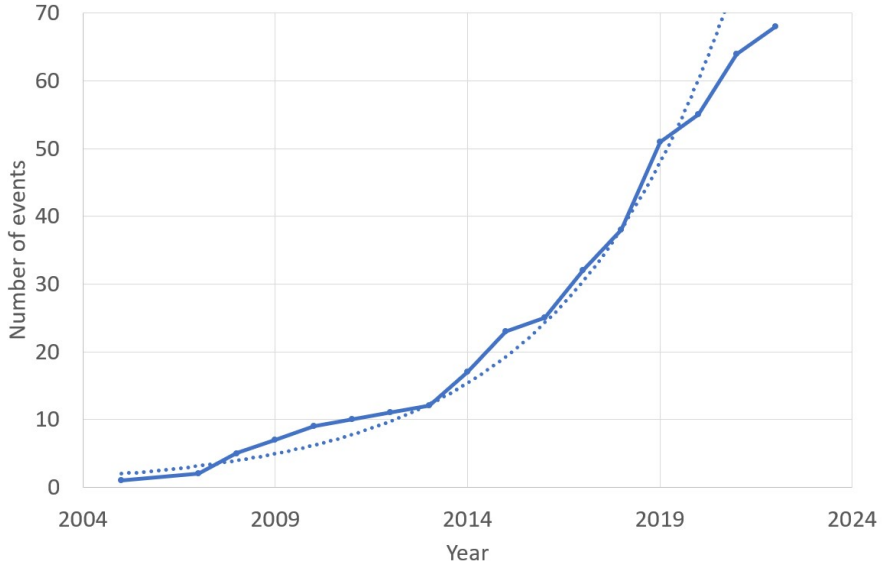

Fig. 1.23. Cumulative number of AM events and significant developments in HEP field [85], [86].

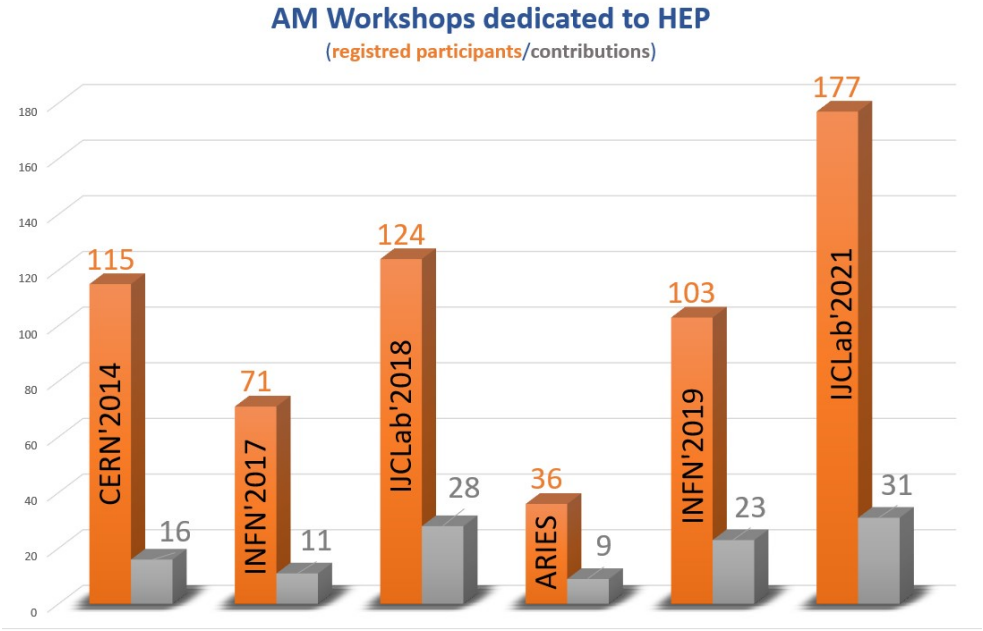

Fig. 1.24. AM Workshops organized by EU accelerator community centers [85], [86].

1.6. Conclusions

During last decades number of metal AM applications for accelerators has been developed and numbers raising pogresively. Unfortunately number of successful and indus-

trialized cases in accelerator field is still minimal. In general the cause of low level AM activities is due to stringent quality requirements for parts as well strongly conservative community. Despite to that majority of AM projects and applications carried in the field already now gives feeling that AM has high potential for nearest future to become a major provider for high performance part manufacturing. The AM has large number of advantages over traditional machining. The most attractive of them are: higher design freedom, improved topology and performance, manufacturing flexibility, level of production automation, minimized number of processing steps and digitization level. During the last 10 years majority of progress oriented countries focus on non-discovered potential of AM and supporting technology development internally. Current reserch will be focused on AM design and manufacturing technology development for 1/4 RFQ sector involving latest 515 nm "green laser" PBF-LB/M/Cu-ETP process, postprocesing and metrology steps.

2. FOCUS AND SCOPE OF RESEARCH

The current research is limited to an examination of metal AM as majority of accelerator components are metallic parts with specific properties like high conductivity, hihg purity and excellent density to be able to provide high or ultrahigh vacuum tightness and outgasing properties. Therefore PBF-LB/M/Cu-ETP process was chosen for technology development. From other side HF-RFQ structure was chosen as object for design improvement and manufacturing technology development. Research is limited to a quarter sector of RFQ development and manufacturing as it including most of manufacturing challenges and later can be scaled to full size body. Quarter sector also allow to access and inspect waveguide area what is inacessible in case of full sector.

2.1. Statement of research gaps and identification of the case study

Modern RFQ's are composed of a great variety of components, necessitating the utilisation of cutting-edge technological solutions. The majority of RFQ components are produced by using conventional high precision machining. Firstly, the conventional machining process necessitates high material removal rates and results in a considerable quantity of material being transferred to chips. Moreover, the standard machining process and technology are highly time-consuming, with machine time and human labour representing a major portion of the final cost. RFQ is manufactured from oxygen-free pure copper (Cu-OFE, C10100), with a purity level exceeding 99.98 %. This presents a significant challenge to the traditional machining process, especially for high precision contouring and surface finishing as high purity copper tends to delaminate at cuuting depths above 11μm, largely due to plastic deformation and stress state of the workpiece material in the subsurface area [87], in overall German Copper Institute classifies Cu-OFE(C10100) as material of machinability group III (Copper-based materials with moderate to poor machining properties) [88].

The majority of the most sophisticated and intricate accelerator components cannot be manufactured from a single piece of material. Instead, they necessitate the utilisation of advanced technological solutions, such as bridges, supports and channels. Consequently, complex components are frequently constrained by unattainable technological challenges. Nevertheless, PBF-LB/M/Cu represents one of the most promising technologies with the potential to realise the ambitious concepts based on new-generation designs.

PBF-LB/M has the potential to become a pivotal technology in the accelerator industry, provided that AM-manufactured parts can attain the pinnacle of quality standards, which are even more arduous to achieve through conventional manufacturing techniques. Nevertheless, AM offers a distinct advantage over traditional methods due to its boundless design potential to create intricate structures that have yet to be attained. One of

the minor challenges in this regard is the lack of trust in new technologies among the accelerator community's decision-makers.

Nevertheless, a considerable proportion of the accelerator community harbours reservations about the potential of AM. The primary reason for this scepticism is the dearth of activities, research, and publications on high-performance, exotic materials and technologies. The current research represents the inaugural official trial to manufacture a realistic RFQ prototype. This will entail tests, analysis, and technology mapping to ensure successful outcomes. However, it is conceivable that some trials may have already been conducted under military or top-secret projects.

The RFQ itself is an RF cavity that contains a vane profile specifically designed to accelerate one type of particle at a given current and for a given energy range (input and output energy) [89].

The RFQ is distinctive in terms of its intricate design and high-precision geometry, representing a pivotal component within the accelerator complex. Furthermore, the cost of the RFQ section represents a considerable proportion of the overall price of the accelerator machine. Additionally, the materials and specifications for the RFQ body are highly specific. A quadrupole represents one of the most expensive and complex components in the assembly process. Moreover, these are relatively new developments for accelerating structures, with a history that is slightly more recent than that of AM technology. Despite this, over the past decades, there has been a notable advancement in the design and size of RFQs [90].

2.2. Overall objective and tasks

The aim of this Thesis is to develop the design and manufacturing technology of RFQ prototype for AM-based technology in order to achieve enhanced performance. To reach the aforementioned objective, the following tasks have been identified:

1. To develop possible RFQ design and performance improvement methodology as well as validation methods.

2. To develop novel RFQ manufacturing methodology and manufacture prototype by using novel technology and encompassing proposed design improvements.

3. To perform the required technological post-processing steps for the RFQ prototype.

4. To perform metrological evaluation of attained geometrical parameters and surface roughness quality – at all technological stages of RFQ prototype production.

5. To evaluate RFQ design/performance improvements by using scientific validation tools – to model RFQ performance, thermal management and geometrical precision.

6. To conduct a quantitative comparison of both: developed and conventional technologies.

7. To identify future research issues and provide practical recommendations for RFQ manufacturing technology advancements.

2.3. Thesis statements to be defended

1. The developed mathematical model for 2-dimensional Q factor calculation for the design stage is applicable for 750 MHz pure copper RFQ cavities and can be scaled.

2. The AM 1/4 RFQ design with balanced smooth transition geometry leads to Q-factor improvement by 2.81 % versus the conventionally designed HF-RFQ.

3. The design of cooling channels, which provides 32 % in average and more than ten times reduced thermal deformation for vane tip region.

4. The used AM and post-processing techniques are capable of providing geometrical tolerances that are practically within the 20 µm on RFQ waveguide profile and modulation region. Furthermore, applied methods are capable of providing surface roughness profile values of Ra = 0.4 µm.

5. The AM method significantly reduces the number of RFQ production operations from 58 to 30 and the production time by 75 %.

2.4. Scientific novelty

Significant contribution to the mechanical engineering and accelerator technology development:

1. An innovative AM RFQ model has been created and validated based on the developed manufacturing method, providing improved performance and heat transmission.

2. An alternative calculation method for Q value based on the RFQ cavity geometry parameters and a coefficient containing the physical properties of the manufacturing material has been developed and validated.

3. The development and validation of an innovative technological process and method for the production of RFQ.

4. For the first time in the world, the production of high purity, complex design and geometric accuracy copper component (RFQ prototype), with AM technology, has been demonstrated and scientifically justified.

5. A comparison of the developed technological process with the traditional manufacturing technology has been carried out, and the advantages of the new technology have been demonstrated.

2.5. Practical significance and applications

The new RFQ design is the first of its kind and represents a significant advancement in particle accelerator and AM-based technology. This is a significant development that will have an impact across a range of fields, particularly in medicine, but also in other areas. The integration of new RFQ designs and AM technologies will undoubtedly boost performance, lower production costs, and push the limits of scientific exploration. The combination of innovative RFQ designs and AM technology is a game-changing development in the creation of particle accelerator components. The developed design and technology, along with the express Q factor calculation model, represent a valuable contribution that can be further developed into more advanced designs. It will lead to improved cost and time efficiency, as well as broader applications across science, medicine, and industry. The ongoing evolution of novel manufacturing technology, coupled with its integration into RFQ design, will undoubtedly drive remarkable advancements, expanding the horizons of particle accelerator technology in general. The main contribution is to compact accelerators. There is no doubt that more compact accelerator technology is a key factor for all applications. The development of superconducting components in the medium term is crucial. As stated in EuCARD^2, improved designs and cost-effectiveness are needed. To increase application area of accelertaors We must have simpler and lower-cost designs and concepts. Higher efficiency, reliability, robustness, and reduced costs of operation are needed in many accelerator applications, particularly in health, industry, and security. The ready mobility of accelerator equipment is also a growing need for some applications. This is the first advanced design development based on monobody multiphysics analysis and is adapted and tuned for novel AM technology. It will lead to improvement RFQ efficiency.

3. RESEARCH METHODOLOGY

The research on potential RFQ design development by metal AM application is based on in-depth scrutiny research in accelerator and AM field. Literature and state of art analysis implies, by using mixed structure by time and project topic. This includes comprehensive analysis of several type of resources: literature, data bases, conference proceedings, standards, patents and EU co-financed projects as well as prior publicly known studies of AM applications within accelerator community, in general most of design improvement research is based on comparative study basis; by using quantitative and qualitative analysis tools.

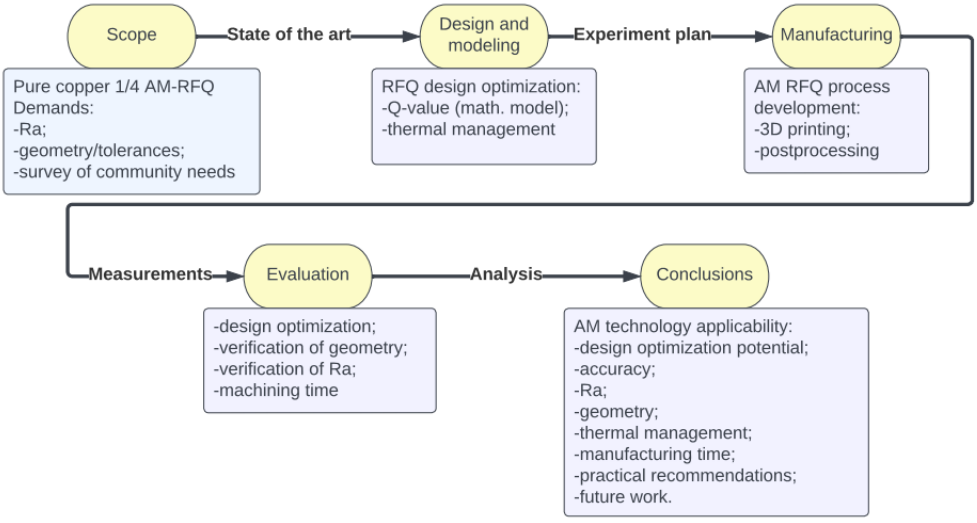

Fig. 3.1. General research plan and used methods.

As the **first step** for the research is to pre-identify feasibility to build RFQ by AM technology. This step includes checking of specific technical limits of proposed manufacturing steps. As well to recognize potential advantages and improvements in the performance of RFQ, and level of efforts applied in manufacturing cycle, to be able reach acceptable level of geometrical accuracy and surface roughness parameters.

The **second step** is conducting of literature review as it is important to explore and study the existing research activities and developments on AM field within accelerators, therefore to gain knowledge improvement in current state of art, and identify research gaps and potential problematics. The review were conducted through specific detailed searches in online databases, such as Google Scholar, Scopus, Web of Science, IEEE Xplore Digital, and by AI search tool application.

The **third step** is development of research plan, which is based on literature review and state of art analysis, by defining procedures and methods that will be used. One of

goals of this step is to define the data that will be collected during further research steps

The designing step is starting from the previous conventional design adaptation to AM technology by using CATIA, ANSYS Mechanical, Poisson/SUPERFISH software. The step includes development of major internal structure changes for cooling channels as well as minor cavity shape improvements. Besides structural changes the step helps to simulate and develop thermal performance behavior and validate obtained results by Ansys and Poisson/SUPERFISH simulations.

Further the prototype build, postprocessing and metrology tests and validation were planned. The manufacturing includes machining data capturing during build process as much as it is allowed by machine manufacturer. Sequentially after manufacturing first metrological tests were planned to understand accuracy as well surface quality for "as-built" part. Further postprocessing and second metrology tests are planned, to find performance and limits of dedicated post-treatment technology.

The final and last step of research methodology is analysis and interpretation of obtained results, including final validation.

3.1. Quantitative analysis methods and tools

Quantitative tools used in reserch are Poisson/SUPERFISH (LANL) codes [91] utilized to validate cavity geometry; CAD software Catia V5R27 was used for part design-redesign stage, as well as to find 2D cavity geometry coordinates for application in Poisson/SUPERFISH codes, in CATIA mostly used workbenches were part design, generative shape design, rapid prototyping and digital shape editor workbenches); Ansys'2019 (steady state thermal, Static Structural and Fluent workbenches) was used in design validation as well as in designing process, and finally ZEISS GOM Inspect'2018 and 2022 version metrology software were used in final stages for metrology data analysis. At several research stages concepts were validated by Autodesk Fusion 360, NetFabb Premium 2023, eDrawings'2021 x64, student version software to prove major visual details of models.

For initial visual evaluation several rapid prototyping PLA material samples were manufactured by using Ultimaker2^{+}Extended and BambuLab X1E 3D FDM printing machines and Ultimaker Cura 4.13.1. version as well Bambu Studio open source software for G-code generation.

3.2. Qualitative analysis methods and tools

Qualitative tools: comparative analysis and simulations were used for result interpretation and validation of results. To accelerator community targeted survey was carried out to better understand needs of the community.

Design, inspection and publicly available information research tools and methods were used to ensure detailed level of research. List of sources used: CERN EDMS; CERN

PLM SmarTeam; INDICO (CERN); INDICO (INFN); INDICO (IN2P3/CNRS); JACoW Publishing; ResearchGate; Espacenet; Google Scholar; Autodesk Netfabb Premium 2023; etc.

Result validation tools: Results at different development stages of prototype were obtained by various tools. At initial stage concept design validation carried out by Poisson/SUPERFISH codes to check quality parameters of RFQ, then ANSYS Static Structural and Steady State Thermal workbenches were used for validation and designing of internal cooling channels. Catia V5R27 /Mechanical Design/Part Design, Shape/Generative Shape Design, Shape/Digitized Shape Editor, Shape/Sketch Tracer and /Machining/Rapid Prototyping workbenches were utilized during whole design workflow.

Build prototype optical scan comparison to model and surface geometry validation on ZEISS GOM Inspect'2018 and Polyworks MS2020 software.

For HF-RFQ geometry development, evaluation and calculations Poisson/SUPERFISH (LANL) codes were used. Further CAD models were developed, inspected, .stl file (mesh) preparation on CatiaV5R27 (Dassault Systems) enviroment. During CAD model development ANSYS'2019 Steady State Thermal, Static Structural and CFD workbenches used to evaluate cooling channel design and static structural behavior. Model slicing and preparation for build job on Truprint1000 machine carried out on Materialise Magics [92] software.

Manufacturing process were executed on TRUMPF TruPrint1000 Green Edition machine in combination with a green TruDisk1020 laser, providing the wavelength of 515 nm and maximum laser power of 500 W. The build experiment was carried out at Fraunhofer IWS in Dresden. Dedicated machine allows cylindrical build volume of 100 mm in diameter and 97 mm in height. The original TRUMPF pre-set pure copper processing parameters and laser scanning algorithms were used throughout whole build experiment by simultaneous automatic monitoring during manufacturing process.

The initial surface roughness profiles were measured at Fraunhofer IWS by perthometer Surfcom Touch 50, which is a contact profilometer from Accretech (Japan). Similarly the first "as-built" part optical scan was also performed in Fraunhofer's IWS metrology lab. After cross check was done at CERN EN-MME metrology lab on Creaform MetraSCAN BLACK™ – Elite scanner with 0.025 mm measurement accuracy and volumetric precision of 0.064 mm at 9.1 m^3 [93], the software Polyworks MS2020 applied for optical scan inspection at lab. Further more detailed alignment and analysis carried out independently on ZEISS GOM 2018 software.

Several Series of measurements on ZEISS Prismo Ultra 12-18-10, which is Bridge-type CMM with a moveable bridge were executed in CERN's MME metrology laboratory. ZEISS Prismo Ultra 12-18-10 which can provide readings up to 1µm precision [94].

3.3. Design of experiments

AM technology workflow in general similarly like most of technologies is a multi-step process. Samples of detailed process-planning for metal AM technologies are described by several authors such as Dotcheva [95], is shown in see Fig. 3.2. . The main activities, there is in association within the model, and the whole AM workflow. The model has three main areas which obviously is one of more simplest ways how to structure higher complexity AM projects.

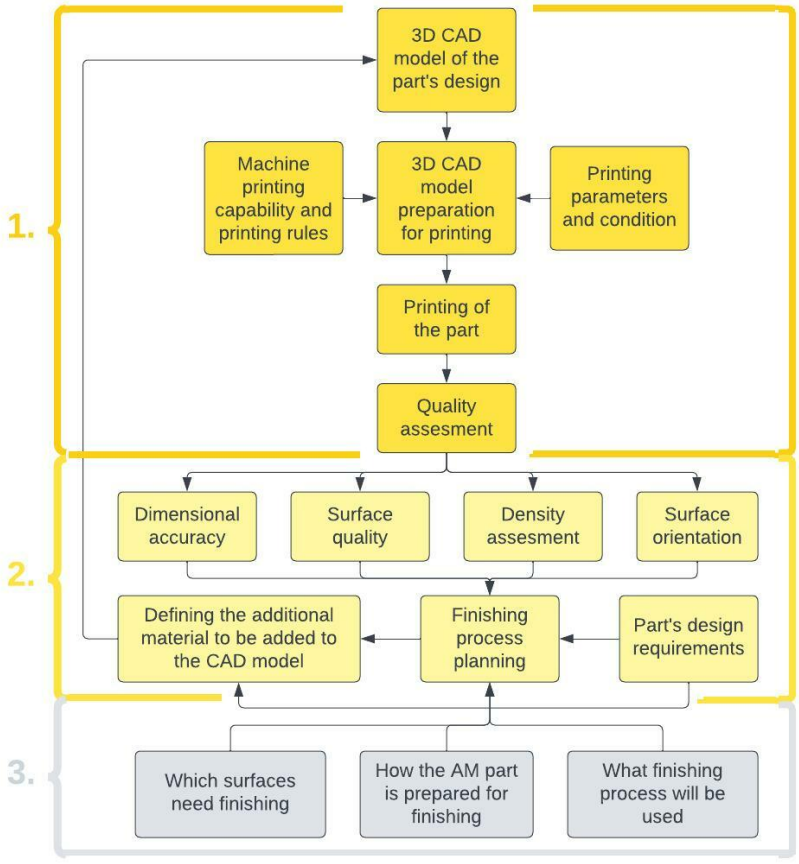

Fig. 3.2. Metal AM process planing model [95].

The first area of the diagram in Fig. 3.2. represents the traditional approach of AM parts fabrication that is still used in most industries. Often the parts quality of more demanding applications are not adequate to the design requirements. It is because of impossibility to predict in advance, or even theoretically estimate, the exact influence of each of the above listed factors on the part quality, and subsequently apply corrections to

the model geometry. Therefore, test parts or the actual parts, whichever is more efficient, need to be printed, their properties measured (Fig. 3.2., area 2), the quality analysed, and corrections applied back to the 3D model (Fig. 3.2., area 3)

3.4. Validation of results

The validation of research results is primarily based on a comparative and statistical analysis of authentic conventionally manufactured and additively manufactured HF-RFQ critical data values. For conventionally manufactured RFQs, the values were retrieved from CERN's EDMS and PLM systems. Furthermore, the presentations of results at scientific conferences and articles in which the manufacturing accuracy and precision of additive manufactured prototype samples were presented were also taken into consideration. At the outset of the AM prototype design process, Poisson/SUPERFISH codes were employed to validate the geometric shape of the cavity. Subsequently, Ansys19.0 Mechanical Steady State Thermal and Static Structural were utilised to validate the thermal performance and its impact on structural stability, which is a critical factor for the stable operation of the accelerator.

4. CONVENTIONAL RFQ AND MANUFACTURING TECHNOLOGY

4.1. Conventional manufacturing basics

Conventionally the pure copper RFQ's are manufactured by multistep machining and brazing technology. Several literature sources referencing on complex multistep manufacturing technologies for linear accelerators [5]. Eleven step manufacturing technology of pure copper PIXE-RFQ was introduced at CERN more than 10 years ago by S. Mathot, however the technology is developing accordingly to the latest advances in machining, brazing technologies and accumulated experience. The last published version were presented and updated by development team in 2018 [96].

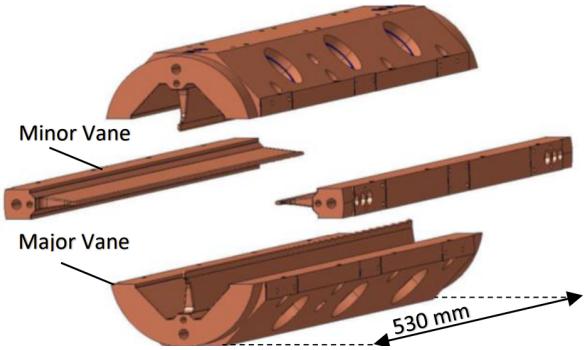

Fig. 4.1. Exploded view of PIXE-RFQ module assembly, two major vanes and two minor vanes [97].

4.2. Challenges of conventional manufacturing process

The eleven steps of RFQ fabrication includes complete technology, starting from solid pure copper block machining to already tuned and ready for beam RFQ. The first step of conventional technology is machining of forged, multi-way hammered Cu-OFE ingot. The first processing step includes rough milling to several cm allowance in length and one millimeter positive offset for all other external surfaces and finally wire EDM cutting for length allowing several centimeters. The next (second) step starts with pre-rough machining, cooling holes drilling and first thermal treatment at 600 °C.

Indeed, the conventional manufacturing procedure is more intricate and time-consuming than additive manufacturing (AM) technology. It encompasses 11 principal steps and 58 sub-steps in total, as documented in reference [96]. Furthermore, it is not uncommon for sub-steps to encompass a multitude of tasks, encompassing diverse processing techniques.

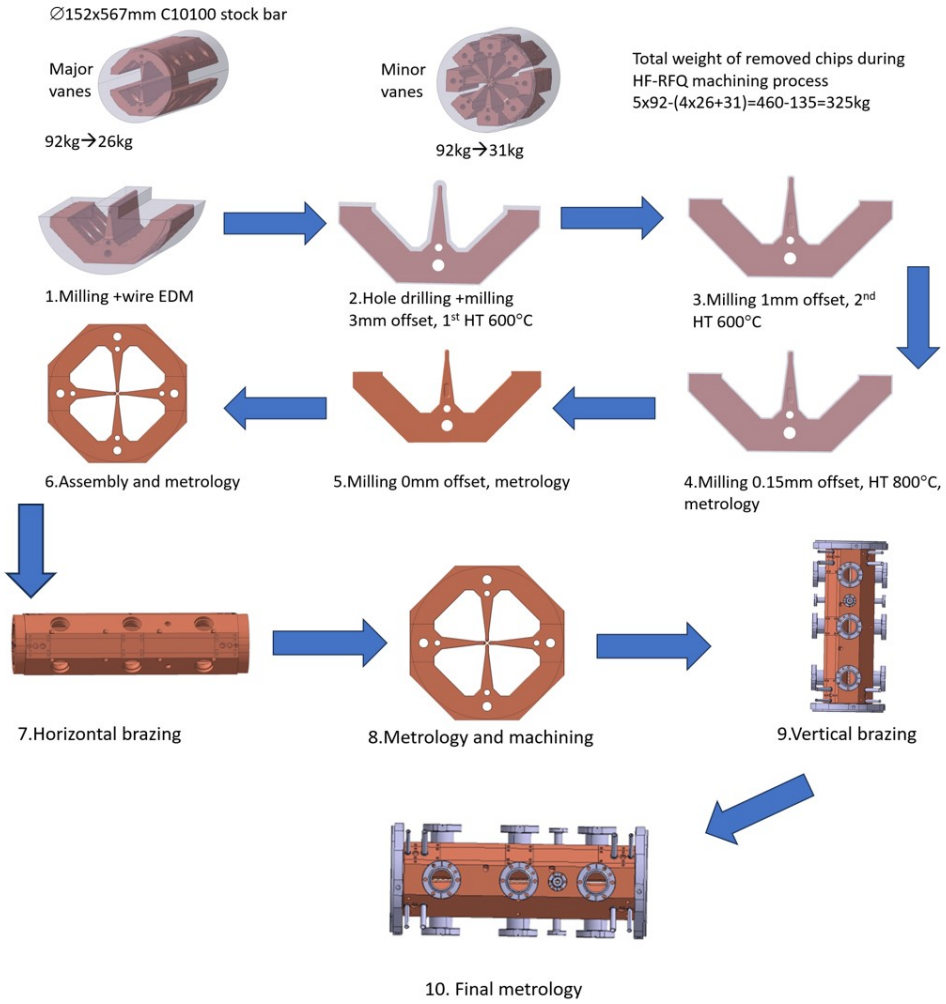

Fig. 4.2. The major steps in conventional manufacturing technology of RFQ.

The comprehensive machining cycle for the two-module PIXE RFQ for ELISA project spanned 16 months, as documented in reference [98]. The extensive machining time can be attributed to the multitude of cleaning, metrology, and stress relief treatments that are conducted between major manufacturing stages.

Table 4.1.

PIXE-RFQ Manufacturing Procedure (rev.1.-July 12, 2017.)[96]

№	Manufacturing steps and substeps
1.	**Machining of the raw material – Copper rods**
	1.1. $L = L_{\mathrm{f}}$ + several cm

1.2 Over thickness: 1 mm on all external surfaces

1.3. Wire cut of the rod

---

2. Pre-rough machining: Over thickness >3mm on all internal surfaces

2.1. Vane length unchanged, $L = L_f$+ several cm

2.2. Pre-rough machining

2.3. Drilling of the cooling channels

2.4. Degreasing and 1st heat treatment (600°C)

---

3. Rough machining: Overthickness 1mm on all surfaces

3.1. Vane lenght adjustment: $L = L_f + 2$ mm(1 mm per side)

3.2. Rough machining of the internal and external surfaces, pumping and RF ports, input and output coupling cells: over thickness 1 mm

3.3. Rough machining of the modulation profile, with a cylindrical cutter

3.4. Rough machining of the reference surfaces for metrology

3.5. Degreasing and 2nd heat treatment (600 °C)

---

4. Pre-finishing: over thickness of 0.15mm for the modulation profiles and brazing surfaces

4.1. Machining of the inlet and outlet sides. $L = L_f + 1.5$ mm (0.75 mm per side)

4.2. Finishing for the external and internal surfaces, opening for pumping and RF ports

4.3. Finishing of the 7 °slopes

4.4. Finishing of the metrology reference surfaces

4.5. Finishing for the water plugs

4.6. Finishing of the brazing grooves but with a depth of 1.3 mm

4.7. Pre-finishing of the input and output coupling cells, over thickness 0.15 mm

4.8. Pre-finishing for the CF40/CF16 flange boring holes and water tubes, over thickness 0.5 mm

4.9. Pre-finishing for the brazing surfaces, over thickness 0.15 mm

4.10. Prefinishing for the modulation profile using a shaped tool, over thickness 0.15 mm

4.11. Pre-finishing of the straight part of the modulation (z > – 8), over thickness 0.15 mm

4.12. Degreasing and 3rd heat treatment (800 °C)

4.13. 1st three dimensional vane metrology

---

5. Finishing: except input and output faces and bore holes for the flanges

5.1. For all vanes, machining on a same plane, the three reference surfaces at the back side

5.2. The vane length is NOT machined now. $L = L_f + 1.5$ mm (0.75 mm per side)

5.3. Finishing of the major vanes

5.4. Metrology of the major vanes, measure of the optimum beam axis, measure of the references point on the internal and external surfaces

5.5. Finishing of the modulation and coupling cells for the minor vanes

5.6. Metrology of the minor vanes, measure of the optimum beam axis

5.7. Finishing for the brazing surfaces for the minor vanes

---

6. Assembly before first brazing

6.1. Four vanes assembly using the external reference points, blocking in position

6.2. Machining of common side reference surfaces

6.3. Machining of the input and output sides. $L = L_f + 1$ mm (0.5 mm per side)

6.4. Metrology of the vane positions

6.5. Vanes disassembly and chemical etching

---

7. First brazing

7.1. First brazing in horizontal position

7.2. Vanes and water plugs brazing

---

8. Machining after first brazing (alcohol lubrication)

8.1. First metrology of the module

8.2. Machining of the input and output faces. $L = L_f + 0.7$ mm (0.35 mm per side)

8.3. Finishing for the CF40/CF16 flange and water tubes boring holes

8.4. Finishing for the diameters and depths for the input and output flanges (CF150)

8.5. Machining of the flanges

8.6. Surface treatment of the flanges

---

9. Second brazing

9.1. Degreasing with alcohol and acetone, heat treatment at 700 °C

9.2. Brazing in vertical position for the flanges and cooling pipes

9.3. Vacuum test

9.4. Second metrology of the module, determination of the over thickness on the inlet and outlet faces, optimum module beam axis

and external reference surfaces for final machining of the inlet and outlet flanges

10. Final finishing

10.1. Machining with alcohol lubrication and dust protections

10.2. Finishing of the inlet and outlet sides. $L = L_f$

10.3. Machining of the CF150 flange contact surface over thickness for the 0.1 mm gap diameter for the centering ring groove for rotation pin and flange flat surfaces

10.4. 3rd and final module metrology

10.5. RF measure of the module

11. RFQ assembly

11.1. Machining of the centering rings and pins

11.2. Assembly also with coupling flanges

11.3. Vacuum test

11.4. RF measure of the RFQ

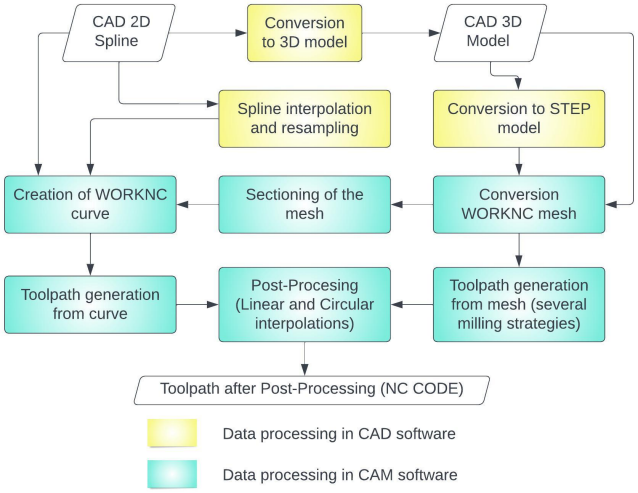

Fig. 4.3. Flow chart of the CAM workflows to produce milling toolpaths [99].

In addition this multistep and complex conventional technology needs NC code development for correct compensation of machining tool radius, shape and wise machining strategy, which in basics are described by developers of PIXE-RFQ machining code and strategy development for cutting toolpath is described by CERN's MME machining experts, see Fig. 4.3. [99].

As RFQ's are relatively new devices, and accelerating structures still are not mass production, number of registered patents is still low. Currently while accelerator community

looks on AM with suspicions there isn't any patent, which involved AM techniques for RFQ's. However few convention manufacturing design and technology patents are available. One of most comprehensive and well described patent is CERN's WO2016023597A1, which was published in February of 2016. It describes complete RFQ technology and especially high frequency RFQ design [100].

Table 4.2.

Potential LINAC Manufacturing Imperfections[5]

Manufacturing Imperfection	**Impact on Linac Operation or Quality of Manufacturing**
Visible machining marks or scratches on the linac inner surface	Increase in arcing → Less efficient linac
Contaminated machining coolant or lubricant	Impurities embedded inside the copper surface → Increase in outgasing time Increase in RF conditioning time Increase in arcing
Imperfect alignment of cavities	Less efficient linac Lower output dose-rate
Excess brazing material inside the linac	Possible effects: Increase in outgasing time Increase in RF conditioning time Increase in arcing Difficulty in tuning and possible shift in the linac's operating frequency Increase in linac's wall loss → Less efficient linac
Having pockets of trapped gas (virtual leak)	Increase in outgasing time
Error in tuning a cavity or more	Shift in the linac operating frequency Less efficient linac
Misaligned electron gun	Less efficient linac Lower output dose-rate
Excessive heat in welding	Change in frequency of adjacent cavities
Incomplete thermal outgasing	Increase in RF conditioning time Increase in arcing
Incomplete gun activation	Unstable beam output
Incomplete RF conditioning	Increase in arcing Missed pulses in beam output

5. NOVEL DESIGN OF RFQ ENABLED BY ADDITIVE MANUFACTURING ADVANTAGES

AM represents a profound transformation in the foundational principles of manufacturing. Moreover, AM enables the creation of design solutions that are not only implausible but also astonishing when considered within the context of conventional technologies. Furthermore, complex and high-performance-focused design parts manufactured by additive technology are less expensive than the same-level performance parts manufactured by conventional methods. AM is a completely different manufacturing method that enables a higher level of design freedom and high-level manufacturing process control and automation, thereby eliminating the impact of human errors during the manufacturing process.

5.1. Mathematical model for AM RFQ Q factor

From a technical standpoint, the development and validation of structures in the majority of RFQ design cases commences with the input parameters for the general design, including the type of accelerating structure, the intended application field, and the utilized materials. Subsequently, the most effective structure, which is tailored to specific performance, is devised through the shaping of its development. However, the methodology employed in the present study differs from that described above. The initial source for the design was CERN's developed HF-RFQ, which has already been proven and accepted by field experts as well as patented [100]. Minor alterations to the shape of the cavity were implemented with the objective of enhancing the static quality value through the exploitation of AM advantages. Nevertheless, the most substantial gains were achieved in the internal structures. The preliminary design of the AM prototype commenced with CERN's HF RFQ, which represents a relatively recent advancement within the field of accelerators. HF-RFQ was introduced to the accelerator community at the conclusion of 2016. The HF-RFQ project was developed over a period of approximately two years [6].

It is widely acknowledged within the accelerator community that LANL has made a substantial contribution to the field of RF devices, pioneering numerous developments in this area. In the 1980s, the Los Alamos Accelerator Theory and Simulation Group (AT-6) maintained and distributed a standard version of the Poisson-Group codes (LATTICE, AUTOMESH, TEKPLOT, POISSON, PANDIRA, MIRT, FORCE, SUPERFISH, and SF01). In general, these codes are the result of decades of development guided by R. F. Holsinger and K. Halbach. The primary applications of these codes are in the design of electromagnets (POISSON and PANDIRA) and radio frequency cavities (SUPERFISH). Additionally, the codes are applicable to other fields, including electrostatics, heat transport, and the identification of mathematical surfaces of minimum area. With

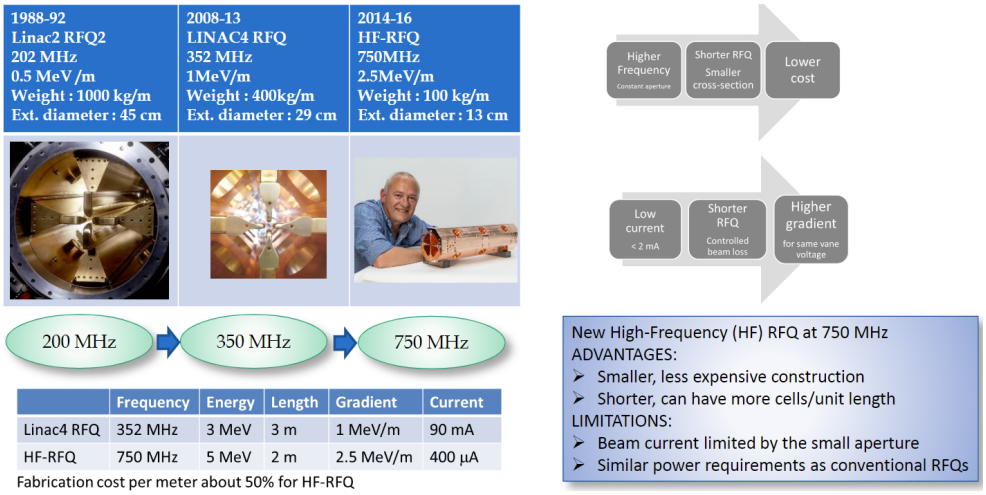

	Frequency	Energy	Length	Gradient	Current
Linac4 RFQ	352 MHz	3 MeV	3 m	1 MeV/m	90 mA
HF-RFQ	750 MHz	5 MeV	2 m	2.5 MeV/m	400 μA

Fabrication cost per meter about 50% for HF-RFQ

Fig. 5.1. RFQ development history at CERN [89].

the provision of special financial support from the Department of Energy's High Energy Physics (DOE-HEP) programme, the codes were revised and corrected to the standard version and a comprehensive manual was written, containing numerous examples and a summary of the underlying theory. In his paper, Warren [101] illustrates some of the capabilities of the codes and provides a summary of the code user manual. The updated codes are currently available upon request via the LANL webpage. Many RF system developers continue to utilise these codes, which are accessible via the LANL homepage upon registration and free of charge [102].

The Poisson/SUPERFISH group of codes were developed by R. Holsinger and K. Halbach for the Los Alamos National Laboratory with the purpose of providing field solutions in two dimensions. The Poisson and Pandira programs employ a conformal triangular mesh to determine the presence and distribution of electrostatic or magnetostatic fields. These codes are capable of handling non-linear and anisotropic materials. The SUPERFISH code is used to calculate resonant electromagnetic modes in two-dimensional resonant structures. Despite its age, the code remains widely used in accelerator science due to its versatility and robustness [103]. To begin a SUPERFISH calculation, the user must first propose an approximate cavity size and shape. This can be done by using existing, validated design samples and modifying them by scaling or making geometrical shape improvements that are tuned to the specific application case.

The Thesis is based on CERN's 750 MHz HF-RFQ design line. These are the most prevalent compact-size RFQs, with common applications in medicine and industry. Therefore, improvement could yield a greater economic and societal impact on human well-being. CERN's compact size RFQs represent a relatively recent development, and it has already become a design line that includes (HF-RFQ, PIXE and carbon-ion RFQ). The SUPRFISH calculation results for these 750 MHz structures are presented in Table 5.1..

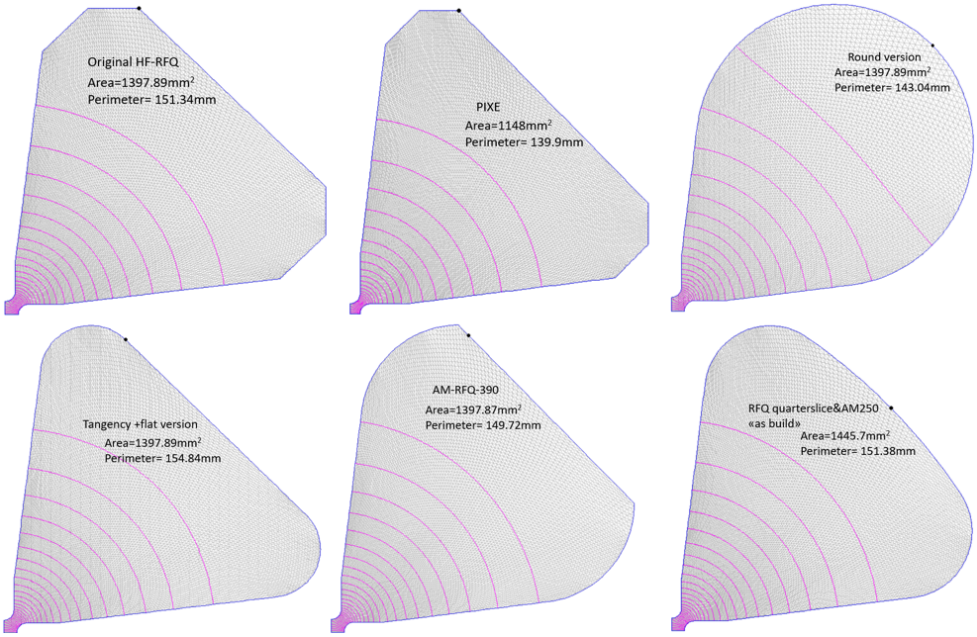

Fig. 5.2. SUPRFISH solutions for 750MHz cavity 2D geometries.

In general designing of new RFQ cavities in most of cases starts with assumption that the cavity's effective quadrant area consists of three quarters of a circle with radius r, plus a square with sides of length r, see figure 5.3., which represent the area nearest the beam axis, yielding a total quadrant area of:

$$A = (4 + 3\pi)r^2/4, \tag{5.1.}$$

where r – circle radius, mm;

π – mathematical constant that is the ratio of a circle's circumference to its diameter, approximately equal to 3.1415.

Then the quadrant inductance

$$L' = \mu_0(4 + 3\pi)r^2/4\ell_V, \tag{5.2.}$$

where μ_0 – permeability of free space (physical constant), μ_0=$4\pi \cdot 10^{-7}$ Tm/A.

Then the cavity resonant frequency is

$$\omega_0{}^2 = (L'C')^{-1} = \frac{16}{\mu_0(4 + 3\pi)r^2C_\ell}, \tag{5.3.}$$

where $(4 + 3\pi)r^2/4$ is total quadrant area of idealized cavity (Fig. 5.3.), m^2, where L' – quadrant shunt inductance, H · m;

Table 5.1.

SUPERFISH Calculation Results for 750 MHz RFQ Cavities [104]

Design name	Perimeter, mm	Area, mm^2	Area/ Perimeter	R. Frequency, MHz	$Q_{0,2D}$ value	Tip R, mm	Aperture R, mm	Shunt impedance, MΩ/m	Stored energy $x10^{-5}$J/cm
HF-RFQ	151.34	1397.89	9.237	716.56	**8028.51**	1.504	1.935	6303.89	6.8775
PIXE	139.9	1148	8.206	728.97	**7156.49**	1.439	1.439	6286.239	6.87484
Carbon	142.15	1202	8.456	709.78	**7273.45**	1.411	1.411	6620.685	6.87443
RoundDesign	143.04	1397.89	9.773	714.75	**8608.20**	1504	1.935	6737.561	6.91407
Tangency+F	154.84	1397.89	9.028	716.59	**7811.74**	1.504	1.935	6133.634	6.90091
AM390	149.72	1397.87	9.337	716.44	**8138.77**	1.504	1.935	6388.894	7.55072
AM 1/4 RFQ	**151.38**	**1445.7**	**9.550**	**703.25**	**8254.51**	**1.504**	**1.935**	**6578.903**	**6.90091**
AM250-200 μm	152.1	1475.2	9.699	736.70	**8569.27**	1.304	2.135	6574.460	4.36554

C' – cavity quadrant shunt capacitance per unit length, H/m;

C_ℓ– shunt capacitance for unit length, assumed $C_\ell = 120 \cdot 10^{-12}$ F/m,

this equation implies that at a fixed frequency, an increase in the capacitive loading reduces the quadrant radius r and the transverse dimensions. The power loss of an eigenmode is commonly quantified by the unloaded quality factor:

$$Q_0 = \frac{\omega_0 W_0}{P_0}, \tag{5.4.}$$

and stored energy per unit length is $W_\ell = C_\ell V^2/2$, and the quality factor is:

$$Q_0 = \frac{\omega_0 W_\ell}{P_\ell} = \sqrt{\frac{8\delta}{(4+3\pi)\omega_0 C_\ell}}, \tag{5.5.}$$

where δ – electric conductivity of Cu-OFE, $\delta = 5.8{\cdot}10^7$S/m.

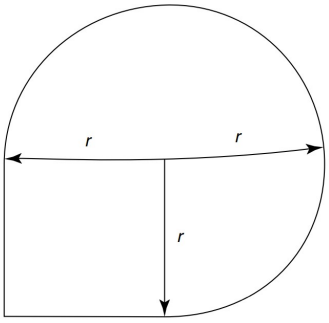

(a) Ideal cavity shape [105]

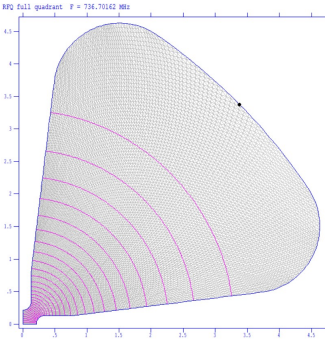

(b) Realistic cavity shape adapted for AM and implemented in 1/4 AM RFQ

Fig. 5.3. Ideal and realistic cavity shapes.

Assuming an $e^{j\omega t}$ time dependence of the currents and voltages, the peak current on the outer wall is given by

$$I = j\omega_0 C_\ell \ell_{\mathrm{V}} V/4, \tag{5.6.}$$

and the magnetic field in the quadrants is

$$B = j\mu_0 \omega_0 C_\ell V/4, \tag{5.7.}$$

Then power loss by assuming the conducting surface area is the perimeter of the quadrant cross section comprised of three quarters of a circle plus a square. Taken over the length ℓ_{V}, the total surface area for all four quadrants is

$$S = 2(4 + 3\pi) r \ell_{\mathrm{V}}, \tag{5.8.}$$

The power dissipation is

$$P = R_{\mathrm{S}} (B/\mu_0)^2 S/2, \tag{5.9.}$$

where

$$R_{\mathrm{S}} = \sqrt{\mu_0 \omega_0 / 2\delta}, \tag{5.10.}$$

is the surface resistance, expressed in terms of the conductivity δ. Substituting for B and eliminating r, we obtain the power per unit length for the whole cavity is

$$P_\ell = \sqrt{\frac{4 + 3\pi}{32\delta}} (\omega_0 C_\ell)^{3/2} V^2, \tag{5.11.}$$

where V - voltage, V.

This shows that for a given vane voltage, the power is proportional to the 3/2 power of the frequency. This is different than the usual $\omega^{-1/2}$ scaling of the power dissipation for typical accelerating cavities, because for this case the ratio of surface magnetic field to vane voltage is proportional to the frequency [105].

The quality factor Q is a ratio of the energy stored in the cavity to the energy dissipated in the walls per RF cycle. A high Q is desirable if it means low power dissipation, but is not necessarily desired if it means large stored energy because it implies a sensitivity to frequency errors. For pulsed systems, high Q also implies a long time constant for filling the cavity with RF energy. The power loss of an eigenmode is commonly quantified by the unloaded quality factor:

$$Q_0 = \frac{\omega_0 W_0}{P_0}, \tag{5.12.}$$

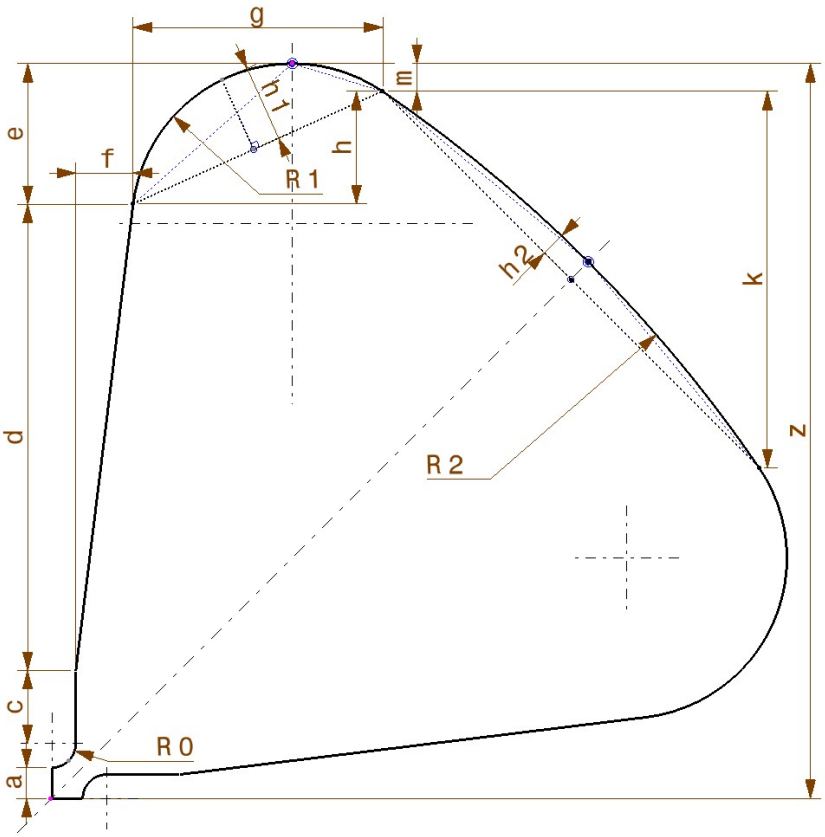

Fig. 5.4. Geometrical elements of RFQ cavity profile.

where W_0 is stored energy for unit lenght, J/m;
P_0 is power dissipation(power loss), kW;
by expanding stored energy equation, quality factor can be calculated:

$$Q_0 = \frac{\omega_0 W_\ell}{P_\ell} = \sqrt{\frac{8\delta}{(4+3\pi)\omega_0 C_\ell}}, \tag{5.13.}$$

where W_ℓ - stored energy for unit length, J/m;
$W_\ell = C_\ell V^2/2$;
further introducing of cavity radius r:

$$Q_0 = \sqrt{\frac{8\delta}{(4+3\pi)\sqrt{\frac{16}{\mu_0(4+3\pi)r^2 C_\ell}}C_\ell}}, \tag{5.14.}$$

and further by adding known values equation becomes dependable from r :

$$Q_{0,2\mathrm{D}} = \sqrt{\frac{8 \cdot 5.8 \cdot 10^7}{(4+3 \cdot 3.14)\sqrt{\frac{16}{4 \cdot 3.14 \cdot 10^{-7}(4+3 \cdot 3.14)r^2 120 \cdot 10^{-12}}} 120 \cdot 10^{-12}}}, \tag{5.15.}$$

Mathematical model for 2-dimensional quality factor $Q_{0,2D}$. Geometrically quality factor of RFQ cavity is equal to cross section area and perimeter deviation multiplied by coefficient.

$$Q_{0,2\mathrm{D}} = \frac{S}{L}\kappa, \tag{5.16.}$$

where

S – cavity cross section area, mm^2

$$S = z^2 - (a + R_0 + c + d + e)^2 - \frac{1}{2}\pi {R_0}^2 - 2R_0 c - 2R_0 d - df - 2R_0 ef -$$
$$2(eg - (gh + {R_1}^2 cos^{-1}(\frac{R_1 - h_1}{R_1}))) - (R_1 - h_1)\sqrt{2R_1 h_1 - {h_1}^2} - 2(k + \frac{l}{2})m -$$
$$(k^2 - (\frac{1}{2}k^2 + {R_2}^2 cos^{-1}(\frac{R_2 - h_2}{R_2})) - (R_2 - h_2)\sqrt{2R_2 h_2 - {h_2}^2}, \tag{5.17.}$$

L – cavity cross section perimeter, mm

$$L = 2a + \pi R_0 + 2c + 2\sqrt{d^2 + f^2} + 2R_1 2cos^{-1}(\frac{R_1 - h_1}{R_1}) + R_2 2cos^{-1}(\frac{R_2 - h_2}{R_2}),$$

$$L = a + \frac{\pi R_0}{2} + c + \sqrt{d^2 + f^2} + 2R_1 cos^{-1}(\frac{R_1 - h_1}{R_1}) + R_2 cos^{-1}(\frac{R_2 - h_2}{R_2}), \tag{5.18.}$$

κ – Q factor coeficient (for 750 MHz RFQ design line κ **= 890.9**), value is obtained by using average value of cavity area and perimeter relation from all listed in Table 5.1. 750MHz RFQ designs, which cahracterizes cavity 2D shape variations.

$a, c, d, e, f, g, h, k, l, m, z, R_\mathrm{i}$ – geometrical elements of cavity (Fig. 5.4.).

Result Validation Table Poisson/SUPERFISH vs Mathmodel *S/L*. From table 5.2. it is visible that **AM 1/4 RFQ** is designed with compromise to allow full capability of tuning options by plungers (relatively flat cavity backwall), but with features of tangential transitions of vane wall to cavity backwall enabled by AM. This feature allows to rise static Q factor by **2.81 %**. In fact increasing of backwall radius $R2$ 5.4. leads to more flat area for tuners, but in same time reduces transition radius $R1$ to vane wall. Therefore balanced values of backwall and transiton radius must be kept to achieve good combination of Q value and flatness of tuning area.

Table 5.2.

Cavity $Q_{0,2D}$ Values S/L vs. SUPERFISH

	Mathmodel				SUPERFISH				
Design name	Perimeter, mm	Area, mm^2	Area/ Perimeter	$Q_{0,2D}$ value	R. Frequency, MHz	$Q_{0,2D}$ value	Tip R, mm	Aperture R, mm	Q value deviation %
HF-RFQ	151.34	1397.89	9.237	8044.26	716.56	8028.51	1.504	1.935	0.19
PIXE	139.9	1148	8.206	7146.45	728.97	7156.49	1.439	1.439	–0.14
Carbon	142.15	1202	8.456	7364.17	709.78	7273.45	1.411	1.411	1.25
RoundDesign	143.04	1397.89	9.773	8511.03	714.75	8608.20	1504	1.935	–1.13
Tangency+F	154.84	1397.89	9.028	7862.43	716.59	7811.74	1.504	1.935	0.65
AM390	149.72	1397.87	9.337	8131.18	716.44	8138.77	1.504	1.935	–0.09
AM 1/4 RFQ	151.38	1445.7	9.550	**8317.19**	703.25	**8254.51**	1.504	1.935	**0.76**
AM250–200 µm	152.1	1475.2	9.699	8446.73	736.70	8569.27	1.304	2.135	–1.43

5.2. Comparison of practically achievable versus original HF-RFQ Q-factor value

From practical point of view for 750 MHz RFQ maximally realisticly achievable Q-factor value relates to "round design" (Fig. 5.2.), because "round design" is more similar to theoretical "ideal design"(square-circle form). If compared versus existing conventionally manufactured HF-RFQ, which was designed and built between years 2016 and 2018 statistic Q factor improvement can reach 7.2 %, Q values 8028.5 and 8608.2 accordingly. In practice it leads to cost reduction on RF power source by 7.2 % as well as reduction of electric consumption during exploitation by same relation.

In general physical accelerator lifetime cost reductions, which is directly related to Q factor value is:

- RF power source size;
- accelerator lifetime power consumption

Sample calculation was done based on HF-RFQ design where the average RF power consumption is 16 kW and the peak power is around 400 kW [106]. In average industrial RF power source cost is $\approx$ 1 Eur/W, therefore 400 kW RF power source cost is 400 000 Eur and theoretical economy on capital costs in case of most economic "Round design" cavity is $\approx$ 28 000 Eur. Further exploitation economy gained from annual power consumption, based on 300 days 24 hour operation and electricity cost 0.2 Eur/kWh reach 1659 Eur/year, what is rather negligible gain if compared to capital investments used to build accelerator facility. However "round design" creates complexities for frequency tuning as well tuners design and calculations, therefore for first prototype **AM 1/4 RFQ** design was chosen. Further were calculated economical gain between conventional HF-RFQ and AM 1/4 RFQ where Q value advantage of AM 1/4 RFQ is **2.81 %**, which in capital costs is 11 240 EUR but exploitation cost reduction is 647 EUR/year.

Although improvement of Q value implies reduction of RF power need, the direct implication on actual RF power source cost is not so trivial, since it also depends on the efficiency of the RF source itself and on the chosen model. Furthermore, the specification for the power source should account for some power buffer to be able to compensate the uncertainty coming from production and from the RFQ operation. The paragraph on energy saving due to a reduction of Q value of few percent is only valid in a theoretical way, but is difficult to be validated.

Furthermore, in different regions of our planet electricity cost varies widely due to market demand and 0.2 EUR/kWh price is rather closer to lowest price offer, as well overall tendency of electricity prices is constantly growing, therefore economy of the exploitation for some periods can easily rise up to five times.

5.3. Modeling of geometry design and thermal management

Geometrical properties

As it was mentioned in subsection 5.1., the design concept for additively manufactured RFQ was based on CERN's developed HF-RFQ, which was already accepted by industry and field experts some time ago [100]. The aim of the Thesis is to improve cavity design for improved quality values. Certain changes of shape were designed to improve static quality factor Q_{2D} by applying AM advantages. However, the most significant improvements were gained from introducing advanced cooling channels. Several key points need to be considered for optimal RFQ – cavity design:

1. to achieve maximum available Q value, cavity 2D shape form must be as possible similar to "ideal" (Fig. 5.3.);

2. as vane thickness can not be infinite thin, there need to consider:

    - the vane form, which is ruled by vane structural stability;
    - the acceptable physical thickness of walls;
    - the whole RFQ heat exchange concept.

Thermal design development. The basic concept of the thermal management for AM produced RFQ was modeled on the ANSYS 19.1 Steady-State Thermal analysis workbench. Input data for ANSYS simulation were based on general approximations and assumptions from the recently built at CERN 750 MHz PIXE RFQ [107]. Crucial input data for the analysis were: 22 °C cooling channel temperature, heat flux on vane tip 2×10^{-3} W/mm^2, flux on the vane and internal walls 8×10^{-3} W/mm^2 , and additional negligible values for heat loss through convection from outer surfaces. Thermal analysis results are provided in Fig. 5.7.. Both CAD models were tested with same heat flux values, to emphasize thermal advantages of AM prototype. From the Steady-State Thermal analysis it is evident that the difference of 0.8 °C, see values on Fig. 5.7. does not posing

any risk for the RFQ functionality. Proposed design concept, especially the internal honeycomb structure and improved cooling channels, could be highly beneficial for the AM manufactured RFQs and other complex (in shape and structure) accelerator components.

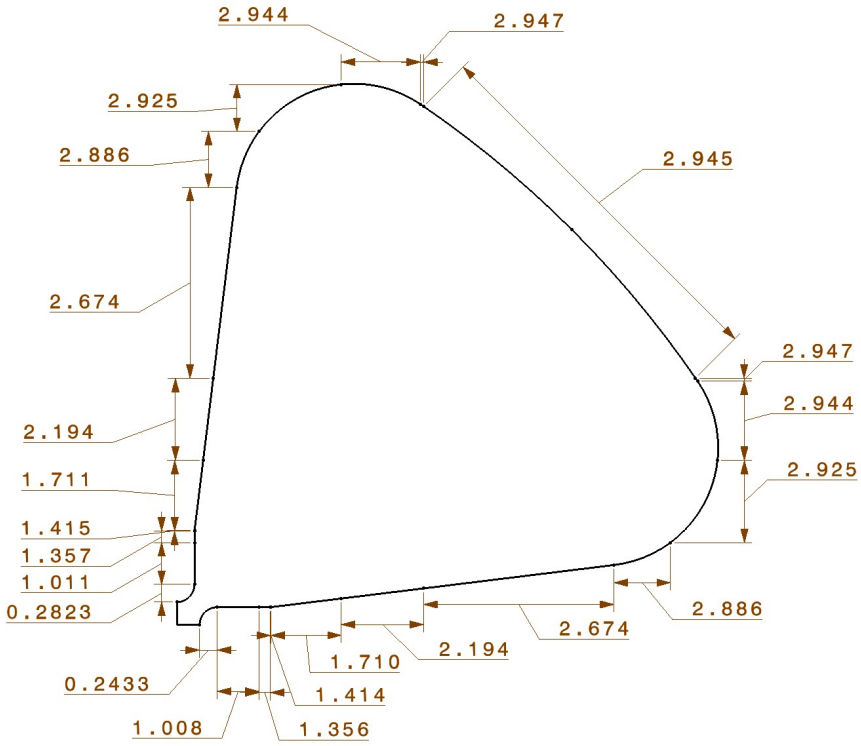

Fig. 5.5. Graphical representation of SUPERFISH calculation results for the power distribution on cavity walls, as well as the average values for length sections, W/cm^2.

In order to address the heat flow distribution in the RFQ model and the thermal stresses dispersion, and the construction of the generated deformation state, in any of its locations, the energy conservation law (Fourier law), described by the differential equation, is used [108], [109]:

$$\rho c \frac{\delta T}{\delta t} - \left(\frac{\delta}{\delta x}(k_x \frac{\delta T}{\delta x}) + \frac{\delta}{\delta y}(k_y \frac{\delta T}{\delta y}) + \frac{\delta}{\delta z}(k_z \frac{\delta T}{\delta z}) \right) - \dot{q} = 0 \qquad (5.19.)$$

, where ρ – the density of the studied solid material, kg/m^3;
c – the specific heat, J·K^{-1}· kg^{-1};
k – the coefficient of thermal conductivity;
$\dot{q}$ – the internal heat generation rate, per unit volume, per unit time, W/m^3/h;
x, y, z – coordinates;
t – time;

T – the variable temperature for the coordinates x, y, z and time t.

For stationary heat transfer, the previous equation becomes:

$$\left(\frac{\delta}{\delta x}(k_{\mathrm{x}}\frac{\delta T}{\delta x})+\frac{\delta}{\delta y}(k_{\mathrm{y}}\frac{\delta T}{\delta y})+\frac{\delta}{\delta z}(k_{\mathrm{z}}\frac{\delta T}{\delta z})\right)+\dot{q}=0 \tag{5.20.}$$

Assuming that the heat transfer takes place in two dimensions, for example, in the X–Y plane, with the coefficient of thermal conductivity, k, constant. In that case, the differential equation is reduced to one with partial derivatives, called the Poisson equation:

$$\frac{\delta^2 T}{\delta x^2}+\frac{\delta^2 T}{\delta y^2}=-\frac{Q}{k} \tag{5.21.}$$

In addition, if no internal heat is generated, the differential equation is reduced to the partial derivative equation, so called the Laplace equation:

$$\frac{\delta^2 T}{\delta x^2}+\frac{\delta^2 T}{\delta y^2}=0 \tag{5.22.}$$

The solution of Laplace's equation is $T(x, y)$. Although Laplace's equation is straightforward, its exact solution is complicated to determine, especially in the case of more complex geometries. As can be seen, the Fourier law relates the components of the conduction heat flux to the temperature gradient. By definition, the element of the conduction heat flux in the x-direction, for an isotropic material, [110] is:

$$q_{\mathrm{x}}=-k\frac{\delta T}{\delta x} \tag{5.23.}$$

Finite element equations for solid problems can be obtained by applying the weighted residue method to the differential equation that governs this problem [108]. Matrix form of the finite element equation:

$$[k]\{\delta\}=\{F\}+\{F_0\} \tag{5.24.}$$

ANSYS Steady-State Thermal and Static Structural finite element method (FEM) application, which is based on equations 5.21., 5.22., 5.23., 5.24. and applied to original HF-RFQ and AM 1/4 RFQ models are showing indisputable advantages of AM 1/4 RFQ cooling channel design, the main advantage is significant decrease of maximum temperature values, which further impress to decreasing of deformation level due to temperature field distribution. Colour maps of temperatures and distortion are shown in Fig. 5.7.. Further temperature and deformation values were compared and are given in Fig. 5.8., which is showing impressive **32 % advantage** of AM manufactured sample. FEM thermal simulation report based on SUPERFISH calculation results is given in ANNEX G.

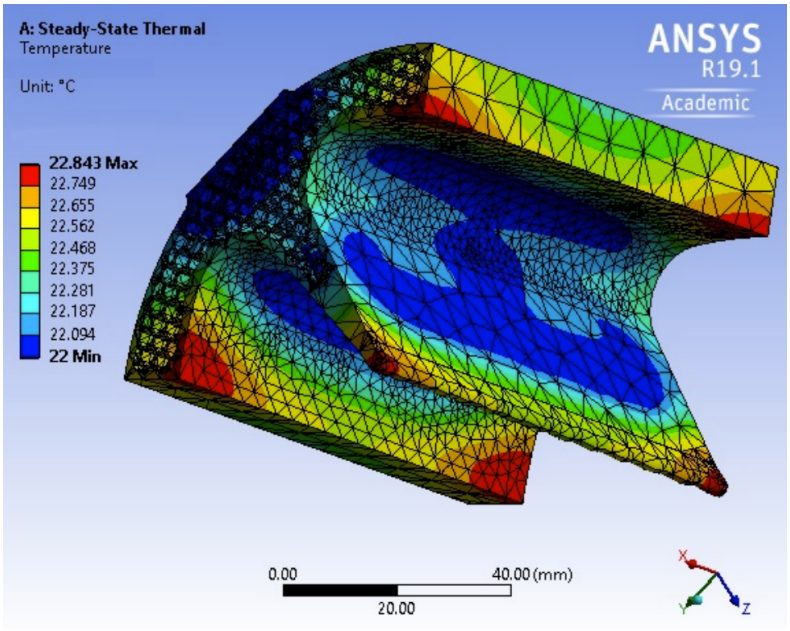

Fig. 5.6. Steady-State Thermal analysis of AM RFQ prototype 1/4 sector.

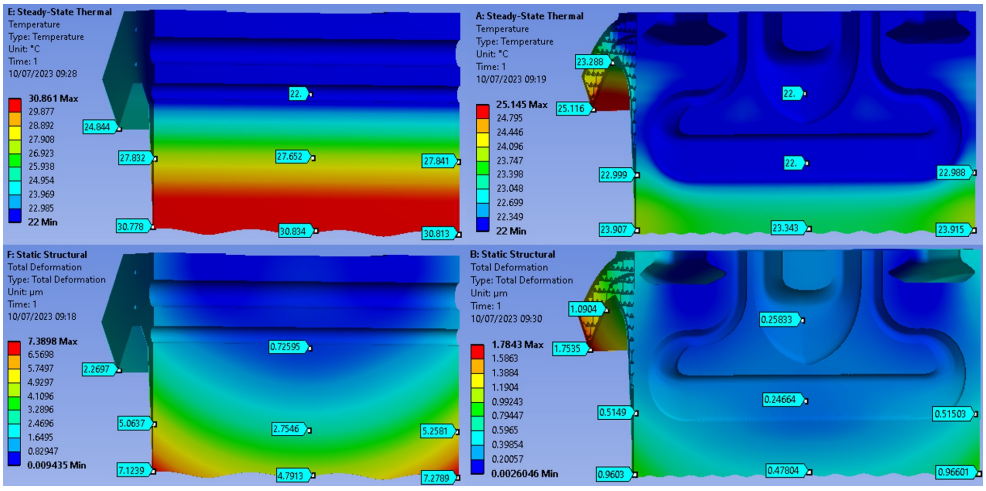

Fig. 5.7. Steady-State Thermal and Static Structural analysis.

5.4. Conclusions

In general lines the CERN's 750 MHz RFQ design line already is highly tuned and does not has gaps for improvements by traditional manufacturing, **but application of AM advantages can allow several meaningful cavity geometry improvements**. The new mathematical model of the cavity shape 2D profile was developed on basic geometrical

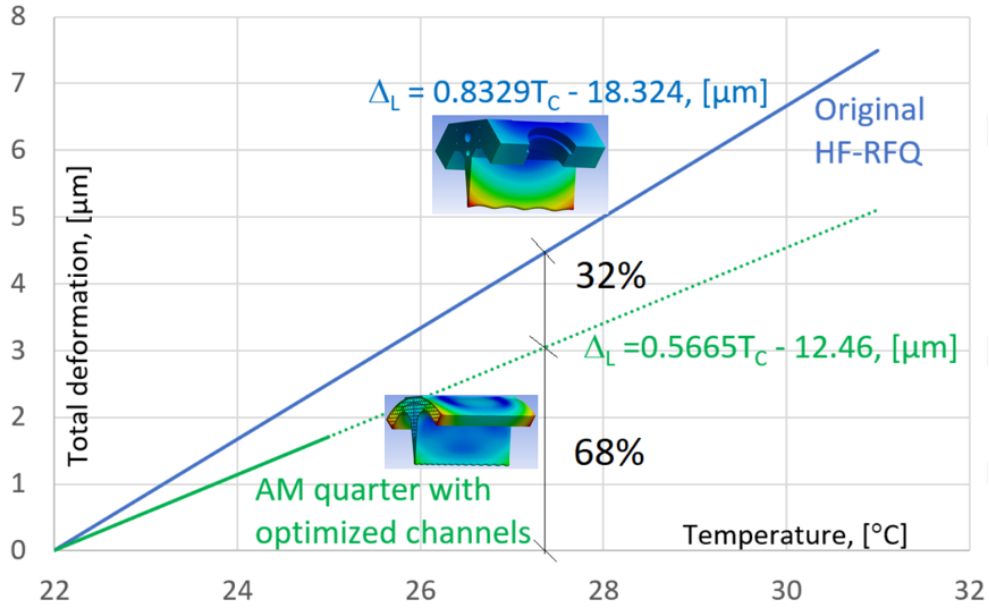

Fig. 5.8. Maximal thermal deformation comparison.

equations 5.16., 5.17., 5.18. including physical form restrictions such as minimum vane, wall thickness, cooling channel implementation in vane volume and ideal cavity shape concept. Further developed mathematical model could be used for other size RFQ's design improvement and adaptation for AM and particularly for cavity quality factor improvement.

Thermal simulation of original HF-RFQ and AM RFQ quartersector prototype 5.8. is showing average **32 % improvement** for maximal thermal deformation over traditionally manufactured HF-RFQ. Thermal distortion simulation and obtained temperature/deformation equation is valid only for current CAD model and stimulation values are strongly affected by cooling channel shape, routing and concept design. The thermal management possibilities of AM RFQ prototype have significant advantages over conventionally manufactured RFQ, the key benefits are based on improved cooling channel shape, routing and increased surface areas. However concept of channels still can be improved by merging of physical modeling and programming tools, to reach higher tunability for thermal efficiency and duty cycle regimes. One of main goals of cooling channel development is to minimize temperature differences in RFQ body therefore reducing structural distortion, which has significant impact on beam stability and quality. This can be achieved by AM technology, as demonstrated in this research.

6. NEW CONCEPT OF AN ADDITIVE MANUFACTURED RFQ

Already at the beginning of the research, it was clear that the goal is ambitious and demanding tuned level AM hardware and well equiped facilities, as well as expert level metrology and postprocessing labs. Therefore, several well known industrial partners and scientific laboratories were involved. From the very start, it was planned to access TRUMPF TruPrint1000 Green Edition AM machine in Fraunhofer IWS(Dresden), similarly postprocessing was planned in Rösler Italiana SRL labs as well further, there appeared an opportunity to realize MMP postprocessing approaches at Binc Industries.

6.1. Challenges of RFQ AM

An RFQ is a critical component of particle accelerators featuring strict technical requirements in order be able successfully operate. At first glance, it appears that its stringent requirements (Table 6.1.) are unreachable by the current state-of-the-art of AM systems. However, the continuous developments in AM systems and related postprocessing technology are steadily approaching the levels of precision, surface quality, and manufacturing predictability required by RFQs. The experimental testing activity of this proof-of-concept was performed on commercially available, state-of-the-art laser-based AM technology, which is suitable for pure copper manufacturing. Table 6.1. and Fig. 6.1. summarizes the main parameters of the design and manufacturing of the pure copper RFQ.

Table 6.1.

Requirements for the RFQ Prototype[111]

Challenge	Target
Geometrical accuracy	20 µm on vane tip, 100 µm elsewhere
Surface roughness	$R_a = 0.4$ µm for all inner surfaces
Cavity Quality factor	> 90 % Q_0
Cooling improvement	$\Delta L < 2$ µm
Limit pressure*	10^{-7} mbar
Electrical conductivity*	95 % of pure copper IACS
Peak electric field on surface*	~ 40 MV/m

* - within scope of this research

The manufacturing experiment was carefully designed and planned, keeping in mind the requirements mentioned in Table 6.1.. To ensure the functionality of the RFQ, the geometrical accuracy and shape of the manufactured surfaces are of utmost importance, as indicated by the values of 20 µm for the vane tip and 100 µm for all other cavity surfaces. The most relevant target value here is the RFQ vane tip and its modulation profile, which is the core element for beam transport; therefore, particular attention and

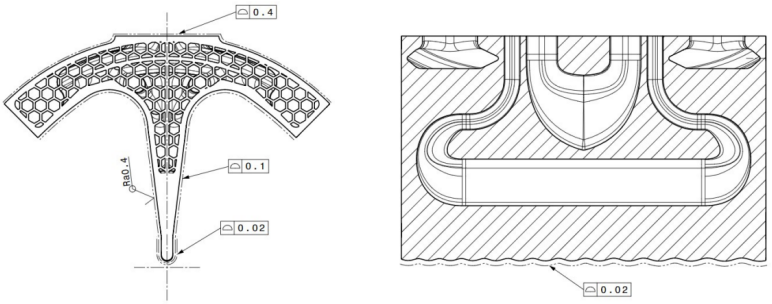

Fig. 6.1. Shape accuracy requirements for prototype.

careful measurements should be devoted to the vane tip. It is clear that, if AM cannot provide enough precision for the modulation geometry, beam transport and acceleration cannot be ensured. Furthermore, the surface arithmetical mean roughness value *Ra* has to be kept at a level of about 0.4 µm. The surface roughness has to be shallower than the penetration of high-frequency currents in the metal "skin depth" to avoid considerable reductions in the Q value of the RFQ resonator and proportional increases in its power consumption and in the cost of the radio frequency system. Moreover, large values of *Ra* might increase the sparking probability of surfaces subject to high electric fields. Although surface roughness is critical for the functionality of RFQ, such values are rather difficult to maintain with conventional AM technology and might require post-processing of the surfaces transporting the radio frequency current. The vacuum value of 10^{-7} mbar was set to minimum required value for the RFQ, as reference circular accelerators often require higher vacuum values. The electrical conductivity is of utmost importance and has a decisive impact on RFQ efficiency. The highest electrical conductivity can be reached only with high chemical purity and density of the base material e.g., copper. In the case of AM, the chemical purity of the final product depends not only on chemical cleanness of powder, but also on the manufacturing chamber's protection against oxidation. It is important to note that the oxygen-free pure copper powder grains tend to oxidize in a standard room environment and at room temperature. The lower electrical conductivity of the RFQ in turn will proportionally increase the required operational power of the accelerator, in a similar way to the roughness, and will generate extra heat on the vane surfaces. Therefore, the target value for the electrical conductivity for this proof-of-concept was set to 90 % that of ideal copper according to the International Annealed Copper Standard (IACS). Finally, the voltage holding properties are crucial for the successful operation of the RFQ. Naturally, these properties are directly affected by any mechanical and chemical inclusions, and the homogeneity of the RFQ material itself. Considering some existing RFQ designs, a target value can be empirically defined at about 40 MV/m peak surface field. However, it was clear that not all RFQ–specific requirements could be achieved at this initial proof-of-concept stage (e.g., roughness, degassing, and voltage holding). In the pro-

posed prototype, design emphasis was given to the verification of AM capabilities for the RFQ geometrical accuracy (manufacturing tolerances) and surface quality (roughness), and to the demonstration of improved mechanical design advantages.

6.2. Additive manufacturing process of pure copper RFQ

In order to attain the best possible results, state–of–the–art AM technology and manufacturing equipment was chosen for the production of the first pure copper RFQ prototype. A TruPrint1000 Green Edition (Fig. 6.2.) in combination with a green TruDisk1020 laser providing the wavelength of 515 nm and maximum laser power of 500 W was used at Fraunhofer IWS in Dresden. Dedicated machine allows cylindrical build volume of 100 mm in diameter and 100 mm in height. The TRUMPF SE+Co.KG pre–set pure copper processing parameters and scanning algorithms were used throughout carefully monitored manufacturing process. As a production material, m4pTM PureCu gas–atomised spher-

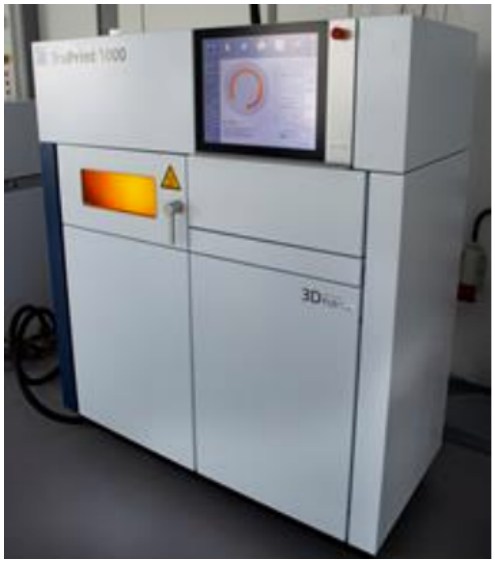

Fig. 6.2. Trumpf TruPrint 1000 Green Edition.

ical shaped powder was used, which was confirmed with the Camsizer X2 and dynamic imaging analysis (see Table 6.2. and Fig. 6.3.). The sphericity was 0.923 according to scanning electron microscope imaging. The particle size distribution was confirmed to be between 19.5 µm and 34.9 µm, which is common for PBF-LB process.

The choice between powder types, which fits better for RFQ requirements and AM process is clarified in previous researches of S. Gruber, where she proved Cu-ETP advantages over Cu-OFC [36]. Therefore final decision fell on 30 µm grain size Cu-ETP powder [111].

Table 6.2.
Main Characteristics of Particle Size Distribution of Cu-ETP [111]

Powder	**D10 in µm**	**D50 in µm**	**D90 in µm**	**Sphericity**
Cu-ETP (Electrolytic Tough-Pitch: pure copper)	19.5	26.2	34.9	0.923

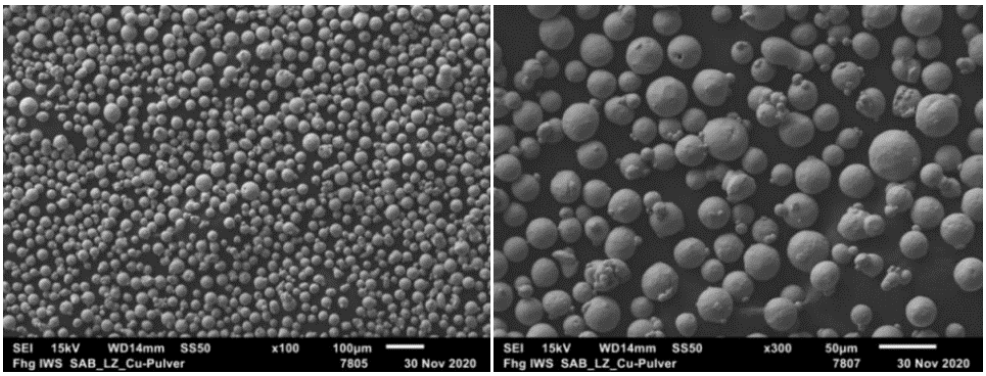

Fig. 6.3. SEM images of Cu-ETP powder: left: magnification of ×100; right: magnification of ×300 [36].

Experimental part of thesis is based on design development and modification of actual CERN's HF-RFQ. Decision to take HF-RFQ as model for development was taken because of size, complexity and potential manufacturing cost reductions. HF-RFQ size fits to current scale of commercial AM machines and our goal is to prove benefits of AM technology for accelerator community. In other hands HF-RFQ is smallest one from RFQ's product line and in that way it is perfect candidate for AM manufacturing, because large volume builds still are too challenging from point of view of AM. Currently in a market are AM machines, which can build micro and nano size parts with exceptionally high precision, but most of them are not acceptable for part manufacturing, which are larger than 100 mm in any dimension, because of build speed and build space. Even large size AM machines with build volume close to 0.25 m^3 and layer thickness 30 µm are comparatively slow at maximum build volume. Often for most of builds processing time varies from couple of hours to weeks. for parts, which are in similar size of HF-RFQ [112].

6.3. Postpocessing

In recent years AM has gained enormous popularity. This is primarily because of its remarkable capability to build intricate shapes and significantly decrease the time and costs of fabrication. Although there are many benefits to using AM, achieving a high-quality surface finish for parts is still a major hurdle for many industries. Dealing with this matter has emphasized the importance of post-processing in the AM process. Post-processing involves a variety of techniques that are carried out after the parts have

been printed to enhance and alter their surface finish quality. There are a wide range of techniques that can be used, including sanding, polishing, heat treatment, and other lesser-known methods. The selection of post-processing technique relies on the particular material, the preferred surface appearance, and the level of required accuracy.

Sandblasting is a well-known post-processing technique in AM. This process utilizes various abrasive media to effectively eliminate surface imperfections and enhance the overall roughness.The treatment can be done either manually or with the help of advanced automated machines. Additionally, the level of roughness can be easily adjusted and controlled to achieve the desired roughness class. Another aspect of postprocessing is polishing, a widely used technique that aims to enhance the surface finish quality of manufactured parts. This process utilizes abrasive materials, like buffing wheels, to eliminate surface imperfections and achieve a polished, glossy surface. You can adjust the polishing time, pressure, and abrasive material to control the degree of shine.

Heat treatment is a crucial post-processing technique for certain metals, which can greatly enhance the quality of the surface finish. This process requires heating the parts to a precise temperature and maintaining that temperature for a designated duration. Heat treatment has the potential to modify the microstructure of the material, resulting in a more refined surface finish and diminished surface roughness.

Post-processing plays a vital role in the AM process, improving the surface finish quality of AM parts. The choice of post-processing technique depends on factors like the material used, the desired surface quality, and the required level of precision. Through the incorporation of post-processing techniques, manufacturers can achieve exceptional quality and improved surface finish in the production of parts using AM. This advancement expands the possibilities of AM, making it a viable option for a wider range of applications.

6.3.1. Traditional mass finishing

The traditional mass finishing is a post-processing method widely used in AM to improve the surface finish of parts produced through 3D printing or other forms of AM. This method involves the use of abrasive media in a vibratory or tumbling action to remove surface anomalies and improve the overall surface quality.

As in AM, parts are built layer by layer, resulting in a characteristic layer structure on the surface of the part. This layer structure can lead to roughness, porosity, and other surface anomalies that negatively impact the functional performance of the part. Mass finishing can effectively remove these anomalies, resulting in a smoother, more homogeneous surface that is better suited for functional applications.

There are two main types of mass finishing methods: vibratory finishing and tumbling. Vibratory finishing involves the use of a vibratory machine that holds the part and abrasive media and applies a vibratory motion to the part and media. This motion causes the abrasive media to rub against the surface of the part, removing surface anomalies and

improving the surface quality. Tumbling, on the other hand, involves placing the part and abrasive media into a rotating drum, which subjects the part to a tumbling action that removes surface anomalies and improves the surface quality.

The choice of mass finishing method depends on several factors, including the size and shape of the part, the desired surface finish, and the type of abrasive media being used. For example, vibratory finishing is typically more effective for small, complex parts, while tumbling is more effective for larger, simpler parts.Mass finishing is a critical post-processing step in the manufacturing of AM parts, as it can significantly improve the surface quality and functional performance. Whether using vibratory or tumbling methods, mass finishing provides a cost-effective and efficient means of removing surface anomalies and achieving a smooth, homogeneous surface that is well-suited for functional applications.

For current case study process was performed in Rösler Italiana Srl., which is subsidiary of German company Rösler Gmbh. Both mass finishing methods vibratory finishing and tumbling were applied for post processing cycle development for case study. The surface finishing has been obtained mainly by the mechanical abrasion of the media on the component, due to the relative speed among them. For the finishing of quarter RFQ sample a three-step process was designed.

6.3.2. Chemically assisted finishing

Chemically Assisted Mass Finishing (CAMF) is a variation of mass finishing that combines the mechanical action of vibratory or tumbling methods with the chemical action of a finishing solution. CAMF offers several unique advantages compared to traditional mass finishing methods, making it a popular choice for post-processing of additive manufactured parts.

One of the main peculiarities of CAMF is the ability to achieve a higher degree of surface refinement compared to traditional mass finishing methods. This is due to the presence of the finishing solution, which reacts with the surface of the part to remove surface anomalies and improve the overall surface quality. The chemical action of the finishing solution can also help to remove surface contaminants and impurities, resulting in a cleaner, more homogeneous surface.

Another advantage of CAMF is the ability to control the rate of material removal and the final surface finish. This is achieved by adjusting the chemical composition and concentration of the finishing solution, as well as the mechanical parameters of the vibratory or tumbling machine. This level of control makes CAMF a versatile and flexible post-processing method that can be tailored to meet the specific requirements of each application. CAMF also offers the benefits of being a closed-loop system, as the finishing solution can be recycled and reused, reducing waste and environmental impact. Additionally, the use of a finishing solution can increase the life of the abrasive media, reducing the frequency of media replacement and further reducing the environmental impact of

Fig. 6.4. RFQ sample piece after chemically assisted treatment at Rösler Italiana Srl.

the process. CAMF is a highly effective and versatile post-processing method for additive manufactured parts, offering several unique advantages compared to traditional mass finishing methods. By combining the mechanical action of vibratory or tumbling methods with the chemical action of a finishing solution, CAMF provides a cost-effective and efficient means of improving the surface quality and functional performance of additive manufactured parts.

6.3.3. MMP TECHNOLOGY®

Micro Machining Process (MMP) technology is a precision machining method that is used to produce micro-scale parts with high accuracy and surface finish. MMP technology is commonly used in the post-processing of additive manufactured parts to remove residual layer structures, improve surface roughness, and enhance the dimensional accuracy of the part.

One of the main peculiarities of MMP technology is its ability to produce parts with very high precision, with dimensional tolerances on the order of a few micrometers. This high level of precision is achieved through the use of specialized micro-scale cutting tools and precision machine tools that are designed to work at the micro-scale.

Another advantage of MMP technology is the ability to produce parts with very high surface finishes, with roughness values on the order of a few nanometers. This high level of surface finish is critical for applications in industries such as biomedical engineering, where surface quality is a key factor in the functional performance of the part.

In addition to its high precision and surface finish, MMP technology offers several

other benefits for post-processing of additive manufactured parts. For example, MMP technology can be used to produce parts with complex geometries and internal features, such as channels and micro-scale fluid systems, that are difficult to produce using traditional manufacturing methods.

In conclusion, MMP technology is a highly effective post-processing method for additive manufactured parts, offering several unique advantages compared to other methods. By leveraging the precision and accuracy of micro-scale machining tools and techniques, MMP technology provides a cost-effective and efficient means of enhancing the dimensional accuracy, surface roughness, and functional performance of additive manufactured parts.

In order to be able to find most suitable and applicable technology for AM pure copper sample part finishing, decision for trial application of MMP TECHNOLOGY® was taken.

In general MMP TECHNOLOGY® (Micro Machining Process) invented by BINC Industries is focusing on high quality part super-finishing, during processing surfaces are treated by selective removal of specific range of roughness. Unlike traditional polishing, MMP TECHNOLOGY® differentiates itself by its ability to finely control the material removal process. MMP TECHNOLOGY® can deliver finely controlled surfaces ranging from matte to brilliant mirror-like finishes. MMP TECHNOLOGY® 's advantages include reproducibility, homogeneity, precise preservation of the exact form of the part, and predictable costs [113].

MMP TECHNOLOGY® consists of a combination of a proprietary mechanical and physical process aided by a catalyst that activates the engineered microtool technology. The mechanical part of the process is provided by a machine whose very high energy movement creates a flux. This flux is composed of aggregated particles of microtools created "in situ" by means of the catalyst. These aggregated microtools are specifically engineered to replicate the micro-roughness of the surface that is to be removed, thus forming a cutting tool that is "keyed" to the roughness being targeted. BinC Industries builds its own machines and microtools, and formulates its own catalysts.

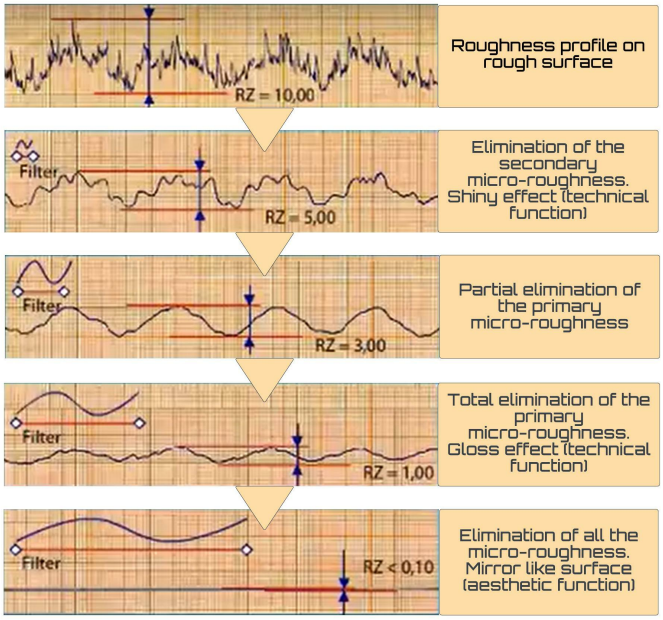

Fig. 6.5. MMP micro-roughness elimination sequence adapted from [113].

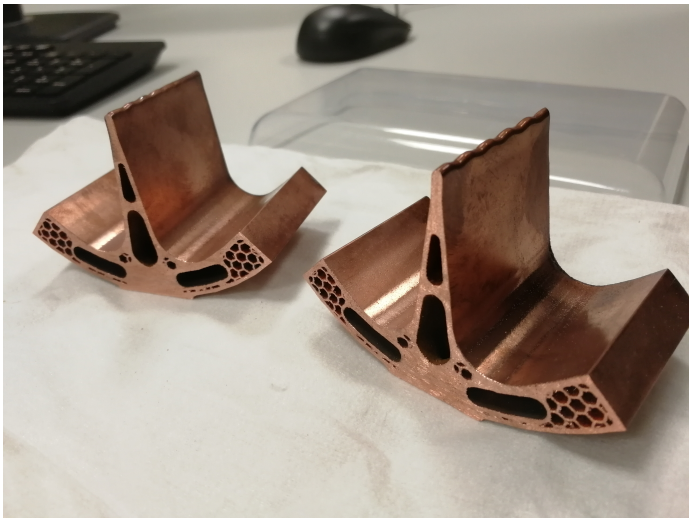

Fig. 6.6. Prototype sample postprocessed by BINC Industries and split after postprocessing.

7. EVALUATION OF GEOMETRICAL ACCURACY AND SURFACE ROUGHNESS QUALITY FOR THE ADDITIVELY MANUFACTURED RFQ PROTOTYPE

7.1. "As-built" part inspection

As previously outlined in the section on research methodology, a series of metrology steps were planned following each manufacturing step. These were designed to verify the geometrical accuracy of the product and to maintain continuous monitoring of any changes in geometrical and surface forms. Indeed, the implementation of a continuous metrological inspection process enables the adjustment of further machining and post-processing parameters, as well as the prediction of the manufacturing process's progress.

7.1.1. Geometry measurements on coordinate measurement machine

Series of measurements were executed in CERN's EN-MME metrology laboratory on

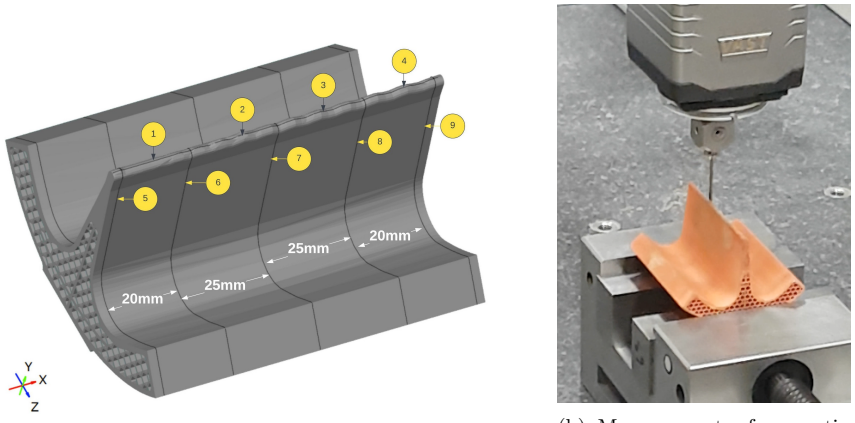

(a) Plan for CMM measurements.

(b) Measurement of vane tip modulation on ZEISS Prismo Ultra CMM.

Fig. 7.1. CMM metrology of AM RFQ quarter.

ZEISS Prismo Ultra 12-18-10 Bridge type CMM with a movable bridge. In top configuration and appropriate conditions Prismo Ultra is able to measure such size parts with accuracy up to 0.5 µm + L / 500 mm [114]. However current measurement was executed with standard accuracy tooling and enviromental conditions providing measuring accuracy at 1.2 µm + L / 500 mm. There also need to mention choice of tip size for measurement tool as it impacts measurement accuracy. The tip radius must be chosen

enough large to filter out surface roughness irregularities and in same time do not miss shape of geometrical forms of object. For vane tip modulation probe tip radius was chosen 1.0004 mm and probe speed 1 mm/s, as vane tip modulation is more challenging part of RFQ, but for the cavity shape measurements, probe tip radius 1.5008 mm and traversing speed 3 mm/s were used.

7.1.2. Optical scanning of geometry

For the better visibility and understanding of the build prototype matching to input stl model the first "as-built" part scan was performed in Fraunhofer IWS (Fig. 7.2.), afterwards optical scan test for same sample was repeated at CERN EN-MME metrology lab by using high-end 3D scanner Creaform METRASCAN Elite Black, which has garanteed resolution of 0.10 mm and volumetric precision in 9.1 m^3 – 0.064 mm. At CERN EN-MME lab first Polyworks MS2020 software was used, but for further more detailed alignment and inspection analysis ZEISS GOM INSPECTION was used.

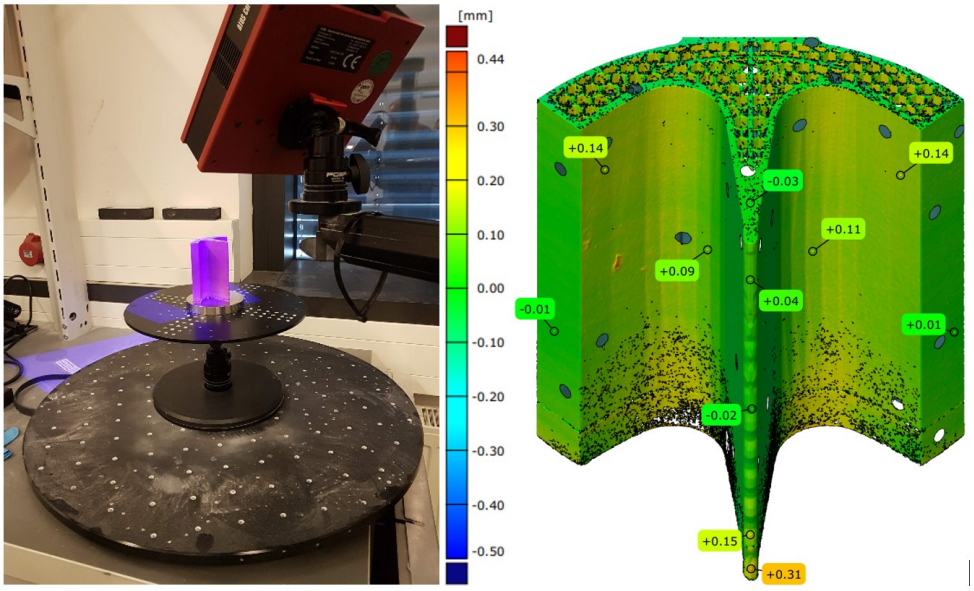

Fig. 7.2. Optical scanning and Point cloud data comparison with original CAD model at Fraunhofer IWS.

7.1.3. Surface roughness measurements

The initial surface roughness profile was measured at Fraunhofer IWS by perthometer Surfcom Touch 50, which is a contact profilometer from Accretech, for surfaces where *Ra* = 0.4 µm is required on both sides of the vane (Fig. 7.3.. measurement numbers 9 and

10) and RFQ internal surfaces (Fig. 7.3.. measurement numbers 6 and 8). Measurements have been repeated three times at each area.

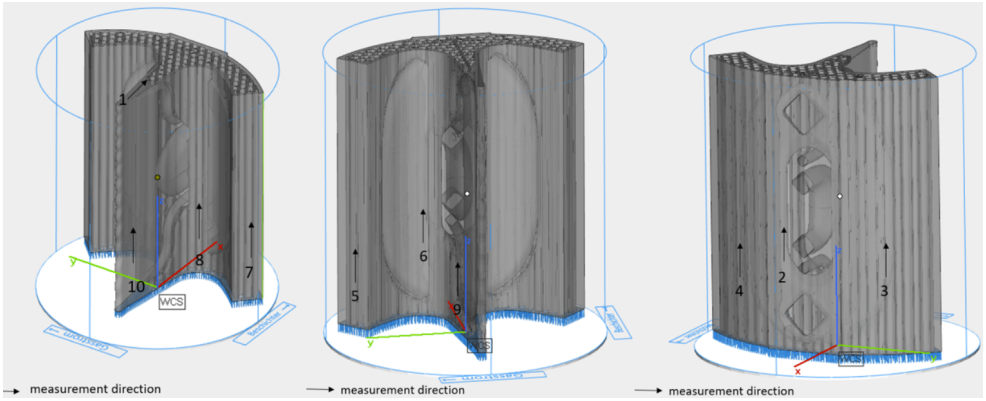

Fig. 7.3. "As-built" part roughness profile measurement locations at Fraunhofer IWS.

The surface arithmetical mean roughness (Ra) average was 14.32 µm, and the maximum height of the profile (Rz) was 116.7 µm. Furthermore measurements were repeated to fulfill the confidence that achieved values are comparable with RFQ prototype requirements 6.1. and obtain a more comprehensive understanding of the surface quality of the prototype. The most indicative surface roughness measurement results are provided in the Table 7.1..

Table 7.1.
RFQ Proof-of-Concept Surface Roughness Values According to ISO 4288 [111]

Location	Measurement No.				Measurement No.			
	Ra (µm)				Rz (µm)			
	1	2	3	Mean	1	2	3	Mean
6	10.4	12.4	12.8	11.9	84.2	89.5	85.6	86.5
8	15.1	15.0	15.3	15.1	148.8	138.7	143.0	143.5
9	13.8	14.9	13.5	14.1	117.2	123.6	104.7	115.1
10	13.9	14.9	14.9	14.6	117.5	134.2	103.3	118.3

Although, these first roughness measurements of the proof-of-concept RFQ show that the obtained surface roughness quality was still far from the required value $Ra = 0.4$ µm, it is important to keep in mind that these results were obtained without any specific adaptations of the AM technological process to achieve better surface roughness outputs. Therefore, even before considering potential post-processing needs and methods for the AM RFQ, there are a range of opportunities to optimize the technological process of the pure copper PBF-LB manufacturing to attain better surface roughness quality.

Additionally all types of surface roughness control were performed at Rösler Italiana Srl. before, after and during whole postprocessing cycle to find and develop the optimal

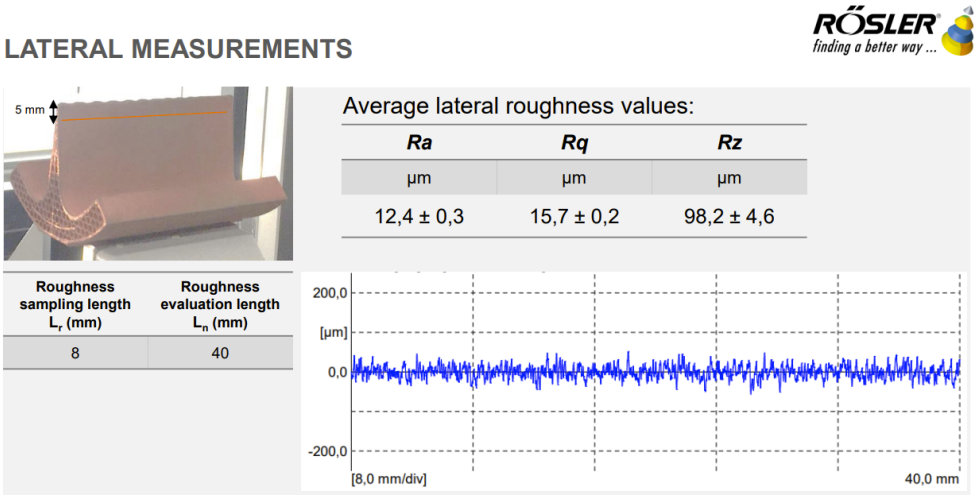

Fig. 7.4. Roughness profile measurement for side surface for "as-built" prototype at Rösler Italiana Srl.

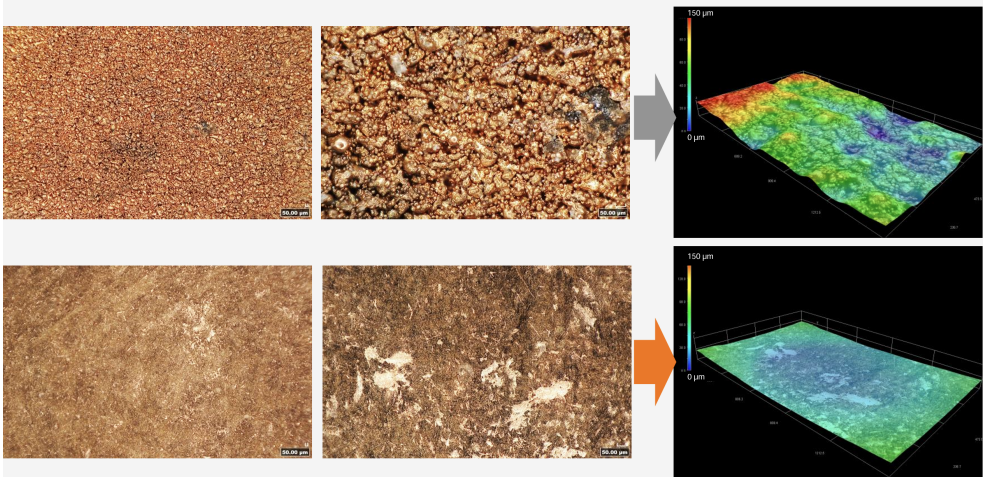

Fig. 7.5. AM RFQ prototype surface optical and 3D images before and after mechanical treatment at Rösler Italiana Srl.

postprocessing techniques and approaches, see Fig. 7.4., 7.9..

7.2. Post-processed part inspection

In scope of this research two quarter prototype parts was manufactured and post processed by two different post processing companies Rösler Italiana Srl. (Italy) and BINC Industries (France). Each of companies were used different postprocessing methods. Rösler Italiana Srl. did purely mechanical and combined mechanical-chemically

assisted [115]. Meantime BINC Industries applied exclusively their own developed MMP TECHNOLOGY®.

7.2.1. Optical scanning of geometry

Similarly as it was done for "as-built" condition optical scanning was repeated after sample post processing step

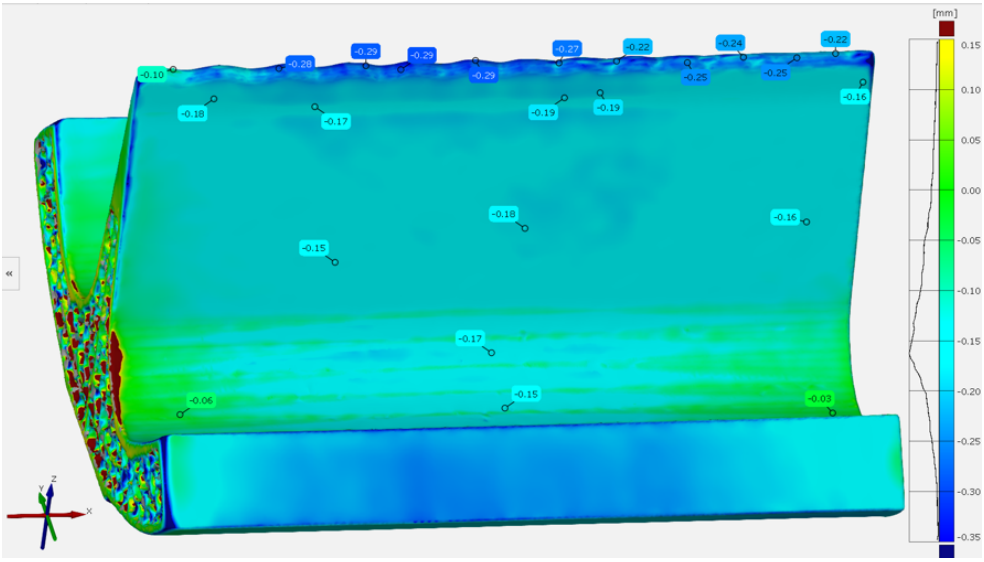

Fig. 7.6. MMP TECHNOLOGY® postprocessed prototype deviation colormap "best fit" scenario for whole body. Image obtained by using ZEISS GOM Inspect software.

and ZEISS GOM INSPECT software applied to compare scanned Point Cloud data with "as-designed" CAD model, which was used for sample build. From the Fig. 7.6. is clearly visible that for post-processed sample surface deviation distribution is slightly shifted to negative values with extremum at – 0.16 mm, that is value, which must be compensated.

The GOM Inspect software allows to align Point Cloud STL data for "best fit" alignment by choosing specific surface areas, so in that way user can adopt alignment and decide how to compensate shrinkage and errors on less critical areas, where is easier to apply compensation methods. For example in Fig. 7.7. vane tip modulation surface is matching in "best fit" mode and compensation is needed only for cavity area, which has less demanding accuracy, as well outside contour of interface ports for cooling and ISO CF vacuum flanges can be more easily adjusted.

As additional feature of "best fit" alignment and visualization of results is geometry sectioning, which allow to see deviation values for sectioned profile diagram.

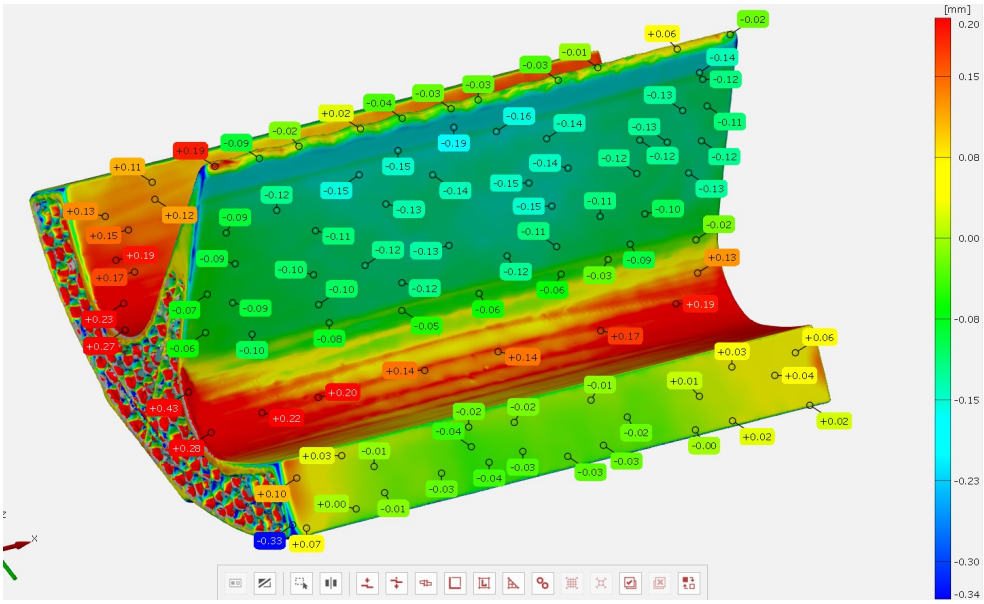

Fig. 7.7. Surface deviation colour map for local “best fit” alignement applied to vane tip, sample post-processed by MMP TECHNOLOGY® . Image generated in ZEISS GOM Inspect.

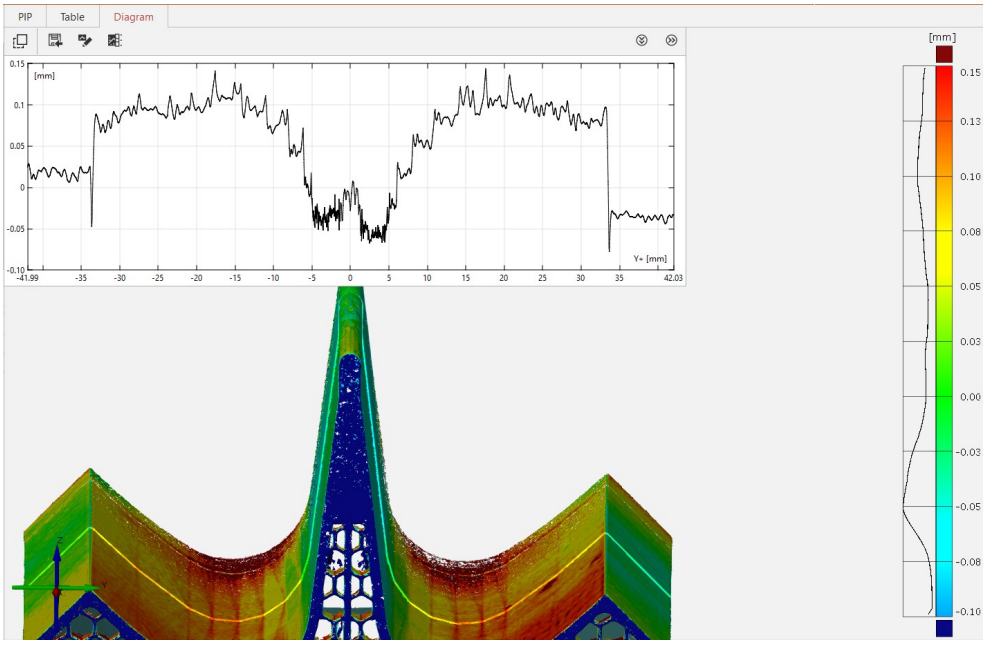

Fig. 7.8. “As-built” prototype normalsection deviation, sectioned in the middle. Diagram, colour map and deviation distibution generated by ZEISS GOM Inspect software.

7.2.2. Surface roughness measurements

Surface roughness parameters were controlled during the whole post processing cycle. Both companies for all three cases of post-processing set roughness target to Ra = 0.4 µm accordingly to initially set values. Additional independent surface roughness measurements were tested at the CERN's MME metrology laboratory. The set surface profile roughness values for all three postprocesing cases for finished product were achieved Ra = 0.4 µm.

Table 7.2.
Values of Surface Roughness Profile for 1/4 RFQ Prototype Samples, Measured Accordingly to ISO 4288 at Italiana Rösler Srl. Metrology Lab During the Tuning of Mechanical and Chemically Assisted Postprocessing Technology

Stage	Vane tip			Vane sides		
	λ_C=0.8mm × 20			λ_C=0.8mm × 5		
	Ra (µm)	Rz (µm)	Rq (µm)	Ra (µm)	Rz (µm)	Rq (µm)
Rough sample	10.7 ± 3.1	68.7 ± 6.7	13.6 ± 1.5	13.82 ± 0.83	48.86 ± 1.56	17.21 ± 1.80
After pretreatment	4.3 ± 1.0	16.0 ± 3.8	5.8 ± 1.5	-	-	-
Mechanical treatment	1.58	4.98	1.89	0.28 ± 0.12	2.09 ± 0.89	0.38 ± 0.15
Chemically assisted	2.31	7.34	2.78	0.28 ± 0.09	1.56 ± 0.50	0.36 ± 0.12

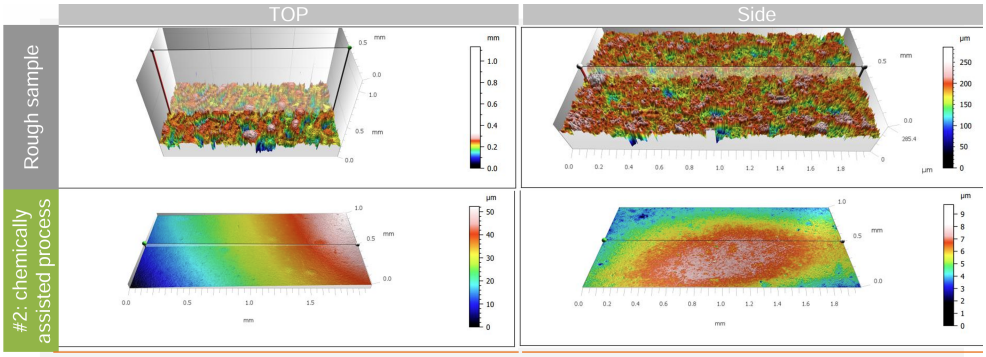

B-5 TOP	Sa (µm)	Sz (µm)	Sq (µm)	B-5 Side	Sa (µm)	Sz (µm)	Sq (µm)
Rough sample	38,18	1137,0	48,52	Rough sample	21,45	281,0	27,90
#2: chemically assisted process	0,58	18,91	0,85	#2: chemically assisted process	0,34	8,08	0,45

Fig. 7.9. AM 1/4RFQ surface 3D rouhness images and parameters for vane tip and side surfaces treated by chemically assisted process at Rösler Italiana Srl.

Surface roughness measurements. Surface profile roughness measurements were carried out in accordance with ISO At final stage additional independent surface roughness measurements were executed at CERN's MME metrology laboratory. Surface profile roughness values for all postprocesing cases were below Ra = 0.4 µm.

Table 7.3.
Surface Roughness Values of 1/4 RFQ Before and After Post-Processing

Post processing method	**Side**	***Ra* (µm)**	***Rz* (µm)**	**Time, h**
Before postprocessing		13.82	48.86	
Trad. mass finishing	A	0.09	0.83	12+
	B	0.07	0.58	12+
Chemically assisted	A	0.07	0.67	1+
	B	0.12	0.97	1+
MMP TECHNOLOGY®	A	0.30	3.24	n.d.
	B	0.11	1.03	n.d.

7.3. Conclusions

The required *Ra* values of less than 0.4 µm were successfully achieved by the three distinct post-processing techniques. In comparison to the chemically assisted process, the conventional surface mass finishing method required a longer processing time, yet resulted in a smaller material removal. The limiting factor for mass finishing processes is the presence of deep valleys on the surface. The preferential mechanical abrasion of peaks by the media results in their retention on the surface at the conclusion of the process. In contrast, chemically assisted surface finishing (Fig. 6.4.) and, presumably, MMP TECHNOLOGY® facilitate significantly higher material removal. In this instance, the external surface layers, which are most susceptible to defects, can be entirely removed, thereby mitigating issues related to the presence of valleys.

8. COMPARISON OF THE MANUFACTURING: NOVEL TECHNOLOGY VERSUS CONVENTIONAL

The comparison of conventional and novel technologies can give more wider view on advantages and disadvantages of each technology, give to reader insight which sometimes looks invisible, but in reality is significant. As one of most driving criteria is the manufacturing time, indirectly it impacts significant part of fabrication expenses. In current case study the quarter sector of the AM RFQ was printed at Fraunhofer IWS on a TRUMPF Truprint 1000 Green Edition machine in a time of 16 hours and 29 minutes, with a total of 3267 layers, each with a layer thickness of 30 µm. As a result, it is possible to calculate the average time for a layer manufacturing cycle, which includes exposure and coating operations:

$$T_{\mathrm{La}} = T_{\mathrm{T}}/n_{\mathrm{L}}, \tag{8.1.}$$

where T_{La}– average time for single layer cycle, s

T_{T} – total time of build, s

n_{L} – number of layers,

Number of layers can be calculated:

$$n_{\mathrm{L}} = H_{\mathrm{T}}/H_{\mathrm{L}}, \tag{8.2.}$$

where H_{T} – total height of build, mm

H_{L} – layer thickness, µm

Accordingly, the 1/4 RFQ prototype required 18.16 seconds for a single-layer cycle. Furthermore, the average build speed was calculated using the value from the model volume, which can be readily extracted from CAD software. Ultimately, the actual AM machine productivity for the Cu-ETP/OFE material prototype is:

$$V_{\mathrm{bs}} = V_{\mathrm{T}}/T_{\mathrm{T}}, \tag{8.3.}$$

where V_{T} – CAD model volume, cm^3

Consequently, the mean volume build speed was determined to be 4.82 cm^3/min. It should be noted, however, that this is merely an indicative value, and that build speed can vary depending on layer thickness, scanning speed, and percentage of exposed surface. Indeed, the TRUMPF Truprint 1000 Green Edition machine is capable of a build speed of up to 25 cm^3/h, which is approximately five times faster than the speed at which the RFQ sample was built. It should be noted that the actual build rate incorporates exposure and

coating phases and is contingent upon system configuration, process parameters, material, and the volume of the build chamber that is filled.

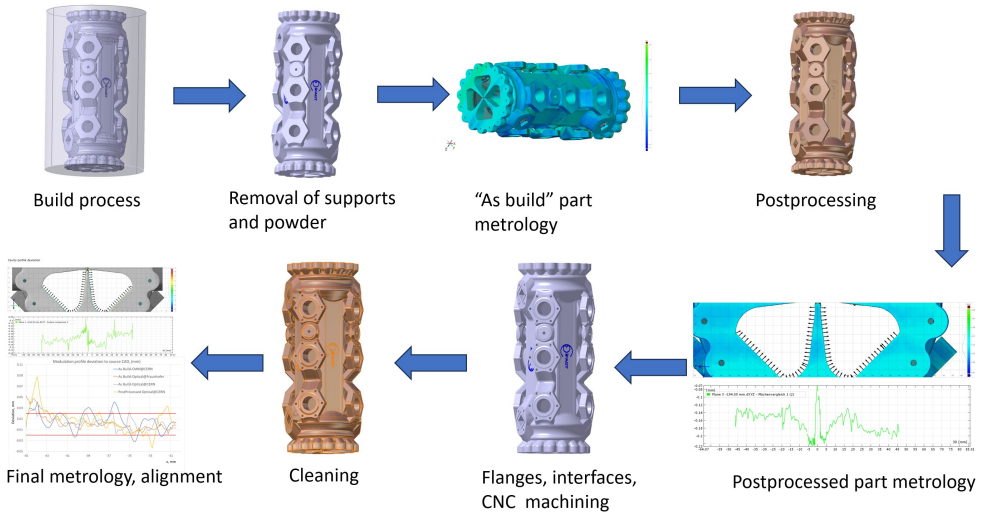

Fig. 8.1. The steps for novel manufacturing technology of RFQ.

Table 8.1.

Comparison of Conventional and AM Manufactured RFQ

Parameter	Conventional	Novel	Improvement, %
Manufacturing time, months	16*	4**	400
Material waste, %	70	2.5	2800
Number of manufacturing substeps	52***	15	346
Weight****, kg/m	67.5	55	18.6
Geometric accuracy	100 %	90 %	– 10
Cooling performance by Δ_L, μm	$0.8329T_C - 18.324$	$0.5665T_C - 12.46$	32
Quality factor Q_{2D}	8028.51	8254.51	2.6

* value from ELISA project for PIXE RFQ;
** empirical values based on IFAST WP10 activities;
*** PIXE technology;
**** weight calculation for full RFQ sector/brazed unit.

Subsequently, the theoretical time required to construct the full-size AM RFQ section with a single laser source machine can be calculated by multiplying the quarter-sector value by four to obtain the full sector, and then by 5.3 to obtain the full length section. Ultimately, the estimated time is 349.8 hours, which is equivalent to 14 days and 13.8 hours. It is also necessary to allow for the time required for de-powdering, removal from the machine, build-plate preparation, support removal and transfer to the post-processing facility, which can collectively take up to one working day. The part should then be transported to the surface improvement facility, where a single, well-organised

and developed post-processing cycle, in an optimistic scenario, can take up to 24 hours. Following this, the metrology inspection is critical for the final flange and port machining.

Conventional manufacturing technology at CERN were developed and described by S. Mathot [96].

Conclusions. It is evident that AM offers substantial benefits over conventional manufacturing, particularly in terms of reduced setups and transportation between diverse manufacturing sites, machines, and facilities throughout the manufacturing process. The novel manufacturing approach replaces the majority of the initial nine steps of conventional machining with three principal construction steps, thereby reducing the potential for human error. Consequently, the AM monolithically built estimate is over three times shorter in terms of machining/manufacturing time than that of a constructed conventionally. The AM-RFQ manufacturing time is estimated based on the data and values obtained in this research.

9. OTHER TECHNICAL VALIDATION TESTS

Within scope of prototype development additional test procedures to validate AM technology applicability were carried out during the research:

HV holding tests. In order to fathom and evaluate behaviour of AM manufactured parts in high voltage field, voltage holding tests were planned and executed, experiments were planned on sample Cu-ETP electrodes, built from same material as RFQ quarter sector. In total several series of tests were planned. Initial tests started from non-postprocessed raw printed electrode pieces for investigation of voltage holding characteristics for raw printed geometry and final experiments with mirror smooth surface and perfect shape geometry. The design of electrodes is adapted for high voltage testing device, which mostly is used for beam electrode tests for CLIC experiment see Fig. 9.1.. The initial tests showing the capability of AM electrodes to hold high vacuum levels and high electric fields with low breakdown rates, approving AM to be a valid candidate for accelerator component manufacturing. The electrodes were tested with two gap heights – 270 µm and 115 µm. The number of breakdowns and breakdown rate are found to be even lower than for a reference of a standard, oxygen free, heat-treated copper electrodes. During the tests, slower conditioning was applied compared to the reference, using approximately twice as many pulses. A stable, electric field of 40 MV/m was reached with the smaller gap height of 115 µm (Table 6.1.).

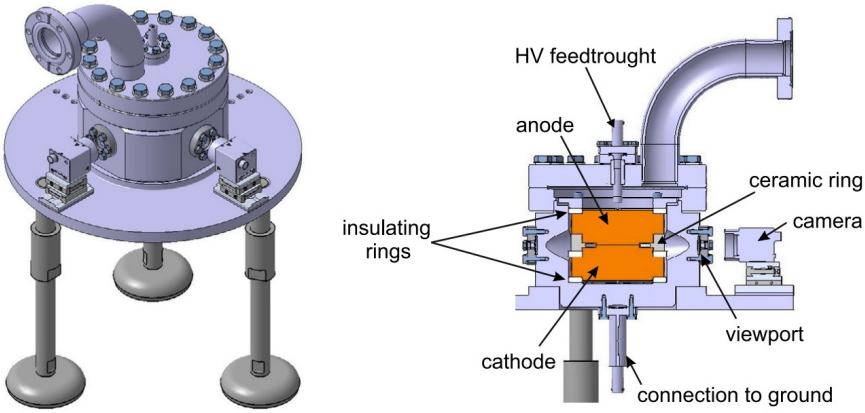

Fig. 9.1. Voltage holding large electrode system (LES) model [116].

He leakage tests. Vacuum tightness is parameter, which mostly is applied to parts for high energy physics. However this parameter is directly related to manufactured product quality – density and porosity. The parts which are designed for HEP purpose mostly must be useable in high or ultrahigh vacuum enviroment as well as must have excellent outgasing parameters. The most simple way to get idea about built object conformity to physics enviroment is to build test vacuum membranes for ISO KF flanges,

those are often used for testing of additively manufactured material and build quality. This step helps to avoid expenses due to fails of vacuum tightness level. Most often practice is manufacture samples with different wall thickness and build angle, and test them afterward.was successfully run for pure copper membranes built by AM with a green laser source (wavelength of 515 nm), with varied wall thicknesses and build angles. Membranes in all wall thicknesses down to 0.5 mm were successfully built with the green laser system. The test conclusions drawn that.

- The green laser source is applicable for thin wall up to 0.5 mm UHV applications.
- 1 mm wall thickness can provide UHV leak tightness in all three applied build angles (90°; 67° and 45°).
- 0.5 mm wall thickness samples deserve more accurate investigation before drawing concluding results. AM technology can be applied to accelerators and vacuum systems that are operating at room temperatures, such as linear accelerators, beam transfer lines and injectors with larger designing flexibility.

Conductivity tests. For additive manufactured samples were accomplished in PoliMi (Milan) labs [117]. The general conclusions were highlighted on test results.

- Almost fully dense and defect free pure copper parts were successfully manufactured by PBF/LB/M using both high–power infrared and "green" laser sources.
- The nature of the laser source does not significantly affect the mechanical, thermal, and electrical properties of pure copper processed through PBF-LB when optimal processing parameters are selected.
- The roughness of planar surfaces of "as build" parts can be significantly reduced by using abrasive media, but chemical solutions are also needed to achieve a good finish in hard-to-reach areas.
- slightly lower electrical and thermal properties were found in the transversal direction than in the build direction, due to process-induced microstructural anisotropy. However, values above 90 % of the copper standard were achieved.

10. VALIDATION OF RESULTS AND ANALYSIS

Validation of AM technology for manufacturing high-precision geometry surface roughness quality is critical to proving the hypothesis on AM applicability for accelerator parts. If AM technology can be tuned to the same accuracy level to build the parts as conventional precision machines, it will create significant technological acceleration in industrial and medical applications. Already at the first steps of the Thesis was identified a set of target parameters for the AM prototype (Table 6.1.). However, additional data, which are significant in proving the advantages of additively manufactured parts, were found during the research. The final list of validation parameters is based on general requirements, and several specific ones were added during development. All output results and validation parameters are collected in Table 10.1. for main geometrical and surface roughness validation, and second Table 10.2. for other crucial parameters.

Table 10.1.
Requirements and Result Validation of HF- RFQ Prototype Geometry and Surface Roughness

Challenge	Target	Result	Compliance
Geometrical accuracy for "as build" part:			
on vane tip,	$\leqslant$ 20 µm	20 µm	with compensation
elsewhere on cavity	$\leqslant$ 100 µm	75 µm	with compensation
Vane shape	$\pm$ 5 µm	$\pm$ 5 µm	with compensation
Vane relative position	$\pm$ 15 µm	$\pm$ 10 µm	with compensation
Cavity shape	$\pm$ 20 µm	–	with compensation
Displacement max $(X - Y)$	$\pm$ 50 µm	–	with compensation
Surface roughness profile R_a for all inner surfaces	$\leqslant$ 0.4 µm	$\approx$ 15 µm	none
Geometrical accuracy for post-processed part:			
on vane tip,	$\leqslant$ 20 µm	25 µm	with compensation
elsewhere on cavity	$\leqslant$ 100 µm	80 µm	with compensation
Vane shape	$\pm$ 5 µm	$\pm$ 5 µm	with compensation
Vane relative position	$\pm$ 15 µm	$\pm$ 15 µm	with compensation
Cavity shape	$\pm$ 20 µm	–	with compensation
Displacement max $(X - Y)$	$\pm$ 50 µm	–	with compensation
Surface roughness profile R_a for all inner surfaces	$\leqslant$ 0.4 µm	$\leqslant$ 0.4 µm	fully

The result values of geometrical accuracy and surface roughness were obtained from a series of metrological measurements at Rösler Italiana Srl. and CERN EN-MME Metrology labs, as well as from additional analysis carried out in the ZEISS GOM Inspect'2022 environment.

Table 10.2.
Requirements and Results of 1/4 RFQ Prototype Secondary Research Parameters

Requirements	Target	Result	Compliance
Measured parameter:			
Electrical conductivity % of pure copper IACS	$\geqslant$ 90%	$\geqslant$ 99%	fully
Simulated parameters:			
Max temperature difference	$\leqslant$ 8.9°C	3.1 °C	fully
Max temperature difference on tip	$\leqslant$ 8.9 °C	0.9 °C	fully
Max total deformation	$\leqslant$ 7.3 µm	1.8 µm	fully
Max total deformation on tip	$\leqslant$ 7.3 µm	0.98 µm	fully
RFQ cavity shape Q value	$\geqslant$ 8028	8254	fully

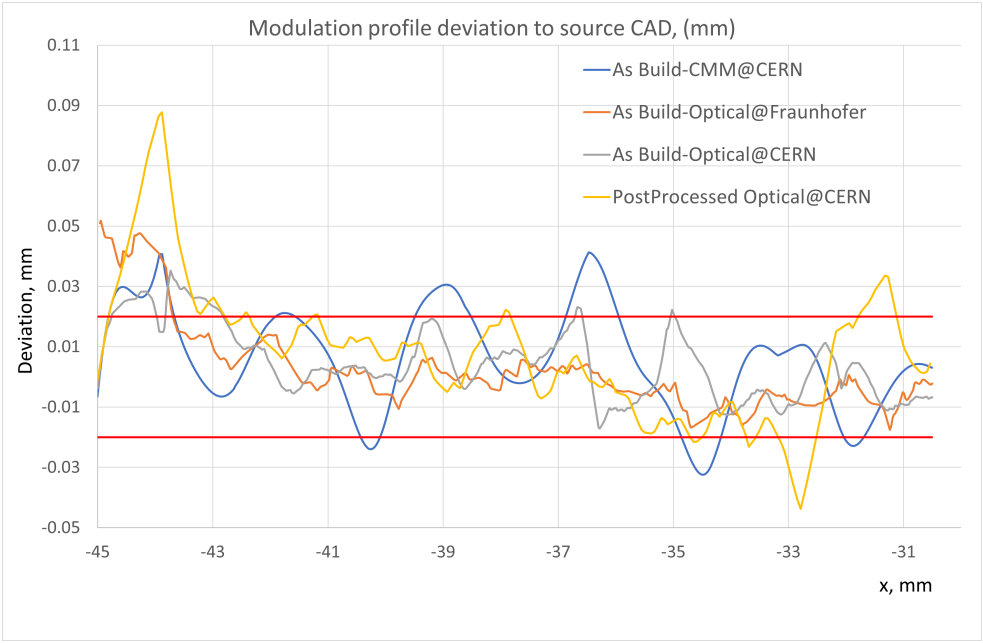

Fig. 10.1. Indicative metrology results for AM build RFQ vane tip modulation deviation.

Vane tip, vane, and cavity measurement analysis gives a comprehensive picture that on surface regions where STL mesh does not have sharp triangulation edges, geometrical accuracy measured by two different methods – CMM and optical, is remarkably close to requirements, but in regions where STL mesh triangulation has relatively narrow and sharp edges with angles smaller than 120° "green laser" spot size 200 µm physically is not able to copy contours in range of 20 µm accuracy (Fig. 10.1.). PBF-LB technology, as well as further post-processing, is giving additional surface deviation error, which in some areas

is higher than the set target for the vane tip area, which also is characterised by yellow deviation line in Fig. 10.1.. Technically, this means that surface STL mesh triangulation for vane tip and cavity curved areas must have a larger curvature radius than "green laser" melt pool radii. In addition, post-processing magnifies deviation values on sharp edges. This phenomenon has a simple and obvious explanation: small and sharp edges during post-processing will be smoothed at the initial process stage. In general Fig. 10.1. is showing that CMM and optical 3D scanning techniques are giving highly similar and repeatable results as well as shows post-processing impact on surface deviation. In fact post-processing is giving significant improvement in roughness, but small radii inner and outer edges still are challenging due to relatively large laser beam spot size. There need to mention that in metrology result graph is well visible slope of deviation along lenght of prototype, which can be explained as thermal shrinkage and impact of fact that first build layers are constrained to 316L solid body build plate.

Values of electrical conductivity for AM samples were tested at Fraunhofer IWS (Dresden) and PoliMi (Milano) [117] and are practically identical to pure copper C10100 values.

For analysis of vane, vane tip modulation and cavity surface profile deviations between measured point cloud and original CAD models standard descriptive statistics were applied. General descriptive statistics formulas were used to calculate arithmetic mean:

$$\overline{x} = \frac{x_1 + x_2 + x_3 + ... + x_\mathrm{n}}{n}, \tag{10.1.}$$

where standard deviation:

$$s = \sqrt{\frac{1}{n-1}\sum_{i=1}^{n}(x_\mathrm{i} - \overline{x})^2}, \tag{10.2.}$$

where standard error value:

$$SE = \frac{\sqrt{\frac{1}{n-1}\sum_{i=1}^{n}(x_\mathrm{i} - \overline{x})^2}}{\sqrt{n}}, \tag{10.3.}$$

where skewness:

$$Sk = \frac{n}{(n-1)(n-2)}\sum\left(\frac{x_\mathrm{i} - \overline{x}}{\sqrt{\frac{1}{n-1}\sum_{i=1}^{n}(x_\mathrm{i} - \overline{x})^2}}\right)^3, \tag{10.4.}$$

where kurtosis:

$$Ku = \left\{ \frac{n(n+1)}{(n-1)(n-2)(n-2)} \sum \left(\frac{x_\mathrm{i} - \overline{x}}{\sqrt{\frac{1}{n-1} \sum_{i=1}^{n} (x_\mathrm{i} - \overline{x})^2}} \right)^4 \right\} - \frac{3(n-1)^2}{(n-2)(n-3)}, \quad (10.5.)$$

95 % confidence interval:

$$CI = \overline{x} \pm (1.96 \times SE) \quad (10.6.)$$

Table 10.3.
Descriptive Statistics Parameters for Vane Tip Modulation Measurements

Parameter	"As-built" short section		Scan.vs.Scan.	Optical long section	
	Optical	CMM	"As-built"	"As-built"	Postprocessed
Mean	–0.00025	0.03315	–0.00862	–0.02776	–0.014
Standard Error	0.000235	0.000208	0.000136	0.0003538	0.000757
Median	–0.00033	0.032655	–0.00879	–0.02770	–0.0108
Mode	0.000186	0.027824	–0.0287	–0.02838	0.00189
Standard Deviation	0.00969	0.014434	0.01080	0.01582	0.02045
Sample Variance	0.000094	0.0002083	0.0001168	0.0002503	0.000418
Kurtosis	0.9641	–0.59378	0.8337	–0.4778	0.1326
Skewness	0.2034	0.19665	–0.1776	0.1092	–0.3719
Range	0.05888	0.07511	0.07905	0.0807	0.1077
Minimum	-0.02526	0.004182	-0.04988	–0.065125	–0.0638
Maximum	0.03361	0.079292	0.029168	0.015658	0.0439
Sum	–0.4228	159.583	–54.0736	–55.503938	–10.225
Count	1691	4814	6268	1999	730
Largest	0.03361	0.079292	0.029168	0.015658	0.0439
Smallest	–0.02526	0.004182	–0.04988	–0.065125	–0.0638
Confidence Level(95.0%)	0.0004624	0.0004078	0.000267	0.0006939	0.001486

Descriptive statistics calculations were calculated in MS Excel environment, the results for "as-built" and post-processed parts were extracted from CMM and optical scan output files, which were processed in CATIA and ZEISS GOM Inspect environments and further summarized in Tab. 10.3.

Thermal and structural performance values were obtained from ANSYS Steady-State Thermal and Static Structural simulations. In case of improved design model maximal temperature and deformation values of sample relocated from vane tip area to periphery of cavity which gives less distortion on most critical region(vane tip) and therefore converging to minimized loss of theoretical performance and stability. See colormap of temperature distribution and deformation presented in Fig. 5.7..

The last value in the result validation Table 10.1. is RFQ cavity shape statistic quality value Q, which normally is starting point for new RFQ design. In the Thesis Q value is

used as quality evaluation value, which is 2.81 % higher than standard HF-RFQ's quality value.

11. CONCLUSIONS

The study has demonstrated that AM can facilitate a substantial advancement in the fabrication of an RFQ through the integration of PBF-LB/M and the application of adopted post-processing technologies. Contemporary advancements in powder bed fusion present a valuable opportunity to enhance the manufacturing processes and design of the RFQ, while simultaneously reducing the machining duration and associated expenses. The present Thesis research has yielded the following findings:

1. AM technology is particularly **well suited to the mechanical complexity of accelerator components**. When combined with the latest processing developments, it offers significant design and optimisation freedom that cannot be achieved by conventional manufacturing technology. Furthermore, **AM technology allows for a reduction in manufacturing time from 16 to 4 months due to a reduction in the number of machining operations by a factor of four**.

2. **The external and internal shapes of the RFQ were successfully optimised**. For instance, the lightened RFQ structure was developed by using lattice structures as honeycomb patterns, whereby the most massive sections were replaced in regions where full material density was not required. The minimum acceptable **wall thickness of 0.5 mm for stable lattice structures and 1.5 mm for helium leak tightness were achieved**.

3. The shape and topology of **the RFQ cooling channels were significantly enhanced in accordance with the optimal thermal management and static structural simulations**. The conventional manufacturing constraints are no longer a limiting factor in cooling channel configurations. The steady-state thermal and static structural simulations conducted by utilising Superfish heat flux calculations, demonstrated that **thermal distortions in the AM prototype exhibit a 32 % advantage in average performance and exceed 100 % in the beam axis area under identical conditions**.

4. The case study demonstrates that the implementation and optimisation of the honeycomb structure and cooling channels result in **a substantial reduction in weight, amounting to approximately 37 % (approximately 21 % and 16 %, respectively)**. However, certain design limitations exist with regard to wall overhangs, closed pockets and powder removal solutions.

5. The **pure copper HF-RFQ prototype** quarter-sector, with a length of 95mm, was constructed using an L-PBF/M system equipped with a green laser. **The manufacturing process was completed in 16 hours and 29 minutes, with 3267 layers and 30 µm layer thickness settings**. The successful production of the prototype validated the viability of industrial manufacturing.

6. The surface roughness measurements for the **"as-built"** model indicated that the prototype surface roughness quality is still far from the required Ra = 0.4 µm. The **surface arithmetical mean roughness average** (Ra) **was measured as 14.32 µm, and the ten-point irregularities value** (Rz) **as 116.7 µm**. However, these results are encouraging since they were obtained without the unique adaption of the AM technological process for improved surface roughness outputs.

7. The **geometrical accuracy measurements after post-processing revealed promising results** – with the standard AM PBF-LB method **approaching the required accuracy of 20 µm on the vane tip and fully reaching 100 µm on other surfaces**. The highest deviation of 0.31 mm on the vane tip can be attributed to a technological glitch – distortion of the support during the built process and stl file meshing quality. Moreover, there still is vast potential to reach a higher level of accuracy by distortion compensations and tuned laser beam scanning approaches.

8. Significant AM technology advantage is the **ease of free-form manufacturing and single set-up build for complex shape parts**. This allows to avoid assembly misalignment during the brazing stage. This advantage is also given the option for improvement of cavity Q factor as no more brazed seams are needed. In current research static Q value of the RFQ, **cavity was improved by 2.81 %** by implementing smoother cavity shape transitions.

9. **The geometrical model for static 2-dimensional RFQ cavity quality factor was developed** and tuned for 750 MHz cavities. For design line of 750 MHz RFQ's **mathematical model works with ± 1.5% accuracy**. The model concept can be used and adapted for different size AM RFQ designs.

11.1. Practical recommendations

The current research constitutes a significant step towards developing additive manufacturing technology for the complex accelerator component, the high-frequency radio frequency quadrupole (HF-RFQ). Based on the findings of this study, the following recommendations are proposed to support further developments in this area:

1. While additive manufacturing technology holds **high potential** to become a viable option **for the production of compact-size RFQs**, further research and developments are needed to reach complete "ready to go" technology;

2. Surface **post-processing techniques are critical** for achieving the desired **roughness values of Ra = 0.4 µm** for the RFQ internal surfaces like cavity and vane;

3. The **required level of geometrical precision** of 2 µm for the vane tip and 100 µm for the cavity is a challenging task, and it **can be accomplished by using com-**

pensation techniques, which are applied either during the CAD modelling phase and/or the manufacturing cycle;

4. The current research shows that **additional 3-dimensional compensation**, in the range of 150 µm – 200 µm, **is necessary to compensate radial shrinkage** of the cavity surface and material removal during post-processing.

11.2. Future research challenges

The present study is initial phase of utilizing PBF-LB/M technology for manufacturing of so complex and unique scientific instrument as is RFQ. Further the subsequent stage of advancement must entail the creation and design of a complete sector RFQ prototype on a scale that represents the final product. The technology will entail meticulous physical and metrological examinations to ensure that the prototype meets the predetermined performance specifications. The required tests comprise a comprehensive array of evaluations, including the fabrication of a complete-sector and full–length RFQ, assessments of vacuum integrity and outgassing, evaluations of voltage holding capacity, examination of watertight and safe design, as well assessments of radio frequency performance and the final validation with the beam. These assessments are designed to evaluate the functionality of the RFQ prototype and identify and resolve any potential challenges that may emerge during the development phase. It is therefore essential to engage in thorough planning and meticulous attention to detail throughout the development process to ensure that the RFQ prototype meets the essential performance specifications and is suitable for practical implementation.

LIST OF TABLES

LIST OF FIGURES

BIBLIOGRAPHY

[1] S. A. Johansson, J. L. Campbell, and K. G. Malmqvist, *Particle-induced X-ray emission spectrometry (PIXE)*. Wiley New York, 1995, vol. 133.

[2] M. Vretenar, "Applications of Particle Accelerators in Europe," CERN, Report, 2017. [Online]. Available: http://apae.ific.uv.es/apae/wp-content/uploads/2015/04/EuCARD_Applications-of-Accelerators-2017.pdf.

[3] E. Wilson, E. J. Wilson, and E. Wilson, *An introduction to particle accelerators*. Clarendon Press, 2001.

[4] F. Taccetti, "MACHINA, the Movable Accelerator for Cultural Heritage In-situ Non-destructive Analysis: project overview," *Rendiconti Lincei. Scienze Fisiche e Naturali*, 2023. [Online]. Available: https://flore.unifi.it/retrieve/df364629-4bda-42b5-96d7-b3f7f0468046/2023%20-%20machina.pdf.

[5] S. Hanna, *RF linear accelerators for medical and industrial applications*. Artech House, 2012.

[6] A. W. Chao, K. H. Mess, *et al.*, *Handbook of accelerator physics and engineering*. World scientific, 2013.

[7] R. Gerard. "Additive manufacturing for accelerators components," CERN. (2016), [Online]. Available: https://indico.cern.ch/event/438866/contributions/1085192/attachments/1256338/1854748/AdditiveManufacturingforAcceleratorsComponents_FCCWEEK16.pdf.

[8] R. Jemghili, A. A. Taleb, and K. Mansouri, "Additive Manufacturing Progress as a New Industrial Revolution," in *2020 IEEE 2nd International Conference on Electronics, Control, Optimization and Computer Science (ICECOCS)*, IEEE, 2020, pp. 1–8.

[9] U. M. Dilberoglu, B. Gharehpapagh, U. Yaman, and M. Dolen, "The role of additive manufacturing in the era of industry 4.0," *Procedia Manufacturing*, vol. 11, pp. 545–554, 2017.

[10] E. Toyserkani, *Metal Additive Manufacturing*. 2021. [Online]. Available: https://www.wiley.com/en-cn/Metal+Additive+Manufacturing-p-9781119210832.

[11] "Metals." (Oct. 26, 2022), [Online]. Available: https://www.britannica.com/science/metal-chemistry.

[12] "Metal industries." (2022), [Online]. Available: https://single-market-economy.ec.europa.eu/sectors/raw-materials/related-industries/metal-industries_en.

[13] "Joint Accelerator Conferences Website." (2022), [Online]. Available: https://www.jacow.org/.

[14] D. I. Wimpenny, P. M. Pandey, L. J. Kumar, *et al.*, *Advances in 3D printing & additive manufacturing technologies*. Springer, 2017.

[15] C. L. Weber, V. Peña, M. K. Micali, *et al.*, "The role of the national science foundation in the origin and evolution of additive manufacturing in the united states," *Science & Technology Policy Institute*, vol. 1, pp. 1–175, 2013.

[16] W. Gao, Y. Zhang, D. Ramanujan, *et al.*, "The status, challenges, and future of additive manufacturing in engineering," *Computer-Aided Design*, vol. 69, pp. 65–89, 2015.

[17] "Horseshoe." (1899), [Online]. Available: https://patentimages.storage.googleapis.com/74/00/41/99b14da4df2c25/US632423.pdf.

[18] R. Baker, "Method of Making Decorative Articles," US1533300, Apr. 14, 1925.

[19] L. Yang, K. Hsu, B. Baughman, *et al.*, *Additive manufacturing of metals: the technology, materials, design and production*. Springer, 2017.

[20] "Metal Additive Manufacturing History." (2019), [Online]. Available: https://additive-manufacturing-report.com/technology/metal/metal-additive-manufacturing-history/.

[21] "Wohlers associates." (2022), [Online]. Available: https://wohlersassociates.com/company/.

[22] T. Wohlers, I. Campbell, O. Diegel, J. Kowen, and N. Mostow, "Wohlers report 2022: 3d printing and additive manufacturing global state of the industry," *Wohlers Associates, Fort Collins, Colorado*, 2022.

[23] J. O. Milewski, *Additive manufacturing of metals*. Springer, 2017, vol. 258.

[24] ISO/ASTM, Ed., *ISO/ASTM 52900:2021(en) Additive manufacturing — General principles — Fundamentals and vocabulary*, 2021. [Online]. Available: https://www.iso.org/obp/ui/#iso:std:iso-astm:52900:ed-2:v1:en.

[25] ISO, *17296-2, 2015 Additive manufacturing: Overview of process categories and feedstock, Geneva, Switzerland*.

[26] "eBook 12: Additive Manufacturing: Metallurgy, Cut Analysis & Porosity, Additive Manufacturing Process Classification, Applications, Trends, Opportunities, and Challenges." (2022), [Online]. Available: https://advancedopticalmetrology.com/additive-manufacturing/additive-manufacturing-metallurgy-cut-analysis-porosity.html.

[27] "Copper 3D Printing – The Ultimate Guide." (2022), [Online]. Available: https://all3dp.com/1/copper-3d-printing-the-ultimate-guide/.

[28] J. Liu, "A review of machine learning techniques for process and performance optimization in laser beam powder bed fusion additive manufacturing," *Journal of Inteligent Manufacturing*, Sep. 15, 2022. [Online]. Available: https://doi.org/10.1007/s10845-022-02012-0.

[29] R. Leach and S. Carmignato, *Precision metal additive manufacturing*. CRC Press, 2020.

[30] "AMCM ups the Game in 3D Printed Rockets with World's Biggest Aerospike Engine." (May 17, 2022), [Online]. Available: https://3dprint.com/291291/amcm-ups-the-game-in-3d-printed-rockets-with-worlds-biggest-aerospike-engine/.

[31] "EOS and Hyperganic team up to evelate the design and performance of space propulsion components." (May 10, 2022), [Online]. Available: https://www.eos.info/en/presscenter/press-releases/eos-and-hyperganic.

[32] "Eplus3d ep-m2050." (2024), [Online]. Available: https://www.eplus3d.com/products/ep-m2050-metal-3d-printer/.

[33] R. Hönl, *World premiere at Formnext: green laser from TRUMPF prints copper and gold, TRUMPF Glob. Press Release.(2018)*. [Online]. Available: https://www.trumpf.com/en_US/newsroom/global-press-releases/press-release-detail-page/release/world-premiere-at-formnext-green-laser-from-trumpf-prints-copper-and-gold/.

[34] "Whitepaper TruPrint 1000 Green Edition." (Oct. 2020), [Online]. Available: https://www.apricon.fi/wp-content/uploads/trumpf_whitepaper_truprint-1000_green_3d-printing_copper.pdf.

[35] A. Hess, R. Schuster, A. Heider, R. Weber, and T. Graf, "Continuous wave laser welding of copper with combined beams at wavelengths of 1030 nm and of 515 nm," *Physics Procedia*, vol. 12, pp. 88–94, 2011.

[36] S. Gruber, L. Stepien, E. López, F. Brueckner, and C. Leyens, "Physical and geometrical properties of additively manufactured pure copper samples using a green laser source," *Materials*, vol. 14, no. 13, p. 3642, 2021. [Online]. Available: https://www.mdpi.com/1996-1944/14/13/3642/pdf?version=1625103967.

[37] "Additive manufacturing." (2022), [Online]. Available: https://eurotech-universities.eu/focus-area/focus-area-additive-manufacturing/.

[38] AM-motion, "Analysis of synergies and best practices based in eu, national and regional am projects," CEA, report, Dec. 22, 2017. [Online]. Available: https://rm-platform.com/images/DOCUMENTS/D2.5_EU_National_and_Regional_AM_projects.pdf (visited on 10/02/2022).

[39] AM-motion, "Report on European and national initiatives and RDI programmes," CEA, report, 2017. [Online]. Available: https://rm-platform.com/images/DOCUMENTS/AM_Inititatives_and_RDI_programmes.pdf.

[40] "Additive Manufacturing Aiming Towards Zero Waste and Efficient Production of High-Tech Metal Products." (2017), [Online]. Available: https://cordis.europa.eu/project/id/313781.

[41] "Precision Additive Metal Manufacturing." (2021), [Online]. Available: https://pam2.eu/.

[42] "Community Research and Development Information Service." (1994), [Online]. Available: https://cordis.europa.eu/about/en.

[43] "Driving up reliability and efficiency of additive manufacturing." (2016), [Online]. Available: https://www.dream-euproject.eu/.

[44] "Additive manufacturing using metal pilot line." (2018), [Online]. Available: https://manuela-project.eu/.

[45] "Novel Fabrication Techniques for the Production of RF Photoinjectors." (2007), [Online]. Available: https://www.sbir.gov/node/287453.

[46] L. Waganer, D. Deuser, K. Slattery, G. Wille, F. Arcella, and B. Cleveland, "Ultra-low cost coil fabrication approach for ARIES-ST," *Fusion Engineering and Design*, vol. 65, no. 2, pp. 339–352, 2003.

[47] L. M. Waganer, K. T. Slattery, J. C. Waldrop III, and A. Team, "ARIES-CS coil structure advanced fabrication approach," *Fusion science and technology*, vol. 54, no. 3, pp. 878–889, 2008.

[48] P. Frigola, R. Agustsson, S. Boucher, *et al.*, "A novel fabrication technique for the production of RF photoinjectors," *Proceedings of EPAC08*, pp. 13–27, 2008.

[49] P. Frigola, R. Agustsson, S. Boucher, *et al.*, "Development of solid freeform fabrication (SFF) for the production of RF Photoinjectors," in *Particle Accelerator Conference*, 2009.

[50] L. Faillace, L. Palumbo, B. Spataro, *et al.*, "An Ultra-high repetition rate S-band RF Gun," in *FEL Conference*, 2008.

[51] R. Veness *et al.*, "Design of a High-Precission Fast Wire Scanner for the SPS at CERN," in *IBIC2012: Proceedings of the 1st International Beam Instrumentation Conference*, 2012.

[52] S. Samuelsson, "Mechanical optimisation of a high-precision fast wire scanner at CERN," M.S. thesis, 2013.

[53] R. Veness, J. Emery, S. Samuelsson, *et al.*, "Experience from the construction of a new fast wire scanner prototype for the CERN-SPS and its optimisation for installation in the CERN-PS booster," 2016.

[54] P. Kilburn, "Overview of Additive Manufacturing and Materials," *CERN, Zurich, Switzerland*, p. 76, 2012.

[55] "Metallic Additive Manufacturing@CERN." (2014), [Online]. Available: `https://indico.cern.ch/event/333735/contributions/779099/attachments/651316/895585/WS_AM_05112014_V1.pdf`.

[56] P. Frigola, R. Agustsson, L. Faillace, *et al.*, "Development of a CW NCRF Photoinjector using solid freeform fabrication (SFF)," *Proc. IPAC '10*, vol. 100523, pp. 3804–3806, 2010.

[57] "Croft Additive Manufacturing." (Dec. 18, 2013), [Online]. Available: `https://www.cernbic.stfc.ac.uk/Pages/Q-and-A-with-Croft-Additive-Manufacturing.aspx`.

[58] "Additive Manufacturing for X-band applications." (2014), [Online]. Available: `https://indico.cern.ch/event/275412/contributions/1617680/attachments/498818/689089/AG_AdditiveManufacturing4Xband.pdf`.

[59] "Developing an additively manufactured X-band RF load." (Aug. 26, 2014), [Online]. Available: `https://indico.cern.ch/event/320241/contributions/1698172/attachments/617452/849607/Developing_an_X-band_RF_load.pdf`.

[60] N. Catalán Lasheras, G. McMonagle, A. Solodko, *et al.*, "JACoW: High Power Conditioning of X-Band RF Components," Tech. Rep., 2018.

[61] P. Frigola, O. Harrysson, T. Horn, *et al.*, "Fabricating copper components," *Adv. Mater. Process*, vol. 172, pp. 20–24, 2014.

[62] C. Terrazas, S. Gaytan, J. Mireles, P. Frigola, D. Espalin, and R. Wicker, "EBM Fabrication and Characterization of High Purity Niobium for Superconductor Applications," in *2014 International Solid Freeform Fabrication Symposium*, University of Texas at Austin, 2014.

[63] R. Rimmer, "Additive manufacturing method for SRF components of various geometries," US9023765B1, May 5, 2015. [Online]. Available: `https://worldwide.espacenet.com/patent/search/family/053001651/publication/US9023765B1?q=pn%5C%3DUS9023765B1`.

[64] P. Frigola, "Development of Nuclear Quality Components using Metal Additive Manufacturing," RadiaBeam Systems, LLC, Santa Monica, CA (United States), Tech. Rep., 2018.

[65] P. Frigola, R. Agustsson, L. Faillace, *et al.*, "Advance additive manufacturing method for SRF cavities of various geometries," Thomas Jefferson National Accelerator Facility (TJNAF), Newport News, VA ..., Tech. Rep., 2015.

[66] "Workshop "Challenges on Additive Manufacturing for High Energy Physics"." (Nov. 5, 2014), [Online]. Available: https://indico.cern.ch/event/333735/.

[67] G. L. D'Alessandro, "Development of X-band high-power RF load for CLIC applications using additive manufacturing techniques," Salento U., 2015.

[68] A. Grudiev, "Development of X-band RF load using additive manufacturing," CERN CLIC, 2017.

[69] H. Bursali, A. Grudiev, P. Morales Sánchez, *et al.*, "JACoW: X-Band RF Spiral Load Optimization for Additive Manufacturing Mass Production," *JACoW IPAC*, vol. 2021, pp. 1143–1146, 2021.

[70] M. Delonca, "LIEBE project:WP3 – Construction and tests," CERN LIEBE, Geneva, report, Jan. 30, 2015. [Online]. Available: https://indico.cern.ch/event/367917/contributions/1786366/attachments/731476/1003620/Melanie%5C_LIEBE-WP3-coordinationmeeting-30012015.pdf.

[71] R. Gerard, "Metal Additive Manufacturing Overview of the process, mechanical properties and MME facility," CERN MME, report, Jan. 30, 2016. [Online]. Available: https://indico.cern.ch/event/567462/contributions/2293345/attachments/1353055%5C%5C/2044352/PS%5C_DUMPREVIEW%5C_Metal%5C_Additive%5C_Manufacturing%5C_RG.pdf.

[72] S. Jenzer, M. Alves, N. Delerue, *et al.*, "Study of the suitability of 3D printing for ultra-high vacuum applications," in *Journal of Physics: Conference Series*, IOP Publishing, vol. 874, 2017, p. 012 097.

[73] S. Jenzer, D. Auguste, J. Bonis, *et al.*, "Study of the performances of a 3D printed BPM," in *Journal of Physics: Conference Series*, IOP Publishing, vol. 1067, 2018, p. 082 026.

[74] I. Santillana, "Mechanical testing and metallographic observations of tensile specimens manufactured via additive manufacturing," CERN MME, report, Jan. 15, 2014. [Online]. Available: https://edms.cern.ch/ui/%5C#!master/navigator/document?D:1480201714:1480201714:subDocs.

[75] G. Romagnoli. "3D Printing Developments." (2016), [Online]. Available: https://indico.cern.ch/event/567462/contributions/2293345/attachments/1353055/2044370/3D_printing_developments.pdf.

[76] J. Gargiulo. "Vacuum characterisation of 3D printed metals." (May 29, 2017), [Online]. Available: https://edms.cern.ch/ui/file/1905096/1/FCCW_GARGIULO_VC_3DPM_pptx_cpdf.pdf (visited on 05/29/2017).

[77] M. Sinico, G. Cogo, M. Benettoni, I. Calliari, and A. Pepato, "Influence of powder particle size distribution on the printability of pure copper for selective laser melting," in *Proceedings of the 30th Annual International Solid Freeform Fabrication Symposium–An Additive Manufacturing Conference*, SFF Symposium Proceedings, 2019, pp. 657–667.

[78] M. Bonesso. "SLM Development on Copper and Copper Alloy for Nuclear Fusion Physics (DTT, ITER, DEMO)." (2019), [Online]. Available: https://agenda.infn.it/event/19247/contributions/100154/attachments/66906/82004/BONESSO_-_wokshop_20_settembre_2019_-_Massimiliano_Bonesso.pdf.

[79] C. Torregrosa. "HRMT48-PROTAD Experiment and Relevance for BIDs," CERN. (2018), [Online]. Available: https://indico.cern.ch/event/718767/contributions/3232507/ (visited on 08/07/2022).

[80] "Fabrication Additive au CERN." (2018), [Online]. Available: https://indico.ijclab.in2p3.fr/event/4990/contributions/16695/attachments/13619/16418/I3DMetal_-_AMCERN.pdf.

[81] T. Sahner. "Short Introduction to the AM Technology." (Mar. 27, 2015), [Online]. Available: https://indico.cern.ch/event/383382/attachments/764675/1049011/04_Sahner_AdditiveManufacturing_27032015.pdf.

[82] DIAM. "Developments and Innovations on Additive Manufacturing." (2016), [Online]. Available: https://www.pd.infn.it/eng/diam/.

[83] N. Cooper, L. Coles, S. Everton, *et al.*, "Additively manufactured ultra-high vacuum chamber for portable quantum technologies," *Additive Manufacturing*, vol. 40, p. 101 898, 2021.

[84] "First survey results: "Accelerator community response to the use of AM in the production and repairs of accelerator components"." (2022), [Online]. Available: https://indico.cern.ch/event/1143029/contributions/4833040/attachments/2438862/4177453/I.FAST_Workshop_A.Ratkus.pdf.

[85] G. Pikurs, "Additive manufacturing applied to particle accelerators," IJCLab, report, Mar. 18, 2022. [Online]. Available: https://indico.cern.ch/event/1126958/contributions/4730216/attachments/2393754/4124387/I.FAST_Paris_G.pdf.

[86] "Additive Manufacturing applied to Particle Accelerators." (2022), [Online]. Available: https://indico.cern.ch/event/1133254/contributions/4853087/attachments/2438320/4176612/I.FAST_1st_Annual_WS_GP_ND.pdf.

[87] J. Han, " Investigation on the formation of surface defects of OFHC copper in diamond micro-grooving process," *Int J Adv Manuf Technol*, 2017. DOI: https://doi.org/10.1007/s00170-017-0848-2. [Online]. Available: https://link.springer.com/article/10.1007/s00170-017-0848-2#preview.

[88] "Recommended machining parameters for copper and copper alloys." (2010), [Online]. Available: https://www.copper.org/applications/marine/cuni/pdf/DKI-Machining.pdf.

[89] M. Vretenar. "Compact Radio Frequency Quadrupoles for medical and industrial applications." (Mar. 9, 2018), [Online]. Available: https://indico.cern.ch/event/686876/contributions/2817924/attachments/1614164/2564508/compact_RFQ_KT_03_18.pdf.

[90] H. W. Pommerenke, "Compact Radio-Frequency Quadrupoles for Industrial and Medical Applications," Ph.D. dissertation, Universität Rostock, 2020. [Online]. Available: https://rosdok.uni-rostock.de/file/rosdok_disshab_0000002457/rosdok_derivate_0000099121/Pommerenke_Dissertation_2021.pdf.

[91] J. Billen and L. Young, "Poisson Superfish Documentation," *LA-UR*, pp. 96–1834, 1996.

[92] "Materialise Magics 3D Print Suite." (2022), [Online]. Available: https://www.materialise.com/en/industrial/software.

[93] "Technical Specifications MetraSCAN BLACK™—Elite." (Oct. 10, 2022), [Online]. Available: https://www.creaform3d.com/en/optical-3d-scanner-metrascan/technical-specifications.

[94] "ZEISS PRISMO Specifications Version: November 2017." (2017), [Online]. Available: https://www.msiviking.com/documents/ZEISS/CMMs/Specifications_ZEISS_PRISMO.pdf.

[95] M. Dotcheva, J. Favrot, K. Dotchev, and J. Zekonyte, "Planning for metal additive manufacturing," *Procedia Manufacturing*, vol. 51, pp. 710–716, 2020. [Online]. Available: https://doi.org/10.1016/j.promfg.2020.10.100.

[96] S. Mathot. "Manufacturing of the High Frequency RFQ." (2018), [Online]. Available: https://indico.cern.ch/event/686876/contributions/2817925/attachments/1614272/2564777/Manufacturing_of_the_HF-RFQ_v1.pptx.

[97] K. Scibor, "PIXE-RFQ modulation and cavity machining.," [Online]. Available: https://www.euspen.eu/knowledge-base/ICE20189.pdf.

[98] *Private conversation with Serge Mathot(CERN EN-MME)*, 2023.

[99] A. Saillet, K. Scibor, P. Naisson, and S. Atieh, "Evaluation of computer-aided manufacturing software accuracy for high precision machining.& Euspen's 20th International Conference & Exhibition, Geneva, CH, June 2020," 2020. [Online]. Available: https://www.euspen.eu/knowledge-base/ICE20187.pdf.

[100] A. Lombardi, "High frequency compact low-energy linear accelerator design," WO2016023597A1, Feb. 18, 2016. [Online]. Available: https://worldwide.espacenet.com/patent/search/family/051429257/publication/WO2016023597A1?q=WO2016023597A1.

[101] J. L. Warren, G. P. Boicourt, M. T. Menzel, G. W. Rodenz, and M. C. Vasquez, "Revision of and documentation for the standard version of the poisson group codes," *IEEE Transactions on Nuclear Science*, vol. 32, no. 5, pp. 2870–2872, 1985. DOI: 10.1109/TNS.1985.4334210.

[102] K. Halbach, "Superfish a computer program for evaluation of RF cavities with cylindrical symmetry," 1976.

[103] S. Humphries, "Poisson/Superfish codes for personal computers," Tech. Rep., 1992.

[104] G. Pikurs, "Research on design improvement of accelerator components by additive manufacturing," National Centre of Physical and Technological Sciences, report, Oct. 12, 2022. [Online]. Available: https://indico.cern.ch/event/1147717/contributions/5082259/attachments/2526799/4346280/CBC2022_GP.pdf.

[105] T. P. Wangler, *RF Linear accelerators*. John Wiley & Sons, 2008.

[106] "Compact radio frequency quadrupoles for medical and industrial applications." (Mar. 9, 2018), [Online]. Available: https://indico.cern.ch/event/686876/contributions/2817924/attachments/1614164/2564508/compact_RFQ_KT_03_18.pdf.

[107] H. W. Pommerenke and A. Grudiev, "RF Measurements and Tuning of the PIXE-RFQ," 2020. [Online]. Available: https://cds.cern.ch/record/2746335.

[108] S. S. Rao, *The finite element method in engineering*. Butterworth-heinemann, 2017.

[109] H.-H. Lee, *Finite element simulations with ANSYS workbench 2019*. SDC publications, 2019.

[110] N. S. Gokhale, *Practical finite element analysis*. Finite to infinite, 2008.

[111] T. Torims, G. Pikurs, S. Gruber, *et al.*, "First Proof-of-Concept Prototype of an Additive Manufactured Radio Frequency Quadrupole," *Instruments*, vol. 5, no. 4, p. 35, 2021. [Online]. Available: https://doi.org/10.3390/instruments5040035.

[112] S. Möller, *Accelerator Technology: Applications in Science, Medicine, and Industry*. Springer Nature, 2020.

[113] "BINC Industries." (2022), [Online]. Available: https://www.youtube.com/user/BestinClassch/videos.

[114] "Creating more flexibility in production. zeiss bridge-type measuring machines," Carl Zeiss Industrielle Messtechnik GmbH. (2018), [Online]. Available: https://www.tqscorp.com/docs/products/Bridge-Machine-Brochure.pdf.

[115] T. Torims, A. Ratkus, G. Pikurs, D. Krogere, A. Cherif, S. Gruber, *et al.*, "Evaluation of geometrical precision and surface roughness quality for the additively manufactured radio frequency quadrupole prototype," *Proceedings of IPAC2022*, pp. 787–791, 2022. [Online]. Available: https://cds.cern.ch/record/2845877/files/document.pdf.

[116] I. Profatilova, X. Stragier, S. Calatroni, A. Kandratsyeu, E. R. Castro, and W. Wuensch, "Breakdown localisation in a pulsed DC electrode system," *Nuclear Instruments and Methods in Physics Research Section A: Accelerators, Spectrometers, Detectors and Associated Equipment*, vol. 953, p. 163 079, 2020.

[117] T. Romano, "18th I.FAST AM group meeting," PoliMi, report, Nov. 17, 2022. [Online]. Available: https://indico.cern.ch/event/1211623/contributions/5096591/attachments/2549403/4391027/task%2010.2%2013th%20IFAST%20meeting.pdf.

Appendices

1. ANNEX A

MÉTROLOGIE EN-MME-MM

RAPPORT DE CONTRÔLE

EDMS	**2644691**
Job	J3073560
Client	TORIMS Toms
Contrôleur	BULAT Bartosz
Machine	ZEISS Prismo Ultra 12-18-10
Précision des mesures	1,2 µm + L/500mm
Température	20°C ±1°C

Date de la mesure	11/10/2021 13:43
N° de plan	-
Désignation	3D printed AM-RFQ
Fournisseur	-
N° de pièce	**-01-**
Valeurs rouges	11

Commentaire

Nom du programme AM_RFQ

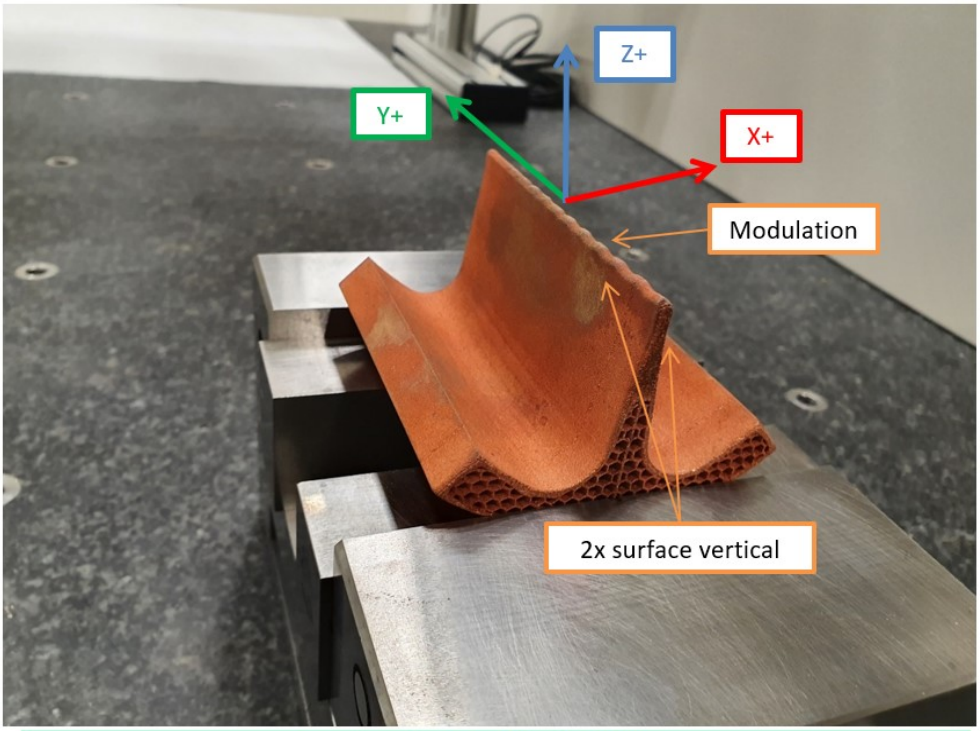

Construction du référentiel de base:

- Orientation primaire: Modulation
- Orientation secondaire: Symetrie 2x surface vertical
- Origine: X = Symetrie 2x surface vertical
  Y = Modulation
  Z = Modulation

EDMS	**2644691**
N° de plan	-
Désignation	3D printed AM-RFQ
N° de pièce	**-01-**
Date/Heure	11/10/2021 13:43

	Nom	Valeur mesurée	Valeur nominale	Tolérance supérieure	Tolérance inférieure	Deviation	+/-
Modulation							
7	FRM-MODULATION	1,1560	0,0000	0,0500	0,0000	1,1560	1,1060
Internal surface							
9	FRM-SURF-INT-1	0,5891	0,0000	0,0500	0,0000	0,5891	0,5391
10	FRM-SURF-INT-2	0,6661	0,0000	0,0500	0,0000	0,6661	0,6161
11	FRM-SURF-INT-3	0,5887	0,0000	0,0500	0,0000	0,5887	0,5387
12	FRM-SURF-INT-4	0,6399	0,0000	0,0500	0,0000	0,6399	0,5899
13	FRM-SURF-INT-5	0,5199	0,0000	0,0500	0,0000	0,5199	0,4699
Modulation surface							
15	FRM-SURF-MOD-1	0,2187	0,0000	0,0500	0,0000	0,2187	0,1687
16	FRM-SURF-MOD-2	0,1400	0,0000	0,0500	0,0000	0,1400	0,0900
17	FRM-SURF-MOD-3	0,1059	0,0000	0,0500	0,0000	0,1059	0,0559
18	FRM-SURF-MOD-4	0,3397	0,0000	0,0500	0,0000	0,3397	0,2897
19	FRM-SURF-MOD-5	0,1277	0,0000	0,0500	0,0000	0,1277	0,0777

EDMS	**2644691**
N° de plan	-
Désignation	3D printed AM-RFQ
N° de pièce	**-01-**
Date/Heure	11/10/2021 13:43

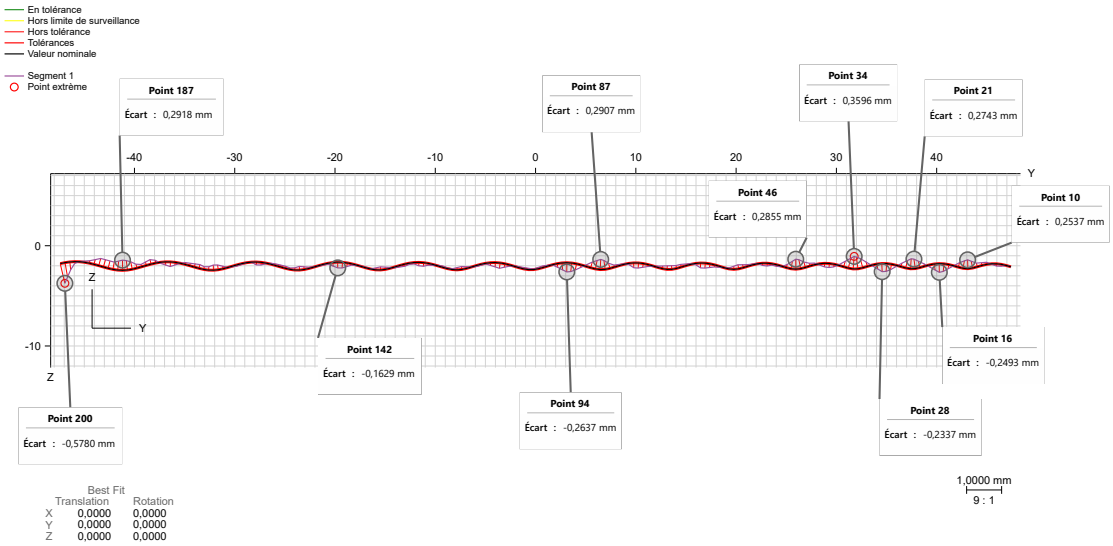

	Nom	Valeur mesurée	Limite supérieure Limite inférieure	Points	Filter type	Lc	Probe radius	Vmess[mm/sec]	Evaluation method
⌒	FRM-MODULATION	1,1560	0,0500 0,0000	200	Gauss	1 -	1,0004	1,000	Direction vecteur nominal

EDMS	**2644691**
N° de plan	-
Désignation	3D printed AM-RFQ
N° de pièce	**-01-**
Date/Heure	11/10/2021 13:43

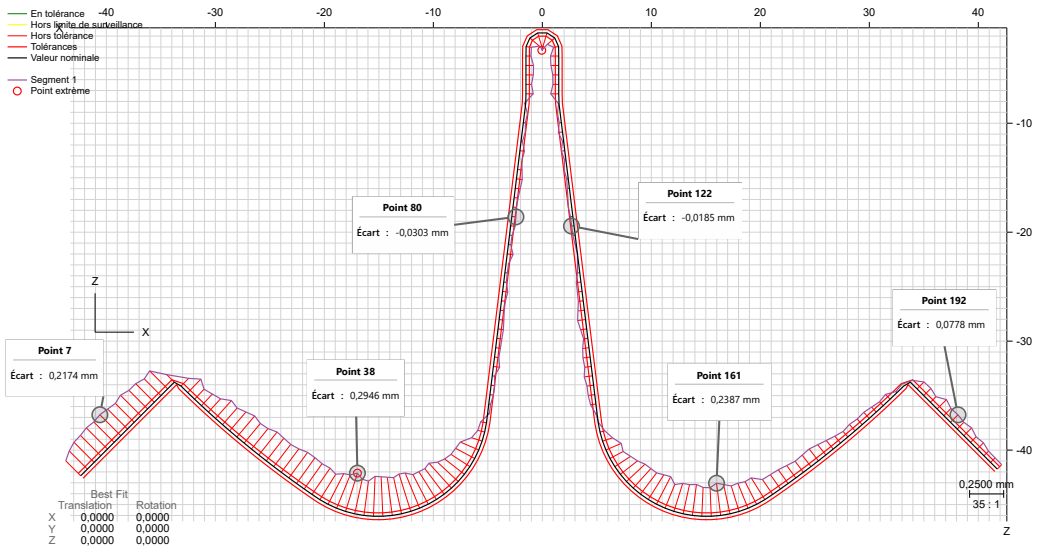

Nom	Valeur mesurée	Limite supérieure Limite inférieure	Points	Filter type	Lc	Probe radius	Vmess[mm/sec]	Evaluation method
FRM-SURF-INT-1	0,5891	0,0500 0,0000	199	Gauss	1 -	1,5008	3,000	Direction vecteur nominal

EDMS	**2644691**
N° de plan	-
Désignation	3D printed AM-RFQ
N° de pièce	**-01-**
Date/Heure	11/10/2021 13:43

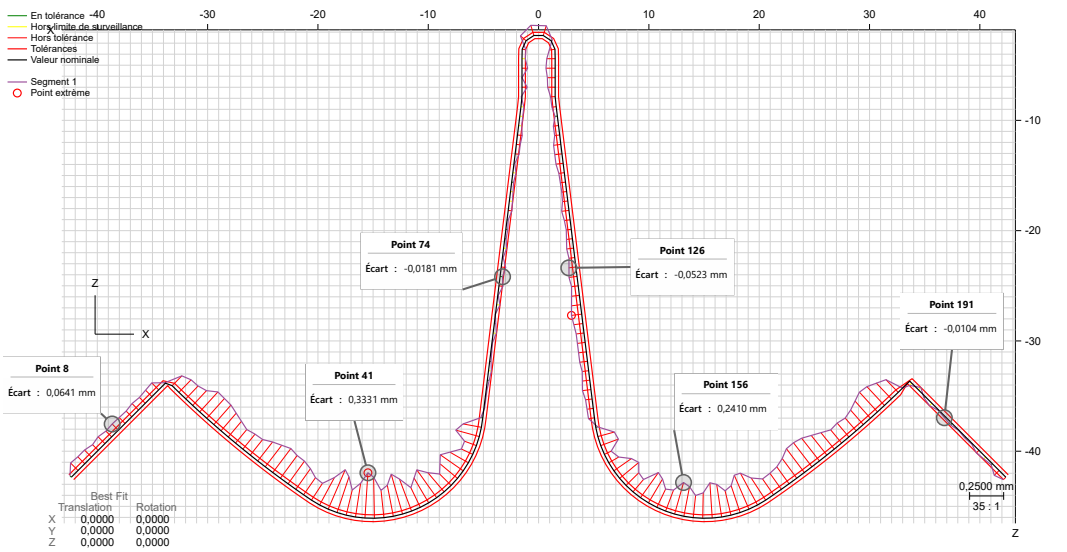

	Nom	Valeur mesurée	Limite supérieure Limite inférieure	Points	Filter type	Lc	Probe radius	Vmess[mm/sec]	Evaluation method
⌒	FRM-SURF-INT-2	0,6661	0,0500 0,0000	200	Gauss	1 -	1,5008	3,000	Direction vecteur nominal

EDMS	**2644691**
N° de plan	-
Désignation	3D printed AM-RFQ
N° de pièce	**-01-**
Date/Heure	11/10/2021 13:43

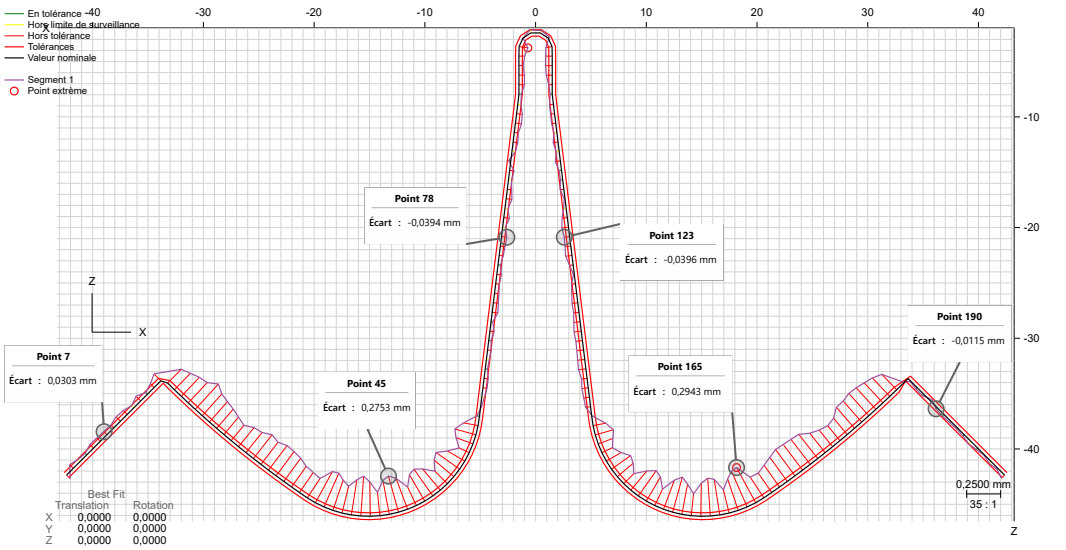

	Nom	Valeur mesurée	Limite supérieure Limite inférieure	Points	Filter type	Lc	Probe radius	Vmess[mm/sec]	Evaluation method
⌒	FRM-SURF-INT-3	0,5887	0,0500 0,0000	200	Gauss	1 -	1,5008	3,000	Direction vecteur nominal

EDMS	**2644691**
N° de plan	-
Désignation	3D printed AM-RFQ
N° de pièce	**-01-**
Date/Heure	11/10/2021 13:43

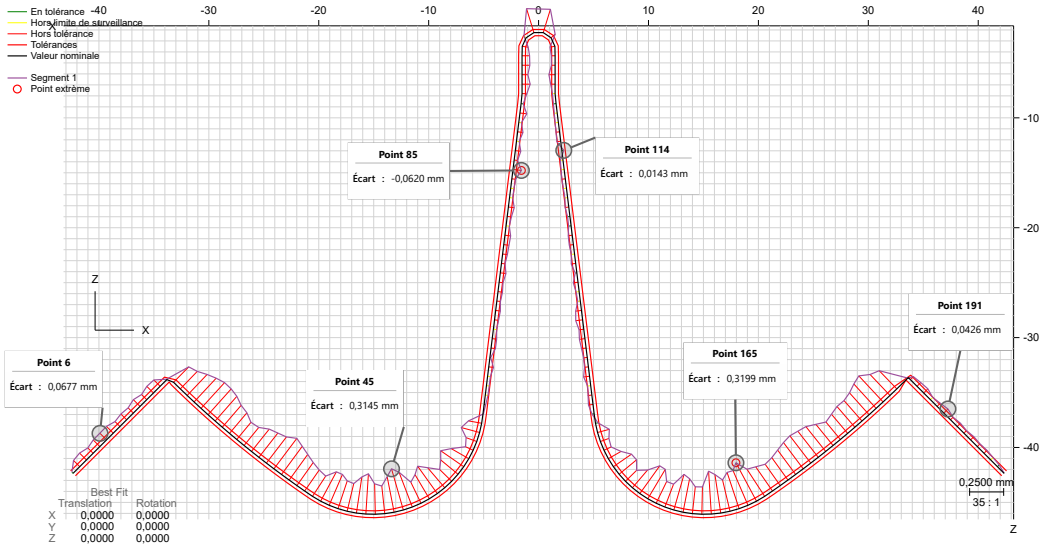

	Nom	Valeur mesurée	Limite supérieure Limite inférieure	Points	Filter type	Lc	Probe radius	Vmess[mm/sec]	Evaluation method
⌒	FRM-SURF-INT-4	0,6399	0,0500 0,0000	200	Gauss	1 -	1,5008	3,000	Direction vecteur nominal

EDMS	**2644691**
N° de plan	-
Désignation	3D printed AM-RFQ
N° de pièce	**-01-**
Date/Heure	11/10/2021 13:43

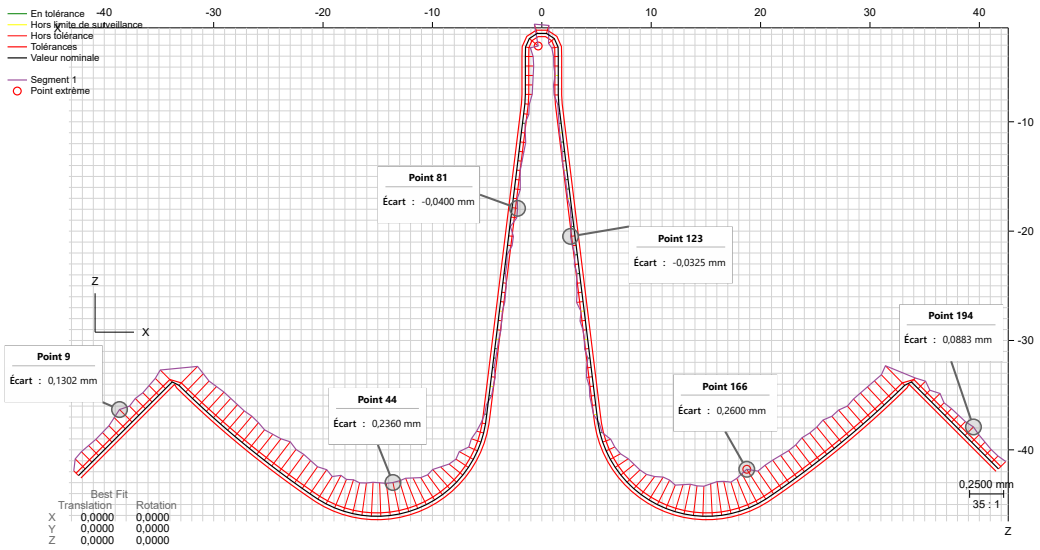

	Nom	Valeur mesurée	Limite supérieure Limite inférieure	Points	Filter type	Lc	Probe radius	Vmess[mm/sec]	Evaluation method
⌒	FRM-SURF-INT-5	0,5199	0,0500 0,0000	199	Gauss	1 -	1,5008	3,000	Direction vecteur nominal

EDMS	**2644691**
N° de plan	-
Désignation	3D printed AM-RFQ
N° de pièce	**-01-**
Date/Heure	11/10/2021 13:43

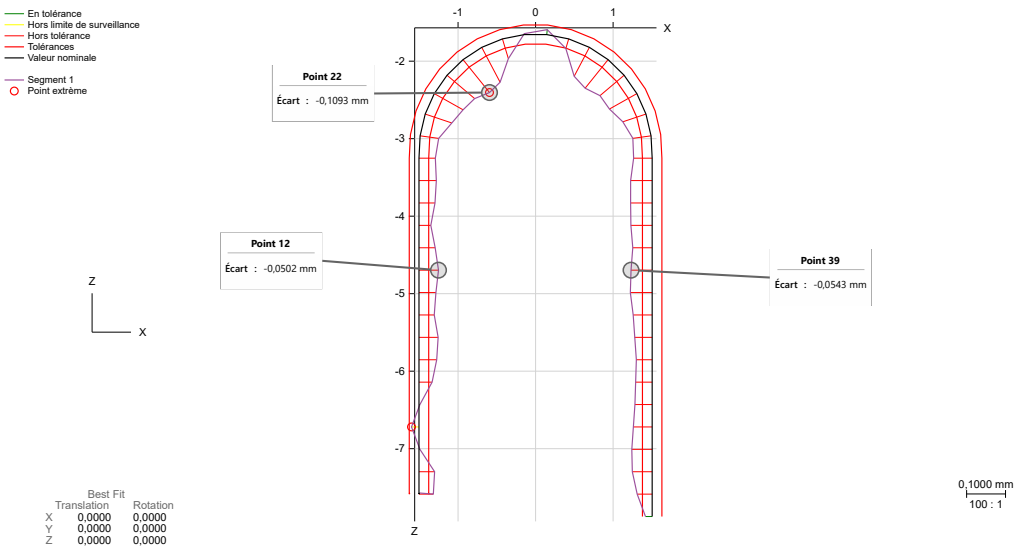

Nom	Valeur mesurée	Limite supérieure Limite inférieure	Points	Filter type	Lc	Probe radius	Vmess[mm/sec]	Evaluation method
FRM-SURF-MOD-1	0,2187	0,0500 0,0000	49	Gauss	1 -	1,5008	3,000	Direction vecteur nominal

EDMS	**2644691**
N° de plan	-
Désignation	3D printed AM-RFQ
N° de pièce	**-01-**
Date/Heure	11/10/2021 13:43

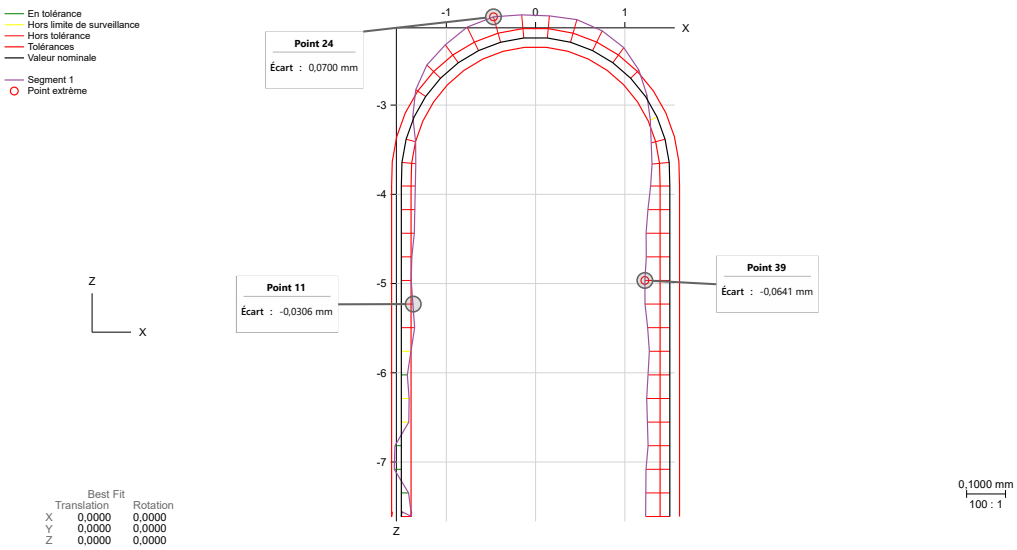

Nom	Valeur mesurée	Limite supérieure Limite inférieure	Points	Filter type	Lc	Probe radius	Vmess[mm/sec]	Evaluation method
FRM-SURF-MOD-2	0,1400	0,0500 0,0000	48	Gauss	1 -	1,5008	3,000	Direction vecteur nominal

EDMS	**2644691**
N° de plan	-
Désignation	3D printed AM-RFQ
N° de pièce	**-01-**
Date/Heure	11/10/2021 13:43

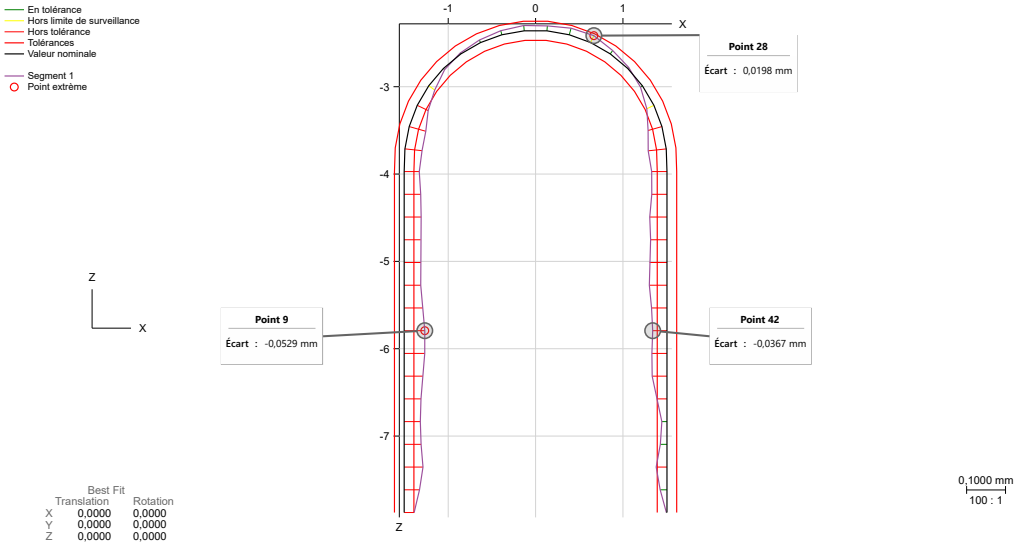

	Nom	Valeur mesurée	Limite supérieure Limite inférieure	Points	Filter type	Lc	Probe radius	Vmess[mm/sec]	Evaluation method
⌒	FRM-SURF-MOD-3	0,1059	0,0500 0,0000	50	Gauss	1 -	1,5008	3,000	Direction vecteur nominal

EDMS	**2644691**
N° de plan	-
Désignation	3D printed AM-RFQ
N° de pièce	**-01-**
Date/Heure	11/10/2021 13:43

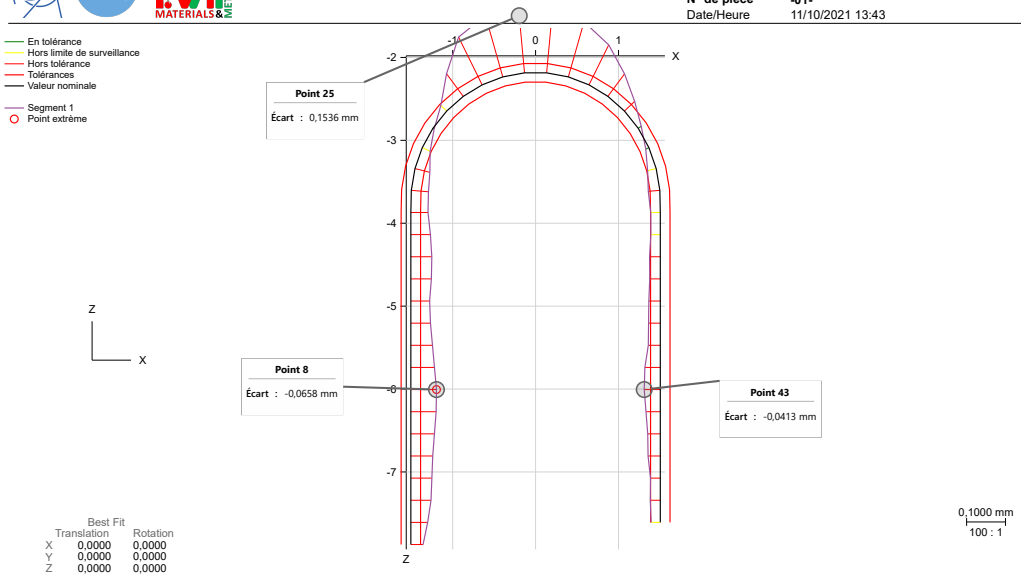

Best Fit

	Translation	Rotation
X	0,0000	0,0000
Y	0,0000	0,0000
Z	0,0000	0,0000

	Nom	Valeur mesurée	Limite supérieure Limite inférieure	Points	Filter type	Lc	Probe radius	Vmess[mm/sec]	Evaluation method
◠	FRM-SURF-MOD-4	0,3397	0,0500 0,0000	49	Gauss	1 -	1,5008	3,000	Direction vecteur nominal

EDMS	**2644691**
N° de plan	-
Désignation	3D printed AM-RFQ
N° de pièce	**-01-**
Date/Heure	11/10/2021 13:43

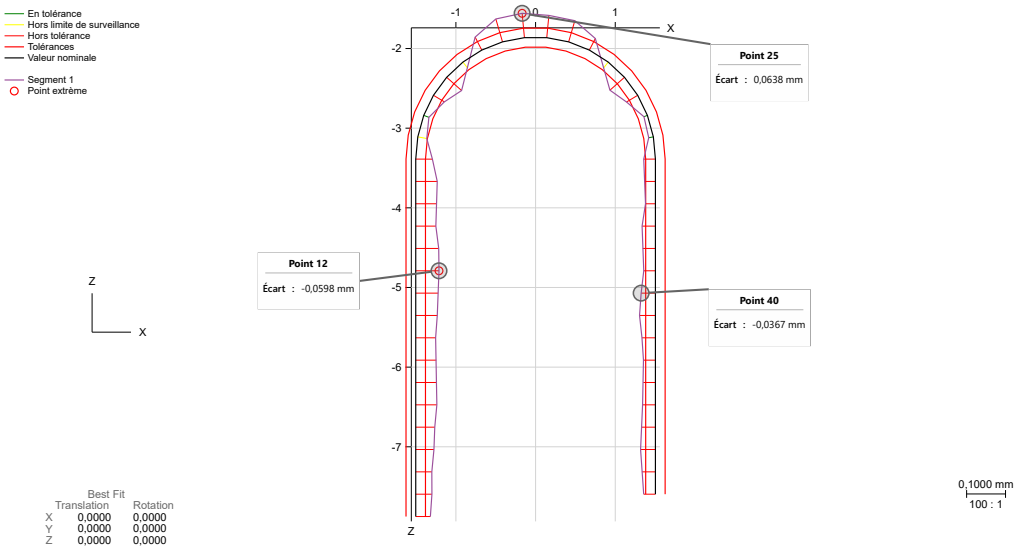

Nom	Valeur mesurée	Limite supérieure Limite inférieure	Points	Filter type	Lc	Probe radius	Vmess[mm/sec]	Evaluation method
FRM-SURF-MOD-5	0,1277	0,0500 0,0000	49	Gauss	1 -	1,5008	3,000	Direction vecteur nominal

Scan performed with Creaform METRASCAN Elite Black

Resolution: 0.10 mm

Volumetric precision in 9.1 m^3 – 0.064 mm

Analysis software: Polyworks MS 2020

Operator: Bartosz BULAT

Date: 2021/10/14

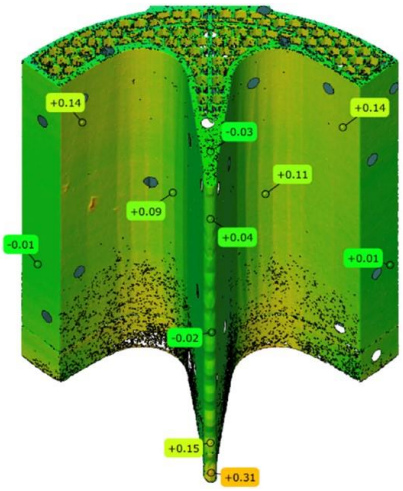

Customer measurement

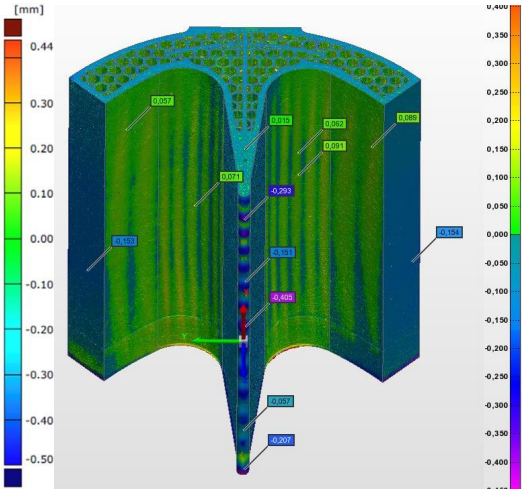

CERN measurement

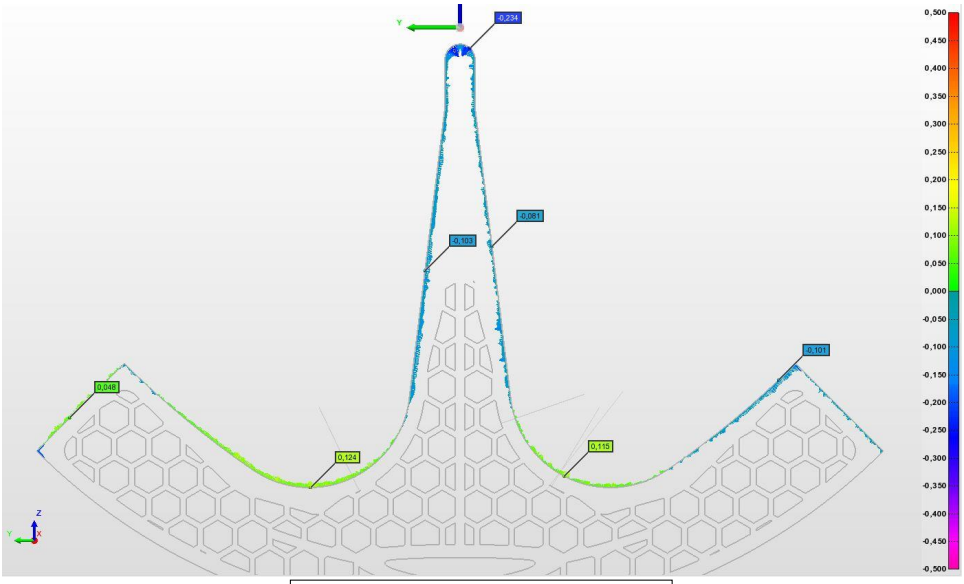
-0,234
-0,061
-0,103
-0,101
0,048
0,124
0,115
0,500
0,450
0,400
0,350
0,300
0,250
0,200
0,150
0,100
0,050
0,000
-0,050
-0,100
-0,150
-0,200
-0,250
-0,300
-0,350
-0,400
-0,450
-0,500

Section 1

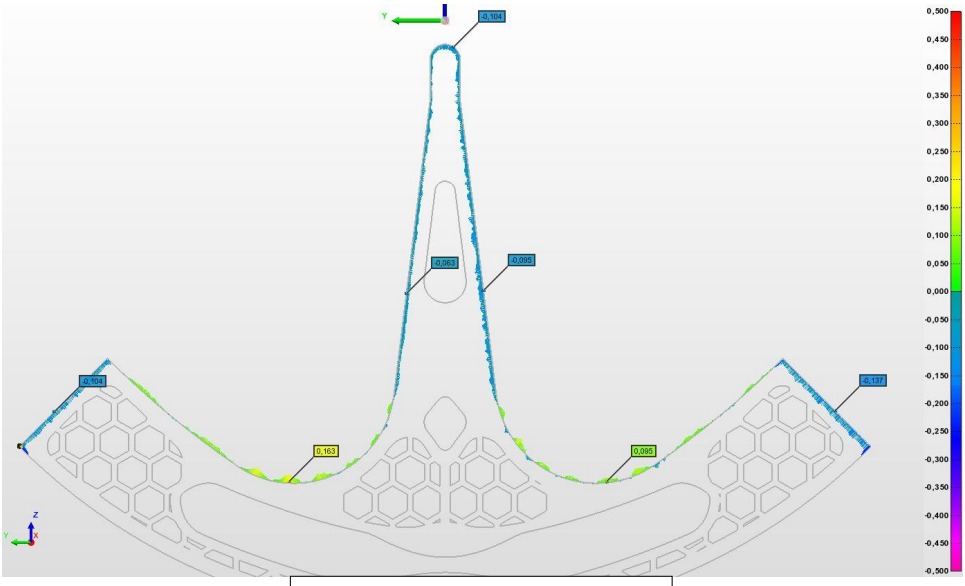
-0,104
-0,053
0,095
-0,104
0,163
0,095
-0,137
0,500
0,450
0,400
0,350
0,300
0,250
0,200
0,150
0,100
0,050
0,000
-0,050
-0,100
-0,150
-0,200
-0,250
-0,300
-0,350
-0,400
-0,450
-0,500

Section 2

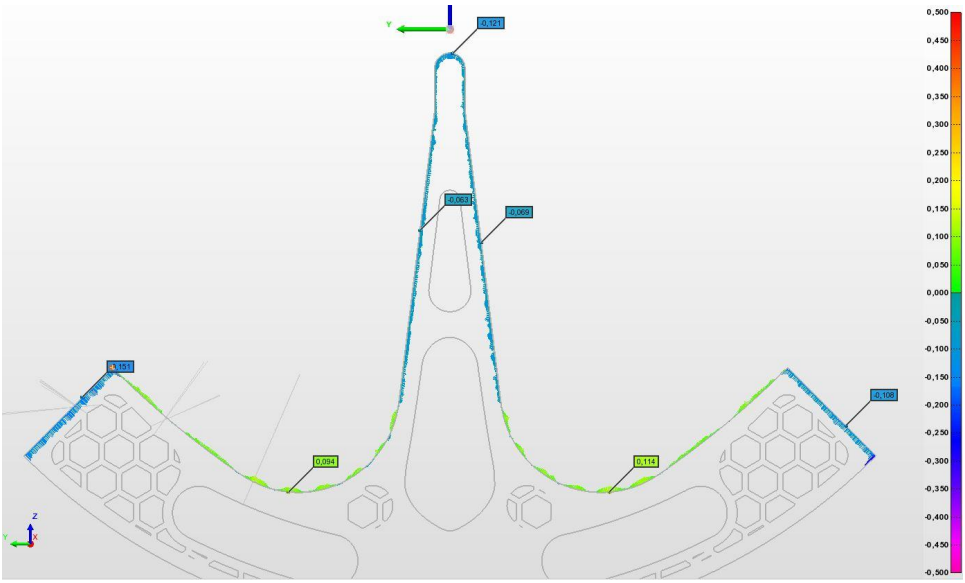
0,121
-0,063
-0,069
-0,151
0,094
0,114
-0,108
0,500
0,450
0,400
0,350
0,300
0,250
0,200
0,150
0,100
0,050
0,000
-0,050
-0,100
-0,150
-0,200
-0,250
-0,300
-0,350
-0,400
-0,450
-0,500

Section 3

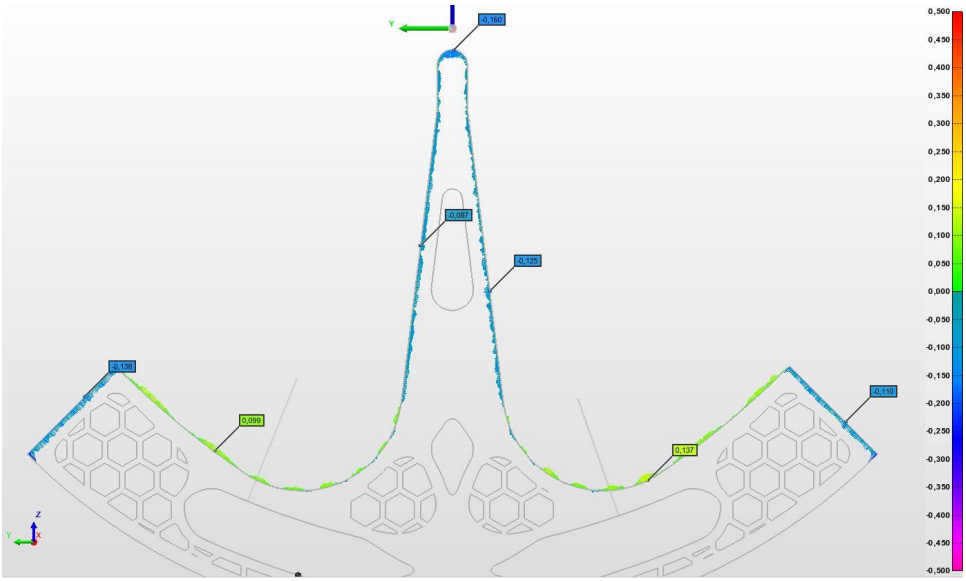
-0,160
-0,087
-0,120
-0,139
0,098
0,137
-0,110
0,500
0,450
0,400
0,350
0,300
0,250
0,200
0,150
0,100
0,050
0,000
-0,050
-0,100
-0,150
-0,200
-0,250
-0,300
-0,350
-0,400
-0,450
-0,500

Section 4

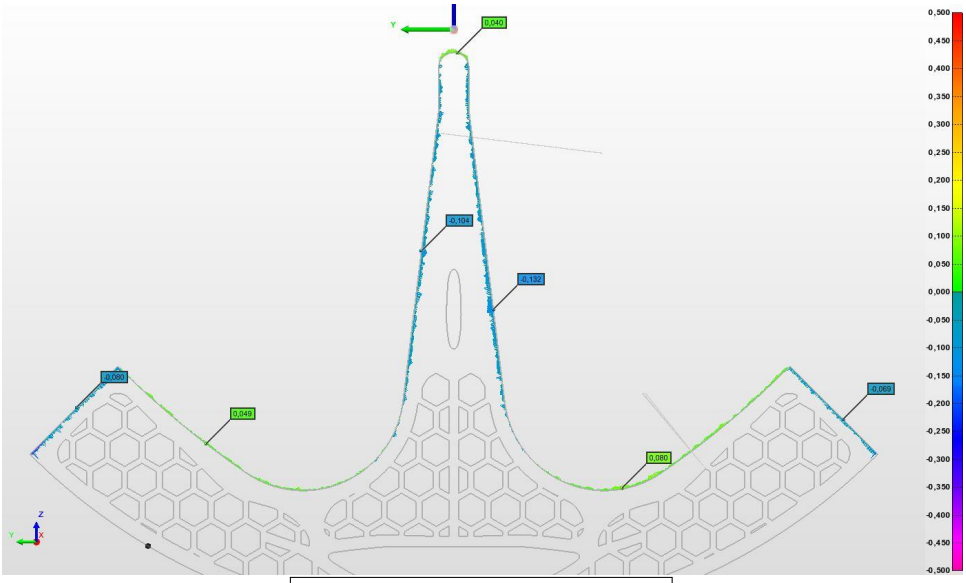
0,040
-0,104
-0,132
0,049
-0,060
0,080
-0,069
0,500
0,450
0,400
0,350
0,300
0,250
0,200
0,150
0,100
0,050
0,000
-0,050
-0,100
-0,150
-0,200
-0,250
-0,300
-0,350
-0,400
-0,450
-0,500

Section 5

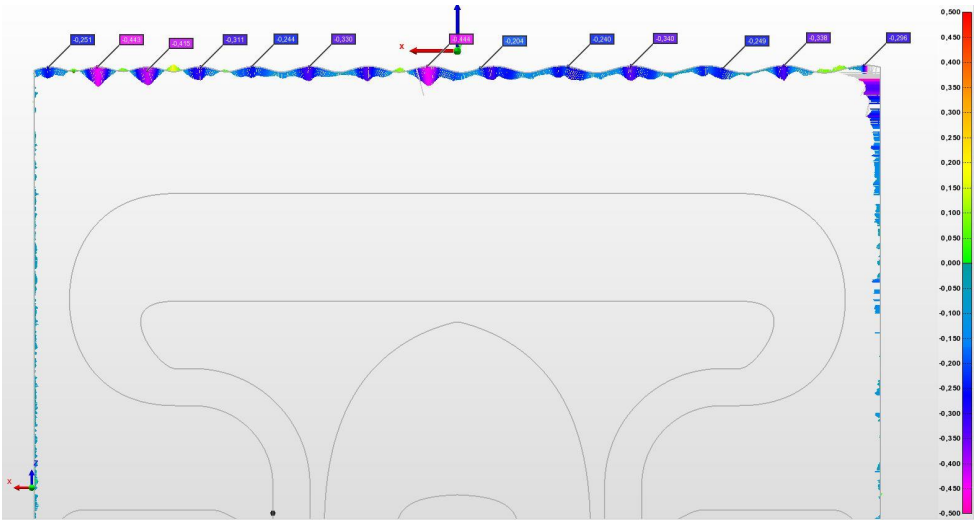

Section - modulation

2. ANNEX B

RAPPORT DE CONTRÔLE

N°EDMS: 2739166

Contrôleur:	RIGAUD J.Ph.	Demandeur:	TORIMS T.
N°JOB:	---	Projet:	iFAST
Date:	19.05.2022	Désignation:	---
Machine:	SCAN CREAFORM	N°plan/indice:	ind. --

Second proto

RAPPORT DE CONTRÔLE

N°EDMS: 2739166

Contrôleur:	RIGAUD J.Ph.	Demandeur:	TORIMS T.
N°JOB:	---	Projet:	iFAST
Date:	19.05.2022	Désignation:	---
Machine:	SCAN CREAFORM	N°plan/indice:	ind. --

Second proto

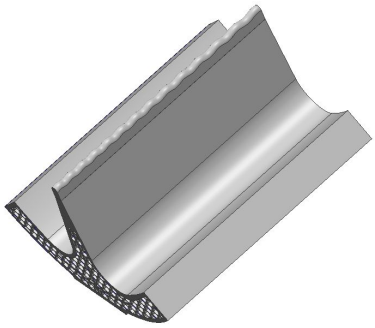

modèle CAO

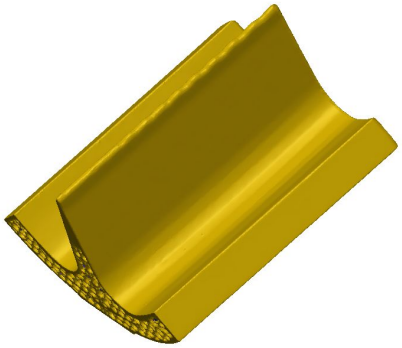

SCAN 3D

RAPPORT DE CONTRÔLE

N°EDMS: 2739166

Contrôleur:	RIGAUD J.Ph.	Demandeur:	TORIMS T.
N°JOB:	---	Projet:	iFAST
Date:	19.05.2022	Désignation:	---
Machine:	SCAN CREAFORM	N°plan/indice:	ind. --

Second proto

écarts à surface

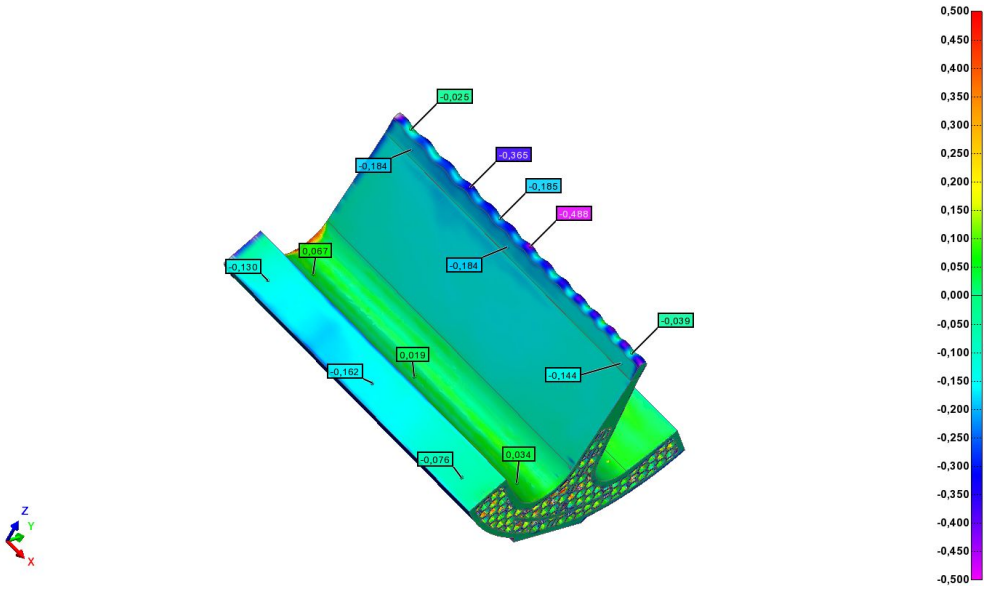

RAPPORT DE CONTRÔLE

N°EDMS: 2739166

Contrôleur:	RIGAUD J.Ph.	Demandeur:	TORIMS T.
N°JOB:	---	Projet:	iFAST
Date:	19.05.2022	Désignation:	---
Machine:	SCAN CREAFORM	N°plan/indice:	ind. --

Second proto

écarts à surface

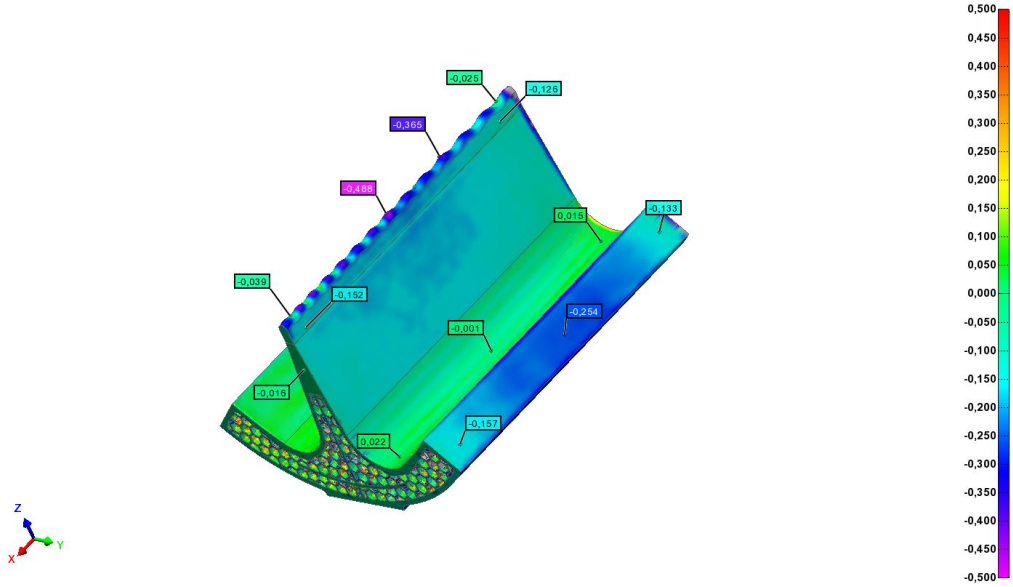

3. ANNEX C

Rapport de contrôle

EDMS.2739166

iFAST

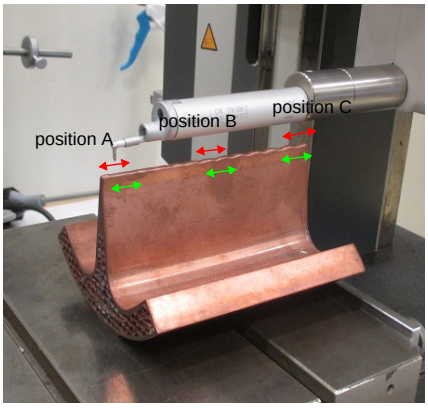

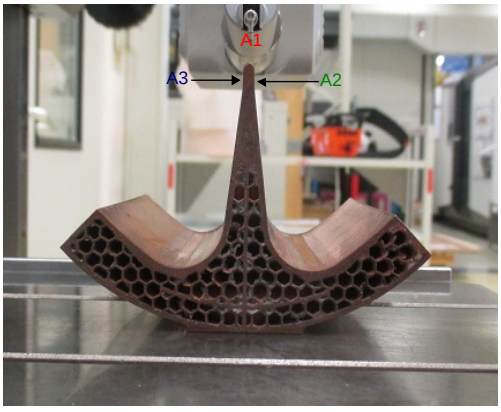

Contrôleur: RIGAUD J.Ph.

Client:TORIMS

Date: 19/05/2022 11:26:40

Rapport de contrôle

EDMS.2739166

iFAST

Profil=R_ISO - Section=[1] X Mag: x100 Z Mag: x50000 <Rugosité_1>

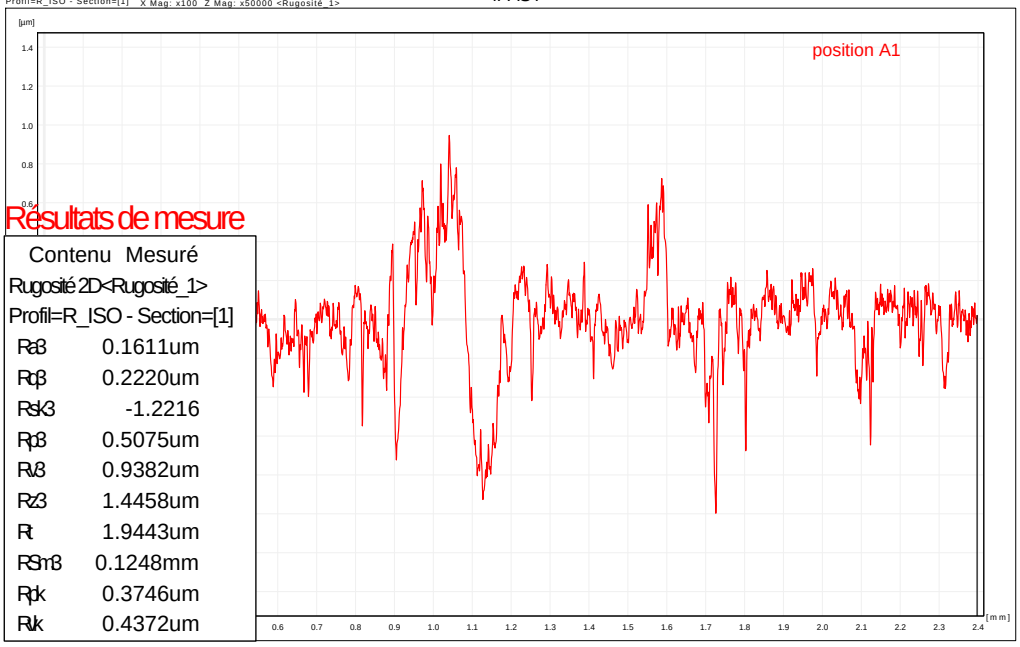

Résultats de mesure

Contenu	Mesuré
Rugosité 2D<Rugosité_1>	
Profil=R_ISO - Section=[1]	
Ra3	0.1611um
Rq3	0.2220um
Rsk3	-1.2216
Rp3	0.5075um
Rv3	0.9382um
Rz3	1.4458um
Rt	1.9443um
RSm3	0.1248mm
Rpk	0.3746um
Rvk	0.4372um

Rapport de contrôle

EDMS.2739166

iFAST

Profil=R_ISO - Section=[1] X Mag: x100 Z Mag: x50000 <Rugosité_1>

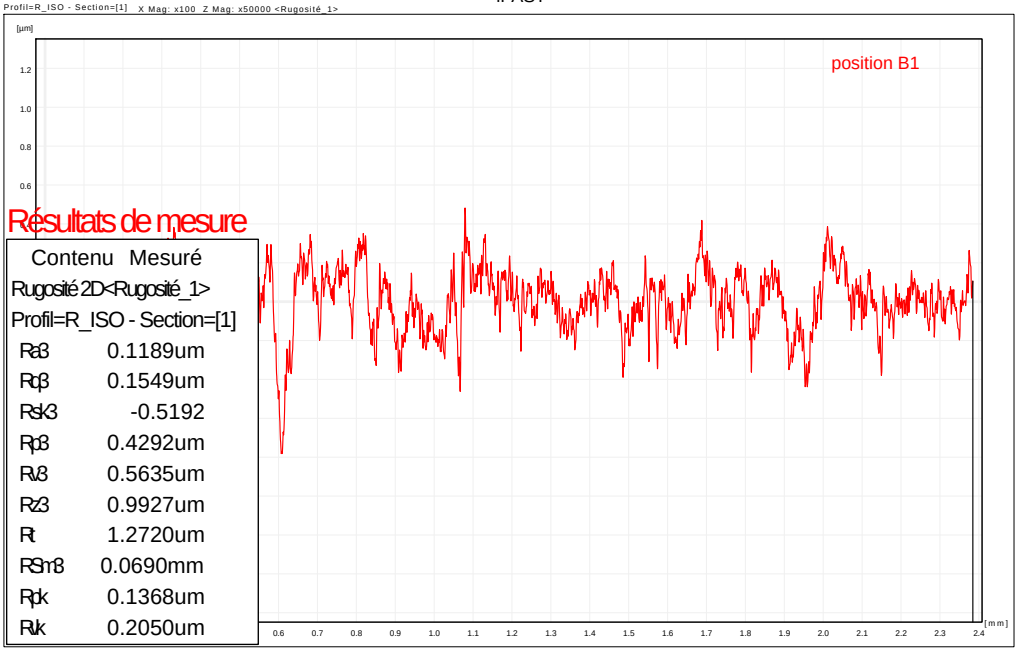

Résultats de mesure

Contenu	Mesuré
Rugosité 2D<Rugosité_1>	
Profil=R_ISO - Section=[1]	
Ra3	0.1189um
Rq3	0.1549um
Rsk3	-0.5192
Rp3	0.4292um
Rv3	0.5635um
Rz3	0.9927um
Rt	1.2720um
RSm3	0.0690mm
Rpk	0.1368um
Rvk	0.2050um

Rapport de contrôle

EDMS.2739166

iFAST

Profil=R_ISO - Section=[1] X Mag: x200 Z Mag: x50000 <Rugosité_1>

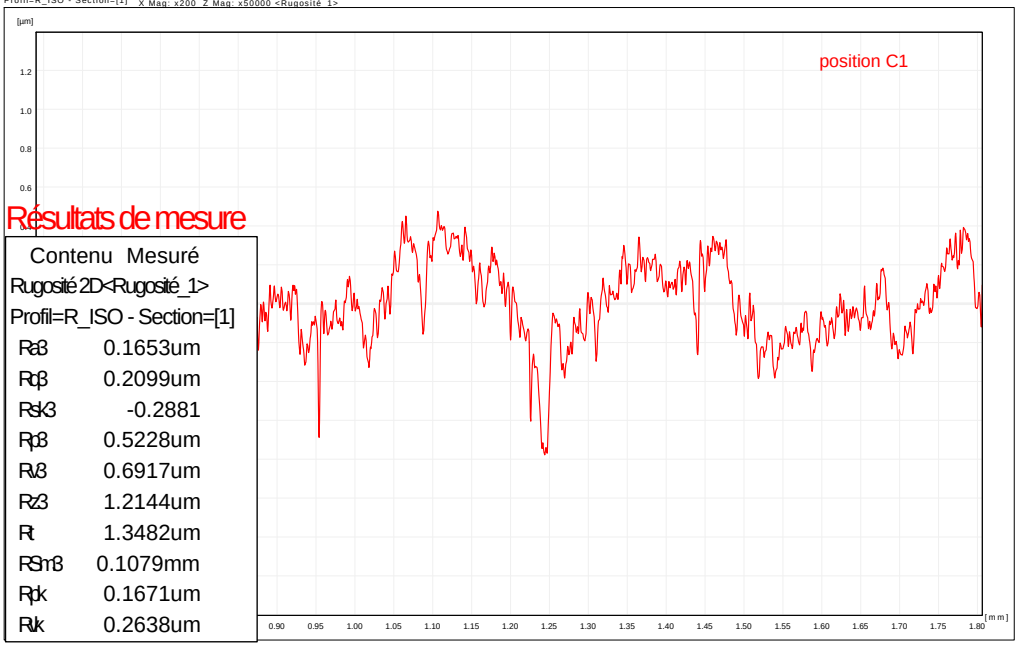

Résultats de mesure

Contenu	Mesuré
Rugosité 2D<Rugosité_1>	
Profil=R_ISO - Section=[1]	
Ra	0.1653um
Rq	0.2099um
Rsk	-0.2881
Rp	0.5228um
Rv	0.6917um
Rz	1.2144um
Rt	1.3482um
RSm	0.1079mm
Rpk	0.1671um
Rvk	0.2638um

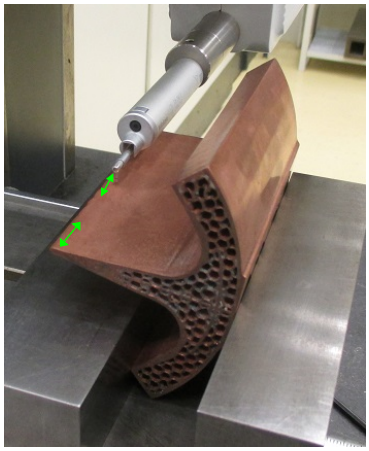

Rapport de contrôle

EDMS.2739166

iFAST

Profil=R_ISO - Section=[1] X Mag: x100 Z Mag: x50000 <Rugosité_1>

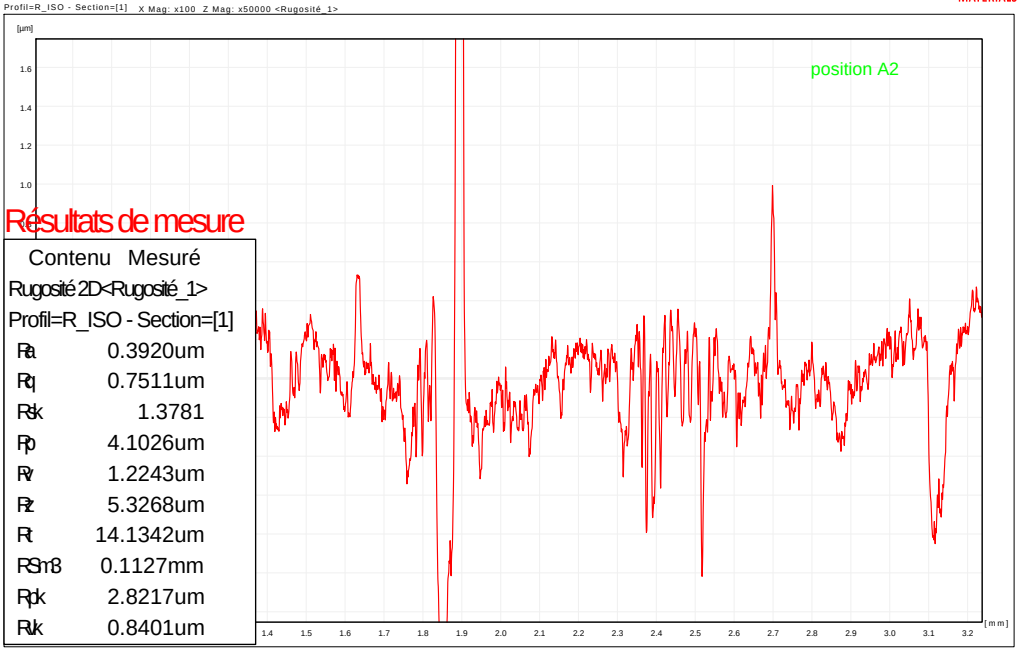

Résultats de mesure

Contenu	Mesuré
Rugosité 2D<Rugosité_1>	
Profil=R_ISO - Section=[1]	
Pa	0.3920um
Pq	0.7511um
Psk	1.3781
Pp	4.1026um
Pv	1.2243um
Pz	5.3268um
Pt	14.1342um
PSm	0.1127mm
Ppk	2.8217um
Pvk	0.8401um

Rapport de contrôle

EDMS.2739166

iFAST

Profil=R_ISO - Section=[1] X Mag: x100 Z Mag: x50000 <Rugosité_1>

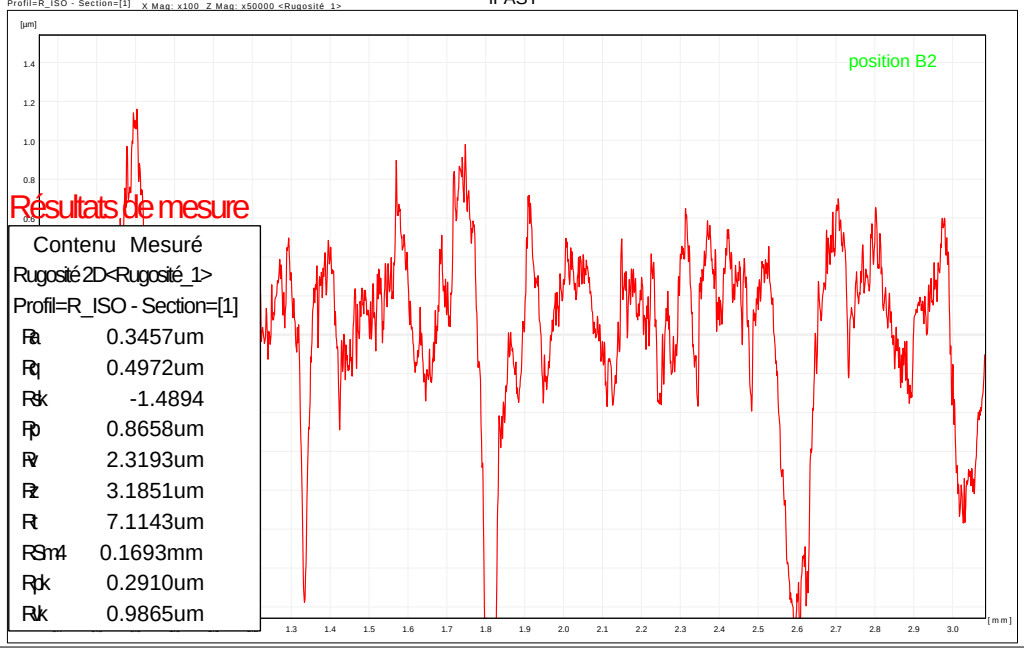

Résultats de mesure

Contenu	Mesuré
Rugosité 2D<Rugosité_1>	
Profil=R_ISO - Section=[1]	
Ra	0.3457um
Rq	0.4972um
Rsk	-1.4894
Rp	0.8658um
Rv	2.3193um
Rz	3.1851um
Rt	7.1143um
RSm	4 0.1693mm
Rpk	0.2910um
Rvk	0.9865um

Rapport de contrôle

EDMS.2739166

iFAST

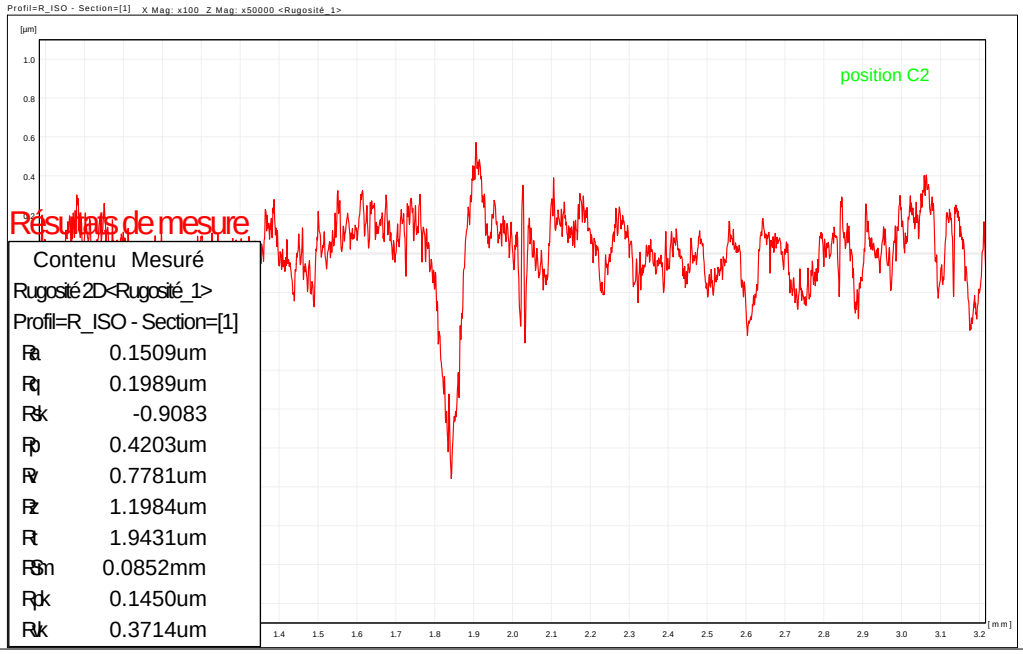

Résultats de mesure

Contenu	Mesuré
Rugosité 2D<Rugosité_1>	
Profil=R_ISO - Section=[1]	
Ra	0.1509um
Rq	0.1989um
Rsk	-0.9083
Rp	0.4203um
Rv	0.7781um
Rz	1.1984um
Rt	1.9431um
RSm	0.0852mm
Rpk	0.1450um
Rvk	0.3714um

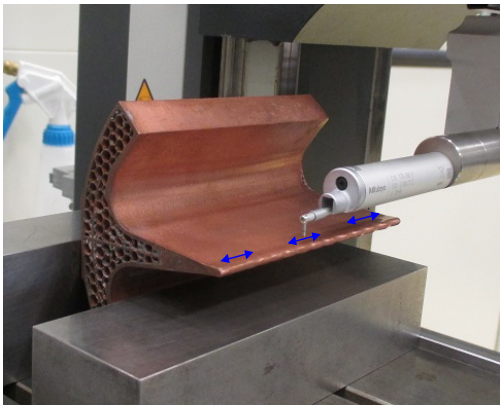

Rapport de contrôle

EDMS.2739166

iFAST

Profil=R_ISO - Section=[1] X Mag: x100 Z Mag: x50000 <Rugosité_1>

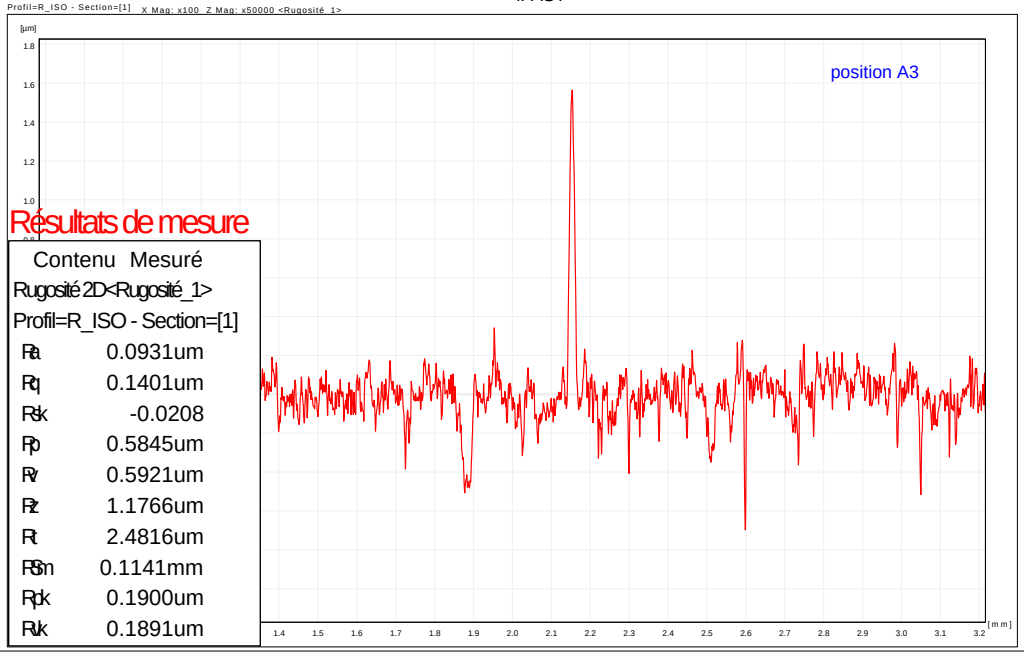

Résultats de mesure

Contenu	Mesuré
Rugosité 2D<Rugosité_1>	
Profil=R_ISO - Section=[1]	
Ra	0.0931um
Rq	0.1401um
Rsk	-0.0208
Rp	0.5845um
Rv	0.5921um
Rz	1.1766um
Rt	2.4816um
RSm	0.1141mm
Rpk	0.1900um
Rvk	0.1891um

Rapport de contrôle

EDMS.2739166

iFAST

Profil=R_ISO - Section=[1] X Mag: x100 Z Mag: x50000 <Rugosité_1>

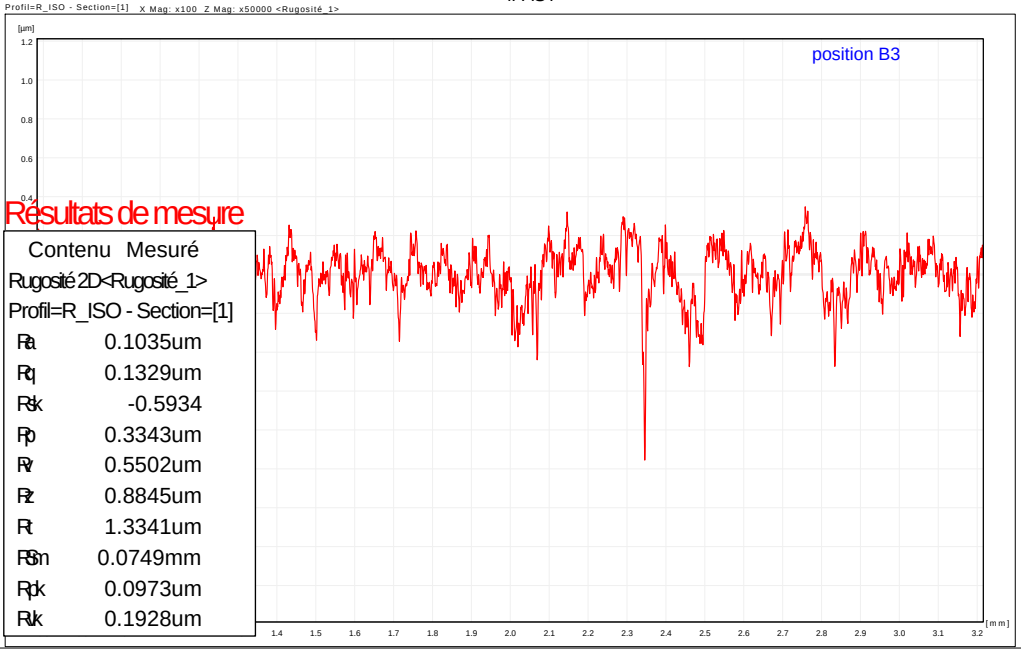

Résultats de mesure

Contenu	Mesuré
Rugosité 2D<Rugosité_1>	
Profil=R_ISO - Section=[1]	
Ra	0.1035um
Rq	0.1329um
Rsk	-0.5934
Rp	0.3343um
Rv	0.5502um
Rz	0.8845um
Rt	1.3341um
RSm	0.0749mm
Rpk	0.0973um
Rvk	0.1928um

Rapport de contrôle

EDMS.2739166

iFAST

Profil=R_ISO - Section=[1] X Mag: x100 Z Mag: x50000 <Rugosité_1>

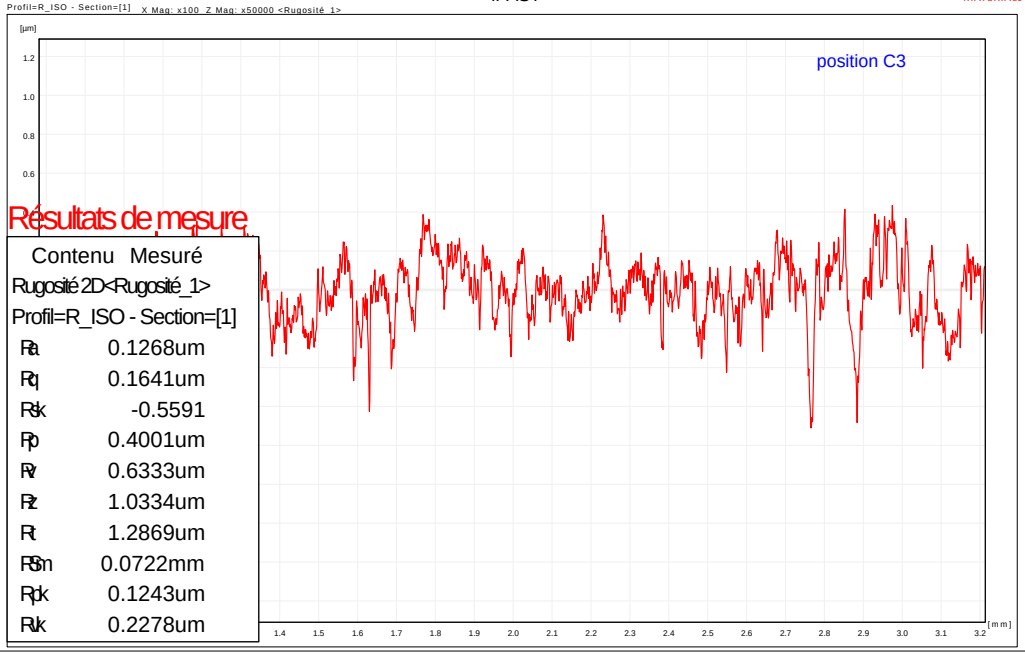

Résultats de mesure

Contenu	Mesuré
Rugosité 2D<Rugosité_1>	
Profil=R_ISO - Section=[1]	
Ra	0.1268um
Rq	0.1641um
Rsk	-0.5591
Rp	0.4001um
Rv	0.6333um
Rz	1.0334um
Rt	1.2869um
RSm	0.0722mm
Rdq	0.1243um
Rku	0.2278um

4. ANNEX D

Rapport de contrôle

EDMS.2739166

iFAST test 1

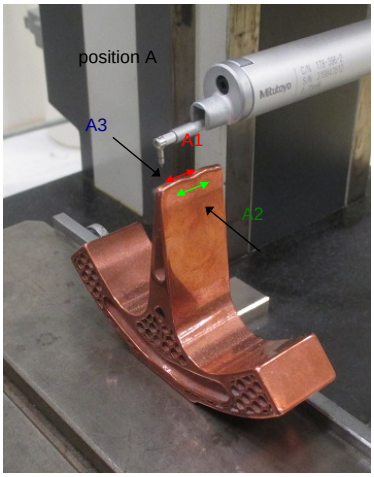

Contrôleur: RIGAUD J.Ph.

Client:TORIMS

Date: 19/05/2022 13:21:15

Rapport de contrôle

EDMS.2739166

iFAST

test 1

Profil=R_ISO - Section=[1] X Mag: x100 Z Mag: x20000 <Rugosité_1>

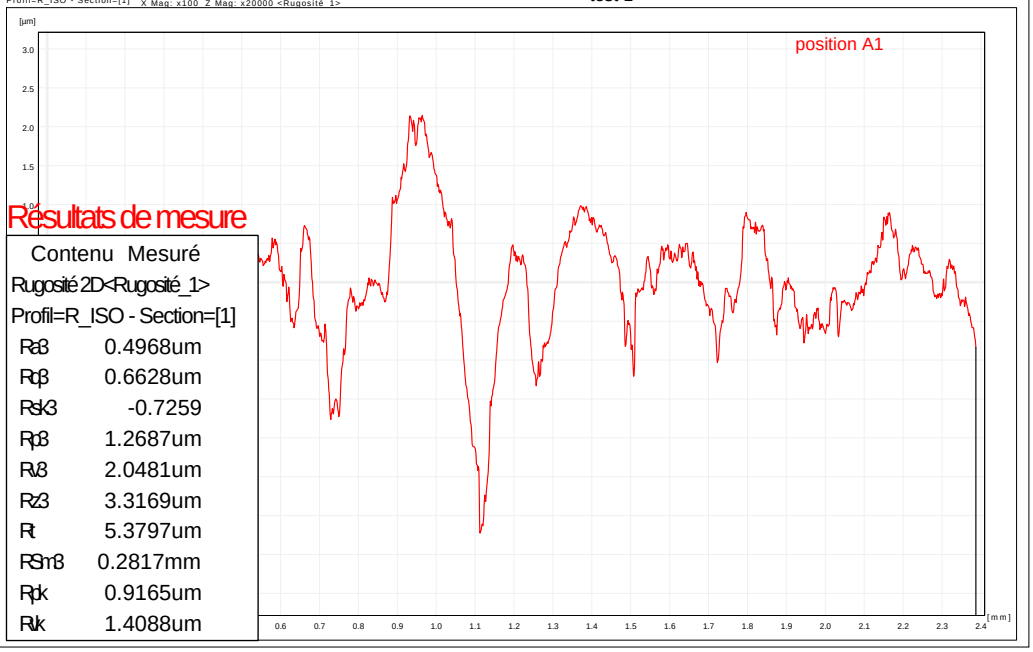

Résultats de mesure

Contenu	Mesuré
Rugosité 2D<Rugosité_1>	
Profil=R_ISO - Section=[1]	
Ra	0.4968um
Rq	0.6628um
Rsk	-0.7259
Rp	1.2687um
Rv	2.0481um
Rz	3.3169um
Rt	5.3797um
RSm	0.2817mm
Rpk	0.9165um
Rvk	1.4088um

Rapport de contrôle

EDMS.2739166

iFAST test 1

Profil=R_ISO - Section=[1] X Mag: x100 Z Mag: x50000 <Rugosité_1>

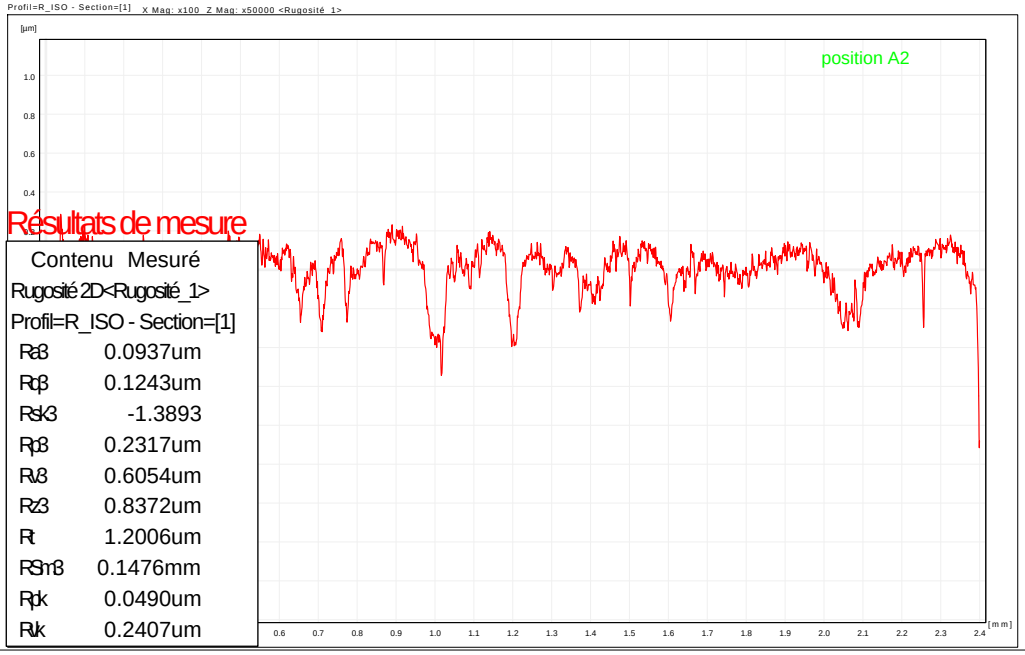

Résultats de mesure

Contenu	Mesuré
Rugosité 2D<Rugosité_1>	
Profil=R_ISO - Section=[1]	
Ra3	0.0937um
Rq3	0.1243um
Rsk3	-1.3893
Rp3	0.2317um
Rv3	0.6054um
Rz3	0.8372um
Rt	1.2006um
RSm3	0.1476mm
Rpk	0.0490um
Rvk	0.2407um

Rapport de contrôle

EDMS.2739166

iFAST test 1

Profil=R_ISO - Section=[1] X Mag: x100 Z Mag: x50000 <Rugosité_1>

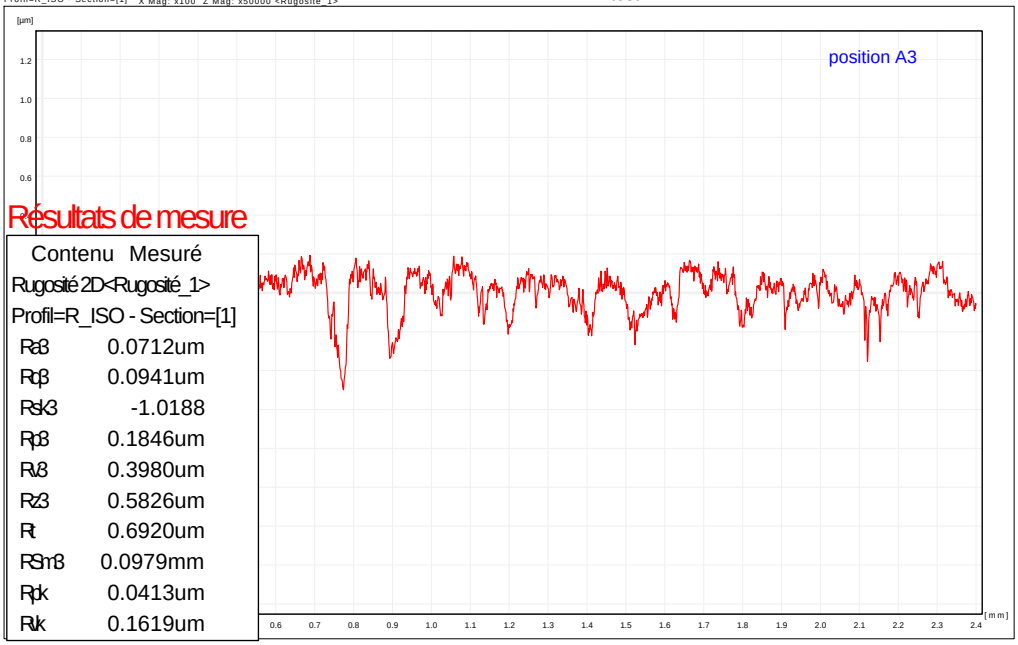

Résultats de mesure

Contenu	Mesuré
Rugosité 2D<Rugosité_1>	
Profil=R_ISO - Section=[1]	
Ra3	0.0712um
Rq3	0.0941um
Rsk3	-1.0188
Rp3	0.1846um
Rv3	0.3980um
Rz3	0.5826um
Rt	0.6920um
RSm3	0.0979mm
Rpk	0.0413um
Rvk	0.1619um

5. ANNEX E

Rapport de contrôle

EDMS.2739166

iFAST test 2

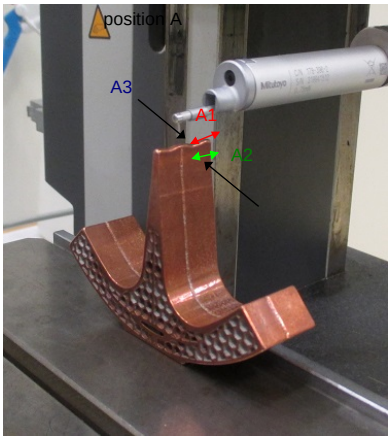

Contrôleur: RIGAUD J.Ph.

Client:TORIMS

Date: 19/05/2022 13:28:41

Rapport de contrôle

EDMS.2739166

iFAST

test 2

Profil=R_ISO - Section=[1] X Mag: x100 Z Mag: x20000 <Rugosité_1>

Résultats de mesure

Contenu	Mesuré
Rugosité 2D<Rugosité_1>	
Profil=R_ISO - Section=[1]	
Ra	0.4299um
Rq	0.5596um
Rsk	-0.2378
Rp	1.4796um
Rv	1.6742um
Rz	3.1538um
Rt	3.7159um
RSm	0.2232mm
Rpk	0.6605um
Rvk	0.7599um

Rapport de contrôle

EDMS.2739166

iFAST test 2

Profil=R_ISO - Section=[1] X Mag: x100 Z Mag: x50000 <Rugosité_1>

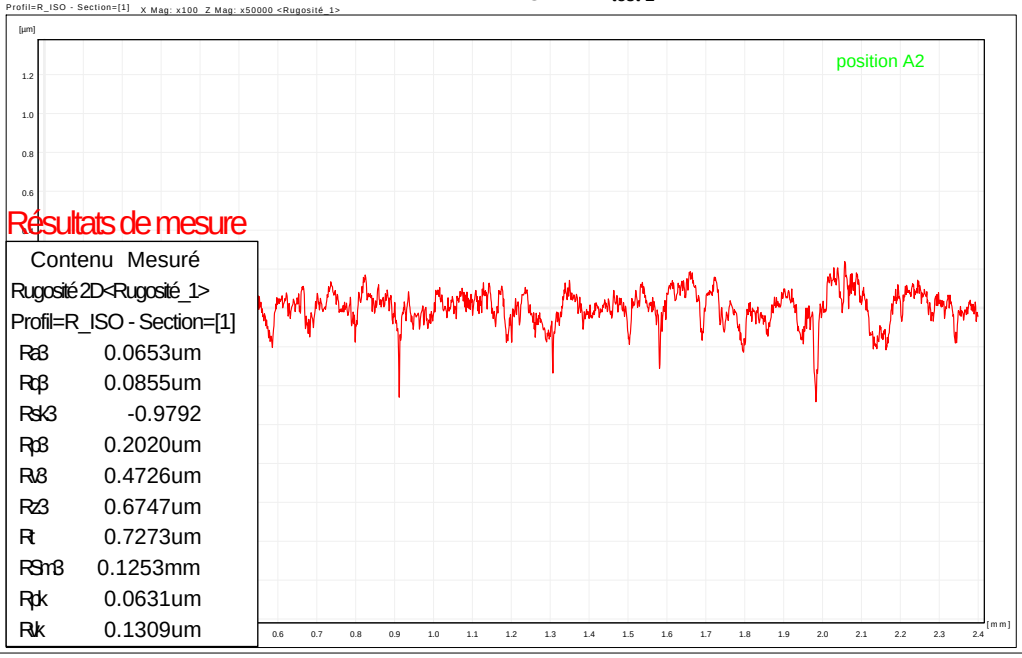

Résultats de mesure

Contenu	Mesuré
Rugosité 2D<Rugosité_1>	
Profil=R_ISO - Section=[1]	
Ra	0.0653um
Rq	0.0855um
Rsk	-0.9792
Rp	0.2020um
Rv	0.4726um
Rz	0.6747um
Rt	0.7273um
RSm	0.1253mm
Rpk	0.0631um
Rvk	0.1309um

Rapport de contrôle

EDMS.2739166

iFAST test 2

Profil=R_ISO - Section=[1] X Mag: x100 Z Mag: x50000 <Rugosité_1>

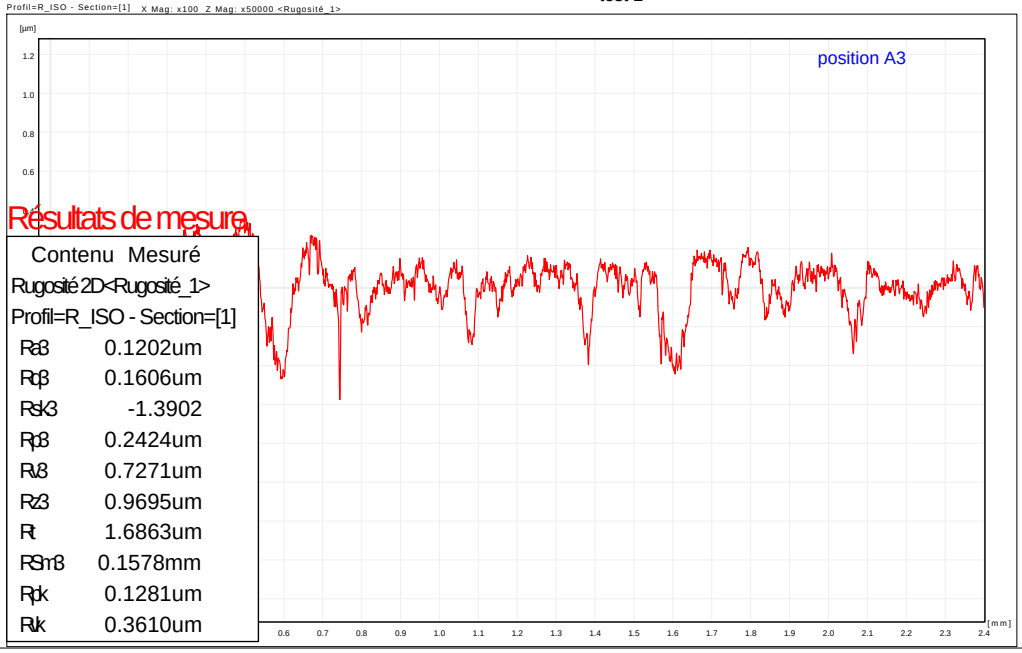

Résultats de mesure

Contenu	Mesuré
Rugosité 2D<Rugosité_1>	
Profil=R_ISO - Section=[1]	
Ra3	0.1202um
Rq3	0.1606um
Rsk3	-1.3902
Rp3	0.2424um
Rv3	0.7271um
Rz3	0.9695um
Rt	1.6863um
RSm3	0.1578mm
Rpk	0.1281um
Rvk	0.3610um

6. ANNEX F

Los Alamos National Laboratory Poisson Superfish

Program SFO written by James H. Billen and Lloyd M. Young

The original Poisson Superfish codes were developed
by Ron F. Holsinger in collaboration with Klaus Halbach.
These programs are provided as a service to the accelerator
community by the Los Alamos Accelerator Code Group (LAACG).

Program SFO 7.17 released 1-13-2006

Solution file C:\LANL\Examples\RadioFrequency\RFQCavity\4THRFQ.T35.
More input from file C:\LANL\Examples\RadioFrequency\RFQCavity\4THRFQ.SEG.
Program file: C:\LANL\AUTOFISH.EXE
SF.INI file: C:\LANL\SF.INI 8-16-2022 18:57:22
Memory used for 4THRFQ.T35 arrays: 535.824 K

Problem description:
RFQ full quadrant
Lowest dipole-mode frequency = 750 MHz

Bore radius at quadrupole symmetry point r0 = 0.1935 cm

Vane-tip radius of curvature rho = 0.1504 cm

Problem file: C:\LANL\EXAMPLES\RADIOFREQUENCY\RFQCAVITY\4THRFQ.AF 2-09-2023 14:42:54

Problem file length: 1546 bytes

Originating program: Autofish Problem type: RFQ

Coordinates and lengths have dimensions of centimeters.

Problem constants and variables.

Letter A in the code column indicates a value supplied in the

Automesh input file.

Letter S in the code column indicates a value supplied in the

SFO input file.

Variable	Code	Value	Description
ALPHAT		3.930000000E-03	Temperature coefficient of resistance
ASCALE		3767.30313	Scaling factor for H at drive point
BETA		0.0	Particle velocity
BETA1		0.100000000	Starting BETA in transit-time table
BETA2		0.950000000	Ending BETA in transit-time table
CCLDELK		1.00000000	Increment for coupling for table in SFO
CCLMAXK		6.00000000	Highest coupling for table in SFO
CCLMINK		1.00000000	Lowest coupling for table in SFO
CLENGTH		0.0	Cavity length for normalization in SFO
CLIGHT		2.997924580E+10	Exact speed of light in cm/sec
CONV		1.00000000	Length conversion (number of units per cm)
DBETA		5.000000000E-02	BETA increment in transit-time table
DELFR		0.0	Frequency step size for a resonance search
DIAGDLL		0	If 1, DLL writes diagnostics to DiagDLL.txt

DKSQ 5.884690478E-10 Change in k^2 after an iteration in Fish

DPHI 180.000000 Phase length of the problem geometry

DSLOPE -0.996981004 Slope of D(k^2) function

DSTOLER 2.000000000E-02 Tolerance required on D(k^2)

DX1 1.428571429E-02 First X mesh interval (at XMIN)

DXMIN 1.428571429E-02 Minimum X mesh interval (found by Automesh)

DYMIN 1.428571429E-02 Minimum Y mesh interval (found by Automesh)

ENORM 1000000.00 Field normalization for NORM=4 option

EPS0 8.854187818E-12 Permittivity of free space

EPSIK 1.000000000E-04 Frequency convergence parameter

EPSO 1.000000000E-05 Convergence parameter in mesh optimization

ERG 12.9137162 Integral (H^2 r dr dz)

EZERO S 11207000.0 E0 for normalization in SFO when NORM=0

EZEROT 1000000.00 E0*T for normalization in SFO when NORM=1

FMU0 1.256637061E-06 Permeability of free space

FREQ 703.252969 RF cavity resonant frequency

FREQD 0.0 Design frequency for a cavity (MHz)

HPHI 5000.00000 Normalization magnetic field for NORM=2

IBETA 0 If >0, SFO writes transit-time vs BETA

ICCC 1 1 for real arrays, 2 for complex arrays

ICCP 1 If 1, compute material power loss

ICORNER1 0 First corner segment for computing average H

ICORNER2 0 Last corner segment for computing average H

ICYCLE 3 Present iteration number

ICYLIN A 0 0 for X,Y problems, 1 for Z,R problems

IMAX 122 KMAX+2

INFODATA 0 Number of tuning-code parameters

IOBSEG -1 First segment of the CCL outer boundary

IPIVOT 1 Pivoting in matrix inversion routines

IRESID	0	If 1, calculate potential residuals
IRMAX	25	Used in optimization of RHOXY
IRTYPE	0	Surface resistance option indicator
ISLOT	0	If 1, SFO computes coupling-slot power loss
ITFILE	0	If 1, SFO writes transit-time plot file
ITOT	14884	(KMAX+2)*(LMAX+2)
KDRI	108	K coordinate of the drive point
KMAX	120	Number of horizontal logical mesh points
KMETHOD	0	Wavenumber computation method (1= use beta)
KPROB A	1	Problem type indicator (Superfish)
LAST35	1	Code for last program to update T35 file
LCYCLE	191	Iteration number in mesh optimization
LDRI	108	L coordinate of the drive point
LINT	1	Logical-mesh coordinate for Ez integration
LMAX	120	Number of vertical logical mesh points
MAXCY	19	Maximum number of cycles (-1: use default)
MAXPPR	413	Maximum points per region
METHOD	2	Method used to get frequency in root finder
NAIR	10175	Number of air points
NBND	14	Number of Dirichlet boundary points
NBSLF A	1	Left-side boundary condition
NBSLO	0	Lower boundary condition
NBSRT	1	Right-side boundary condition
NBSUP	1	Upper boundary condition
NDRI	13285	Drive point index = IRLAX(NPINP)
NEGAT	0	Zero-area triangle indicator
NFE	0	Number of iron points
NHSTEM	1	Number of half stems
NINTER	0	Number of interface points

NMATR	0	Number of material records in T35 file
NORM S	0	Normalization method in SFO
NPBOUND	412	Total number of boundary points in the mesh
NPINP	10190	Total points in problem
NPONTS	9779	Number of unknown relaxation points
NREG	2	Number of regions
NRMSEG	1	Normalization segment number for NORM=2
NSEG	26	Number of boundary segments
NSPL	1	Number of special-potential points
NSTEP	0	Number of steps for a resonance search
OMEGAM	1.000000000E-03	Used in optimization of RHOXY
PI	3.14159265	The number pi to machine precision
PLCELL	360.000000	Phase length per cell for multicell problems
Q2I	0.0	1/2Q passed from CFish to SFO
RESIDR	1.000000000E-08	Residual resistance of a superconductor
RESIK	2.708842748E-08	Residual = DKSQ/XKSQ
RFMU	1.00000000	Permeability for rf surface resistance
RHO	1.724100000E-06	Material resistivity (Ohm-m)
RHOR	1.724100000E-06	Reference resistivity (Ohm-cm) at TEMPR
RHOXY	1.60000000	Over-relaxation factor in mesh optimization
RMASS	-2.00000000	Rest mass energy of particle in SFO
RSTEM	1.00000000	Stem radius in cm
SLOSS	3.000000000E-02	Coupling-slot power factor per % coupling
TC	9.20000000	Critical temperature of a superconductor
TEMPC	20.0000000	Normal conductor operating temperature
TEMPK	2.00000000	Operating temperature of a superconductor
TEMPR	20.0000000	Reference temperature for IRTYPE=3
TRIAVG	7.240105077E-04	Average area of all triangles
TRIMAX	2.929405217E-03	Area of the largest positive-area triangle

TRIMIN 3.660000000E-06 Area of the smallest positive-area triangle

VOLUME 0.0 Cavity volume (cylindrical symmetry only)

XDRI 3.36400000 X coordinate of the drive point

XK0 0.147390923 The wave number k = 2pif/c

XKSQ 2.172408432E-02 Square of the wave number

XMAXG 4.60786424 Upper X bound of the problem geometry

XMING 0.0 Lower X bound of the problem geometry

XNORM1 0.0 Starting X for NORM=4 integration path

XNORM2 0.0 Ending X for NORM=4 integration path

XYAREA 14.4563178 Total cross sectional area

YDRI 3.36400000 Y coordinate of the drive point

YMAXG 4.60778801 Upper Y bound of the problem geometry

YMING 0.0 Lower Y bound of the problem geometry

YNORM1 0.0 Starting Y for NORM=4 integration path

YNORM2 0.0 Ending Y for NORM=4 integration path

ZCTR 0.0 Reference Z in transit-time integrals

Segment numbers for field calculations

[Note: negative values indicate stem segments.]

2 3 4 5 6 7 8 9 10 11 12 13

14 15 16 17 18 19 20 21 22 23 24 25

No materials other than air or empty space.

The field normalization factor ASCALE for this problem is based

upon the calculated cavity length ZLONG = 0.19350000.

Electric field along Y = 0.000000

for normalization ASCALE = 10986.722957:

X(cm)	Ex(V/m)
0.00000	8.802004E+06
0.00893	8.823318E+06
0.01488	8.898260E+06
0.02288	8.962373E+06
0.02977	9.040317E+06
0.03752	9.155027E+06
0.04465	9.199781E+06
0.05229	9.337987E+06
0.05954	9.478951E+06
0.06710	9.656742E+06
0.07442	9.838232E+06
0.08193	1.005610E+07
0.08931	1.027922E+07
0.09677	1.053865E+07
0.10419	1.080571E+07
0.11160	1.110656E+07
0.11908	1.142465E+07
0.12644	1.177349E+07
0.13396	1.214749E+07
0.14128	1.255212E+07
0.14885	1.298419E+07
0.15613	1.346985E+07
0.16373	1.398807E+07
0.17097	1.456812E+07
0.17862	1.500246E+07
0.18532	1.562620E+07
0.19350	1.637876E+07

Total cavity stored energy (from program Fish): 6.9009093E-05 Joules/cm

---

Power and fields on wall segment 2. K,L = 1,15 to 11,25

This segment uses surface resistance option IRTYPE = 0

Surface resistance, Rs = 6.918579E-03 Ohm calculated from:

Operating temperature, TEMPC = 20.000 C

Reference resistivity, RHOR = 1.724100E-06 Ohm-cm

Reference temperature, TEMPR = 20.000 C

Temperature coefficient, ALPHAT = 3.930000E-03 /C

Relative permeability, RFMU = 1.000

m	K	L	X (cm)	Y (cm)	H (A/m)	|E| (V/m)
1	1	15	0.00000	0.193500	4.8315E+02	3.6872E+05
			7.370889E-03	0.193862	4.8448E+02	1.0191E+06
2	2	15	1.474178E-02	0.194224	4.8872E+02	1.9494E+06
			2.204168E-02	0.195307	4.9677E+02	2.8040E+06
3	3	15	2.934158E-02	0.196390	5.0627E+02	3.8454E+06
			3.650020E-02	0.198183	5.1925E+02	4.5924E+06
4	4	15	4.365882E-02	0.199976	5.3931E+02	5.9962E+06
			5.060720E-02	0.202462	5.5832E+02	6.8165E+06
5	5	15	5.755559E-02	0.204949	5.8165E+02	7.8572E+06
			6.422683E-02	0.208104	6.0520E+02	8.5529E+06
6	6	16	7.089807E-02	0.211259	6.3199E+02	9.5084E+06
			7.722792E-02	0.215053	6.6036E+02	1.0052E+07
7	7	16	8.355776E-02	0.218847	6.9110E+02	1.0865E+07
			8.948526E-02	0.223243	7.2336E+02	1.1389E+07
8	7	17	9.541275E-02	0.227639	7.5677E+02	1.1849E+07
			0.100881	0.232595	7.9157E+02	1.2170E+07

9	8	17	0.106349	0.237551	8.2702E+02	1.2510E+07
			0.111305	0.243019	8.6347E+02	1.2734E+07
10	9	18	0.116261	0.248487	8.9995E+02	1.2819E+07
			0.120657	0.254415	9.3716E+02	1.2886E+07
11	9	19	0.125053	0.260342	9.7411E+02	1.2780E+07
			0.128847	0.266672	1.0110E+03	1.2580E+07
12	10	20	0.132641	0.273002	1.0473E+03	1.2443E+07
			0.135796	0.279673	1.0830E+03	1.2179E+07
13	10	21	0.138951	0.286344	1.1181E+03	1.1865E+07
			0.141438	0.293293	1.1528E+03	1.1412E+07
14	11	22	0.143924	0.300241	1.1858E+03	1.1063E+07
			0.145717	0.307400	1.2178E+03	1.0572E+07
15	11	23	0.147510	0.314558	1.2484E+03	1.0223E+07
			0.148593	0.321858	1.2780E+03	9.6658E+06
16	11	24	0.149676	0.329158	1.3057E+03	9.1444E+06
			0.150038	0.336529	1.3316E+03	8.7327E+06
17	11	25	0.150400	0.343900	1.3563E+03	8.3146E+06

Summary for the above wall segment:

Emax = 1.2886E+07 V/m

Hmax = 1.3563E+03 A/m

Surface Area = 2.3615E-01 cm^2

Power = 6.6677E-02 W

Maximum P/A = 6.3637E-01 W/cm^2

Average P/A = 2.8234E-01 W/cm^2

df/dz = 4.1172E+01 MHz/mm (for volume added to the cavity)

df/f = 5.8544E-02

df/dr = 3.0317E+01 MHz/mm (for volume added to the cavity)

df/f = 4.3109E-02

Power and fields on wall segment 3. K,L = 11,25 to 11,50

This segment uses surface resistance option IRTYPE = 0

Surface resistance, Rs = 6.918579E-03 Ohm calculated from:

Operating temperature, TEMPC = 20.000 C

Reference resistivity, RHOR = 1.724100E-06 Ohm-cm

Reference temperature, TEMPR = 20.000 C

Temperature coefficient, ALPHAT = 3.930000E-03 /C

Relative permeability, RFMU = 1.000

m	K	L	X (cm)	Y (cm)	H (A/m)	|E| (V/m)
1	11	25	0.150400	0.343900	1.3563E+03	8.3146E+06
			0.150400	0.351022	1.3792E+03	7.9104E+06
2	11	26	0.150400	0.358144	1.4007E+03	7.5464E+06
			0.150400	0.365266	1.4207E+03	7.1394E+06
3	11	27	0.150400	0.372388	1.4392E+03	6.7476E+06
			0.150400	0.379510	1.4575E+03	6.4795E+06
4	11	28	0.150400	0.386632	1.4749E+03	6.2558E+06
			0.150400	0.393754	1.4918E+03	6.0053E+06
5	11	29	0.150400	0.400876	1.5080E+03	5.7857E+06
			0.150400	0.407998	1.5238E+03	5.6001E+06
6	11	30	0.150400	0.415120	1.5390E+03	5.4396E+06
			0.150400	0.422242	1.5538E+03	5.2718E+06
7	11	31	0.150400	0.429364	1.5682E+03	5.1141E+06
			0.150400	0.436486	1.5822E+03	4.9755E+06
8	11	32	0.150400	0.443608	1.5958E+03	4.8506E+06
			0.150400	0.450730	1.6090E+03	4.7178E+06
9	11	33	0.150400	0.457852	1.6219E+03	4.5996E+06

			0.150400	0.464974	1.6345E+03	4.4896E+06
10	11	34	0.150400	0.472096	1.6468E+03	4.3882E+06
			0.150400	0.479218	1.6589E+03	4.2816E+06
11	11	35	0.150400	0.486340	1.6706E+03	4.1853E+06
			0.150400	0.493462	1.6821E+03	4.0949E+06
12	11	36	0.150400	0.500584	1.6933E+03	4.0102E+06
			0.150400	0.507706	1.7043E+03	3.9265E+06
13	11	37	0.150400	0.514828	1.7151E+03	3.8414E+06
			0.150400	0.521950	1.7257E+03	3.7652E+06
14	11	38	0.150400	0.529072	1.7361E+03	3.6930E+06
			0.150400	0.536194	1.7462E+03	3.6180E+06
15	11	39	0.150400	0.543316	1.7562E+03	3.5495E+06
			0.150400	0.550438	1.7659E+03	3.4841E+06
16	11	40	0.150400	0.557560	1.7755E+03	3.4215E+06
			0.150400	0.564682	1.7849E+03	3.3569E+06
17	11	41	0.150400	0.571804	1.7942E+03	3.2976E+06
			0.150400	0.578926	1.8033E+03	3.2405E+06
18	11	42	0.150400	0.586048	1.8122E+03	3.1856E+06
			0.150400	0.593170	1.8210E+03	3.1292E+06
19	11	43	0.150400	0.600292	1.8296E+03	3.0769E+06
			0.150400	0.607414	1.8381E+03	3.0266E+06
20	11	44	0.150400	0.614536	1.8464E+03	2.9777E+06
			0.150400	0.621658	1.8546E+03	2.9278E+06
21	11	45	0.150400	0.628780	1.8627E+03	2.8810E+06
			0.150400	0.635902	1.8707E+03	2.8360E+06
22	11	46	0.150400	0.643024	1.8785E+03	2.7922E+06
			0.150400	0.650146	1.8862E+03	2.7476E+06
23	11	47	0.150400	0.657268	1.8938E+03	2.7045E+06
			0.150400	0.664390	1.9012E+03	2.6631E+06

24	11	48	0.150400	0.671512	1.9086E+03	2.6225E+06
			0.150400	0.678634	1.9158E+03	2.5825E+06
25	11	49	0.150400	0.685756	1.9230E+03	2.5419E+06
			0.150400	0.692878	1.9300E+03	2.5034E+06
26	11	50	0.150400	0.700000	1.9369E+03	2.4650E+06

Summary for the above wall segment:

Emax = 8.3146E+06 V/m

Hmax = 1.9369E+03 A/m

Surface Area = 3.5610E-01 cm^2

Power = 3.5988E-01 W

Maximum P/A = 1.2977E+00 W/cm^2

Average P/A = 1.0106E+00 W/cm^2

df/dz = 1.5186E+01 MHz/mm (for volume added to the cavity)

df/f = 2.1594E-02

Power and fields on wall segment 4. K,L = 11,50 to 11,54

This segment uses surface resistance option IRTYPE = 0

Surface resistance, Rs = 6.918579E-03 Ohm calculated from:

Operating temperature, TEMPC = 20.000 C

Reference resistivity, RHOR = 1.724100E-06 Ohm-cm

Reference temperature, TEMPR = 20.000 C

Temperature coefficient, ALPHAT = 3.930000E-03 /C

Relative permeability, RFMU = 1.000

m	K	L	X (cm)	Y (cm)	H (A/m)	|E| (V/m)
1	11	50	0.150400	0.700000	1.9369E+03	2.4650E+06
			0.150400	0.712200	1.9484E+03	2.4001E+06

2	11	51	0.150400	0.724400	1.9597E+03	2.3361E+06
			0.150400	0.736600	1.9707E+03	2.2680E+06
3	11	52	0.150400	0.748800	1.9814E+03	2.2046E+06
			0.150400	0.761000	1.9918E+03	2.1407E+06
4	11	53	0.150400	0.773200	2.0017E+03	2.0634E+06
			0.150400	0.785400	2.0113E+03	2.0227E+06
5	11	54	0.150400	0.797600	2.0208E+03	1.9758E+06

Summary for the above wall segment:

Emax = 2.4650E+06 V/m

Hmax = 2.0208E+03 A/m

Surface Area = 9.7600E-02 cm^2

Power = 1.3245E-01 W

Maximum P/A = 1.4127E+00 W/cm^2

Average P/A = 1.3570E+00 W/cm^2

df/dz = 9.4643E-01 MHz/mm (for volume added to the cavity)

df/f = 1.3458E-03

Power and fields on wall segment 5. K,L = 11,54 to 12,54

This segment uses surface resistance option IRTYPE = 0

Surface resistance, Rs = 6.918579E-03 Ohm calculated from:

Operating temperature, TEMPC = 20.000 C

Reference resistivity, RHOR = 1.724100E-06 Ohm-cm

Reference temperature, TEMPR = 20.000 C

Temperature coefficient, ALPHAT = 3.930000E-03 /C

Relative permeability, RFMU = 1.000

m	K	L	X (cm)	Y (cm)	H (A/m)	|E| (V/m)

1	11	54	0.150400	0.797600	2.0208E+03	1.9758E+06
			0.150550	0.800050	2.0225E+03	1.9748E+06
2	12	54	0.150700	0.802500	2.0244E+03	1.9440E+06

Summary for the above wall segment:

Emax = 1.9758E+06 V/m

Hmax = 2.0244E+03 A/m

Surface Area = 4.9092E-03 cm^2

Power = 6.9469E-03 W

Maximum P/A = 1.4176E+00 W/cm^2

Average P/A = 1.4151E+00 W/cm^2

df/dz = 3.5895E-02 MHz/mm (for volume added to the cavity)

df/f = 5.1041E-05

df/dr = 2.1976E-03 MHz/mm (for volume added to the cavity)

df/f = 3.1250E-06

Power and fields on wall segment 6. K,L = 12,54 to 17,80

This segment uses surface resistance option IRTYPE = 0

Surface resistance, Rs = 6.918579E-03 Ohm calculated from:

Operating temperature, TEMPC = 20.000 C

Reference resistivity, RHOR = 1.724100E-06 Ohm-cm

Reference temperature, TEMPR = 20.000 C

Temperature coefficient, ALPHAT = 3.930000E-03 /C

Relative permeability, RFMU = 1.000

m	K	L	X (cm)	Y (cm)	H (A/m)	|E| (V/m)
1	12	54	0.150700	0.802500	2.0244E+03	1.9440E+06
			0.152111	0.813990	2.0331E+03	1.9343E+06

2	12	55	0.153521	0.825481	2.0417E+03	1.9179E+06
			0.154932	0.836971	2.0504E+03	1.9112E+06
3	12	56	0.156343	0.848462	2.0590E+03	1.9034E+06
			0.157754	0.859952	2.0676E+03	1.8943E+06
4	12	57	0.159164	0.871442	2.0762E+03	1.8855E+06
			0.160575	0.882933	2.0847E+03	1.8673E+06
5	13	58	0.161986	0.894423	2.0932E+03	1.8505E+06
			0.163397	0.905913	2.1015E+03	1.8316E+06
6	13	59	0.164807	0.917404	2.1098E+03	1.8126E+06
			0.166218	0.928894	2.1180E+03	1.7932E+06
7	13	60	0.167629	0.940385	2.1260E+03	1.7736E+06
			0.169040	0.951875	2.1340E+03	1.7542E+06
8	13	61	0.170450	0.963365	2.1419E+03	1.7346E+06
			0.171861	0.974856	2.1497E+03	1.7134E+06
9	14	62	0.173272	0.986346	2.1575E+03	1.6940E+06
			0.174683	0.997837	2.1651E+03	1.6743E+06
10	14	63	0.176093	1.00933	2.1726E+03	1.6547E+06
			0.177504	1.02082	2.1800E+03	1.6340E+06
11	14	64	0.178915	1.03231	2.1874E+03	1.6158E+06
			0.180326	1.04380	2.1947E+03	1.5981E+06
12	14	65	0.181736	1.05529	2.2019E+03	1.5798E+06
			0.183147	1.06678	2.2090E+03	1.5627E+06
13	14	66	0.184558	1.07827	2.2160E+03	1.5459E+06
			0.185969	1.08976	2.2230E+03	1.5289E+06
14	14	67	0.187379	1.10125	2.2299E+03	1.5113E+06
			0.188790	1.11274	2.2367E+03	1.4930E+06
15	15	68	0.190201	1.12423	2.2434E+03	1.4767E+06
			0.191611	1.13572	2.2500E+03	1.4595E+06
16	15	69	0.193022	1.14721	2.2566E+03	1.4425E+06

			0.194433	1.15870	2.2631E+03	1.4263E+06
17	15	70	0.195844	1.17019	2.2695E+03	1.4113E+06
			0.197254	1.18168	2.2759E+03	1.3969E+06
18	15	71	0.198665	1.19317	2.2822E+03	1.3820E+06
			0.200076	1.20466	2.2884E+03	1.3682E+06
19	15	72	0.201487	1.21615	2.2946E+03	1.3545E+06
			0.202897	1.22764	2.3007E+03	1.3404E+06
20	15	73	0.204308	1.23913	2.3067E+03	1.3258E+06
			0.205719	1.25062	2.3127E+03	1.3103E+06
21	16	74	0.207130	1.26212	2.3186E+03	1.2957E+06
			0.208540	1.27361	2.3244E+03	1.2822E+06
22	16	75	0.209951	1.28510	2.3302E+03	1.2692E+06
			0.211362	1.29659	2.3359E+03	1.2577E+06
23	16	76	0.212773	1.30808	2.3416E+03	1.2453E+06
			0.214183	1.31957	2.3472E+03	1.2306E+06
24	16	77	0.215594	1.33106	2.3527E+03	1.2188E+06
			0.217005	1.34255	2.3582E+03	1.2066E+06
25	17	78	0.218416	1.35404	2.3637E+03	1.1931E+06
			0.219826	1.36553	2.3691E+03	1.1846E+06
26	16	79	0.221237	1.37702	2.3744E+03	1.1731E+06
			0.222648	1.38851	2.3797E+03	1.1610E+06
27	17	80	0.224059	1.40000	2.3849E+03	1.1502E+06

Summary for the above wall segment:

Emax = 1.9440E+06 V/m

Hmax = 2.3849E+03 A/m

Surface Area = 6.0199E-01 cm^2

Power = 1.0297E+00 W

Maximum P/A = 1.9676E+00 W/cm^2

Average P/A = 1.7105E+00 W/cm^2

df/dz = 2.2932E+00 MHz/mm (for volume added to the cavity)

df/f = 3.2609E-03

df/dr = 2.8155E-01 MHz/mm (for volume added to the cavity)

df/f = 4.0036E-04

Power and fields on wall segment 7. K,L = 17,80 to 22,95

This segment uses surface resistance option IRTYPE = 0

Surface resistance, Rs = 6.918579E-03 Ohm calculated from:

Operating temperature, TEMPC = 20.000 C

Reference resistivity, RHOR = 1.724100E-06 Ohm-cm

Reference temperature, TEMPR = 20.000 C

Temperature coefficient, ALPHAT = 3.930000E-03 /C

Relative permeability, RFMU = 1.000

m	K	L	X (cm)	Y (cm)	H (A/m)	|E| (V/m)
1	17	80	0.224059	1.40000	2.3849E+03	1.1502E+06
			0.226923	1.42333	2.3954E+03	1.1281E+06
2	17	81	0.229788	1.44667	2.4057E+03	1.1060E+06
			0.232653	1.47000	2.4157E+03	1.0854E+06
3	18	82	0.235518	1.49333	2.4256E+03	1.0623E+06
			0.238382	1.51667	2.4353E+03	1.0403E+06
4	18	83	0.241247	1.54000	2.4447E+03	1.0207E+06
			0.244112	1.56333	2.4540E+03	1.0031E+06
5	18	84	0.246977	1.58667	2.4632E+03	9.8559E+05
			0.249841	1.61000	2.4722E+03	9.6889E+05
6	18	85	0.252706	1.63333	2.4810E+03	9.5207E+05
			0.255571	1.65667	2.4897E+03	9.3653E+05

7	19	86	0.258436	1.68000	2.4982E+03	9.1852E+05
			0.261301	1.70333	2.5066E+03	9.0222E+05
8	19	87	0.264165	1.72667	2.5148E+03	8.8554E+05
			0.267030	1.75000	2.5229E+03	8.7040E+05
9	20	88	0.269895	1.77333	2.5308E+03	8.5497E+05
			0.272760	1.79667	2.5386E+03	8.4067E+05
10	20	89	0.275624	1.82000	2.5463E+03	8.2643E+05
			0.278489	1.84333	2.5538E+03	8.1270E+05
11	21	90	0.281354	1.86667	2.5612E+03	7.9667E+05
			0.284219	1.89000	2.5685E+03	7.8221E+05
12	21	91	0.287083	1.91333	2.5756E+03	7.6847E+05
			0.289948	1.93667	2.5826E+03	7.5682E+05
13	21	92	0.292813	1.96000	2.5895E+03	7.4506E+05
			0.295678	1.98333	2.5963E+03	7.3379E+05
14	21	93	0.298543	2.00667	2.6030E+03	7.2175E+05
			0.301407	2.03000	2.6096E+03	7.1088E+05
15	22	94	0.304272	2.05333	2.6161E+03	6.9865E+05
			0.307137	2.07667	2.6224E+03	6.8695E+05
16	22	95	0.310002	2.10000	2.6287E+03	6.7520E+05

Summary for the above wall segment:

Emax = 1.1502E+06 V/m

Hmax = 2.6287E+03 A/m

Surface Area = 7.0526E-01 cm^2

Power = 1.5475E+00 W

Maximum P/A = 2.3904E+00 W/cm^2

Average P/A = 2.1942E+00 W/cm^2

df/dz = -1.6028E-01 MHz/mm (for volume added to the cavity)

df/f = -2.2791E-04

df/dr = -1.9679E-02 MHz/mm (for volume added to the cavity)

df/f = -2.7982E-05

Power and fields on wall segment 8. K,L = 22,95 to 36,111

This segment uses surface resistance option IRTYPE = 0

Surface resistance, Rs = 6.918579E-03 Ohm calculated from:

Operating temperature, TEMPC = 20.000 C

Reference resistivity, RHOR = 1.724100E-06 Ohm-cm

Reference temperature, TEMPR = 20.000 C

Temperature coefficient, ALPHAT = 3.930000E-03 /C

Relative permeability, RFMU = 1.000

m	K	L	X (cm)	Y (cm)	H (A/m)	|E| (V/m)
1	22	95	0.310002	2.10000	2.6287E+03	6.7520E+05
			0.314536	2.13693	2.6384E+03	6.5720E+05
2	23	96	0.319070	2.17386	2.6478E+03	6.4021E+05
			0.323604	2.21079	2.6570E+03	6.2350E+05
3	24	96	0.328138	2.24772	2.6660E+03	6.0719E+05
			0.332672	2.28465	2.6747E+03	5.9171E+05
4	24	97	0.337206	2.32158	2.6832E+03	5.7606E+05
			0.341740	2.35851	2.6914E+03	5.6171E+05
5	25	98	0.346274	2.39544	2.6995E+03	5.4682E+05
			0.350808	2.43237	2.7074E+03	5.3315E+05
6	25	99	0.355342	2.46930	2.7150E+03	5.1959E+05
			0.359876	2.50623	2.7225E+03	5.0603E+05
7	26	99	0.364410	2.54315	2.7298E+03	4.9292E+05
			0.368944	2.58008	2.7368E+03	4.7939E+05
8	27	100	0.373478	2.61701	2.7437E+03	4.6601E+05

			0.378012	2.65394	2.7504E+03	4.5400E+05
9	27	101	0.382546	2.69087	2.7569E+03	4.4130E+05
			0.387081	2.72780	2.7632E+03	4.2999E+05
10	28	102	0.391615	2.76473	2.7694E+03	4.1873E+05
			0.396149	2.80166	2.7754E+03	4.0706E+05
11	29	102	0.400683	2.83859	2.7813E+03	3.9589E+05
			0.405217	2.87552	2.7869E+03	3.8433E+05
12	29	103	0.409751	2.91245	2.7924E+03	3.7246E+05
			0.414285	2.94938	2.7978E+03	3.6241E+05
13	30	104	0.418819	2.98631	2.8030E+03	3.5184E+05
			0.423353	3.02324	2.8080E+03	3.4149E+05
14	31	104	0.427887	3.06017	2.8130E+03	3.3140E+05
			0.432421	3.09710	2.8177E+03	3.2063E+05
15	31	105	0.436955	3.13403	2.8223E+03	3.0947E+05
			0.441489	3.17096	2.8267E+03	2.9980E+05
16	32	106	0.446023	3.20789	2.8310E+03	2.8973E+05
			0.450557	3.24482	2.8351E+03	2.8099E+05
17	32	107	0.455091	3.28175	2.8392E+03	2.7159E+05
			0.459625	3.31867	2.8430E+03	2.6234E+05
18	33	107	0.464159	3.35560	2.8468E+03	2.5291E+05
			0.468694	3.39253	2.8504E+03	2.4303E+05
19	34	108	0.473228	3.42946	2.8539E+03	2.3176E+05
			0.477762	3.46639	2.8572E+03	2.2281E+05
20	34	109	0.482296	3.50332	2.8603E+03	2.1311E+05
			0.486830	3.54025	2.8634E+03	2.0416E+05
21	35	110	0.491364	3.57718	2.8663E+03	1.9508E+05
			0.495898	3.61411	2.8691E+03	1.8593E+05
22	36	110	0.500432	3.65104	2.8717E+03	1.7538E+05
			0.504966	3.68797	2.8742E+03	1.6465E+05

23 36 111 0.509500 3.72490 2.8765E+03 1.5243E+05

Summary for the above wall segment:

Emax = 6.7520E+05 V/m

Hmax = 2.8765E+03 A/m

Surface Area = 1.6371E+00 cm^2

Power = 4.3776E+00 W

Maximum P/A = 2.8624E+00 W/cm^2

Average P/A = 2.6740E+00 W/cm^2

df/dz = -3.3951E+00 MHz/mm (for volume added to the cavity)

df/f = -4.8277E-03

df/dr = -4.1683E-01 MHz/mm (for volume added to the cavity)

df/f = -5.9272E-04

Power and fields on wall segment 9. K,L = 36,111 to 50,116

This segment uses surface resistance option IRTYPE = 0

Surface resistance, Rs = 6.918579E-03 Ohm calculated from:

Operating temperature, TEMPC = 20.000 C

Reference resistivity, RHOR = 1.724100E-06 Ohm-cm

Reference temperature, TEMPR = 20.000 C

Temperature coefficient, ALPHAT = 3.930000E-03 /C

Relative permeability, RFMU = 1.000

m	K	L	X (cm)	Y (cm)	H (A/m)	|E| (V/m)
1	36	111	0.509500	3.72490	2.8765E+03	1.5243E+05
			0.514183	3.75533	2.8783E+03	1.4432E+05
2	37	112	0.518866	3.78577	2.8800E+03	1.3615E+05
			0.524170	3.81080	2.8813E+03	1.3001E+05

3	38	112	0.529473	3.83583	2.8826E+03	1.2704E+05
			0.535089	3.85726	2.8837E+03	1.2281E+05
4	38	113	0.540705	3.87869	2.8847E+03	1.1833E+05
			0.546505	3.89757	2.8856E+03	1.1462E+05
5	39	113	0.552305	3.91645	2.8865E+03	1.1121E+05
			0.558224	3.93343	2.8873E+03	1.0821E+05
6	40	113	0.564142	3.95040	2.8881E+03	1.0824E+05
			0.570144	3.96588	2.8888E+03	1.0521E+05
7	41	114	0.576145	3.98136	2.8894E+03	1.0233E+05
			0.582207	3.99563	2.8901E+03	1.0001E+05
8	42	114	0.588269	4.00989	2.8907E+03	9.7916E+04
			0.594377	4.02315	2.8912E+03	9.6331E+04
9	43	114	0.600485	4.03641	2.8918E+03	9.6107E+04
			0.606630	4.04881	2.8923E+03	9.3799E+04
10	43	115	0.612775	4.06121	2.8928E+03	9.1876E+04
			0.618949	4.07287	2.8933E+03	9.0417E+04
11	44	115	0.625122	4.08453	2.8937E+03	8.9298E+04
			0.631321	4.09555	2.8942E+03	8.8190E+04
12	45	115	0.637519	4.10656	2.8946E+03	8.7431E+04
			0.643737	4.11700	2.8950E+03	8.6690E+04
13	46	115	0.649955	4.12744	2.8955E+03	8.5319E+04
			0.656191	4.13736	2.8959E+03	8.3167E+04
14	47	115	0.662426	4.14729	2.8962E+03	8.3741E+04
			0.668676	4.15674	2.8966E+03	8.2449E+04
15	48	116	0.674926	4.16620	2.8970E+03	8.0338E+04
			0.681189	4.17524	2.8973E+03	7.8959E+04
16	49	116	0.687452	4.18427	2.8977E+03	7.7844E+04
			0.693726	4.19292	2.8980E+03	7.7834E+04
17	50	116	0.700000	4.20157	2.8983E+03	7.6523E+04

Summary for the above wall segment:

Emax = 1.5243E+05 V/m

Hmax = 2.8983E+03 A/m

Surface Area = 5.1904E-01 cm^2

Power = 1.4982E+00 W

Maximum P/A = 2.9059E+00 W/cm^2

Average P/A = 2.8865E+00 W/cm^2

df/dz = -1.2599E+00 MHz/mm (for volume added to the cavity)

df/f = -1.7915E-03

df/dr = -5.0529E-01 MHz/mm (for volume added to the cavity)

df/f = -7.1850E-04

Power and fields on wall segment 10. K,L = 50,116 to 80,120

This segment uses surface resistance option IRTYPE = 0

Surface resistance, Rs = 6.918579E-03 Ohm calculated from:

Operating temperature, TEMPC = 20.000 C

Reference resistivity, RHOR = 1.724100E-06 Ohm-cm

Reference temperature, TEMPR = 20.000 C

Temperature coefficient, ALPHAT = 3.930000E-03 /C

Relative permeability, RFMU = 1.000

m	K	L	X (cm)	Y (cm)	H (A/m)	|E| (V/m)
1	50	116	0.700000	4.20157	2.8983E+03	7.6523E+04
			0.710591	4.21534	2.8988E+03	7.6238E+04
2	51	116	0.721182	4.22911	2.8994E+03	7.4279E+04
			0.731831	4.24203	2.8998E+03	7.2689E+04
3	52	116	0.742481	4.25494	2.9003E+03	7.2955E+04

			0.753179	4.26709	2.9008E+03	7.1215E+04
4	52	117	0.763878	4.27923	2.9012E+03	6.8668E+04
			0.774618	4.29067	2.9016E+03	6.7078E+04
5	53	117	0.785358	4.30210	2.9020E+03	6.6080E+04
			0.796135	4.31290	2.9025E+03	6.4675E+04
6	54	117	0.806911	4.32369	2.9028E+03	6.3420E+04
			0.817719	4.33388	2.9032E+03	6.2306E+04
7	55	117	0.828527	4.34407	2.9036E+03	6.3668E+04
			0.839363	4.35371	2.9040E+03	6.2272E+04
8	56	118	0.850199	4.36335	2.9043E+03	6.0721E+04
			0.861059	4.37247	2.9046E+03	5.8460E+04
9	57	118	0.871919	4.38158	2.9050E+03	5.7712E+04
			0.882800	4.39021	2.9053E+03	5.6721E+04
10	58	118	0.893681	4.39884	2.9056E+03	5.6144E+04
			0.904582	4.40701	2.9059E+03	5.5243E+04
11	59	118	0.915483	4.41518	2.9062E+03	5.4781E+04
			0.926401	4.42292	2.9065E+03	5.3504E+04
12	60	118	0.937319	4.43065	2.9068E+03	5.3494E+04
			0.948252	4.43797	2.9071E+03	5.2411E+04
13	61	118	0.959185	4.44529	2.9073E+03	5.1738E+04
			0.970132	4.45221	2.9076E+03	5.0544E+04
14	62	118	0.981080	4.45914	2.9079E+03	5.1515E+04
			0.992039	4.46568	2.9081E+03	5.0431E+04
15	62	119	1.00300	4.47223	2.9084E+03	4.9184E+04
			1.01397	4.47841	2.9086E+03	4.8103E+04
16	63	119	1.02494	4.48459	2.9088E+03	4.6845E+04
			1.03592	4.49042	2.9091E+03	4.5841E+04
17	64	119	1.04690	4.49626	2.9093E+03	4.5709E+04
			1.05790	4.50175	2.9095E+03	4.5504E+04

18	65	119	1.06889	4.50725	2.9097E+03	4.4867E+04
			1.07989	4.51242	2.9100E+03	4.4150E+04
19	66	119	1.09089	4.51759	2.9102E+03	4.3870E+04
			1.10189	4.52244	2.9104E+03	4.3018E+04
20	67	119	1.11290	4.52730	2.9106E+03	4.2880E+04
			1.12392	4.53184	2.9108E+03	4.1916E+04
21	68	119	1.13493	4.53639	2.9110E+03	4.2077E+04
			1.14595	4.54064	2.9112E+03	4.0456E+04
22	69	119	1.15697	4.54489	2.9114E+03	4.0839E+04
			1.16800	4.54884	2.9115E+03	3.9268E+04
23	70	119	1.17902	4.55280	2.9118E+03	3.8809E+04
			1.19006	4.55647	2.9119E+03	3.7822E+04
24	71	120	1.20109	4.56014	2.9121E+03	3.8052E+04
			1.21213	4.56354	2.9123E+03	3.7964E+04
25	72	120	1.22316	4.56693	2.9124E+03	3.8576E+04
			1.23420	4.57005	2.9126E+03	3.6960E+04
26	73	120	1.24525	4.57317	2.9127E+03	3.8089E+04
			1.25629	4.57602	2.9129E+03	3.5835E+04
27	74	120	1.26734	4.57887	2.9131E+03	3.7018E+04
			1.27838	4.58146	2.9132E+03	3.2816E+04
28	75	120	1.28943	4.58404	2.9134E+03	3.3870E+04
			1.30048	4.58637	2.9135E+03	3.1400E+04
29	76	120	1.31154	4.58870	2.9137E+03	3.2537E+04
			1.32259	4.59076	2.9138E+03	3.0181E+04
30	77	120	1.33365	4.59283	2.9139E+03	3.1307E+04
			1.34470	4.59465	2.9141E+03	2.8883E+04
31	78	120	1.35576	4.59646	2.9142E+03	2.9912E+04
			1.36682	4.59803	2.9144E+03	2.7570E+04
32	79	120	1.37788	4.59959	2.9145E+03	2.8338E+04

1.38894 4.60091 2.9146E+03 2.6634E+04

33 80 120 1.40000 4.60222 2.9147E+03 2.6785E+04

Summary for the above wall segment:

Emax = 7.6523E+04 V/m

Hmax = 2.9147E+03 A/m

Surface Area = 8.2988E-01 cm^2

Power = 2.4274E+00 W

Maximum P/A = 2.9389E+00 W/cm^2

Average P/A = 2.9250E+00 W/cm^2

df/dz = -1.0801E+00 MHz/mm (for volume added to the cavity)

df/f = -1.5358E-03

df/dr = -1.8918E+00 MHz/mm (for volume added to the cavity)

df/f = -2.6900E-03

Power and fields on wall segment 11. K,L = 80,120 to 95,118

This segment uses surface resistance option IRTYPE = 0

Surface resistance, Rs = 6.918579E-03 Ohm calculated from:

Operating temperature, TEMPC = 20.000 C

Reference resistivity, RHOR = 1.724100E-06 Ohm-cm

Reference temperature, TEMPR = 20.000 C

Temperature coefficient, ALPHAT = 3.930000E-03 /C

Relative permeability, RFMU = 1.000

m	K	L	X (cm)	Y (cm)	H (A/m)	|E| (V/m)
1	80	120	1.40000	4.60222	2.9147E+03	2.6785E+04
			1.42132	4.60406	2.9150E+03	2.6058E+04
2	81	120	1.44263	4.60589	2.9152E+03	2.6872E+04

			1.46396	4.60682	2.9154E+03	2.5246E+04
3	82	120	1.48529	4.60775	2.9156E+03	2.6698E+04
			1.50662	4.60777	2.9158E+03	2.3522E+04
4	83	120	1.52795	4.60779	2.9160E+03	2.5300E+04
			1.54928	4.60690	2.9162E+03	2.1965E+04
5	84	120	1.57061	4.60602	2.9164E+03	2.3817E+04
			1.59193	4.60422	2.9166E+03	2.0417E+04
6	85	120	1.61324	4.60243	2.9167E+03	2.2223E+04
			1.63454	4.59972	2.9169E+03	1.8701E+04
7	86	120	1.65583	4.59701	2.9170E+03	2.0353E+04
			1.67710	4.59337	2.9172E+03	1.6157E+04
8	87	120	1.69836	4.58973	2.9173E+03	1.6847E+04
			1.71959	4.58516	2.9175E+03	1.4820E+04
9	88	120	1.74081	4.58058	2.9176E+03	1.5479E+04
			1.76199	4.57504	2.9177E+03	1.3515E+04
10	89	120	1.78317	4.56950	2.9178E+03	1.4782E+04
			1.80428	4.56298	2.9179E+03	1.5056E+04
11	89	119	1.82540	4.55646	2.9181E+03	1.5350E+04
			1.84644	4.54892	2.9181E+03	1.1383E+04
12	90	119	1.86748	4.54139	2.9182E+03	1.2163E+04
			1.88844	4.53281	2.9183E+03	1.0293E+04
13	91	119	1.90940	4.52423	2.9183E+03	1.0911E+04
			1.93025	4.51457	2.9184E+03	9.5230E+03
14	92	119	1.95110	4.50491	2.9185E+03	1.0141E+04
			1.97184	4.49412	2.9185E+03	8.2604E+03
15	93	119	1.99257	4.48332	2.9186E+03	8.4578E+03
			2.01316	4.47134	2.9186E+03	8.9409E+03
16	94	118	2.03375	4.45936	2.9187E+03	9.1724E+03
			2.05418	4.44613	2.9187E+03	5.5554E+03

17 95 118 2.07460 4.43290 2.9187E+03 6.9747E+03

Summary for the above wall segment:

Emax = 2.6872E+04 V/m

Hmax = 2.9187E+03 A/m

Surface Area = 7.1013E-01 cm^2

Power = 2.0907E+00 W

Maximum P/A = 2.9469E+00 W/cm^2

Average P/A = 2.9442E+00 W/cm^2

df/dz = -4.9190E-01 MHz/mm (for volume added to the cavity)

df/f = -6.9946E-04

df/dr = -1.8376E+00 MHz/mm (for volume added to the cavity)

df/f = -2.6131E-03

Power and fields on wall segment 12. K,L = 95,118 to 95,119

This segment uses surface resistance option IRTYPE = 0

Surface resistance, Rs = 6.918579E-03 Ohm calculated from:

Operating temperature, TEMPC = 20.000 C

Reference resistivity, RHOR = 1.724100E-06 Ohm-cm

Reference temperature, TEMPR = 20.000 C

Temperature coefficient, ALPHAT = 3.930000E-03 /C

Relative permeability, RFMU = 1.000

m	K	L	X (cm)	Y (cm)	H (A/m)	|E| (V/m)
1	95	118	2.07460	4.43290	2.9187E+03	6.9747E+03
			2.08730	4.42425	2.9187E+03	6.2756E+03
2	95	119	2.10000	4.41559	2.9187E+03	6.5918E+03

Summary for the above wall segment:

Emax = 6.9747E+03 V/m

Hmax = 2.9187E+03 A/m

Surface Area = 3.0737E-02 cm^2

Power = 9.0580E-02 W

Maximum P/A = 2.9470E+00 W/cm^2

Average P/A = 2.9469E+00 W/cm^2

df/dz = -4.7206E-02 MHz/mm (for volume added to the cavity)

df/f = -6.7126E-05

df/dr = -6.9273E-02 MHz/mm (for volume added to the cavity)

df/f = -9.8504E-05

Power and fields on wall segment 13. K,L = 95,119 to 108,108

This segment uses surface resistance option IRTYPE = 0

Surface resistance, Rs = 6.918579E-03 Ohm calculated from:

Operating temperature, TEMPC = 20.000 C

Reference resistivity, RHOR = 1.724100E-06 Ohm-cm

Reference temperature, TEMPR = 20.000 C

Temperature coefficient, ALPHAT = 3.930000E-03 /C

Relative permeability, RFMU = 1.000

m	K	L	X (cm)	Y (cm)	H (A/m)	|E| (V/m)
1	95	119	2.10000	4.41559	2.9187E+03	6.5918E+03
			2.13755	4.38948	2.9187E+03	7.5299E+03
2	96	118	2.17511	4.36337	2.9188E+03	8.2651E+03
			2.21239	4.33688	2.9187E+03	9.4567E+03
3	96	117	2.24968	4.31040	2.9187E+03	9.3599E+03
			2.28669	4.28353	2.9187E+03	9.4386E+03

4	97	116	2.32371	4.25666	2.9186E+03	1.0161E+04
			2.36044	4.22942	2.9185E+03	9.9092E+03
5	98	116	2.39718	4.20218	2.9185E+03	1.0886E+04
			2.43364	4.17457	2.9184E+03	1.0696E+04
6	98	115	2.47011	4.14695	2.9183E+03	1.1235E+04
			2.50628	4.11897	2.9182E+03	1.0707E+04
7	99	115	2.54246	4.09099	2.9181E+03	1.1587E+04
			2.57835	4.06264	2.9180E+03	1.1221E+04
8	100	114	2.61425	4.03429	2.9179E+03	1.1375E+04
			2.64985	4.00558	2.9178E+03	1.1170E+04
9	101	114	2.68545	3.97687	2.9177E+03	1.0234E+04
			2.72076	3.94779	2.9176E+03	1.1312E+04
10	101	113	2.75607	3.91872	2.9175E+03	1.1611E+04
			2.79108	3.88929	2.9174E+03	1.0989E+04
11	102	113	2.82609	3.85986	2.9173E+03	1.2368E+04
			2.86080	3.83008	2.9172E+03	1.1448E+04
12	103	112	2.89551	3.80029	2.9171E+03	1.1038E+04
			2.92991	3.77016	2.9170E+03	1.0784E+04
13	103	111	2.96432	3.74002	2.9169E+03	1.1413E+04
			2.99842	3.70954	2.9169E+03	1.1008E+04
14	104	111	3.03251	3.67906	2.9168E+03	1.2201E+04
			3.06630	3.64823	2.9167E+03	1.1163E+04
15	105	110	3.10008	3.61740	2.9166E+03	1.0511E+04
			3.13355	3.58623	2.9166E+03	1.0494E+04
16	105	109	3.16703	3.55506	2.9165E+03	9.9115E+03
			3.20018	3.52355	2.9165E+03	1.0804E+04
17	106	109	3.23333	3.49204	2.9165E+03	9.7342E+03
			3.26616	3.46020	2.9164E+03	1.0234E+04
18	107	108	3.29899	3.42835	2.9164E+03	1.0077E+04

3.33150 3.39618 2.9164E+03 9.8050E+03

19 108 108 3.36400 3.36400 2.9164E+03 9.9246E+03

Summary for the above wall segment:

Emax = 1.2368E+04 V/m

Hmax = 2.9188E+03 A/m

Surface Area = 1.6465E+00 cm^2

Power = 4.8483E+00 W

Maximum P/A = 2.9470E+00 W/cm^2

Average P/A = 2.9446E+00 W/cm^2

df/dz = -2.8655E+00 MHz/mm (for volume added to the cavity)

df/f = -4.0746E-03

df/dr = -3.4445E+00 MHz/mm (for volume added to the cavity)

df/f = -4.8979E-03

Power and fields on wall segment 14. K,L = 108,108 to 117,95

This segment uses surface resistance option IRTYPE = 0

Surface resistance, Rs = 6.918579E-03 Ohm calculated from:

Operating temperature, TEMPC = 20.000 C

Reference resistivity, RHOR = 1.724100E-06 Ohm-cm

Reference temperature, TEMPR = 20.000 C

Temperature coefficient, ALPHAT = 3.930000E-03 /C

Relative permeability, RFMU = 1.000

m	K	L	X (cm)	Y (cm)	H (A/m)	|E| (V/m)
1	108	108	3.36400	3.36400	2.9164E+03	9.9246E+03
			3.40017	3.32740	2.9164E+03	1.0312E+04
2	108	107	3.43633	3.29080	2.9164E+03	1.0198E+04

			3.47209	3.25380	2.9165E+03	1.0604E+04
3	109	106	3.50784	3.21680	2.9165E+03	9.9833E+03
			3.54317	3.17939	2.9165E+03	1.0858E+04
4	109	105	3.57850	3.14198	2.9166E+03	1.0409E+04
			3.61340	3.10417	2.9167E+03	1.2189E+04
5	110	105	3.64829	3.06636	2.9167E+03	1.1474E+04
			3.68276	3.02816	2.9168E+03	1.1620E+04
6	111	104	3.71722	2.98995	2.9169E+03	1.1115E+04
			3.75125	2.95135	2.9170E+03	1.1150E+04
7	111	103	3.78527	2.91276	2.9170E+03	1.0319E+04
			3.81885	2.87377	2.9171E+03	1.1577E+04
8	112	103	3.85243	2.83479	2.9173E+03	1.1657E+04
			3.88557	2.79542	2.9174E+03	1.1644E+04
9	113	102	3.91870	2.75606	2.9175E+03	1.0714E+04
			3.95138	2.71631	2.9176E+03	1.1205E+04
10	113	101	3.98406	2.67657	2.9177E+03	1.0963E+04
			4.01629	2.63646	2.9178E+03	1.1244E+04
11	114	100	4.04851	2.59635	2.9179E+03	1.0806E+04
			4.08027	2.55587	2.9181E+03	1.1684E+04
12	115	100	4.11204	2.51539	2.9182E+03	1.1009E+04
			4.14334	2.47455	2.9183E+03	1.0705E+04
13	115	99	4.17463	2.43371	2.9183E+03	9.0576E+03
			4.20546	2.39252	2.9184E+03	1.0084E+04
14	116	98	4.23629	2.35132	2.9185E+03	8.5530E+03
			4.26665	2.30978	2.9186E+03	9.5577E+03
15	116	97	4.29701	2.26823	2.9186E+03	7.6995E+03
			4.32689	2.22634	2.9187E+03	8.7878E+03
16	117	96	4.35677	2.18446	2.9187E+03	7.1415E+03
			4.38616	2.14223	2.9187E+03	7.6594E+03

17 117 95 4.41556 2.10000 2.9187E+03 6.6070E+03

Summary for the above wall segment:

Emax = 1.2189E+04 V/m

Hmax = 2.9187E+03 A/m

Surface Area = 1.6465E+00 cm^2

Power = 4.8482E+00 W

Maximum P/A = 2.9469E+00 W/cm^2

Average P/A = 2.9445E+00 W/cm^2

df/dz = -3.4444E+00 MHz/mm (for volume added to the cavity)

df/f = -4.8979E-03

df/dr = -2.8654E+00 MHz/mm (for volume added to the cavity)

df/f = -4.0745E-03

Power and fields on wall segment 15. K,L = 117,95 to 118,95

This segment uses surface resistance option IRTYPE = 0

Surface resistance, Rs = 6.918579E-03 Ohm calculated from:

Operating temperature, TEMPC = 20.000 C

Reference resistivity, RHOR = 1.724100E-06 Ohm-cm

Reference temperature, TEMPR = 20.000 C

Temperature coefficient, ALPHAT = 3.930000E-03 /C

Relative permeability, RFMU = 1.000

m	K	L	X (cm)	Y (cm)	H (A/m)	|E| (V/m)
1	117	95	4.41556	2.10000	2.9187E+03	6.6070E+03
			4.42423	2.08735	2.9187E+03	7.0176E+03
2	118	95	4.43290	2.07470	2.9187E+03	6.5737E+03

Summary for the above wall segment:

Emax = 7.0176E+03 V/m

Hmax = 2.9187E+03 A/m

Surface Area = 3.0670E-02 cm^2

Power = 9.0381E-02 W

Maximum P/A = 2.9469E+00 W/cm^2

Average P/A = 2.9469E+00 W/cm^2

df/dz = -6.8999E-02 MHz/mm (for volume added to the cavity)

df/f = -9.8114E-05

df/dr = -4.7281E-02 MHz/mm (for volume added to the cavity)

df/f = -6.7232E-05

Power and fields on wall segment 16. K,L = 118,95 to 120,80

This segment uses surface resistance option IRTYPE = 0

Surface resistance, Rs = 6.918579E-03 Ohm calculated from:

Operating temperature, TEMPC = 20.000 C

Reference resistivity, RHOR = 1.724100E-06 Ohm-cm

Reference temperature, TEMPR = 20.000 C

Temperature coefficient, ALPHAT = 3.930000E-03 /C

Relative permeability, RFMU = 1.000

m	K	L	X (cm)	Y (cm)	H (A/m)	|E| (V/m)
1	118	95	4.43290	2.07470	2.9187E+03	6.5737E+03
			4.44695	2.05289	2.9187E+03	8.1793E+03
2	118	94	4.46100	2.03108	2.9186E+03	6.4972E+03
			4.47366	2.00910	2.9186E+03	7.6008E+03
3	118	93	4.48631	1.98712	2.9185E+03	7.7329E+03
			4.49762	1.96498	2.9185E+03	9.7689E+03

4	119	92	4.50893	1.94284	2.9184E+03	1.0318E+04
			4.51897	1.92057	2.9184E+03	1.1586E+04
5	119	91	4.52900	1.89829	2.9183E+03	1.1311E+04
			4.53782	1.87591	2.9182E+03	1.1900E+04
6	119	90	4.54663	1.85352	2.9181E+03	1.1382E+04
			4.55427	1.83104	2.9180E+03	1.3484E+04
7	119	89	4.56191	1.80857	2.9179E+03	1.3897E+04
			4.56841	1.78601	2.9178E+03	1.5332E+04
8	120	88	4.57491	1.76346	2.9177E+03	1.6294E+04
			4.58030	1.74084	2.9176E+03	1.6311E+04
9	119	87	4.58570	1.71822	2.9174E+03	1.6771E+04
			4.59001	1.69555	2.9173E+03	1.8627E+04
10	120	86	4.59433	1.67288	2.9171E+03	1.8847E+04
			4.59758	1.65018	2.9170E+03	1.9411E+04
11	119	85	4.60083	1.62747	2.9168E+03	1.9500E+04
			4.60304	1.60474	2.9167E+03	2.1931E+04
12	120	84	4.60525	1.58200	2.9165E+03	2.2321E+04
			4.60642	1.55925	2.9163E+03	2.3105E+04
13	119	83	4.60759	1.53650	2.9161E+03	2.3265E+04
			4.60773	1.51374	2.9159E+03	2.5158E+04
14	120	82	4.60786	1.49099	2.9157E+03	2.5790E+04
			4.60697	1.46823	2.9155E+03	2.6682E+04
15	119	81	4.60608	1.44548	2.9152E+03	2.6830E+04
			4.60415	1.42274	2.9150E+03	2.8229E+04
16	120	80	4.60223	1.40000	2.9147E+03	2.9106E+04

Summary for the above wall segment:

Emax = 2.9106E+04 V/m

Hmax = 2.9187E+03 A/m

Surface Area = 7.1021E-01 cm^2

Power = 2.0910E+00 W

Maximum P/A = 2.9468E+00 W/cm^2

Average P/A = 2.9441E+00 W/cm^2

df/dz = -1.8379E+00 MHz/mm (for volume added to the cavity)

df/f = -2.6134E-03

df/dr = -4.9228E-01 MHz/mm (for volume added to the cavity)

df/f = -7.0001E-04

Power and fields on wall segment 17. K,L = 120,80 to 116,50

This segment uses surface resistance option IRTYPE = 0

Surface resistance, Rs = 6.918579E-03 Ohm calculated from:

Operating temperature, TEMPC = 20.000 C

Reference resistivity, RHOR = 1.724100E-06 Ohm-cm

Reference temperature, TEMPR = 20.000 C

Temperature coefficient, ALPHAT = 3.930000E-03 /C

Relative permeability, RFMU = 1.000

m	K	L	X (cm)	Y (cm)	H (A/m)	|E| (V/m)
1	120	80	4.60223	1.40000	2.9147E+03	2.9106E+04
			4.60082	1.38820	2.9146E+03	2.9618E+04
2	119	79	4.59941	1.37640	2.9145E+03	3.0126E+04
			4.59771	1.36461	2.9143E+03	3.0692E+04
3	120	78	4.59602	1.35281	2.9142E+03	3.1010E+04
			4.59404	1.34102	2.9140E+03	3.1468E+04
4	119	77	4.59205	1.32922	2.9139E+03	3.1979E+04
			4.58978	1.31743	2.9137E+03	3.3187E+04
5	120	76	4.58751	1.30564	2.9136E+03	3.3285E+04

			4.58495	1.29385	2.9134E+03	3.3663E+04
6	119	75	4.58238	1.28207	2.9133E+03	3.4182E+04
			4.57952	1.27028	2.9131E+03	3.5402E+04
7	120	74	4.57666	1.25850	2.9129E+03	3.5592E+04
			4.57350	1.24672	2.9128E+03	3.6043E+04
8	119	73	4.57033	1.23494	2.9126E+03	3.6596E+04
			4.56686	1.22316	2.9124E+03	3.7430E+04
9	120	72	4.56339	1.21139	2.9122E+03	3.7971E+04
			4.55960	1.19962	2.9121E+03	3.8705E+04
10	119	71	4.55581	1.18785	2.9119E+03	3.7857E+04
			4.55170	1.17609	2.9117E+03	3.9209E+04
11	119	70	4.54760	1.16432	2.9115E+03	3.9624E+04
			4.54316	1.15256	2.9113E+03	4.0480E+04
12	119	69	4.53872	1.14081	2.9111E+03	4.1269E+04
			4.53395	1.12906	2.9109E+03	4.2082E+04
13	119	68	4.52917	1.11731	2.9107E+03	4.2871E+04
			4.52405	1.10556	2.9104E+03	4.3420E+04
14	119	67	4.51893	1.09382	2.9102E+03	4.4127E+04
			4.51345	1.08209	2.9100E+03	4.5052E+04
15	119	66	4.50797	1.07035	2.9098E+03	4.5978E+04
			4.50212	1.05863	2.9095E+03	4.5768E+04
16	118	65	4.49626	1.04690	2.9093E+03	4.6678E+04
			4.49003	1.03519	2.9090E+03	4.6956E+04
17	119	64	4.48380	1.02348	2.9088E+03	4.8004E+04
			4.47716	1.01178	2.9086E+03	4.9227E+04
18	118	63	4.47053	1.00008	2.9083E+03	5.0090E+04
			4.46348	0.988387	2.9080E+03	5.0400E+04
19	119	62	4.45644	0.976699	2.9077E+03	5.1319E+04
			4.44895	0.965025	2.9075E+03	5.2464E+04

20	118	61	4.44147	0.953352	2.9072E+03	5.3599E+04
			4.43354	0.941694	2.9069E+03	5.3469E+04
21	118	60	4.42560	0.930036	2.9066E+03	5.4474E+04
			4.41718	0.918397	2.9063E+03	5.4578E+04
22	118	59	4.40876	0.906758	2.9060E+03	5.5852E+04
			4.39984	0.895139	2.9056E+03	5.7347E+04
23	118	58	4.39092	0.883520	2.9053E+03	5.8349E+04
			4.38146	0.871925	2.9050E+03	5.9584E+04
24	117	57	4.37199	0.860329	2.9046E+03	6.1219E+04
			4.36196	0.848759	2.9042E+03	6.0681E+04
25	117	56	4.35192	0.837190	2.9039E+03	6.2159E+04
			4.34127	0.825650	2.9035E+03	6.2671E+04
26	117	55	4.33062	0.814110	2.9031E+03	6.4189E+04
			4.31931	0.802605	2.9027E+03	6.6363E+04
27	117	54	4.30799	0.791099	2.9023E+03	6.7857E+04
			4.29596	0.779633	2.9018E+03	6.8141E+04
28	116	53	4.28392	0.768168	2.9014E+03	6.9005E+04
			4.27110	0.756748	2.9009E+03	6.9601E+04
29	117	52	4.25828	0.745328	2.9004E+03	7.1346E+04
			4.24459	0.733963	2.8999E+03	7.3325E+04
30	116	51	4.23090	0.722598	2.8994E+03	7.5135E+04
			4.21624	0.711299	2.8989E+03	7.6569E+04
31	116	50	4.20158	0.700000	2.8983E+03	7.8544E+04

Summary for the above wall segment:

Emax = 7.8544E+04 V/m

Hmax = 2.9146E+03 A/m

Surface Area = 8.2987E-01 cm^2

Power = 2.4274E+00 W

Maximum P/A = 2.9386E+00 W/cm^2

Average P/A = 2.9250E+00 W/cm^2

df/dz = -1.8917E+00 MHz/mm (for volume added to the cavity)

df/f = -2.6900E-03

df/dr = -1.0801E+00 MHz/mm (for volume added to the cavity)

df/f = -1.5358E-03

Power and fields on wall segment 18. K,L = 116,50 to 111,37

This segment uses surface resistance option IRTYPE = 0

Surface resistance, Rs = 6.918579E-03 Ohm calculated from:

Operating temperature, TEMPC = 20.000 C

Reference resistivity, RHOR = 1.724100E-06 Ohm-cm

Reference temperature, TEMPR = 20.000 C

Temperature coefficient, ALPHAT = 3.930000E-03 /C

Relative permeability, RFMU = 1.000

m	K	L	X (cm)	Y (cm)	H (A/m)	|E| (V/m)
1	116	50	4.20158	0.700000	2.8983E+03	7.8544E+04
			4.19088	0.692280	2.8979E+03	7.8112E+04
2	115	49	4.18019	0.684560	2.8975E+03	7.9699E+04
			4.16889	0.676857	2.8971E+03	8.0354E+04
3	116	48	4.15760	0.669155	2.8966E+03	8.1891E+04
			4.14563	0.661473	2.8962E+03	8.3653E+04
4	115	47	4.13367	0.653792	2.8957E+03	8.5414E+04
			4.12095	0.646135	2.8952E+03	8.7021E+04
5	115	46	4.10823	0.638477	2.8947E+03	8.8878E+04
			4.09464	0.630850	2.8941E+03	8.9566E+04
6	114	45	4.08106	0.623223	2.8936E+03	9.1142E+04

			4.06647	0.615634	2.8930E+03	9.2274E+04
7	115	44	4.05188	0.608044	2.8924E+03	9.4198E+04
			4.03611	0.600504	2.8917E+03	9.6436E+04
8	114	43	4.02034	0.592963	2.8911E+03	9.8683E+04
			4.00314	0.585486	2.8904E+03	1.0024E+05
9	114	42	3.98593	0.578010	2.8896E+03	1.0307E+05
			3.96694	0.570621	2.8888E+03	1.0519E+05
10	113	41	3.94795	0.563232	2.8879E+03	1.0845E+05
			3.92664	0.555973	2.8870E+03	1.1172E+05
11	113	40	3.90534	0.548713	2.8860E+03	1.1537E+05
			3.88087	0.541660	2.8848E+03	1.1939E+05
12	112	39	3.85641	0.534607	2.8836E+03	1.2387E+05
			3.82730	0.527925	2.8821E+03	1.2861E+05
13	112	38	3.79819	0.521243	2.8806E+03	1.3563E+05
			3.76160	0.515371	2.8786E+03	1.4387E+05
14	111	37	3.72500	0.509500	2.8764E+03	1.5412E+05

Summary for the above wall segment:

Emax = 1.5412E+05 V/m

Hmax = 2.8979E+03 A/m

Surface Area = 5.1894E-01 cm^2

Power = 1.4979E+00 W

Maximum P/A = 2.9050E+00 W/cm^2

Average P/A = 2.8864E+00 W/cm^2

df/dz = -5.0524E-01 MHz/mm (for volume added to the cavity)

df/f = -7.1843E-04

df/dr = -1.2595E+00 MHz/mm (for volume added to the cavity)

df/f = -1.7910E-03

Power and fields on wall segment 19. K,L = 111,37 to 95,23

This segment uses surface resistance option IRTYPE = 0

Surface resistance, Rs = 6.918579E-03 Ohm calculated from:

Operating temperature, TEMPC = 20.000 C

Reference resistivity, RHOR = 1.724100E-06 Ohm-cm

Reference temperature, TEMPR = 20.000 C

Temperature coefficient, ALPHAT = 3.930000E-03 /C

Relative permeability, RFMU = 1.000

m	K	L	X (cm)	Y (cm)	H (A/m)	|E| (V/m)
1	111	37	3.72500	0.509500	2.8764E+03	1.5412E+05
			3.68967	0.505163	2.8742E+03	1.6322E+05
2	111	36	3.65435	0.500826	2.8719E+03	1.7316E+05
			3.61902	0.496489	2.8694E+03	1.8314E+05
3	110	36	3.58370	0.492152	2.8668E+03	1.9277E+05
			3.54837	0.487816	2.8640E+03	2.0239E+05
4	109	35	3.51304	0.483479	2.8611E+03	2.1157E+05
			3.47772	0.479142	2.8581E+03	2.2051E+05
5	108	35	3.44239	0.474805	2.8550E+03	2.2929E+05
			3.40707	0.470468	2.8517E+03	2.3892E+05
6	108	34	3.37174	0.466131	2.8483E+03	2.4782E+05
			3.33641	0.461794	2.8448E+03	2.5704E+05
7	107	33	3.30109	0.457457	2.8412E+03	2.6627E+05
			3.26576	0.453120	2.8374E+03	2.7524E+05
8	106	33	3.23043	0.448784	2.8335E+03	2.8448E+05
			3.19511	0.444447	2.8295E+03	2.9425E+05
9	106	32	3.15978	0.440110	2.8254E+03	3.0343E+05
			3.12446	0.435773	2.8211E+03	3.1287E+05

10	105	32	3.08913	0.431436	2.8166E+03	3.2201E+05
			3.05380	0.427099	2.8121E+03	3.3272E+05
11	104	31	3.01848	0.422762	2.8074E+03	3.4249E+05
			2.98315	0.418425	2.8025E+03	3.5273E+05
12	104	30	2.94783	0.414088	2.7976E+03	3.6294E+05
			2.91250	0.409751	2.7924E+03	3.7298E+05
13	103	30	2.87717	0.405415	2.7872E+03	3.8320E+05
			2.84185	0.401078	2.7818E+03	3.9445E+05
14	102	29	2.80652	0.396741	2.7762E+03	4.0525E+05
			2.77120	0.392404	2.7705E+03	4.1643E+05
15	102	28	2.73587	0.388067	2.7646E+03	4.2759E+05
			2.70054	0.383730	2.7586E+03	4.3881E+05
16	101	28	2.66522	0.379393	2.7524E+03	4.5031E+05
			2.62989	0.375056	2.7460E+03	4.6246E+05
17	100	27	2.59457	0.370719	2.7395E+03	4.7442E+05
			2.55924	0.366383	2.7328E+03	4.8668E+05
18	99	27	2.52391	0.362046	2.7260E+03	4.9906E+05
			2.48859	0.357709	2.7189E+03	5.1244E+05
19	99	26	2.45326	0.353372	2.7117E+03	5.2577E+05
			2.41793	0.349035	2.7043E+03	5.3917E+05
20	98	25	2.38261	0.344698	2.6967E+03	5.5286E+05
			2.34728	0.340361	2.6889E+03	5.6694E+05
21	97	25	2.31196	0.336024	2.6809E+03	5.8118E+05
			2.27663	0.331687	2.6727E+03	5.9560E+05
22	97	24	2.24130	0.327351	2.6643E+03	6.1089E+05
			2.20598	0.323014	2.6557E+03	6.2672E+05
23	96	24	2.17065	0.318677	2.6469E+03	6.4249E+05
			2.13533	0.314340	2.6378E+03	6.5781E+05
24	95	23	2.10000	0.310003	2.6286E+03	6.7438E+05

Summary for the above wall segment:

Emax = 6.7438E+05 V/m

Hmax = 2.8742E+03 A/m

Surface Area = 1.6372E+00 cm^2

Power = 4.3778E+00 W

Maximum P/A = 2.8578E+00 W/cm^2

Average P/A = 2.6740E+00 W/cm^2

df/dz = -4.1670E-01 MHz/mm (for volume added to the cavity)

df/f = -5.9253E-04

df/dr = -3.3942E+00 MHz/mm (for volume added to the cavity)

df/f = -4.8265E-03

Power and fields on wall segment 20. K,L = 95,23 to 80,17

This segment uses surface resistance option IRTYPE = 0

Surface resistance, Rs = 6.918579E-03 Ohm calculated from:

Operating temperature, TEMPC = 20.000 C

Reference resistivity, RHOR = 1.724100E-06 Ohm-cm

Reference temperature, TEMPR = 20.000 C

Temperature coefficient, ALPHAT = 3.930000E-03 /C

Relative permeability, RFMU = 1.000

m	K	L	X (cm)	Y (cm)	H (A/m)	|E| (V/m)
1	95	23	2.10000	0.310003	2.6286E+03	6.7438E+05
			2.08056	0.307616	2.6234E+03	6.8356E+05
2	94	23	2.06111	0.305229	2.6181E+03	6.9286E+05
			2.04167	0.302842	2.6127E+03	7.0244E+05
3	94	22	2.02222	0.300454	2.6073E+03	7.1220E+05

			2.00278	0.298067	2.6018E+03	7.2200E+05
4	93	22	1.98333	0.295680	2.5962E+03	7.3298E+05
			1.96389	0.293293	2.5906E+03	7.4364E+05
5	92	22	1.94444	0.290906	2.5848E+03	7.5388E+05
			1.92500	0.288519	2.5790E+03	7.6455E+05
6	91	21	1.90556	0.286132	2.5731E+03	7.7580E+05
			1.88611	0.283744	2.5671E+03	7.8646E+05
7	90	21	1.86667	0.281357	2.5611E+03	7.9824E+05
			1.84722	0.278970	2.5549E+03	8.0958E+05
8	89	21	1.82778	0.276583	2.5486E+03	8.2098E+05
			1.80833	0.274196	2.5423E+03	8.3314E+05
9	89	20	1.78889	0.271809	2.5359E+03	8.4549E+05
			1.76944	0.269422	2.5294E+03	8.5744E+05
10	88	20	1.75000	0.267034	2.5227E+03	8.7054E+05
			1.73056	0.264647	2.5160E+03	8.8318E+05
11	87	20	1.71111	0.262260	2.5092E+03	8.9604E+05
			1.69167	0.259873	2.5023E+03	9.0974E+05
12	86	19	1.67222	0.257486	2.4953E+03	9.2353E+05
			1.65278	0.255099	2.4881E+03	9.3707E+05
13	85	19	1.63333	0.252712	2.4809E+03	9.5190E+05
			1.61389	0.250324	2.4735E+03	9.6622E+05
14	84	19	1.59444	0.247937	2.4661E+03	9.8087E+05
			1.57500	0.245550	2.4585E+03	9.9625E+05
15	84	18	1.55556	0.243163	2.4508E+03	1.0118E+06
			1.53611	0.240776	2.4430E+03	1.0273E+06
16	83	18	1.51667	0.238389	2.4351E+03	1.0446E+06
			1.49722	0.236002	2.4270E+03	1.0612E+06
17	82	18	1.47778	0.233614	2.4188E+03	1.0783E+06
			1.45833	0.231227	2.4105E+03	1.0953E+06

18	81	17	1.43889	0.228840	2.4020E+03	1.1125E+06
			1.41944	0.226453	2.3934E+03	1.1297E+06
19	80	17	1.40000	0.224066	2.3847E+03	1.1469E+06

Summary for the above wall segment:

Emax = 1.1469E+06 V/m

Hmax = 2.6234E+03 A/m

Surface Area = 7.0526E-01 cm^2

Power = 1.5473E+00 W

Maximum P/A = 2.3807E+00 W/cm^2

Average P/A = 2.1940E+00 W/cm^2

df/dz = -1.9509E-02 MHz/mm (for volume added to the cavity)

df/f = -2.7742E-05

df/dr = -1.5891E-01 MHz/mm (for volume added to the cavity)

df/f = -2.2597E-04

Power and fields on wall segment 21. K,L = 80,17 to 54,11

This segment uses surface resistance option IRTYPE = 0

Surface resistance, Rs = 6.918579E-03 Ohm calculated from:

Operating temperature, TEMPC = 20.000 C

Reference resistivity, RHOR = 1.724100E-06 Ohm-cm

Reference temperature, TEMPR = 20.000 C

Temperature coefficient, ALPHAT = 3.930000E-03 /C

Relative permeability, RFMU = 1.000

m	K	L	X (cm)	Y (cm)	H (A/m)	|E| (V/m)
1	80	17	1.40000	0.224066	2.3847E+03	1.1469E+06
			1.38970	0.222801	2.3800E+03	1.1584E+06

2	79	17	1.37939	0.221536	2.3753E+03	1.1680E+06
			1.36909	0.220271	2.3705E+03	1.1787E+06
3	78	17	1.35879	0.219006	2.3657E+03	1.1907E+06
			1.34848	0.217741	2.3609E+03	1.2013E+06
4	78	16	1.33818	0.216476	2.3560E+03	1.2125E+06
			1.32788	0.215211	2.3510E+03	1.2240E+06
5	77	16	1.31757	0.213946	2.3460E+03	1.2357E+06
			1.30727	0.212681	2.3410E+03	1.2474E+06
6	76	16	1.29697	0.211417	2.3359E+03	1.2580E+06
			1.28666	0.210152	2.3308E+03	1.2682E+06
7	75	16	1.27636	0.208887	2.3256E+03	1.2812E+06
			1.26606	0.207622	2.3204E+03	1.2925E+06
8	74	16	1.25575	0.206357	2.3151E+03	1.3057E+06
			1.24545	0.205092	2.3098E+03	1.3182E+06
9	73	15	1.23514	0.203827	2.3044E+03	1.3308E+06
			1.22484	0.202562	2.2990E+03	1.3435E+06
10	72	15	1.21454	0.201297	2.2935E+03	1.3564E+06
			1.20423	0.200032	2.2879E+03	1.3698E+06
11	71	15	1.19393	0.198767	2.2823E+03	1.3826E+06
			1.18363	0.197502	2.2767E+03	1.3960E+06
12	70	15	1.17332	0.196237	2.2710E+03	1.4095E+06
			1.16302	0.194972	2.2653E+03	1.4228E+06
13	69	15	1.15272	0.193708	2.2595E+03	1.4377E+06
			1.14241	0.192443	2.2536E+03	1.4525E+06
14	69	14	1.13211	0.191178	2.2477E+03	1.4671E+06
			1.12181	0.189913	2.2417E+03	1.4818E+06
15	68	14	1.11150	0.188648	2.2356E+03	1.4965E+06
			1.10120	0.187383	2.2295E+03	1.5120E+06
16	67	14	1.09090	0.186118	2.2234E+03	1.5269E+06

			1.08059	0.184853	2.2171E+03	1.5422E+06
17	66	14	1.07029	0.183588	2.2108E+03	1.5586E+06
			1.05999	0.182323	2.2045E+03	1.5750E+06
18	65	13	1.04968	0.181058	2.1980E+03	1.5914E+06
			1.03938	0.179793	2.1915E+03	1.6080E+06
19	64	13	1.02908	0.178528	2.1850E+03	1.6244E+06
			1.01877	0.177263	2.1784E+03	1.6419E+06
20	63	13	1.00847	0.175999	2.1717E+03	1.6589E+06
			0.998166	0.174734	2.1649E+03	1.6762E+06
21	62	13	0.987862	0.173469	2.1580E+03	1.6935E+06
			0.977559	0.172204	2.1511E+03	1.7107E+06
22	61	13	0.967255	0.170939	2.1441E+03	1.7288E+06
			0.956952	0.169674	2.1371E+03	1.7471E+06
23	61	12	0.946648	0.168409	2.1300E+03	1.7650E+06
			0.936345	0.167144	2.1228E+03	1.7829E+06
24	60	12	0.926041	0.165879	2.1155E+03	1.8008E+06
			0.915738	0.164614	2.1081E+03	1.8187E+06
25	59	12	0.905434	0.163349	2.1007E+03	1.8362E+06
			0.895131	0.162084	2.0932E+03	1.8526E+06
26	58	12	0.884828	0.160819	2.0856E+03	1.8690E+06
			0.874524	0.159554	2.0780E+03	1.8828E+06
27	57	12	0.864221	0.158290	2.0703E+03	1.8966E+06
			0.853917	0.157025	2.0625E+03	1.9028E+06
28	56	11	0.843614	0.155760	2.0548E+03	1.9101E+06
			0.833310	0.154495	2.0471E+03	1.9209E+06
29	55	11	0.823007	0.153230	2.0392E+03	1.9306E+06
			0.812703	0.151965	2.0315E+03	1.9571E+06
30	54	11	0.802400	0.150700	2.0236E+03	1.9737E+06

Summary for the above wall segment:

Emax = 1.9737E+06 V/m

Hmax = 2.3800E+03 A/m

Surface Area = 6.0209E-01 cm^2

Power = 1.0295E+00 W

Maximum P/A = 1.9595E+00 W/cm^2

Average P/A = 1.7100E+00 W/cm^2

df/dz = 2.8267E-01 MHz/mm (for volume added to the cavity)

df/f = 4.0195E-04

df/dr = 2.3025E+00 MHz/mm (for volume added to the cavity)

df/f = 3.2741E-03

Power and fields on wall segment 22. K,L = 54,11 to 54,12

This segment uses surface resistance option IRTYPE = 0

Surface resistance, Rs = 6.918579E-03 Ohm calculated from:

Operating temperature, TEMPC = 20.000 C

Reference resistivity, RHOR = 1.724100E-06 Ohm-cm

Reference temperature, TEMPR = 20.000 C

Temperature coefficient, ALPHAT = 3.930000E-03 /C

Relative permeability, RFMU = 1.000

m	K	L	X (cm)	Y (cm)	H (A/m)	|E| (V/m)
1	54	11	0.802400	0.150700	2.0236E+03	1.9737E+06
			0.800000	0.150550	2.0218E+03	1.9798E+06
2	54	12	0.797600	0.150400	2.0199E+03	1.9859E+06

Summary for the above wall segment:

Emax = 1.9859E+06 V/m

Hmax = 2.0218E+03 A/m

Surface Area = 4.8094E-03 cm^2

Power = 6.8004E-03 W

Maximum P/A = 1.4140E+00 W/cm^2

Average P/A = 1.4140E+00 W/cm^2

df/dz = 2.0749E-03 MHz/mm (for volume added to the cavity)

df/f = 2.9504E-06

df/dr = 3.3198E-02 MHz/mm (for volume added to the cavity)

df/f = 4.7207E-05

Power and fields on wall segment 23. K,L = 54,12 to 50,12

This segment uses surface resistance option IRTYPE = 0

Surface resistance, Rs = 6.918579E-03 Ohm calculated from:

Operating temperature, TEMPC = 20.000 C

Reference resistivity, RHOR = 1.724100E-06 Ohm-cm

Reference temperature, TEMPR = 20.000 C

Temperature coefficient, ALPHAT = 3.930000E-03 /C

Relative permeability, RFMU = 1.000

m	K	L	X (cm)	Y (cm)	H (A/m)	|E| (V/m)
1	54	12	0.797600	0.150400	2.0199E+03	1.9859E+06
			0.785400	0.150400	2.0106E+03	2.0078E+06
2	53	12	0.773200	0.150400	2.0010E+03	2.0743E+06
			0.761000	0.150400	1.9911E+03	2.1608E+06
3	52	12	0.748800	0.150400	1.9806E+03	2.2249E+06
			0.736600	0.150400	1.9699E+03	2.2863E+06
4	51	12	0.724400	0.150400	1.9589E+03	2.3459E+06
			0.712200	0.150400	1.9475E+03	2.4091E+06

5	50	12	0.700000	0.150400	1.9359E+03	2.4714E+06

Summary for the above wall segment:

Emax = 2.4714E+06 V/m

Hmax = 2.0106E+03 A/m

Surface Area = 9.7600E-02 cm^2

Power = 1.3234E-01 W

Maximum P/A = 1.3984E+00 W/cm^2

Average P/A = 1.3560E+00 W/cm^2

df/dr = 9.5191E-01 MHz/mm (for volume added to the cavity)

df/f = 1.3536E-03

Power and fields on wall segment 24. K,L = 50,12 to 25,12

This segment uses surface resistance option IRTYPE = 0

Surface resistance, Rs = 6.918579E-03 Ohm calculated from:

Operating temperature, TEMPC = 20.000 C

Reference resistivity, RHOR = 1.724100E-06 Ohm-cm

Reference temperature, TEMPR = 20.000 C

Temperature coefficient, ALPHAT = 3.930000E-03 /C

Relative permeability, RFMU = 1.000

m	K	L	X (cm)	Y (cm)	H (A/m)	|E| (V/m)
1	50	12	0.700000	0.150400	1.9359E+03	2.4714E+06
			0.692878	0.150400	1.9290E+03	2.5108E+06
2	49	12	0.685756	0.150400	1.9219E+03	2.5488E+06
			0.678634	0.150400	1.9148E+03	2.5889E+06
3	48	12	0.671512	0.150400	1.9075E+03	2.6289E+06
			0.664390	0.150400	1.9001E+03	2.6706E+06

4	47	12	0.657268	0.150400	1.8927E+03	2.7119E+06
			0.650146	0.150400	1.8850E+03	2.7562E+06
5	46	12	0.643024	0.150400	1.8773E+03	2.7995E+06
			0.635902	0.150400	1.8695E+03	2.8457E+06
6	45	12	0.628780	0.150400	1.8615E+03	2.8913E+06
			0.621658	0.150400	1.8534E+03	2.9399E+06
7	44	12	0.614536	0.150400	1.8451E+03	2.9881E+06
			0.607414	0.150400	1.8367E+03	3.0393E+06
8	43	12	0.600292	0.150400	1.8282E+03	3.0904E+06
			0.593170	0.150400	1.8196E+03	3.1448E+06
9	42	12	0.586048	0.150400	1.8107E+03	3.1991E+06
			0.578926	0.150400	1.8018E+03	3.2570E+06
10	41	12	0.571804	0.150400	1.7926E+03	3.3150E+06
			0.564682	0.150400	1.7833E+03	3.3768E+06
11	40	12	0.557560	0.150400	1.7739E+03	3.4389E+06
			0.550438	0.150400	1.7642E+03	3.5051E+06
12	39	12	0.543316	0.150400	1.7544E+03	3.5719E+06
			0.536194	0.150400	1.7443E+03	3.6432E+06
13	38	12	0.529072	0.150400	1.7341E+03	3.7152E+06
			0.521950	0.150400	1.7237E+03	3.7923E+06
14	37	12	0.514828	0.150400	1.7131E+03	3.8703E+06
			0.507706	0.150400	1.7022E+03	3.9540E+06
15	36	12	0.500584	0.150400	1.6911E+03	4.0389E+06
			0.493462	0.150400	1.6797E+03	4.1303E+06
16	35	12	0.486340	0.150400	1.6682E+03	4.2232E+06
			0.479218	0.150400	1.6563E+03	4.3236E+06
17	34	12	0.472096	0.150400	1.6442E+03	4.4257E+06
			0.464974	0.150400	1.6317E+03	4.5369E+06
18	33	12	0.457852	0.150400	1.6190E+03	4.6500E+06

			0.450730	0.150400	1.6059E+03	4.7741E+06
19	32	12	0.443608	0.150400	1.5925E+03	4.9003E+06
			0.436486	0.150400	1.5787E+03	5.0405E+06
20	31	12	0.429364	0.150400	1.5646E+03	5.1827E+06
			0.422242	0.150400	1.5499E+03	5.3433E+06
21	30	12	0.415120	0.150400	1.5350E+03	5.5056E+06
			0.407998	0.150400	1.5194E+03	5.6932E+06
22	29	12	0.400876	0.150400	1.5035E+03	5.8814E+06
			0.393754	0.150400	1.4868E+03	6.1070E+06
23	28	12	0.386632	0.150400	1.4698E+03	6.3305E+06
			0.379510	0.150400	1.4517E+03	6.6151E+06
24	27	12	0.372388	0.150400	1.4334E+03	6.8908E+06
			0.365266	0.150400	1.4135E+03	7.3085E+06
25	26	12	0.358144	0.150400	1.3930E+03	7.6185E+06
			0.351022	0.150400	1.3707E+03	8.1201E+06
26	25	12	0.343900	0.150400	1.3477E+03	8.5557E+06

Summary for the above wall segment:

Emax = 8.5557E+06 V/m

Hmax = 1.9290E+03 A/m

Surface Area = 3.5610E-01 cm^2

Power = 3.5880E-01 W

Maximum P/A = 1.2872E+00 W/cm^2

Average P/A = 1.0076E+00 W/cm^2

df/dr = 1.5672E+01 MHz/mm (for volume added to the cavity)

df/f = 2.2284E-02

Power and fields on wall segment 25. K,L = 25,12 to 14,1

This segment uses surface resistance option IRTYPE = 0

Surface resistance, Rs = 6.918579E-03 Ohm calculated from:

Operating temperature, TEMPC = 20.000 C

Reference resistivity, RHOR = 1.724100E-06 Ohm-cm

Reference temperature, TEMPR = 20.000 C

Temperature coefficient, ALPHAT = 3.930000E-03 /C

Relative permeability, RFMU = 1.000

m	K	L	X (cm)	Y (cm)	H (A/m)	|E| (V/m)
1	25	12	0.343900	0.150400	1.3477E+03	8.5557E+06
			0.336961	0.150079	1.3247E+03	9.0021E+06
2	24	11	0.330023	0.149758	1.2997E+03	9.4493E+06
			0.323143	0.148799	1.2722E+03	1.0007E+07
3	23	11	0.316264	0.147839	1.2442E+03	1.0438E+07
			0.309503	0.146249	1.2138E+03	1.1019E+07
4	22	11	0.302741	0.144659	1.1831E+03	1.1435E+07
			0.296155	0.142451	1.1502E+03	1.2000E+07
5	21	11	0.289569	0.140244	1.1169E+03	1.2456E+07
			0.283215	0.137438	1.0820E+03	1.2850E+07
6	20	11	0.276861	0.134633	1.0462E+03	1.3269E+07
			0.270793	0.131253	1.0079E+03	1.3796E+07
7	20	10	0.264725	0.127873	9.7007E+02	1.4120E+07
			0.258994	0.123947	9.3116E+02	1.4410E+07
8	19	10	0.253264	0.120022	8.9176E+02	1.4710E+07
			0.247920	0.115584	8.5010E+02	1.5155E+07
9	18	9	0.242576	0.111147	8.0872E+02	1.5356E+07
			0.237665	0.106235	7.6665E+02	1.5565E+07
10	17	9	0.232753	0.101324	7.2417E+02	1.5734E+07
			0.228316	9.598004E-02	6.8064E+02	1.6035E+07

11	17	8	0.223878	9.063625E-02	6.3686E+02	1.6148E+07
			0.219953	8.490582E-02	5.9317E+02	1.6349E+07
12	16	7	0.216027	7.917540E-02	5.4841E+02	1.6463E+07
			0.212647	7.310722E-02	5.0374E+02	1.6535E+07
13	16	6	0.209267	6.703905E-02	4.5867E+02	1.6619E+07
			0.206462	6.068490E-02	4.1332E+02	1.6624E+07
14	15	5	0.203656	5.433075E-02	3.6803E+02	1.6698E+07
			0.201449	4.774483E-02	3.2212E+02	1.6702E+07
15	15	4	0.199241	4.115891E-02	2.7675E+02	1.6698E+07
			0.197651	3.439742E-02	2.3054E+02	1.6714E+07
16	14	3	0.196061	2.763593E-02	1.8513E+02	1.6764E+07
			0.195101	2.075654E-02	1.3426E+02	1.6660E+07
17	15	2	0.194142	1.387716E-02	8.9246E+01	1.6494E+07
			0.193821	6.938581E-03	4.4546E+01	1.6423E+07
18	14	1	0.193500	0.00000	0.0000E+00	1.6379E+07

Summary for the above wall segment:

Emax = 1.6764E+07 V/m

Hmax = 1.3247E+03 A/m

Surface Area = 2.3616E-01 cm^2

Power = 5.7461E-02 W

Maximum P/A = 6.0702E-01 W/cm^2

Average P/A = 2.4331E-01 W/cm^2

df/dz = 8.5434E+01 MHz/mm (for volume added to the cavity)

df/f = 1.2148E-01

df/dr = 6.4737E+01 MHz/mm (for volume added to the cavity)

df/f = 9.2054E-02

Problem variables computed by this code.

Variable Code		Value	Description
ASCALE		10986.7230	Scaling factor for H at drive point
CAPK		0.0	2pi/beta*lambda, phase change/length
EMAX		16763730.6	Peak electric field on boundary segments
ENERGY		6.900909298E-05	Total stored energy in RF fields
EZERO	S	11207000.0	E0 for normalization in SFO when NORM=0
FREQC		703.252969	Frequency corrected for stems and posts
HCORNER		0.0	Average H at corner arc with coupling slot
HMAX		2918.75128	Peak H on specified boundary segments
HPHI		483.132253	Normalization magnetic field for NORM=2
NCELL		0	Number of cells for multicell problems
NPEG		24	Number of FieldSegments entries
NRESIST		0	Number of segments with unique resistivity
NSTEM		0	Number of stems for multicell problems
POWER		36.9407937	Power on conducting boundaries
RHOC		1.724100000E-06	Computed resistivity for IRTYPE=3
RS		6.918578637E-03	RF surface resistance (Ohms)
SAREA		14.7508435	Total surface area in power calculations
T		0.0	Transit-time factor
ZLONG		0.193500000	Length in SFO used to define E0

Superfish output summary for problem description:

RFQ full quadrant

Lowest dipole-mode frequency = 750 MHz

Bore radius at quadrupole symmetry point r0 = 0.1935 cm

Vane-tip radius of curvature rho = 0.1504 cm

Problem file: C:\LANL\EXAMPLES\RADIOFREQUENCY\RFQCAVITY\4THRFQ.AF 2-09-2023 14:42:54

All calculated values below refer to the mesh geometry only.

Field normalization (NORM = 0): EZERO = 11.20700 MV/m

Frequency = 703.25297 MHz

Normalization factor for E0 = 11.207 MV/m = 10986.723

Stored energy = 6.90091E-05 Joules/cm

Using standard room-temperature copper.

Surface resistance = 6.91858 milliOhm

Normal-conductor resistivity = 1.72410 microOhm-cm

Operating temperature = 20.0000 C

Power dissipation = 36.9408 W/cm

Q = 8254.51 Shunt impedance = 6578.903 MOhm/m

r/Q = 12.279 Ohm Wake loss parameter = 0.01356 V/pC

Average magnetic field on the outer wall = 2914.98 A/m, 2.93939 W/cm^2

Maximum H (at X,Y = 2.17511,4.36337) = 2918.75 A/m, 2.94701 W/cm^2

Maximum E (at X,Y = 0.196061,0.027636) = 16.7637 MV/m, 0.681677 Kilp.

Ratio of peak fields Bmax/Emax = 0.2188 mT/(MV/m)

Peak-to-average ratio Emax/E0 = 1.4958

Wall segments:

Segment	Xend (cm)	Yend (cm)	Emax (MV/m)	Power (W)	P/A (W/cm^2)	dF/dX (MHz/mm)	dF/dY (MHz/mm)
	0.0000	0.19350					
2	0.15040	0.34390	12.89	6.6677E-02	0.2823	41.17	30.32
3	0.15040	0.70000	8.315	0.3599	1.011	15.19	0.000
4	0.15040	0.79760	2.465	0.1324	1.357	0.9464	0.000
5	0.15070	0.80250	1.976	6.9469E-03	1.415	3.5895E-02	2.1976E-03
6	0.22406	1.4000	1.944	1.030	1.711	2.293	0.2816

7	0.31000	2.1000	1.150	1.547	2.194	-0.1603	-1.9679E-02
8	0.50950	3.7249	0.6752	4.378	2.674	-3.395	-0.4168
9	0.70000	4.2016	0.1524	1.498	2.886	-1.260	-0.5053
10	1.4000	4.6022	7.6523E-02	2.427	2.925	-1.080	-1.892
11	2.0746	4.4329	2.6872E-02	2.091	2.944	-0.4919	-1.838
12	2.1000	4.4156	6.9747E-03	9.0580E-02	2.947	-4.7206E-02	-6.9273E-02
13	3.3640	3.3640	1.2368E-02	4.848	2.945	-2.865	-3.444
14	4.4156	2.1000	1.2189E-02	4.848	2.945	-3.444	-2.865
15	4.4329	2.0747	7.0176E-03	9.0381E-02	2.947	-6.8999E-02	-4.7281E-02
16	4.6022	1.4000	2.9106E-02	2.091	2.944	-1.838	-0.4923
17	4.2016	0.70000	7.8544E-02	2.427	2.925	-1.892	-1.080
18	3.7250	0.50950	0.1541	1.498	2.886	-0.5052	-1.260
19	2.1000	0.31000	0.6744	4.378	2.674	-0.4167	-3.394
20	1.4000	0.22407	1.147	1.547	2.194	-1.9509E-02	-0.1589
21	0.80240	0.15070	1.974	1.030	1.710	0.2827	2.303
22	0.79760	0.15040	1.986	6.8004E-03	1.414	2.0749E-03	3.3198E-02
23	0.70000	0.15040	2.471	0.1323	1.356	0.000	0.9519
24	0.34390	0.15040	8.556	0.3588	1.008	0.000	15.67
25	0.19350	0.0000	16.76	5.7461E-02	0.2433	85.43	64.74

Total 36.94

7. ANNEX G

Project*

First Saved	Sunday, September 11, 2022
Last Saved	Wednesday, September 14, 2022
Product Version	2019 R1
Save Project Before Solution	No
Save Project After Solution	No

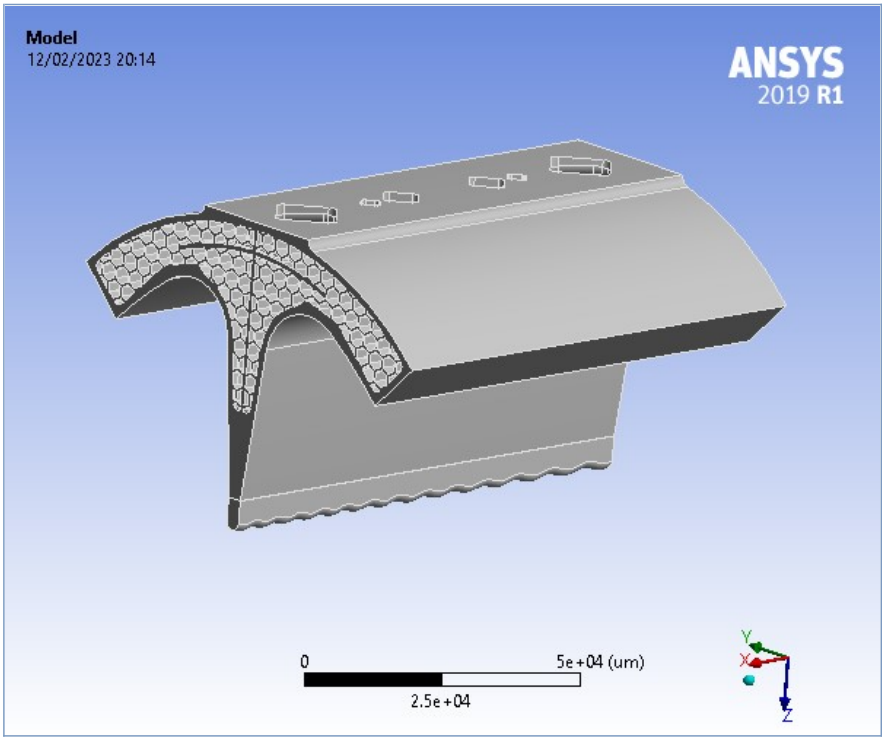

Contents

Units

TABLE 1

Unit System	Metric (µm, kg, µN, s, V, mA) Degrees rad/s Celsius
Angle	Degrees
Rotational Velocity	rad/s
Temperature	Celsius

Model (A4, B4)

Geometry

TABLE 2
Model (A4, B4) > Geometry

Object Name	*Geometry*
State	Fully Defined
Definition	
Source	C:\Users\gpikurs\Downloads\QS2407-a.CATPart
Type	Catia5
Length Unit	Millimeters
Element Control	Program Controlled

Display Style	Body Color
Bounding Box	
Length X	96117 µm
Length Y	84853 µm
Length Z	59193 µm
Properties	
Volume	7.9214e+013 µm³
Mass	0.70817 kg
Scale Factor Value	1.
Statistics	
Bodies	1
Active Bodies	1
Nodes	820441
Elements	484011
Mesh Metric	None
Update Options	
Assign Default Material	No
Basic Geometry Options	
Solid Bodies	Yes
Surface Bodies	Yes
Line Bodies	No
Parameters	Independent
Parameter Key	ANS;DS
Attributes	No
Named Selections	No
Material Properties	No
Advanced Geometry Options	
Use Associativity	Yes
Coordinate Systems	No
Reader Mode Saves Updated File	No
Use Instances	Yes
Smart CAD Update	Yes
Compare Parts On Update	No
Analysis Type	3-D
Mixed Import Resolution	None
Clean Bodies On Import	No
Stitch Surfaces On Import	None
Decompose Disjoint Geometry	Yes
Enclosure and Symmetry Processing	Yes

TABLE 3
Model (A4, B4) > Geometry > Parts

Object Name	*PartBody|Assemble.1*
State	Meshed
Graphics Properties	
Visible	Yes
Transparency	1
Definition	
Suppressed	No
Stiffness Behavior	Flexible
Coordinate System	Default Coordinate System
Reference Temperature	By Environment
Behavior	None
Material	
Assignment	Copper, cast
Nonlinear Effects	Yes

Thermal Strain Effects	Yes
Bounding Box	
Length X	96117 µm
Length Y	84853 µm
Length Z	59193 µm
Properties	
Volume	7.9214e+013 µm³
Mass	0.70817 kg
Centroid X	-1.2488 µm
Centroid Y	1.2237 µm
Centroid Z	-43079 µm
Moment of Inertia Ip1	3.7422e+008 kg·µm²
Moment of Inertia Ip2	6.2231e+008 kg·µm²
Moment of Inertia Ip3	7.788e+008 kg·µm²
Statistics	
Nodes	820441
Elements	484011
Mesh Metric	None

TABLE 4
Model (A4, B4) > Materials > Copper, cast Assignment

Object Name	*Copper, cast Assignment*
State	Fully Defined
General	
Scoping Method	Geometry Selection
Geometry	1 Body
Definition	
Material	Copper, cast
Nonlinear Effects	Yes
Thermal Strain Effects	Yes
Reference Temperature	By Environment
Suppressed	No

Coordinate Systems

TABLE 5
Model (A4, B4) > Coordinate Systems > Coordinate System

Object Name	*Global Coordinate System*
State	Fully Defined
Definition	
Type	Cartesian
Coordinate System ID	0.
Origin	
Origin X	0. µm
Origin Y	0. µm
Origin Z	0. µm
Directional Vectors	
X Axis Data	[1. 0. 0.]
Y Axis Data	[0. 1. 0.]
Z Axis Data	[0. 0. 1.]

Mesh

TABLE 6
Model (A4, B4) > Mesh

Object Name	*Mesh*

State	Solved
Display	
Display Style	Use Geometry Setting
Defaults	
Physics Preference	Mechanical
Element Order	Program Controlled
Element Size	1000.0 µm
Sizing	
Use Adaptive Sizing	Yes
Resolution	Default (2)
Mesh Defeaturing	Yes
Defeature Size	Default
Transition	Fast
Span Angle Center	Coarse
Initial Size Seed	Assembly
Bounding Box Diagonal	1.4122e+005 µm
Average Surface Area	3.3408e+007 µm²
Minimum Edge Length	1.1657 µm
Quality	
Check Mesh Quality	Yes, Errors
Error Limits	Standard Mechanical
Target Quality	Default (0.050000)
Smoothing	Medium
Mesh Metric	None
Inflation	
Use Automatic Inflation	None
Inflation Option	Smooth Transition
Transition Ratio	0.272
Maximum Layers	5
Growth Rate	1.2
Inflation Algorithm	Pre
View Advanced Options	No
Advanced	
Number of CPUs for Parallel Part Meshing	Program Controlled
Straight Sided Elements	No
Rigid Body Behavior	Dimensionally Reduced
Triangle Surface Mesher	Program Controlled
Topology Checking	Yes
Pinch Tolerance	Please Define
Generate Pinch on Refresh	No
Statistics	
Nodes	820441
Elements	484011

Steady-State Thermal (A5)

TABLE 7
Model (A4, B4) > Analysis

Object Name	*Steady-State Thermal (A5)*
State	Solved
Definition	
Physics Type	Thermal
Analysis Type	Steady-State
Solver Target	Mechanical APDL
Options	
Generate Input Only	No

TABLE 8
Model (A4, B4) > Steady-State Thermal (A5) > Initial Condition

Object Name	*Initial Temperature*
State	Fully Defined
Definition	
Initial Temperature	Uniform Temperature
Initial Temperature Value	22. °C

TABLE 9
Model (A4, B4) > Steady-State Thermal (A5) > Analysis Settings

Object Name	*Analysis Settings*
State	Fully Defined
Step Controls	
Number Of Steps	1.
Current Step Number	1.
Step End Time	1. s
Auto Time Stepping	Program Controlled
Solver Controls	
Solver Type	Program Controlled
Solver Pivot Checking	Program Controlled
Radiosity Controls	
Radiosity Solver	Program Controlled
Flux Convergence	1.e-004
Maximum Iteration	1000.
Solver Tolerance	0.1 pW/μm²
Over Relaxation	0.1
Hemicube Resolution	10.
Nonlinear Controls	
Heat Convergence	Program Controlled
Temperature Convergence	Program Controlled
Line Search	Program Controlled
Output Controls	
Calculate Thermal Flux	Yes
Nodal Forces	No
Contact Miscellaneous	No
General Miscellaneous	No
Store Results At	All Time Points
Analysis Data Management	
Solver Files Directory	C:\Users\gpikurs\Documents\RFQ-Q_files\dp0\SYS\MECH\
Future Analysis	None
Scratch Solver Files Directory	
Save MAPDL db	No
Contact Summary	Program Controlled
Delete Unneeded Files	Yes
Nonlinear Solution	No
Solver Units	Active System
Solver Unit System	μmks

TABLE 10
Model (A4, B4) > Steady-State Thermal (A5) > Loads

Object Name	*Heat Flux Vane Tip*	*Heat Flux Cavity*	*Temperature*	*Convection*	*Heat Flux*	*Heat Flux 2*	*Heat Flux 3*
State	Fully Defined						
Scope							
Scoping Method	Geometry Selection						
Geometry	1 Face	2 Faces	443 Faces	5 Faces	2 Faces		4 Faces

Definition							
Type	Heat Flux		Temperature	Convection	Heat Flux		
Magnitude	100. pW/μm² (ramped)	22000 pW/μm² (ramped)	22. °C (ramped)		27500 pW/μm² (ramped)	30000 pW/μm² (ramped)	6000. pW/μm² (ramped)
Suppressed	No						
Film Coefficient				500. pW/μm²·°C (step applied)			
Ambient Temperature				22. °C (ramped)			
Convection Matrix				Program Controlled			

FIGURE 1
Model (A4, B4) > Steady-State Thermal (A5) > Heat Flux Vane Tip

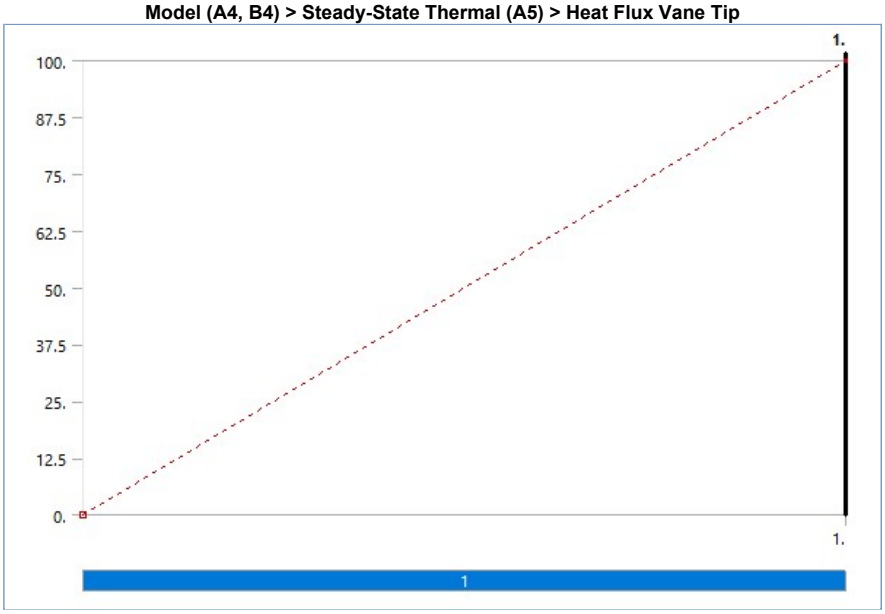

FIGURE 2
Model (A4, B4) > Steady-State Thermal (A5) > Heat Flux Cavity

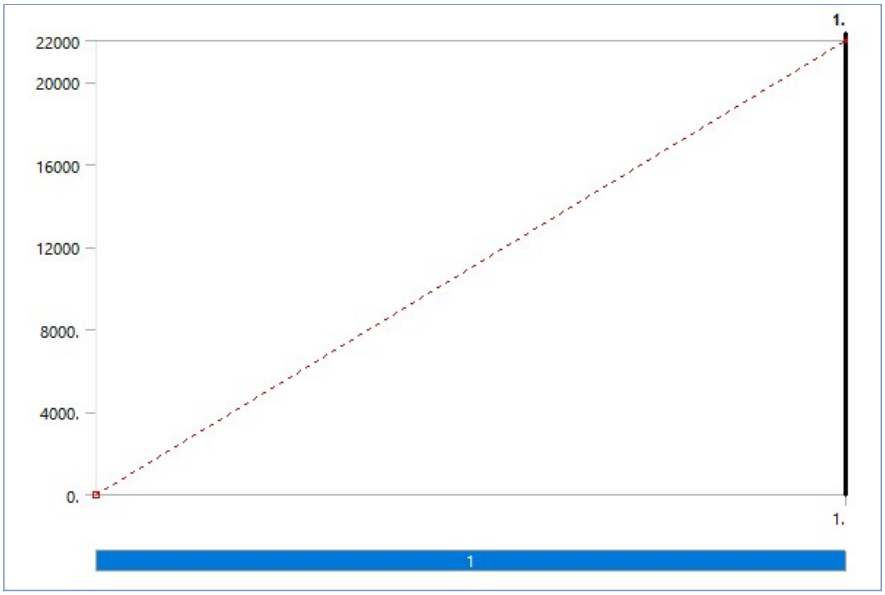

FIGURE 3
Model (A4, B4) > Steady-State Thermal (A5) > Temperature

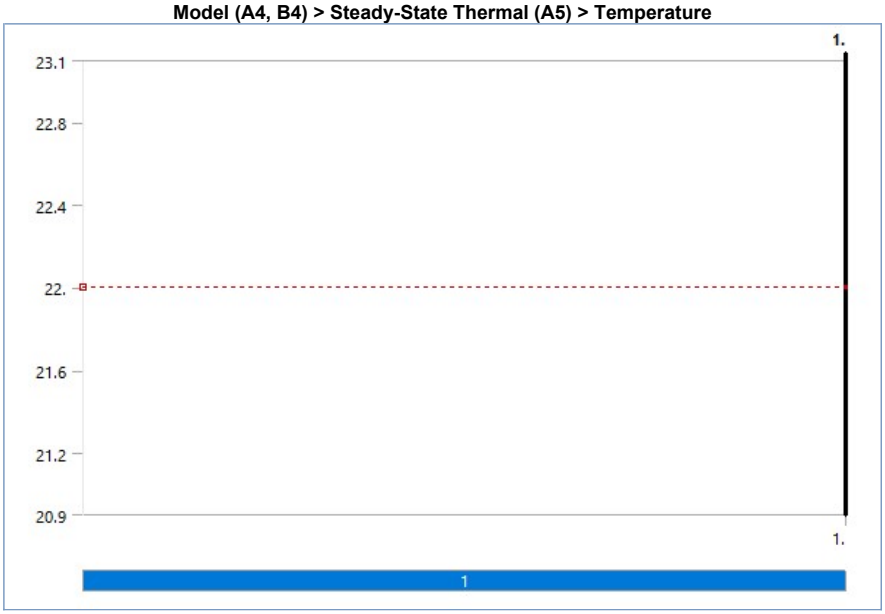

FIGURE 4
Model (A4, B4) > Steady-State Thermal (A5) > Convection

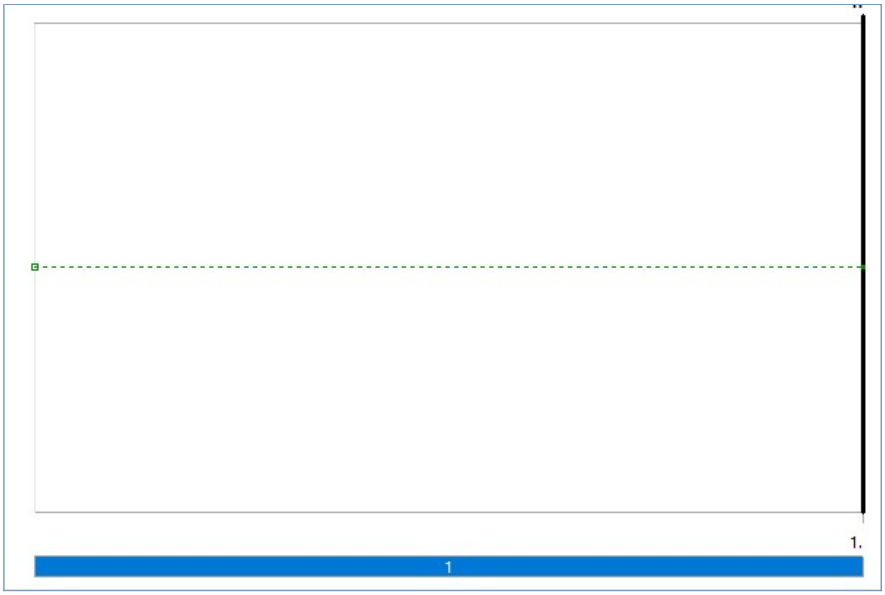

TABLE 11
Model (A4, B4) > Steady-State Thermal (A5) > Convection

Steps	Time [s]	Convection Coefficient [pW/µm²·°C]	Temperature [°C]
1	0.	= 500.	= 22.
	1.	500.	22.

FIGURE 5
Model (A4, B4) > Steady-State Thermal (A5) > Heat Flux

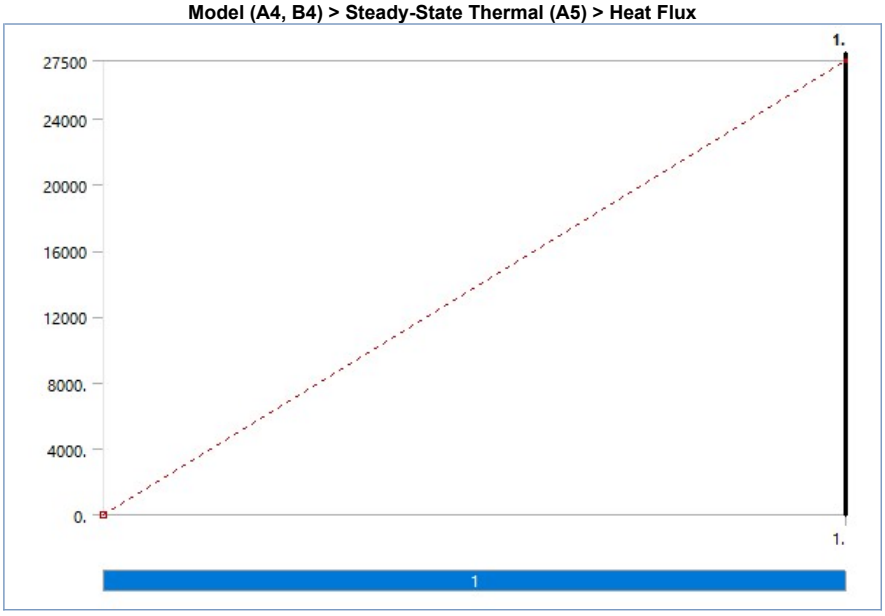

FIGURE 6
Model (A4, B4) > Steady-State Thermal (A5) > Heat Flux 2

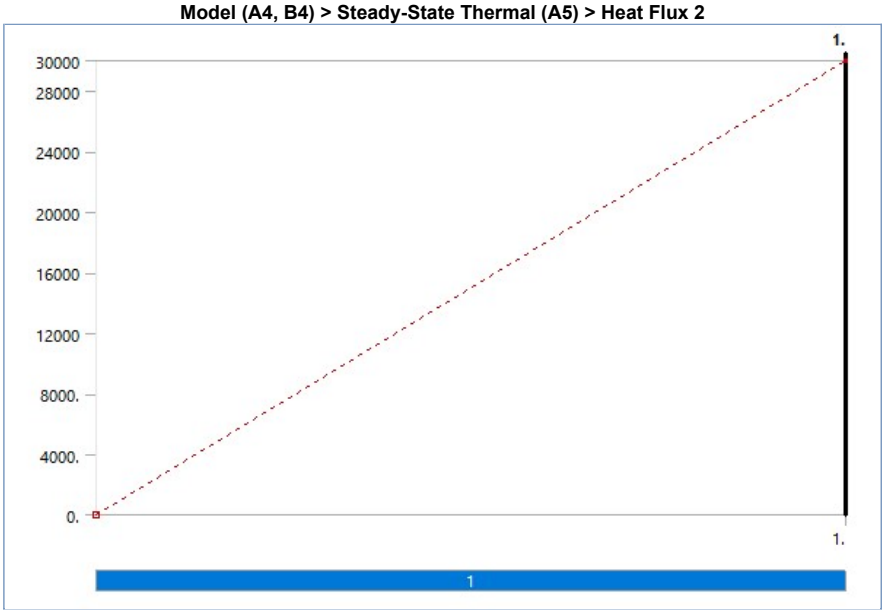

FIGURE 7
Model (A4, B4) > Steady-State Thermal (A5) > Heat Flux 3

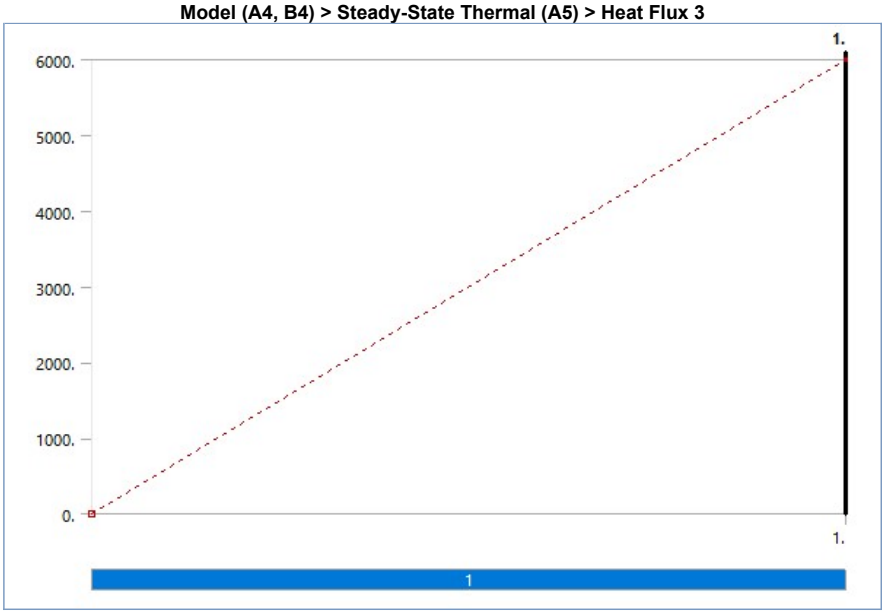

Solution (A6)

TABLE 12
Model (A4, B4) > Steady-State Thermal (A5) > Solution

Object Name	*Solution (A6)*
State	Solved
Adaptive Mesh Refinement	
Max Refinement Loops	1.
Refinement Depth	2.
Information	
Status	Done
MAPDL Elapsed Time	32. s
MAPDL Memory Used	4.3955 GB
MAPDL Result File Size	274.19 MB
Post Processing	
Beam Section Results	No
On Demand Stress/Strain	No

TABLE 13
Model (A4, B4) > Steady-State Thermal (A5) > Solution (A6) > Solution Information

Object Name	*Solution Information*
State	Solved
Solution Information	
Solution Output	Solver Output
Update Interval	2.5 s
Display Points	All
FE Connection Visibility	
Activate Visibility	Yes
Display	All FE Connectors
Draw Connections Attached To	All Nodes
Line Color	Connection Type
Visible on Results	No
Line Thickness	Single
Display Type	Lines

TABLE 14
Model (A4, B4) > Steady-State Thermal (A5) > Solution (A6) > Results

Object Name	*Temperature*
State	Solved
Scope	
Scoping Method	Geometry Selection
Geometry	All Bodies
Definition	
Type	Temperature
By	Time
Display Time	Last
Calculate Time History	Yes
Identifier	
Suppressed	No
Results	
Minimum	22. °C
Maximum	25.145 °C
Average	22.625 °C
Minimum Occurs On	PartBody|Assemble.1
Maximum Occurs On	PartBody|Assemble.1
Information	
Time	1. s
Load Step	1
Substep	1
Iteration Number	1

FIGURE 8
Model (A4, B4) > Steady-State Thermal (A5) > Solution (A6) > Temperature

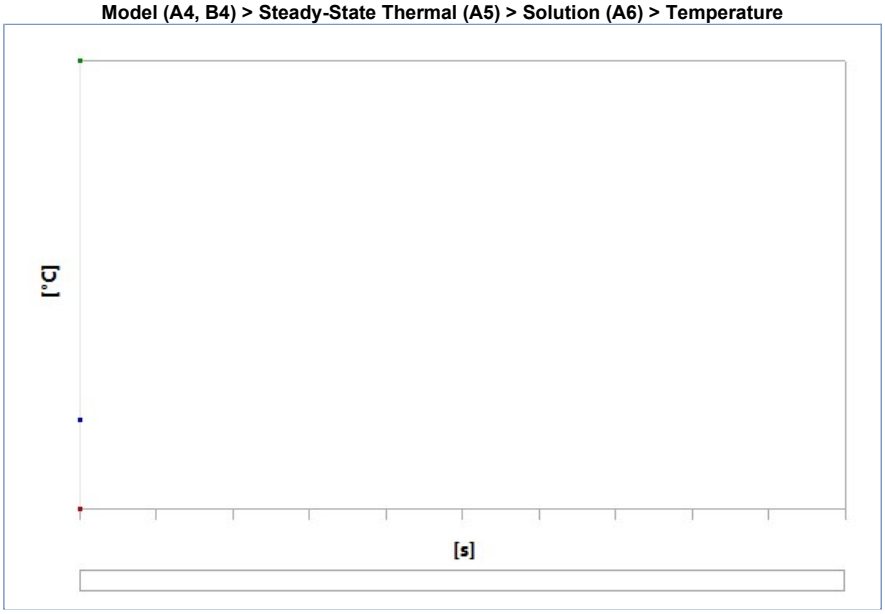

TABLE 15
Model (A4, B4) > Steady-State Thermal (A5) > Solution (A6) > Temperature

Time [s]	Minimum [°C]	Maximum [°C]	Average [°C]
1.	22.	25.145	22.625

Static Structural (B5)

TABLE 16
Model (A4, B4) > Analysis

Object Name	*Static Structural (B5)*
State	Solved
Definition	
Physics Type	Structural
Analysis Type	Static Structural
Solver Target	Mechanical APDL
Options	
Environment Temperature	22. °C
Generate Input Only	No

TABLE 17
Model (A4, B4) > Static Structural (B5) > Analysis Settings

Object Name	*Analysis Settings*
State	Fully Defined
Step Controls	
Number Of Steps	1.
Current Step Number	1.
Step End Time	1. s
Auto Time Stepping	Program Controlled
Solver Controls	
Solver Type	Program Controlled

Weak Springs	Off
Solver Pivot Checking	Program Controlled
Large Deflection	Off
Inertia Relief	Off
Rotordynamics Controls	
Coriolis Effect	Off
Restart Controls	
Generate Restart Points	Program Controlled
Retain Files After Full Solve	No
Combine Restart Files	Program Controlled
Nonlinear Controls	
Newton-Raphson Option	Program Controlled
Force Convergence	Program Controlled
Moment Convergence	Program Controlled
Displacement Convergence	Program Controlled
Rotation Convergence	Program Controlled
Line Search	Program Controlled
Stabilization	Off
Output Controls	
Stress	Yes
Strain	Yes
Nodal Forces	No
Contact Miscellaneous	No
General Miscellaneous	No
Store Results At	All Time Points
Analysis Data Management	
Solver Files Directory	C:\Users\gpikurs\Documents\RFQ-Q_files\dp0\SYS-2\MECH\
Future Analysis	None
Scratch Solver Files Directory	
Save MAPDL db	No
Contact Summary	Program Controlled
Delete Unneeded Files	Yes
Nonlinear Solution	No
Solver Units	Active System
Solver Unit System	µmks

TABLE 18
Model (A4, B4) > Static Structural (B5) > Loads

Object Name	*Remote Displacement*
State	Fully Defined
Scope	
Scoping Method	Geometry Selection
Geometry	1 Face
Coordinate System	Global Coordinate System
X Coordinate	5.4251e-002 µm
Y Coordinate	4.3682e-005 µm
Z Coordinate	-60000 µm
Location	Defined
Definition	
Type	Remote Displacement
X Component	0. µm (ramped)
Y Component	0. µm (ramped)
Z Component	0. µm (ramped)
Rotation X	0. ° (ramped)
Rotation Y	0. ° (ramped)
Rotation Z	0. ° (ramped)

Suppressed	No
Behavior	Deformable
Advanced	
Pinball Region	All

FIGURE 9
Model (A4, B4) > Static Structural (B5) > Remote Displacement

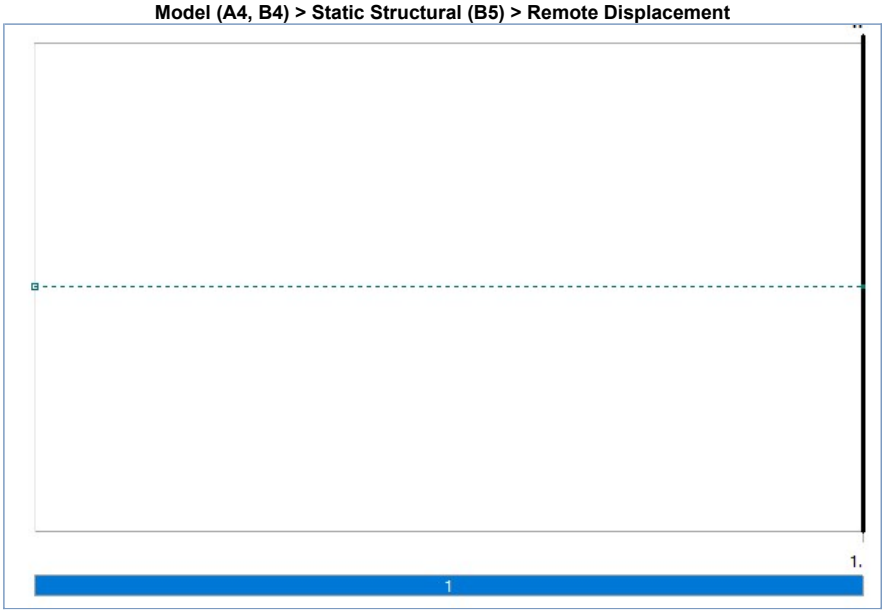

TABLE 19
Model (A4, B4) > Static Structural (B5) > Imported Load (A6)

Object Name	*Imported Load (A6)*
State	Fully Defined
Definition	
Type	Imported Data
Interpolation Type	Mechanical Results Transfer
Suppressed	No
Source	A6::Solution

TABLE 20
Model (A4, B4) > Static Structural (B5) > Imported Load (A6) > Imported Body Temperature

Object Name	*Imported Body Temperature*
State	Solved
Scope	
Scoping Method	Geometry Selection
Geometry	1 Body
Definition	
Type	Imported Body Temperature
Tabular Loading	Program Controlled
Suppressed	No
Source Environment	Steady-State Thermal (A5)
Source Time	Worksheet

FIGURE 10

Model (A4, B4) > Static Structural (B5) > Imported Load (A6) > Imported Body Temperature

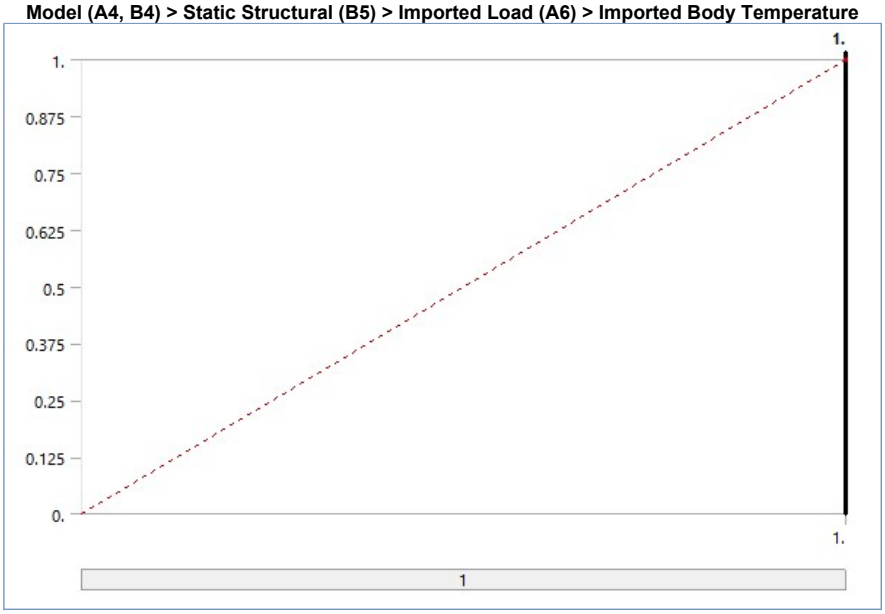

Model (A4, B4) > Static Structural (B5) > Imported Load (A6) > Imported Body Temperature

	Source Time (s)	Analysis Time (s)
1	End Time	1
*		

Solution (B6)

TABLE 21
Model (A4, B4) > Static Structural (B5) > Solution

Object Name	*Solution (B6)*
State	Solved
Adaptive Mesh Refinement	
Max Refinement Loops	1.
Refinement Depth	2.
Information	
Status	Done
MAPDL Elapsed Time	2 m 17 s
MAPDL Memory Used	4.4424 GB
MAPDL Result File Size	452.19 MB
Post Processing	
Beam Section Results	No
On Demand Stress/Strain	No

TABLE 22
Model (A4, B4) > Static Structural (B5) > Solution (B6) > Solution Information

Object Name	*Solution Information*
State	Solved
Solution Information	
Solution Output	Solver Output
Newton-Raphson Residuals	0
Identify Element Violations	0

Update Interval	2.5 s
Display Points	All
FE Connection Visibility	
Activate Visibility	Yes
Display	All FE Connectors
Draw Connections Attached To	All Nodes
Line Color	Connection Type
Visible on Results	No
Line Thickness	Single
Display Type	Lines

TABLE 23
Model (A4, B4) > Static Structural (B5) > Solution (B6) > Results

Object Name	*Total Deformation*
State	Solved
Scope	
Scoping Method	Geometry Selection
Geometry	All Bodies
Definition	
Type	Total Deformation
By	Time
Display Time	Last
Calculate Time History	Yes
Identifier	
Suppressed	No
Results	
Minimum	2.6046e-003 µm
Maximum	1.7843 µm
Average	0.41487 µm
Minimum Occurs On	PartBody|Assemble.1
Maximum Occurs On	PartBody|Assemble.1
Information	
Time	1. s
Load Step	1
Substep	1
Iteration Number	1

FIGURE 11
Model (A4, B4) > Static Structural (B5) > Solution (B6) > Total Deformation

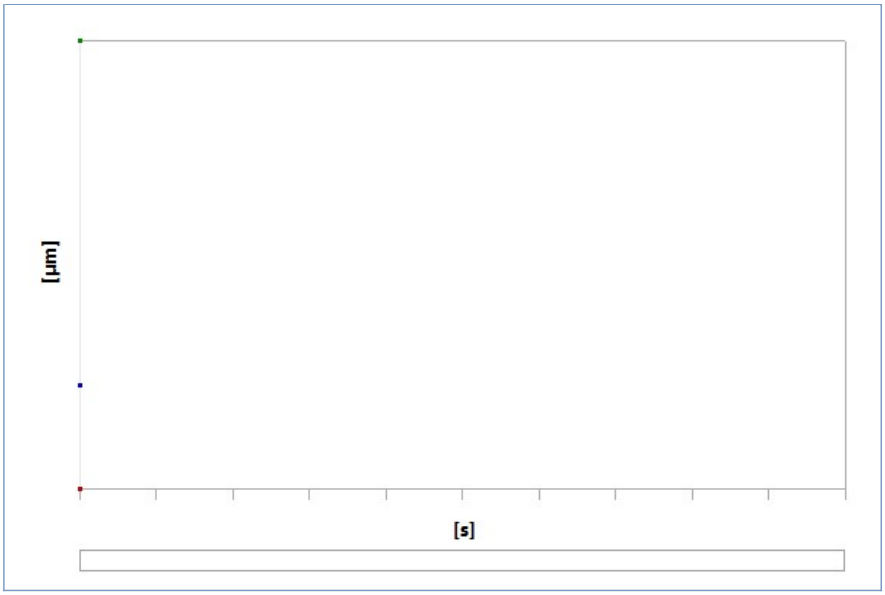

TABLE 24
Model (A4, B4) > Static Structural (B5) > Solution (B6) > Total Deformation

Time [s]	Minimum [µm]	Maximum [µm]	Average [µm]
1.	2.6046e-003	1.7843	0.41487

Material Data

Copper, cast

TABLE 25
Copper, cast > Constants

Isotropic Resistivity	19.3 mohm um

TABLE 26
Copper, cast > Density

Density kg um^-3
8.94e-015

TABLE 27
Copper, cast > Isotropic Elasticity

Young's Modulus MPa	Poisson's Ratio	Bulk Modulus MPa	Shear Modulus MPa
1.25e+005	0.345	1.3441e+005	46468

TABLE 28
Copper, cast > Isotropic Thermal Conductivity

Thermal Conductivity pW um^-1 C^-1
3.94e+008

TABLE 29
Copper, cast > Isotropic Secant Coefficient of Thermal Expansion

Coefficient of Thermal Expansion C^-1
1.68e-005

Zero-Thermal-Strain Reference Temperature C
22

TABLE 30
Copper, cast > Specific Heat Constant Pressure

Specific Heat pJ kg^-1 C^-1
3.85e+014

TABLE 31
Copper, cast > Color

Red	Green	Blue
255	153	0

TABLE 32
Copper, cast > Tensile Yield Strength

Tensile Yield Strength MPa
33.5

TABLE 33
Copper, cast > Tensile Ultimate Strength

Tensile Ultimate Strength MPa
152

8. ANNEX H

Vane tip surface deviation generated from CMM measurements vs source .STL model

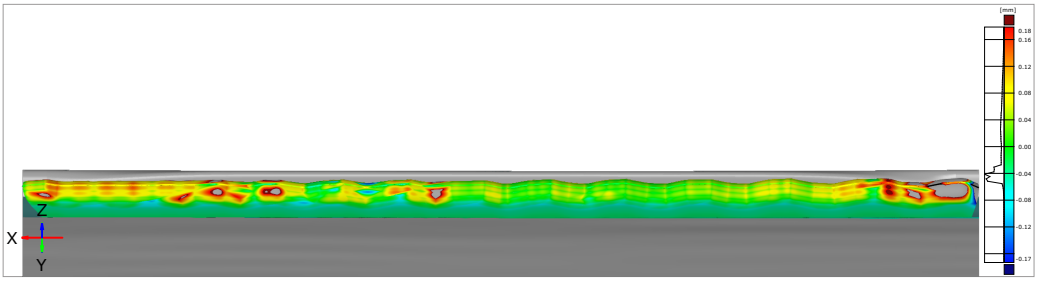

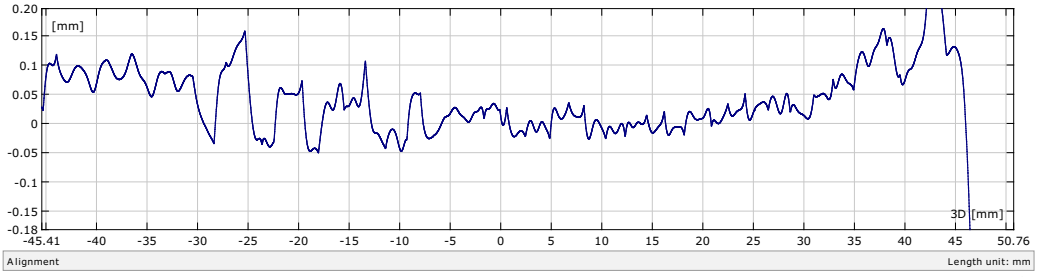

Alignment

Length unit: mm

Vane tip surface deviation CMM vs source STL

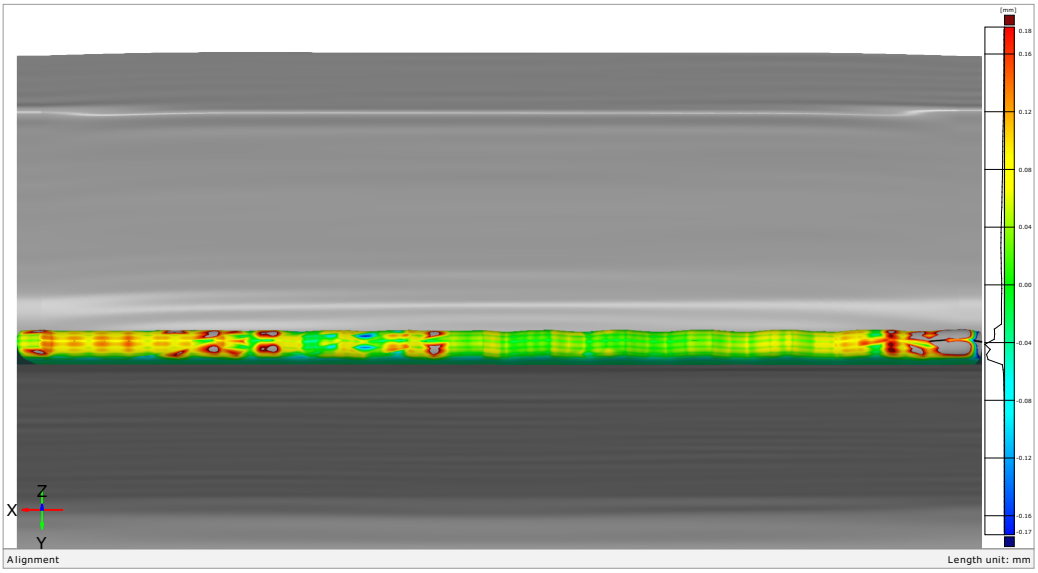

Vanetip surface deviation CMM vs source STL

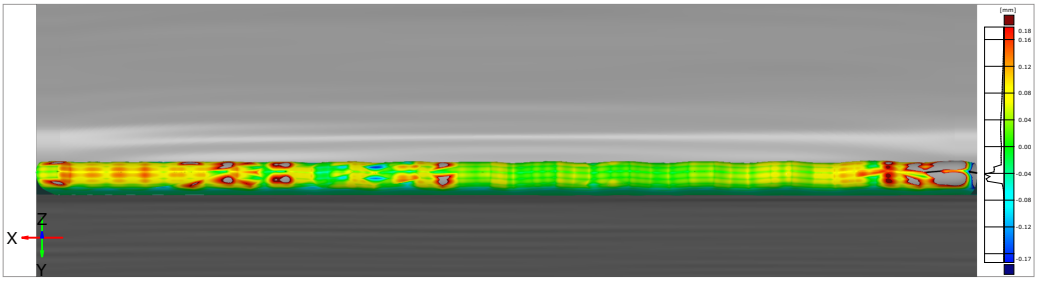

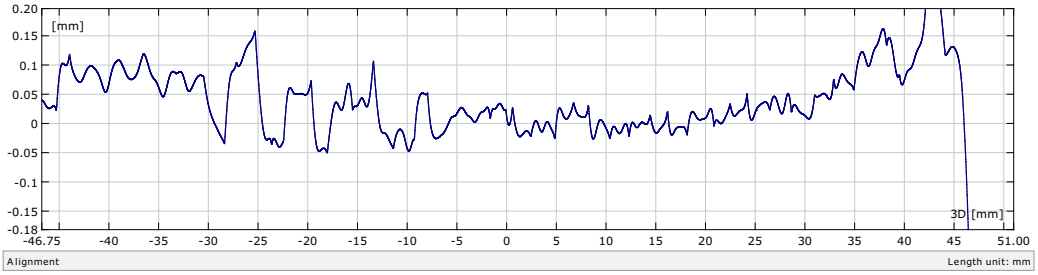

Guntis Pikurs was born in 1973 in Cēsis. He holds a Bachelor's (1995), Engineer's (1996) and Master's degree in Railway Transport (1999) from Riga Technical University (RTU). Since 2003, he has been working at RTU in various positions (research assistant, engineer, lecturer). He is currently a researcher at the Institute of Particle Physics and Accelerator Technology of the Faculty of Natural Sciences and Technology, RTU. His research interests are in mechanical engineering, manufacturing technology, materials processing, and additive manufacturing.